Corrosion Rates of STEEL in CONCRETE

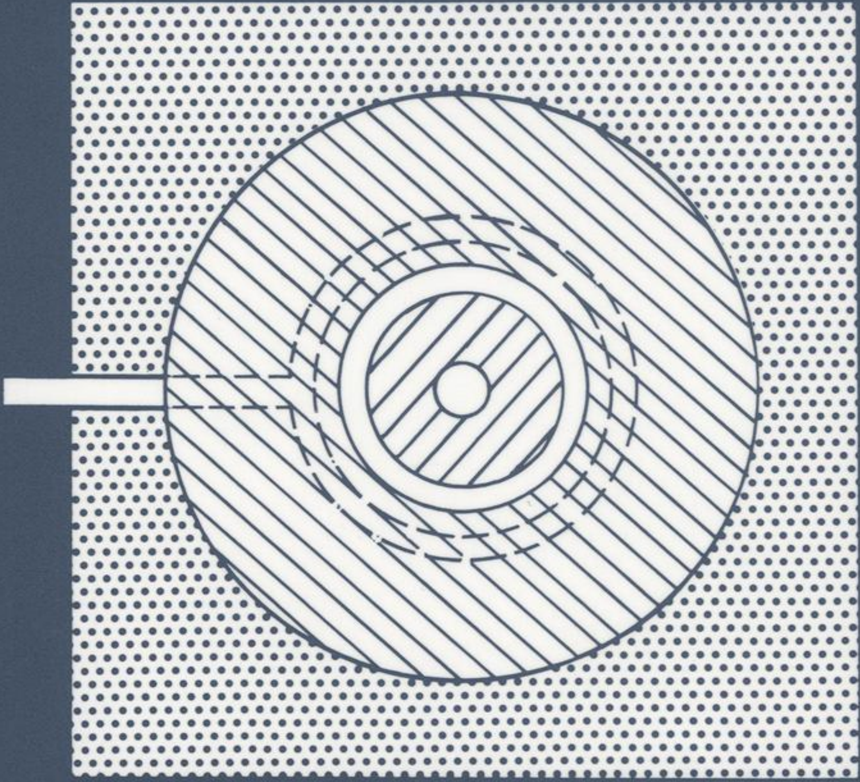

Berke/Chaker/Whiting, editors

ASTM

STP 1065

STP 1065

Corrosion Rates of Steel in Concrete

Neal S. Berke, Victor Chaker, and David Whiting, editors

ASTM
1916 Race Street
Philadelphia, PA 19103

Library of Congress Cataloging-in-Publication Data

Corrosion rates of steel in concrete/Neal S Berke, Victor Chaker, and David Whiting, editors
(STP 1065)
Proceedings of a symposium held in Baltimore, Md , June 29, 1988 and sponsored by the ASTM Committee G-1 on Corrosion of Metals and others
Includes bibliographical references
"ASTM publication code number (PCN) 04-010650-07"—T p verso
ISBN 0-8031-1458-3
1 Reinforcing bars—Corrosion—Congresses 2 Chlorides—Congresses I Berke, Neal Steven, 1952- II Chaker, Victor III Whiting, D (David) IV American Society for Testing and Materials Committee G-1 on Corrosion of Metals V Series ASTM special technical publication, 1065
TA445 5 C69 1990
620 1'723—dc20 90-509
CIP

Peer Review Policy

Each paper published in this volume was evaluated by three peer reviewers The authors addressed all of the reviewers' comments to the satisfaction of both the technical editor(s) and the ASTM Committee on Publications

The quality of the papers in this publication reflects not only the obvious efforts of the authors and the technical editor(s), but also the work of these peer reviewers The ASTM Committee on Publications acknowledges with appreciation their dedication and contribution of time and effort on behalf of ASTM

Printed in Ann Arbor, MI
August 1990

Foreword

The symposium on Corrosion Rates of Steel in Concrete was held in Baltimore, Maryland, on 29 June 1988 The symposium was sponsored by ASTM Committee G01 on Corrosion of Metals and ASTM Committee C09 on Concrete and Concrete Aggregates and its Subcommittees C09 03 08 on Admixtures and C09 03 15 on Concrete's Resistance to Its Environment Neal S Berke, W R Grace and Company, Victor Chaker, Port Authority of New York and New Jersey, and David Whiting, Construction Technology Laboratories, Presided as symposium cochairmen and are editors of this publication

Contents

STP1065-EB/Aug. 1990

Overview

Steel reinforced concrete is a widely used and durable structural material The concrete environment protects the steel from direct atmospheric corrosion However, this protective environment can be compromised due to the ingress or addition of chloride ions, or by carbonation, or both Indeed, the widespread use of steel reinforced concrete in bridge and parking decks subjected to chloride deicing salts, and the use of reinforced concrete in marine environments has resulted in early need of repair due to reinforcement corrosion Other failures have occurred in reinforced pipes and other structures where carbonation has reached the reinforcement level Often the corrosion damage cannot be determined until visible signs of cracking and spalling are evident

ASTM Committee G01 on Corrosion of Metals is actively involved in the writing and evaluation of test methods related to corrosion of metals Subcommittee G01 14 on Corrosion of Reinforcing Steel is the committee addressing rebar corrosion An active goal of Subcommittee G01 14 is to develop test methods that can be used to determine and predict the corrosion rates of steel in concrete Nondestructive techniques would be quite useful in assessing the condition of reinforced concrete in laboratory and more importantly field conditions The results could be used to develop maintenance and repair schedules, and to evaluate new corrosion protection methods The symposium thus provides a useful starting point in the evaluation of test methods to be developed by ASTM

Realizing that corrosion of steel in concrete is also of interest to ASTM Committee C09 on Concrete and Concrete Aggregates, G01 14 is cooperating closely with subcommittees in C09 This Special Technical Publication (STP) is the result of a joint symposium cosponsored by Subcommittees G01 14, C09 03 08 04 (Corrosion Inhibitors), and C09 03 15 on Methods of Testing the Resistance of Concrete to Its Environment

This STP contains eleven papers dealing directly with methods of determining corrosion rates of steel in concrete Several of these papers and the other two papers also address other issues of interest such as chloride ingress, the effects of pozzolans, concrete properties, corrosion inhibitors, different metals and repair techniques, and mechanisms of corrosion Not all of the methods or mechanisms discussed are universally used or accepted, but they do show the active interest in this area of study, and the diversity of views.

Neal S. Berke
W R Grace, Construction Products Division, Cambridge, MA 02140, symposium cochairman and editor

Victor Chaker
Port Authority of NY-NJ, Jersey City, NJ 07310-1397, symposium cochairman and editor

David Whiting
Concrete Technology Laboratories Inc , Skokie, IL 60077-1030, symposium cochairman and editor

Carolyn M. Hansson[1] *and Birgit Sørensen*[1]

The Threshold Concentration of Chloride in Concrete for the Initiation of Reinforcement Corrosion

---

REFERENCE: Hansson, C. M. and Sørensen, B., **"The Threshold Concentration of Chloride in Concrete for the Initiation of Reinforcement Corrosion,"** *Corrosion Rates of Steel in Concrete, ASTM STP 1065,* N. S. Berke, V. Chaker, and D. Whiting, Eds., American Society for Testing and Materials, Philadelphia, 1990, pp. 3–16.

ABSTRACT: The mechanism by which chlorides initiate corrosion is by locally breaking down the passive film which forms on steel in the highly alkaline concrete pore solution. However, the breakdown of passivity requires a certain concentration of chlorides. The aim of the project described in the paper has been to determine the influence of a number of factors on the critical concentration of Cl^- necessary for initiation of corrosion of steel embedded in concrete. The variables investigated include hardening conditions, water/cement ratio, cement type, reinforcing steel surface condition, and salt type.

Mortar samples containing a steel rod have been cast, hardened, and subsequently exposed to a sodium chloride or calcium chloride solution. The corrosion current of the embedded steel has been monitored electrochemically and initially was of the order of 10^{-4} A/m^2, corresponding to a corrosion rate of approximately 0.1 μm/year from the steel surface. After a period of time, the corrosion current increased by several orders of magnitude indicating that the chloride had penetrated to the steel surface and had initiated corrosion. The rate of this penetration, the chloride concentration in the mortar adjacent to the steel at the onset of corrosion, and the subsequent corrosion rate have all been measured to determine the influence of the preceding variables.

KEY WORDS: critical chloride concentration, chloride diffusion, cement type, water/cement ratio, corrosion rates, corrosion, steels, concrete

In good quality portland cement concrete, steel develops a protective passive layer because of the high alkalinity of the pore solution. In the passive state, the steel corrodes at an insignificantly slow rate, typically of the order of 0.1 μm/year [*1,2*]. Unfortunately, however, chloride ions can break down this passivity and allow the steel to actively corrode at rates several orders of magnitude higher than the passive rate.

The critical amount of chloride necessary for the breakdown of the passive film and the onset of active corrosion has been the subject of controversy among scientific investigators for many years. Moreover, its corollary—the amount of chloride which can be tolerated without risk of corrosion—is of major interest to the practicing engineer who would like to use accelerators or other chloride-containing additives in concrete or to those who must build constructions in areas where the mixing water or aggregate are contaminated by chlorides (for example in the Middle East). A knowledge of the chloride threshold value for reinforcement corrosion is also of utmost importance to those involved in inspection,

---

[1] Department head and research engineer, respectively, The Danish Corrosion Centre, Park Allé 345, DK-2605, Brøndby, Denmark.

repair, and maintenance of constructions which are exposed to chlorides from seawater or from de-icing salts

The reason for the scientific controversy and practical confusion is basically a question of "which concrete and when?" because the amount of chloride which can be tolerated is highly dependent on a large number of factors including (1) whether the chloride is present in the original concrete mix or penetrates the concrete from the atmosphere, (2) the composition and history of the concrete, and (3) the atmospheric conditions

The majority of laboratory investigations have either been carried out in synthetic cement pore solution to which chlorides have been added [*3–6*] or cement paste or mortar mixes containing chlorides [*5–12*] On the other hand, the majority of practical investigations of critical values of chloride have involved constructions into which chloride ions have penetrated from the environment [*13–18*]

The present project is aimed at bridging the gap between these two types of investigations by making laboratory investigations of the actual amount of chloride necessary to initiate active reinforcement corrosion in mortar samples when the salt penetrates from the environment

From the viewpoint of reinforcement corrosion, it is the amount of "free" chloride present in the cement paste pore solution rather than the total chloride concentration which is critical The difference between these two, the amount or proportion of "bound" chloride is primarily dependent on the composition of the cement used in the concrete, particularly the cement's aluminium phase content [*19*], its pH [*20,21*] and, probably, its specific surface area [*22*] Thus, the advent of new cement types containing, for example, fly ash, slag, or microsilica, can have a strong influence on the amount of "free" chlorides present in the pore solution

The composition of the concrete and its history (that is, age, temperature, and humidity history) determine the degree of porosity and amount of free water (pore solution) in the cement paste phase These factors, in turn, determine the rate at which chlorides can penetrate into the reinforcement and, thus, the initiation time for corrosion They also determine the concentration of Cl^- in the pore solution which effects the total chloride threshold value for corrosion Finally, they determine the access of oxygen from the environment and the electrical resistivity of the concrete which, together, control the corrosion rate after initiation

In the present investigation, the time to initiate corrosion, the total chloride concentration in the mortar adjacent to the steel at the time of initiation, and the subsequent corrosion rate have been determined with the following parameters as variables (1) cement type, (2) water/cement ratio, (3) curing conditions, (4) state of the reinforcement, and (5) salt type In addition, the proportion of "bound" chloride has been determined for a single sample of each cement type

It should be noted that the exact value of threshold concentration cannot be used in practice because each part of each construction is likely to have its own unique value However, the aim of the project has been to determine the relative influence of the different factors so that the risk of corrosion due to penetrating chlorides can be minimized in future constructions

Experimental Procedure

Sample Preparation

The samples investigated were mortar prisms (40 by 40 by 160 mm^3) with a cement sand ratio of 1 3 and with the cement type and water/cement (w/c) ratios given in Table 1 and

TABLE 1—*Summary of samples tested Six samples of each type were cast and tested*

Mortar Type	Sample Designation	w/c	No of Days at 100% RH	Salt
	EFFECT OF CEMENT TYPE			
Danish ordinary portland cement	DK-OPC	0 50	14	NaCl
Danish low alkali sulphate resistance portland cement	DK-SRPC	0 50	14	NaCl
Danish rapid hardening portland cement	DK-RHPC	0 50	14	NaCl
Danish standard flyash cement	DK-STD	0 50	14	NaCl
Austrian ordinary portland cement	A-OPC	0 50	14	NaCl
Swedish ordinary portland cement	S-OPC	0 50	14	NaCl
90% Swedish ordinary portland cement + 10% microsilica	S-SiO_2	0 50	14	NaCl
	EFFECT OF WATER/CEMENT RATIO			
Danish ordinary portland cement	DK-OPC/40	0 40	14	NaCl
Danish ordinary portland cement	DK-OPC/45	0 45	14	NaCl
Danish ordinary portland cement	DK-OPC/50	0 50	14	NaCl
Danish ordinary portland cement	DK-OPC/60	0 60	14	NaCl
	EFFECT OF HARDENING CONDITIONS			
Danish OPC	DK-OPC-03	0 50	3	NaCl
Danish OPC	DK-OPC-07	0 50	7	NaCl
Danish OPC	DK-OPC-14	0 50	14	NaCl
Danish OPC	DK-OPC-31	0 50	31	NaCl
	EFFECT OF SALT TYPE			
Danish OPC	DK-OPC-Ca	0 50	14	$CaCl_2$
Danish standard flyash cement	DK-STD-Ca	0 50	14	$CaCl_2$
	EFFECT OF STEEL SURFACE CONDITION			
Danish OPC with cleaned reinforcing steel	DK-OPC-cr	0 50	14	NaCl
Danish OPC with as-received reinforcing steel	DK-OPC-ar	0 50	14	NaCl
Danish OPC with rusted reinforcing steel	DK-OPC-rr	0 50	14	NaCl

containing a centrally placed, smooth, plain carbon steel rod, as illustrated in Fig 1 The compositions of the cements investigated are given in Table 2 After casting, the samples were kept for 24 h in 100% relative humidity (RH) before demolding Except where indicated in Table 1, the prisms were then stored in 100% RH (that is, over water in a closed container) for an additional 13 days and, thereafter, in the laboratory atmosphere at approximately 50% RH for 16 days Six samples of each composition or hardening condition or both were prepared and tested

As indicated in the Results section of this paper, the threshold value of chloride concentration measured for these samples was judged to be unrealistically high Therefore, three additional sets of samples were prepared using profiled reinforcing steel instead of the smooth steel rod In one set, the reinforcement was used in the slightly rusted "as-received" condition, in the second set, it was cleaned by sand-blasting, and in the third set, it was further rusted by outdoor exposure for two weeks

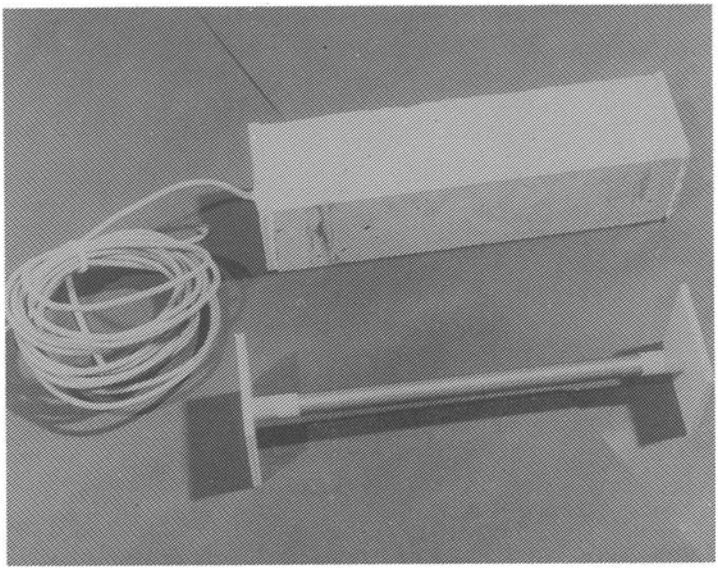

FIG. 1—*Mortar sample containing a centrally placed steel rod.*

Exposure Procedure

Thirty days after casting, the samples were immersed in a 1 *N* sodium chloride (NaCl) or calcium chloride ($CaCl_2$) solution containing calcium hydroxide ($Ca(OH)_2$) and coupled to potentiostat. They were held at a constant applied potential of 0.00 mV saturated calomel electrode (SCE) and the current flowing between each embedded steel rod and an external stainless steel counter electrode was monitored daily. The initial current densities monitored were of the order of 10^{-4} A/m^2 (approximately 0.1 μm/year) and continued unchanged until the chloride penetrated the cover and initiated corrosion at which time the current increased by over three orders of magnitude in the course of a few days.

At this time, three samples of each set were removed and broken to expose the mortar surface adjacent to the steel. Small samples, of the order of 1 g, were removed in approximately 2 to 3 mm from this surface, dissolved in hot nitric acid (HNO_3), cooled and analyzed for Cl^- by potentiometric titration against silver nitrate ($AgNO_3$).

In addition, very small samples, of the order of 5 mg, were scraped from the surface adjacent to both the noncorroding part of the steel and to the corroded part. These were analyzed for Cl^- by energy dispersive X-ray fluorescence spectrometry (XRF). In this technique, the ratio of the intensities of the characteristic X-rays for chlorine and calcium were determined for a number of samples containing known amounts of sodium chloride and the results plotted as a calibration curve. The chloride content of the samples was then determined by comparing their Cl/Ca intensity ratios with those on the calibration curve.

The remaining three samples were disconnected from the potentiostat and positioned vertically with the lower 2 to 3 cm in the chloride solution. Their free potentials were monitored over a period of several weeks and their corrosion rates were determined by polarization resistance measurements. The reason for their being partially exposed to the atmosphere is that earlier experiments showed that the initial corrosion rate is so high that the oxygen dissolved in the pore solution of totally submersed samples is rapidly depleted and the corrosion reaction is stifled despite the high chloride content of the mortar.

TABLE 2—*Analyses of the different cement types investigated Compositions are given in percent by weight*

Cement Type	D-OPC	A-OPC	S-OPC	D-SRPC	D-RHPC	D-STD
Loss on ignition (1000°C)	2 4	2 3	2 3	0 9	0 2	0 2
Insoluble residue	0 6	0 6	0 4			
SiO_2	19 6	19 9	19 6	24 4	22 4	22 4
Al_2O_3	6 0	5 5	4 8	2 6	4 9	4 9
Fe_2O_3	3 0	2 8	2 1	3 1	2 8	2 8
CaO	62 9	61 7	62 8	65 1	66 2	66 2
MgO	0 9	2 4	3 0	0 6	1 0	1 0
SO_3	2 7	2 7	2 8	2 0	0 6	0 6
Alkalis	1 9	2 1	2 2	0 4	0 9	0 9
"Bogue composition"						
C_3S	54 7	51 2	63 4	49 0	58 0	58 0
C_2S	15 0	18 5	8 5	33 0	21 0	21 0135
C_3A	10 8	9 8	9 2	2 0	8 0	8 0
C_4AF	9 1	8 5	6 4	9 0	8 0	8 0
Flyash additions					3 0	22 0
Specific surface area, m^2/kg	300	355	390	300	400	440

At the end of this exposure period, the bound chloride content was determined for a single sample of each cement type by the following procedure The lower half of the sample (that is, that which had been partially submersed in the NaCl solution) was removed and crushed One part was weighed, dried for 48 h at 110°C, and reweighed to determine the free water content The total chloride content of these samples was determined by dissolving the dried mortar in 0 01 *N* HNO_3 and analyzing the solution for Cl^- by potentiometric titration against $AgNO_3$ The pore solution was expressed from the remaining part of the samples and analyzed for both OH^- and Cl^- by chemical and potentiometric titration, respectively

Results and Discussion

The values of time to initiate corrosion, t_o, the critical chloride concentration, C_o, the steady-state corrosion rate, i_o, the proportion of free chloride given as a percentage of the total chloride content, the pH value of the pore solutions expressed from the samples together with the pH values of the same cements without chloride additions, are given in Table 3 The effects of the different parameters investigated are presented in graphical form in association with the following discussions

The pH values (calculated from hydroxyl ion contents) of the pore solutions after long-term exposure to sodium chloride solution vary very little from cement to cement and are all lower than might be expected This may be explained, however, by the previous observation [*20*] that an ion-exchange takes place at the surface of concrete exposed to salt solutions, the hydroxyl ions being leached out while the chloride ions diffuse in Thus, the low, fairly constant values of pH reflect the result of this exchange

It can be seen from Table 3 that the threshold value of chloride concentration at the onset of corrosion is not as pronounced as might be expected and appears, unexpectedly, to be independent of the proportion of the total chloride remaining in the pore solution

The actual value of the threshold concentration determined by potentiometric titration—

TABLE 3—*The average values* ($\overline{x}$) *and standard deviations* (s) *of the values of the time to initiate corrosion* (t_o), *the critical chloride concentration* (C_o), *the subsequent corrosion current density* (i_o), *the electrical resistance, and free* Cl^- *content given as % of the total average chloride content of the sample*

Sample Designation	t_o, days		C_o (titr), % mortar		C_o (XRF), % mortar		i_o, mA/m^2		Electrical Resistance		Free Cl$^-$, % total Cl	pH of Sample	pH of Paste (Ref 25)
	$\overline{x}$	s	$\overline{x}$	s	$\overline{x}$	s	$\overline{x}$	s	$\overline{x}$	s			
DK-OPC-03	27	17	0 139	0 004	0 050	0 026	0 78	0 61	88				
DK-OPC-07	49	19	0 231	0 024	0 102	0 049	0 57	0 31	86	10			
DK-OPC-14	48	19	0 212	0 031	0 085	0 035	0 96	0 91	115	16			
DK-OPC-31	88	14	0 284	0 069	0 173	0 075	1 20	0 70	115	4			
DK-OPC/40	199	39	0 287	0 032	0 170	0 040	2 80	0 10	419	249			
DK-OPC/45	99	8	0 258	0 023	0 137	0 015	0 94	0 39	219	34			
DK-OPC/50	48	19	0 212	0 031	0 085	0 035	0 96	0 91	115	16			
DK-OPC/60	38	11	0 257	0 012	0 080	0 045	7 10	1 10	128	11			
DK-SRPC	78	5	0 212	0 028	0 094	0 030	1 60	1 90	129	15	71	12 75	13 28
DK-RHPC	236	58	0 237	0 120	0 102	0 062	1 60	0 70	372	7	30	12 38	
DK-STD[a]	389	18	0 140	0 017	0 123	0 022	0 83		1087	40	28	12 62	13 42
DK-OPC	48	19	0 212	0 031	0 085	0 035	0 96	0 91	115	16	40	12 38	13 58
A-OPC	110	26	0 263	0 059	0 150	0 037	3 20	2 00	172	25	35	12 60	13 63
S-OPC	80	13	0 252	0 043	0 159	0 054	2 50	0 80	160	2	86	12 56	13 79
S-SiO$_2$	190	96	0 099	0 015	0 051	0 036	4 90	2 90	359	79	33	12 56	12 93
DK-OPC-Ca	58	14	0 343	0 066	0 167	0 018	3 80	3 20	152	4			
DK-STD-Ca	96	5	0 215	0 083	0 125	0 019	1 60	0 90	397	22			
DK-OPC-cr	67	2	0 303	0 115	0 220	0 020	0 60	0 20	103	6			
DK-OPC-ar[b]	59	12	0 260	0 123	0 180	0 033	8 10	8 40	133	14			
DK-OPC-rr[c]	94	13	0 391	0 048					104	7			

[a] Three samples have not yet begun to corrode after 600 days' exposure None of a second series of samples has yet begun to corrode after 120 days' exposure

[b] One sample has not yet begun to corrode after 120 days' exposure

[c] Two samples have not yet begun to corrode after 120 days' exposure

approximately 0.15 to 0.35% by weight of the mortar, giving a value of 0.6 to 1.4% by weight of the cement—is significantly higher than expected from practical measurements of chloride concentrations in constructions in which the reinforcement is actively corroding. There are two possible explanations for this.

First, only a small amount (approximately 1 g) of mortar is removed from the sample adjacent to the steel and it is likely that the cement:sand ratio in this sample is higher than in the bulk of the sample. Therefore, to convert the total amount of chloride present to weight percentage of the cement, the multiplication factor should be lower than the theoretical value of ×4.

Second, the steel used was smooth and clean whereas normal reinforcing steel is both profiled and more or less covered by a rust layer at the time the concrete is cast. The profiling gives a larger specific surface area and, together with the rust, can also give rise to corrosion at lower chloride contents by the phenomenon known as crevice corrosion.

The values of critical concentration determined by X-ray fluorescence are consistently lower than those determined by titration. One reason for this is that they are determined on very small amounts (approximately 5 mg) of material scraped from the layer immediately adjacent to the steel whereas those for titration are obtained from samples drilled from the mortar adjacent to the steel to a depth of approximately 2 mm. Assuming a linear concentration gradient exists from the surface of the sample to the steel, the difference in XRF and titration values can partly be accounted for by the difference in Cl^- concentration over these 2 mm.

A second effect is that the XRF determinations were made by comparison of the intensities of the Cl and Ca characteristic X-ray emissions with those of standard samples prepared in the same manner. By this technique, the uncertainties in the content of sand in the sample are eliminated. It is felt, therefore, that XRF results are the more realistic values.

A very good correlation is observed between the time to initiate corrosion, t_0, and the electrical resistance of all the hardened samples, as illustrated in Fig. 2. This suggests that electrical resistance of fully saturated concrete or mortar could be used as a simple and inexpensively determined parameter to rank their resistance to penetration of salts.

Effect of Curing Time

The transfer of samples from 100% RH to the laboratory atmosphere of approximately 50% RH results in a drying out of the mortar and effectively stops hydration. Thus, samples which were cured at 100% RH for only three days and allowed to dry out for 27 days can be expected to contain significant amounts of unhydrated cement and to be extremely porous. When the sample is subsequently immersed in NaCl solution, the chloride ions will penetrate the mortar very rapidly together with the water as it is drawn in by capillary suction. The unhydrated cement can then begin to react and will be affected by the presence of the Cl^- ions which will have a greater chance of being chemically bound than if they penetrated fully hardened cement paste and may also have an accelerating effect on the hydration.

The longer the period of moist curing, the slower will be the penetration of chlorides but the degree of chemical binding can also be expected to be lower. The first hypothesis is confirmed by the results shown in Fig. 3: the initiation time for corrosion increases approximately linearly with an increasing period of moist curing. On the other hand, any increase in chemical binding is not reflected in a higher critical chloride concentration for corrosion and, in fact, the tendency is the opposite. One possible cause could be that a moist curing period of only three days was not sufficient to allow a fully protective passive film to be formed before the chlorides penetrated the mortar cover.

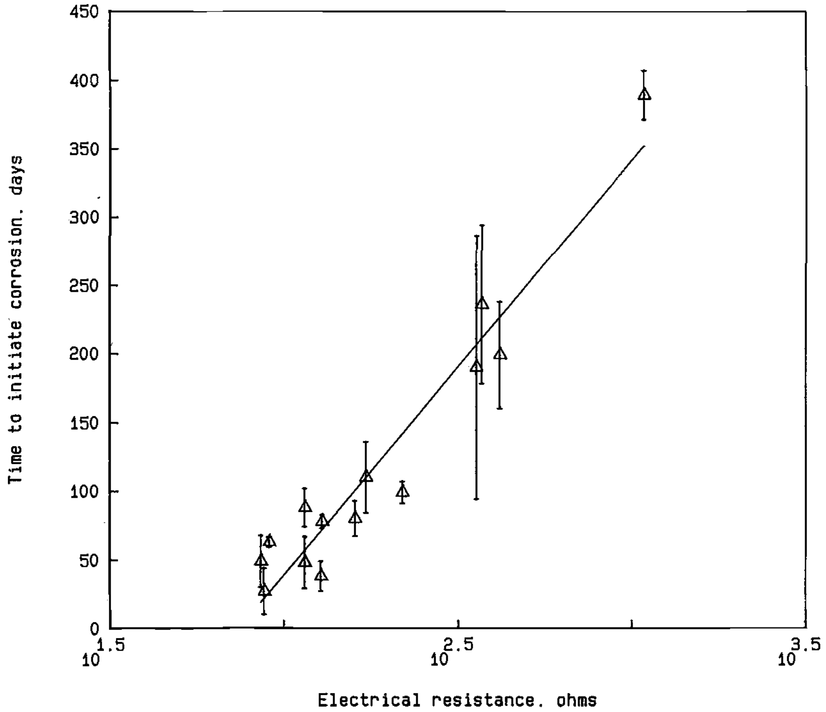

FIG. 2—*The time to initiate corrosion as a function of the electrical resistance of the hardened samples.*

Effect of Water/Cement Ratio

A major effect of increasing the w/c ratio is an increase in the porosity. This has a threefold negative effect from the point of view of reinforcement corrosion: a more rapid diffusion of chloride ions in to the steel surface; easier ingress of oxygen and lower electrical resistivity. Increasing the w/c ratio has two additional effects: first, it results in a lower pH of the pore solution [*20*] which, in turn, influences both the degree of chloride binding [*20,21*] and the critical concentration of chlorides required to break down the passive film [*23*]. Second, a higher w/c ratio gives a greater total amount of free water and, therefore, a more dilute chloride concentration in the pore solution [*20*].

The net effect of these factors is negative, however, as illustrated in Fig. 4, with a rapidly decreasing initiation time for corrosion and a similar decrease in the critical chloride concentration for corrosion (as determined by XRF). It should be noted that the effect of w/c ratio on the initiation time is considerably greater than that of curing shown in Fig. 3.

The Effect of Cement Type

The critical chloride concentrations and the initiation times for corrosion for mortars prepared with all seven types of cement are given in the bar diagram in Fig. 5. In Fig. 6, the values of t_0 for samples prepared with the three Danish cements, sulphate resistant portland cement (SRPC), rapid-hardening portland cement (RHPC) and standard cement,

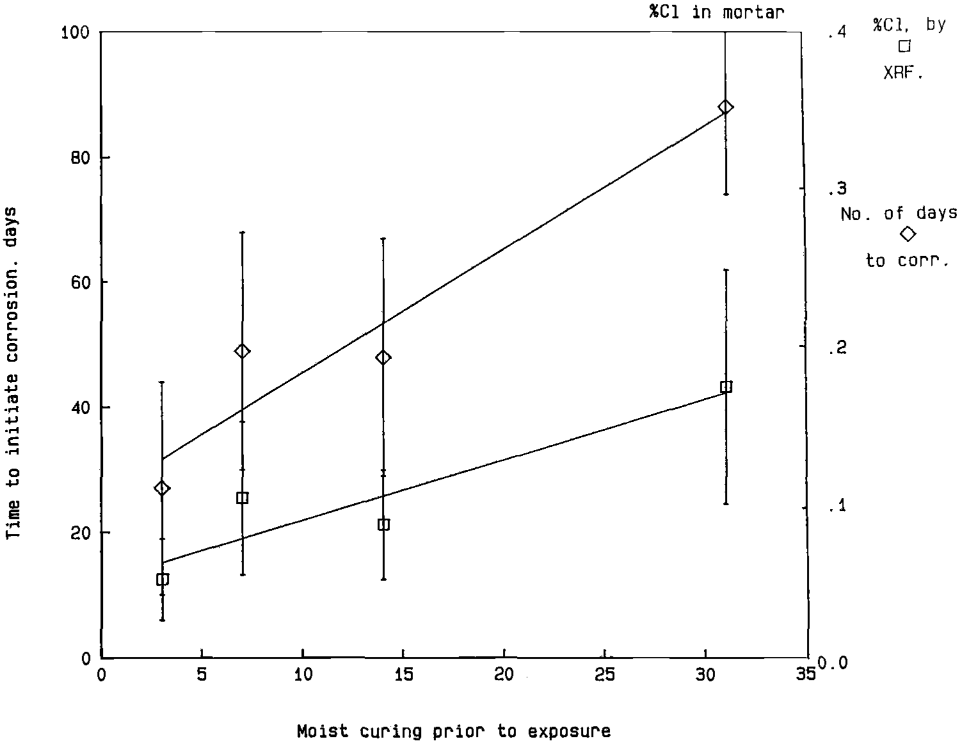

FIG. 3—*The corrosion initiation time and critical chloride concentration (determined by XRF) for Danish OPC mortar samples as a function of the period of moist curing.*

are plotted versus the steady-state diffusion coefficients determined for 28 day old paste samples of the same cements also with w/c = 0.50 published previously [24]. The correlation is excellent and confirms that steady-state diffusion measurements on paste samples can be used as an indication of resistance of mortar and concrete to penetration of chlorides.

The Ordinary Portland Cements (OPCs)—Despite the fact that the composition of all three OPCs lie within the general specification for ordinary portland cement, their response to exposure to chlorides is quite different. The present results confirm a previous observation [25] that the Swedish OPC has a much lower binding capacity for chlorides than do the Danish or Austrian OPCs. The reason for this is not clear but is probably a combination of the effects of the lower total aluminium content (that is, tricalcium aluminate (C_3A) + tetracalcium aluminate ferrite (C_4AF)), the higher pH of the pore solution (which has been shown to decrease the chloride binding [20,21]) and, possibly, the additions of ferrous sulphate to this cement.

Although the concentration of chlorides remaining in solution in the Swedish OPC is much greater than that if the other OPCs, the critical total chloride concentration necessary to initiate corrosion is the highest of the three OPC cements. It must be concluded, therefore, that the high dissolved chloride content which can be tolerated is a result of the very high pH of this cement.

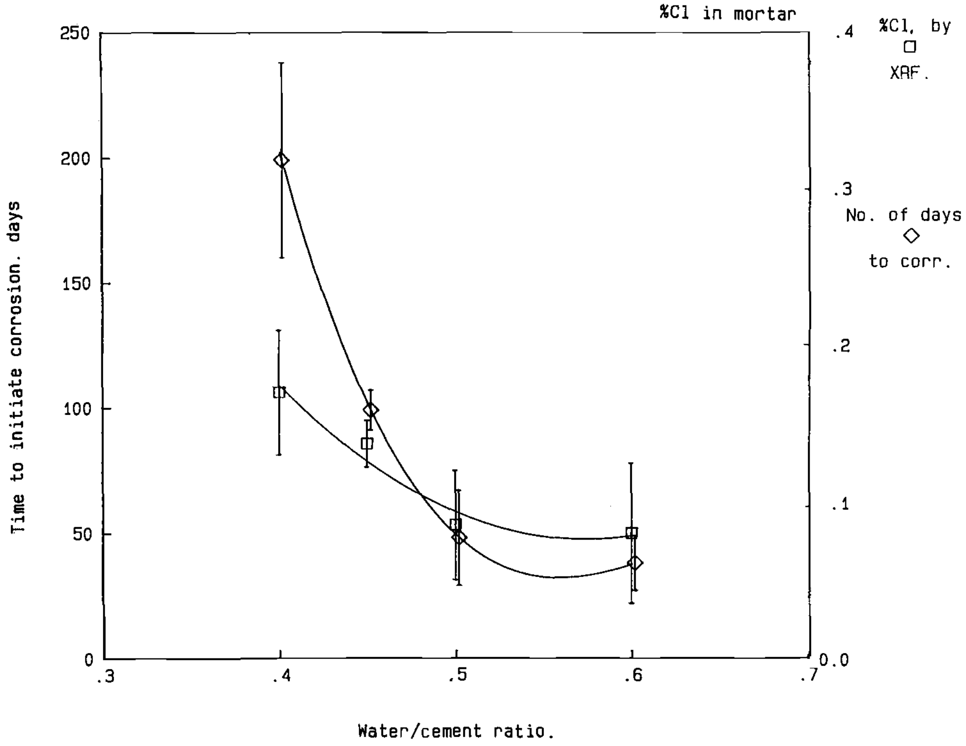

FIG. 4—*The effect of water/cement ratio of Danish OPC mortar samples on the time to initiate corrosion and the critical chloride concentration (determined by XRF).*

There is no relationship between the values of t_0 for samples made with these three cements and, for example, the specific surface area of the cement which must play a role in the pore size distribution of the hardened paste. That the Danish OPC had the lowest value of all seven cements is probably due to its coarse particle size but the Swedish OPC has the highest specific surface area of the three but a lower value of t_0 than the Austrian OPC samples. The additions of ferrous sulphate to the Swedish OPC which have a mild accelerating effect may, however, result a more open pore structure and, thereby. allow more rapid penetration of the chloride solution. Ferrous sulphate is also normally added to Danish cements, but the OPC used in this project was one prepared for experimental purposes and did not contain this additive.

Sulphate Resistant Portland Cement—Apart from the Swedish OPC which was just discussed, samples prepared with SRPC exhibited the lowest degree of chloride binding, as expected from its low C_3A content.

It should be noted, however, that despite previous reports [26] that SRPC has a lower resistance to chloride diffusion than OPC, the present results show very little difference in the behavior of SRPC samples relative to those prepared with the three OPCs.

Cements with Microsilica or Fly Ash—The previous observation [25] of a significant increase in the binding of chlorides by additions of silicon dioxide (SiO_2) to the Swedish OPC

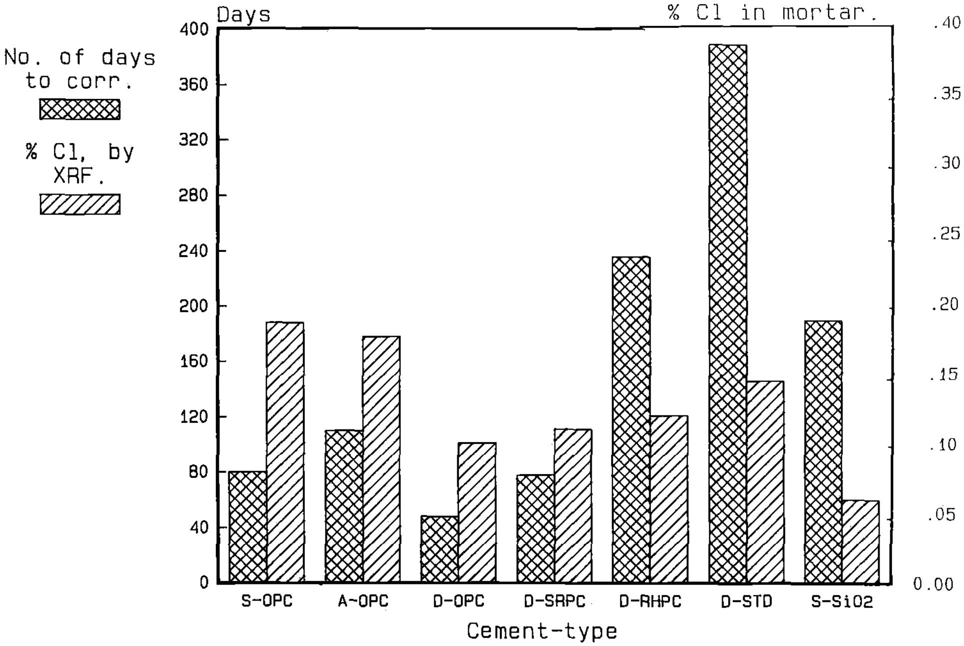

FIG. 5—*The times to initiate corrosion and critical chloride concentration (determined by XRF) for mortar samples prepared with different cement types.*

is confirmed by the present measurements. There are probably two reasons for this: first, the low value of pH which influences the degree of chloride binding [*20,21*] and, second, the enormous increase in internal surface area available for adsorption of the Cl^- resulting from the presence of the extremely fine silica particles.

Despite the high degree of Cl binding, however, the samples of prepared Swedish OPC/SiO_2 exhibited the lowest value of critical chloride concentration. This is also attributable to the low pH of this cement mixture.

The Danish rapid hardening (RHPC) and Standard cements contain 3% and 22% fly ash, respectively, and exhibited the highest values of t_0 suggesting that the fly ash is very effective in reducing the porosity in the hardened paste. In comparison, the SiO_2 probably produces a more open structure in mixes without the use of a superplasticizer.

Effect of Cation Type

It has been reported that chloride as $CaCl_2$ diffuses through hardened cement paste more rapidly than it does as NaCl [*27*]. Moreover, chloride added as $CaCl_2$ to mortar in the mixing water results in a higher corrosion rate than similar additions of NaCl [*28*]. In the present experiments, however, where the chloride penetrates the hardened mortar together with water, there is no significant effect on the time to initiate corrosion of steel in Danish OPC mortar and, in fact, the $CaCl_2$ gives a slightly longer average initiation time than does NaCl.

In contrast, the $CaCl_2$ initiated corrosion of steel in Standard cement considerably more rapidly than did NaCl. It is possible that this is due to the Standard cement's very slow hardening rate relative to that of the OPC. This is supported by the fact that the electrical resistance of the Standard cement samples exposed to $CaCl_2$ solution which was 88 Ω at the

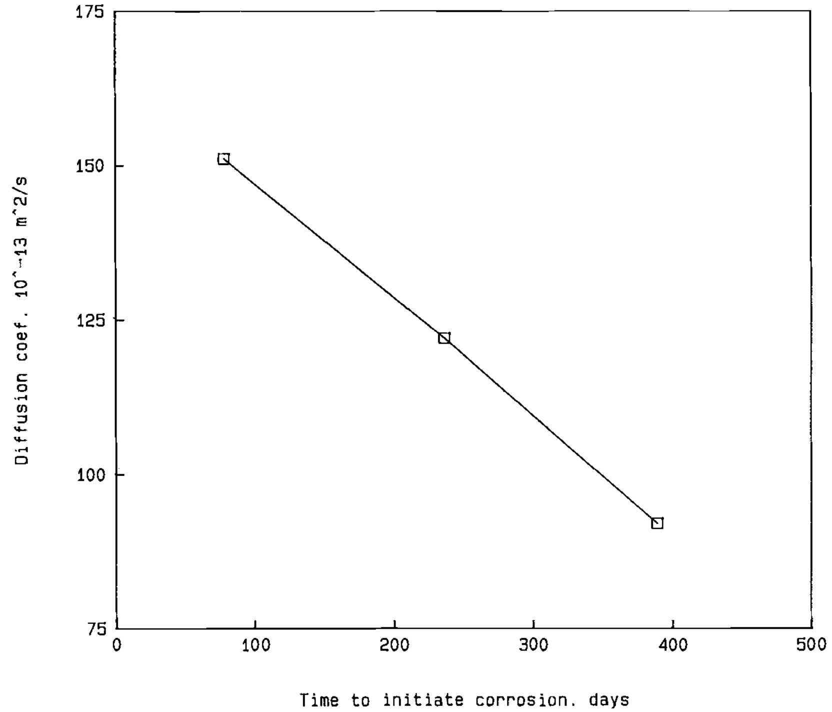

FIG. 6—*The time to initiate corrosion versus the steady-state diffusion rates (from Ref 24) for samples prepared with the Danish cements.*

time of exposure, rose to 397 Ω when corrosion was initiated after 96 days. Compared to that the electrical resistance of the samples exposed to NaCl solution had reached a level of 1087 Ω by the onset of corrosion after 389 days.

Effect of Steel Surface Condition

At the time of writing of this article, that is after 100 days exposure to chloride solution, all the samples containing sand-blast, profiled reinforcement had begun to corrode. Five of the six samples containing as-received reinforcement and only two samples containing reinforcing steel which had been exposed outdoors prior to being embedded in the concrete had begun to corrode. The initiation time for smooth steel in the same cement (Danish OPC) was only 48 days and it must be concluded, therefore, that the profiling or the presence of rust or both have a positive effect on the onset of corrosion. It was noted, however, that, in contrast to the normal single area of corrosion observed on the smooth steel, tiny areas of corrosion were visible on the profiled steel, especially at the corners of the profiling, as illustrated in Fig. 7, suggesting that crevice corrosion can play a role in corrosion of this steel.

Conclusion

The investigation has shown that the initiation time to onset of corrosion is strongly dependent on hardening condition, water/cement ratio and type of cement, including content of microsilica and fly ash. All of these properties are reflected in the electrical resistance

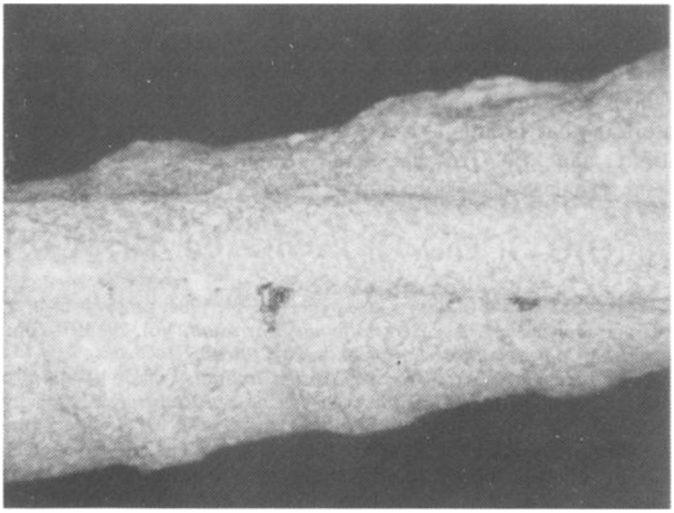

FIG. 7—*Macrograph of profiled reinforcing bar showing corrosion initiation at the corners of the profiling.*

of the concrete. It has been shown that the time to initiation is proportional to the logarithm of the electrical resistance.

The critical chloride concentration is less dependent than the initiation time on the previously mentioned parameters.

Drying test specimens in laboratory atmosphere three days after casting, causes a reduction of 2 to 3 times in the critical chloride concentration and in the initiation time, compared to specimens that has been hardened in 100% RH for 31 days.

Tests performed on specimens with water/cement ratios of 0.4 to 0.6 showed that reducing the w/c ratio has two synergistic effects: (1) the critical chloride content is increased due to the higher pH in the pore solution and: (2) the porosity of the paste is considerably reduced. The combination of these two factors leads to a considerable increase in the time to corrosion.

The replacement of 10% of the cement with microsilica leads to a reduction of the critical chloride concentration to approximately one third of the level for the same cement without microsilica. However, the denser structure in the mortar containing silica leads to an increase in the initiation time of a factor of 2 to 3 and the net effect of microsilica on chloride initiated corrosion is therefore positive.

Fly ash has only a minor, if any, effect on the critical chloride concentration. However, the time to corrosion is increased considerably due to the less porous structure. This effect is even greater if the pozzolanic reaction of the fly ash is allowed to progress before the chloride ions reach the reinforcement.

In the test series with profiled reinforcing steel, the results indicate that the corrosion properties of the profiled steel are at least as good as those of the smooth steel. Further, the presence of a rust layer on the steel prior to casting seems to have a positive effect on the corrosion properties.

Acknowledgments

The authors would like to express their appreciation of the financial support for this project provided by the Danish Technical Research Council (STVF); the Larsen and Nielsen

Foundation, the Thomas B Triges Foundation, Hansen, Carlsen and Frølund A/S, Højgaard and Schultz A/S, and the Danish Corrosion Centre The supply of materials for the investigation by Aalborg Portland Cement Fabrik is also appreciated The work has been carried out as part of the European Community COST 502 Programme and we would like to thank our collaborators in that program, Kajsa Byfors of the Swedish Cement and Concrete Research Institute, and Josef Tritthart of the Technical University of Graz, Austria, for their interest and technical discussions during the course of this project

References

[1] Hansson, C M , *Cement and Concrete Research,* Vol 14, 1984, pp 574–584
[2] Andrade, C and Gonzales, J A , *Werkstoffe und Korrosion,* Vol 29, 1978, pp 515–519
[3] Hausmann, D A , *Materials Protection,* Vol 6, No 19, 1967
[4] Gouda, V K and Halaka, W Y , *British Corrosion Journal,* Vol 5, 1970, pp 204–208
[5] Vassie, P R , in *Corrosion of Steel Reinforcement in Concrete Construction,* Society of the Chemical Industry, London, 1979, pp 57–78
[6] Tuutti, K , "Corrosion of Steel in Concrete," Swedish Cement and Concrete Institute, Report No 4, 1982
[7] Richartz, W , *Zement-Kalk-Gips,* Vol 22, 1969, pp 447–456
[8] Gouda, V K , *British Corrosion Journal,* Vol 5, 1970, pp 198–203
[9] Gouda, V K , *British Corrosion Journal,* Vol 5, 1970, pp 198–203
[10] Rechberger, P , *Zement-Kalk-Gips,* Vol 22, 1983, pp 582–590
[11] Dehgjanian, C and Locke, C E , *Corrosion,* National Association of Corrosion Engineers, Vol 39, No 8, 1983, pp 299–305
[12] Locke, C E and Siman, A , *Corrosion of Reinforcing Steel in Concrete, ASTM STP 713,* American Society of Testing and Materials, Philadelphia, 1980, pp 3–16
[13] Browne, R D and Geoghegan, M P in *Corrosion of Steel Reinforcement in Concrete Construction,* Society of the Chemical Industry, London, 1979, pp 79–98
[14] Van de Veer, J R , *Journal,* American Concrete Institute, Vol 63, 1966, p 697
[15] Sørensen, B and Maahn, E , *Nordic Concrete Research,* Publication No 1, Paper 24, 1982
[16] Stratfull, R F , *Materials Protection,* Vol 7, 1968, pp 29–34
[17] Volkwein, A and Springenschmid, R , *Proceedings,* Second International Conference on the Durability of Building and Components, Sept 1981, pp 199–209
[18] Cady, P D and Weyers, R E , *Cement, Concrete and Aggregates,* Vol 5, 1983, pp 81–87
[19] Rosenberg, A M , *ACI Journal Proceedings,* American Concrete Institute, Vol 61, Oct 1964, pp 1261–1279
[20] Byfors, K , *Nordic Concrete Research,* No 5, 1986, pp 27–38
[21] Tritthart, J in *Chloride Induced Concrete Corrosion,* Road Research Dept , Austrian Ministry of Building and Technology, 1988 (in German)
[22] Hansson, C M and Sørensen, B , *Nordic Concrete Research,* No 6, 1987, pp 57–72
[23] Pourbaix, M , *Corrosion,* Vol 26, 1970, p 431
[24] Hansson, C M , Strunge, H , Markussen, J B , and Frølund, T , *Nordic Concrete Research,* No 4, 1985, pp 70–80
[25] Byfors, K , Hansson, C M , and Tritthart, J , *Cement and Concrete Research,* Vol 16, 1986, pp 760–770
[26] Page, C L , Short, N R , and El Tarras, A , *Cement and Concrete Research,* Vol 11, 1981, pp 395–406
[27] Kondo, R , Satake, M , and Ushiyama, H , *Proceedings,* 28th General Technical Session of the Cement Association of Japan, May 1974, pp 41–43
[28] Hansson, C M , Frølund, T , and Markussen, J B , *Cement and Concrete Research,* Vol 15, 1985, pp 65–73

C. Valentini,[1] *L. Berardo,*[1] *and I. Alanis*[1]

Influence of Blast Furnace Slags on the Corrosion Rate of Steel in Concrete

REFERENCE: Valentini, C , Berardo, L , and Alanis, I , "**Influence of Blast Furnace Slags on the Corrosion Rate of Steel in Concrete,**" *Corrosion Rates of Steel in Concrete, ASTM STP 1065,* N S Berke, V Chaker, and D Whiting, Eds , American Society for Testing and Materials, Philadelphia, 1990, pp 17–28

ABSTRACT: The polarization resistance method was used to measure the corrosion rate of steel bars embedded in mortar specimens The measurements were carried out on specimens, with different percentages of blast furnace slags (0, 20, 45, and 75% weight relative to the weight of cement) During the first 28 days, all the specimens were cured, immersed in water, and subsequently stored partially immersed at 50 and 100% relative humidity In addition to the polarization resistance, the corrosion potential and ohmic resistance of the specimens were recorded The influence of the different storage conditions and the percentage of furnace slags on the corrosion rate of steel bars embedded in the mortar are discussed An analysis of the correlation between the measured parameters is presented

KEY WORDS: steel in concrete, corrosion rate, blast furnace slags, corrosion, steels, concrete

Portland cement blended with blast furnace slags (BFS) have been used in several countries Argentine standards allow up to 20% BFS mixed with cements to be used in reinforced concrete structures Recently, attempts have been made to increase this level up to 75% and controversial opinions appeared For that reason, it was found necessary to survey the performance of steel in BFS blended cements

Two features of BFS are indicated as potentially dangerous in relation to steel passivity presence of sulfide and lower content of alkalis

Longuet [*1*] has studied the chemical composition of the pore solution of several BFS blended cements The results showed that solution compositions were strongly dependent on both cement composition and metallurgical slags composition The influence of sulfide on the electrochemical behavior of iron and steel in alkaline media was studied in connection with corrosion in the pulp and paper industry Tromans [*2*] reported that sulfide might be incorporated into the magnetite lattice yielding a nonprotective film of contaminated magnetite under those conditions On the other hand, Salvarezza et al [*3*] showed that the behavior of iron in high alkaline solutions is related to the concentration ratio of SH^-/OH^- In solutions with pH ranging from 11 0 to 12 0 and with 0 01 *M* of sodium sulfide, they found a strong pH dependent pitting potential and inhibition of the pitting process at pH higher than 12 0

In spite of these worrying reports, in some countries furnace slags are used, as shown by the available information The failure of several prestressed concrete structures have been

---

[1] Research engineer, research engineer, and research chemist, respectively, Sector Electroquimica Aplicada, Instituto Nacional de Tecnologia Industrial, C C 157, 1650 San Martin, Pcia de Buenos Aires, Republica Argentina

ascribed to the use of metallurgical cements, however, Vanden Bosch [*4*] argued that in many cases the true reason was a defective construction (high concrete porosity, poor concrete coverage, etc)

In laboratory experiments Batic [*5*] determined that more than 35% BFS mixed with cements promotes steel corrosion In a previous work [*6*], we found that corrosion rate of rebars embedded in mortar with 20 and 65% BFS was slightly different from that of similar rebars in portland cement mortar Two hundred days after curing the steel rods presented no differences in surface attack

In this paper, the polarization resistance (R_p) technique was used with adaptations introduced by Andrade [*7*] to measure the instantaneous corrosion rate of steel bars embedded in mortar specimens with different contents of BFS

Experimental Procedure

Equipment

Conventional electrochemical equipment has been used PAR (New Hartford, New York) Model 173 potentiostat with ohmic resistance compensation, low rate linear voltage generator constructed in the laboratory and Philips (Waltham, Massachusetts) X-Y recorder PM 8041

Specimen Preparation

Mortar specimens (7 by 6 by 3 5 cm) were constructed with 0, 20, 45, and 75% BFS as a cement replacement and with portland cement with a water/cement (w/c) ratio of 0 5 and cement/sand (c/s) ratio of 1 3 Cement and BFS chemical composition are reported in Table 1

The specimens contained two identical bars and a central auxiliary steel electrode. The steel bars arrangement is displayed in Fig 1. Nine specimens of each composition were prepared and cured, immersed in water for 28 days Three specimens were kept in each storage condition 50 and 100% relative humidity (RH) and partially immersed (PI). Electrochemical measures were performed only for the storage period

Steel bars were cleaned in hydrochloric acid 1 1 solution with 3 g/L of hexametylenetetramine as corrosion inhibitor, washed with water, and dried in hot air

TABLE 1—*Chemical composition of cement and slag*

Substance	Cement, %	Slag, %
Insoluble residue	0 70	2 00
Silicon dioxide	21 60	35 80
Aluminum oxide	4 55	11 00
Ferric oxide	3 06	2 12
Calcium oxide	64 00	42 80
Sodium oxide	0 08	
Potassium oxide	1 06	
Magnesium oxide	0 70	3 54
Sulfur trioxide	3 12	0 12
Loss by calcination	1 90	
Free calcium oxide	0 38	
Total alkalines	0 78	
Manganese oxide		1 07
Sulfide		0 90

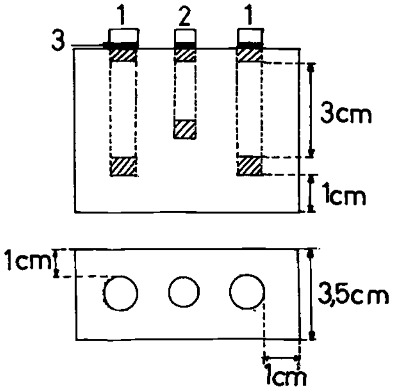

1. Working electrode steel bar 0.8 cm in diameter.
2. Auxiliary electrode steel bar.
3. Insulating tape.

FIG. 1—*Mortar specimen scheme.*

Procedure

In the present work, the R_p was obtained by applying a potentiostatic step of -10 mV from the corrosion potential, and the current value was recorded after 15 to 20 s as suggested elsewhere [*8*]. In order to calculate the instantaneous corrosion current, Stern's formula was used. The constant B values in Expression 1 vary from 13 to 52 mV in the majority of the metal/medium systems. In the present work, B values of 26 mV for steel in the active state and 52 mV for steel in the passive condition were assumed as it was suggested [*12*] elsewhere.

$$\text{current density} = \frac{B}{\text{electrode area} \times R_p} \qquad (1)$$

An electrical circuit (Fig. 2) is assumed to represent the system; where C is the capacitance, R_p the Faradic resistance of the metal electrolyte interphase, and R_Ω is the resistance of the electrolyte and the mortar layers between the metal and the calomel reference electrode. R_Ω is measured through the comparative system of the potentiostat. Expression 2 is used to calculate R_p values.

$$R_p = \frac{\Delta E}{I_{\text{measured}}} - R_\Omega \qquad (2)$$

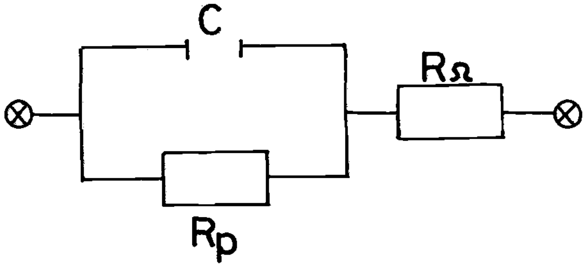

FIG. 2—*Electrical equivalent circuit.*

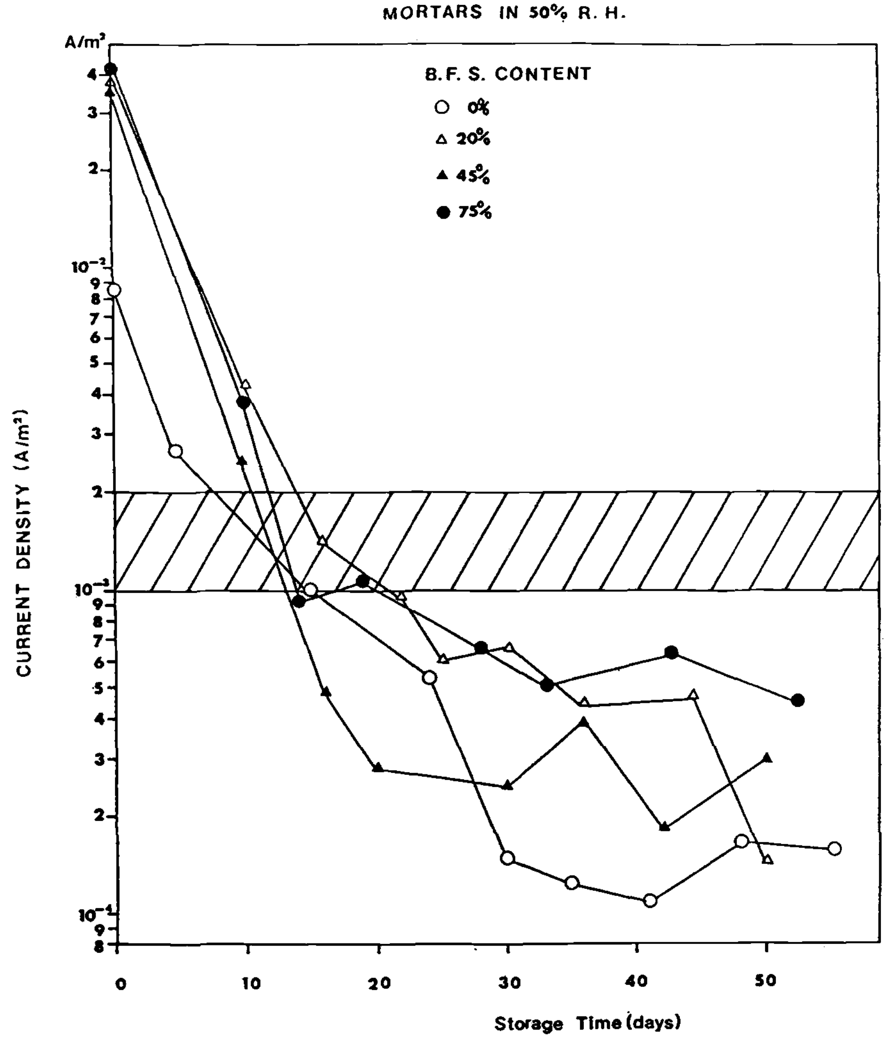

FIG. 3—*Variation of the corrosion intensity of steel bars embedded in BFS concrete mortars, 50% RH.*

where

ΔE = p

R_Ω = measured ohmic resistance.

Corrosion rate is directly proportional to the current density. In the present work, results were expressed as current density.

The corrosion potential (E_c) was measured between each steel rod and a reference standard calomel electrode (SCE).

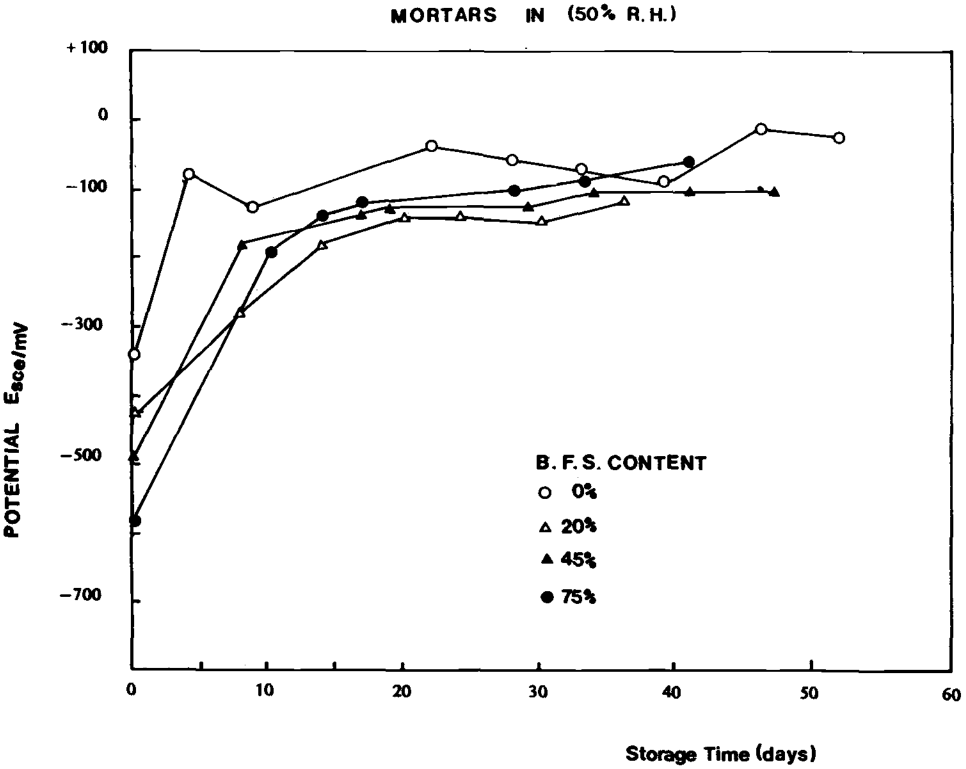

FIG. 4—*Variation of the corrosion potential of steel bars embedded in BFS cement mortars, 50% RH.*

Results

Figures 3 to 8 depict current density and potential versus time curves. The shadow zone marked on the graphs represents an approximate boundary between current densities that are considered significant in terms of their effect on service life and those that are not, as suggested by Andrade [*11*]. In all the cases, corrosion behavior shows a passivation trend (Figs. 3, 5, and 7), the smallest values correspond to the 50% RH stored specimens. The current density immediately after 28 days of curing (t = 0 day in the graphs) is independent on the BFS content and is about 10 times the current for specimens without BFS. On the other hand, there seems not to be another clear influence on the BFS content. Figure 9 shows minimal corrosion rates of rebars embedded in 0 and 75% BFS cement mortars kept in 100% RH and PI. The corrosion potential versus time curves also show a trend of passivation (Figs. 4, 6, and 8).

As it can be seen, the 50% RH condition promotes the higher E_c values. The 100% RH and PI potentials, are very similar to each other but smaller in magnitude. A well-defined dependence of potential on BFS content is apparent only in the 100% RH condition (Fig. 6).

Using ohmic resistance data, an overall conductance value has been computed for each condition and composition with 40 days of storage life. The results are presented in Fig. 10.

Two types of behavior are evident. For 100% RH and PI conditions, the specimens

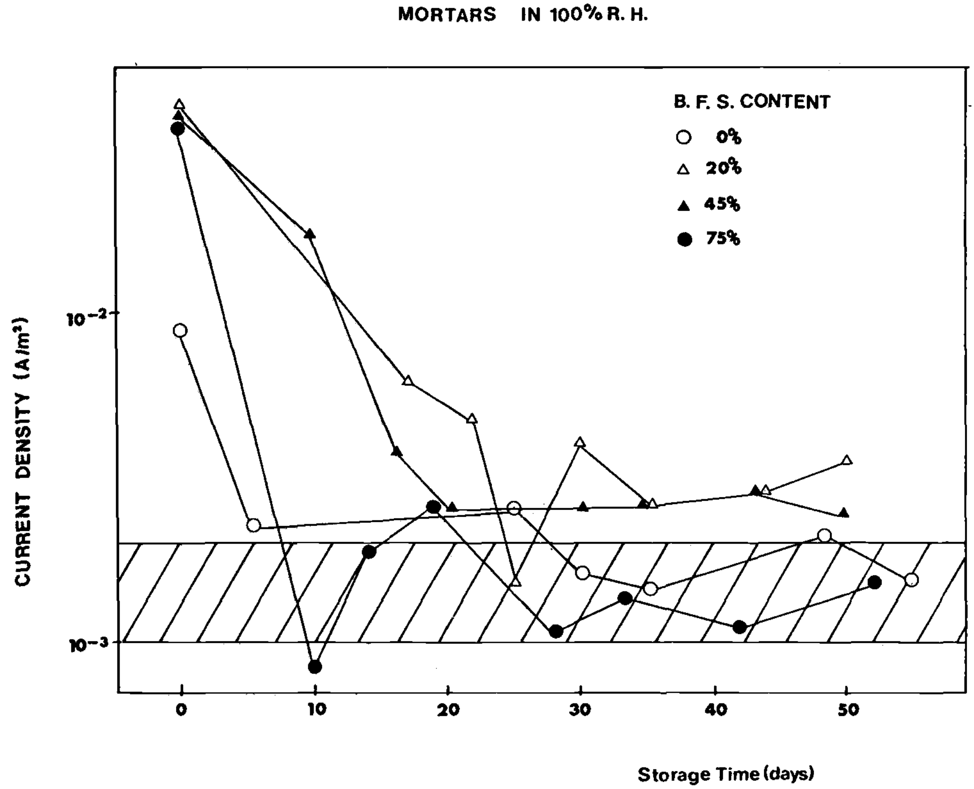

FIG. 5—*Variation of the corrosion intensity of steel bars embedded in BFS cement mortars, 100% RH.*

conductances are strongly dependent on the BFS content, otherwise a weak dependence appears in the 50% RH conditions.

The first set of mortar specimens was broken after 60 days of storage, and the steel appearance was observed. Steels which had been embedded in cements without BFS presented a whitish surface and those in BFS cements a blackish one. No other differences were evident between the steel probes.

The polished bars used as auxiliary electrodes showed a slight, homogeneous attack in the case of BFS cement mortars.

Within the mortar near the steel, some green regions occurred in the specimens containing BFS, except in those stored in the 50% RH conditions. The intensity of those patches increased with the BFS content.

Discussion

Cementitious materials are complex mediums, in the sense that chemical and physical properties change with time during months or even years. Furthermore, steel corrosion behavior can be affected not only by the solution aggresivity but also by oxygen availability, medium conductance, etc.

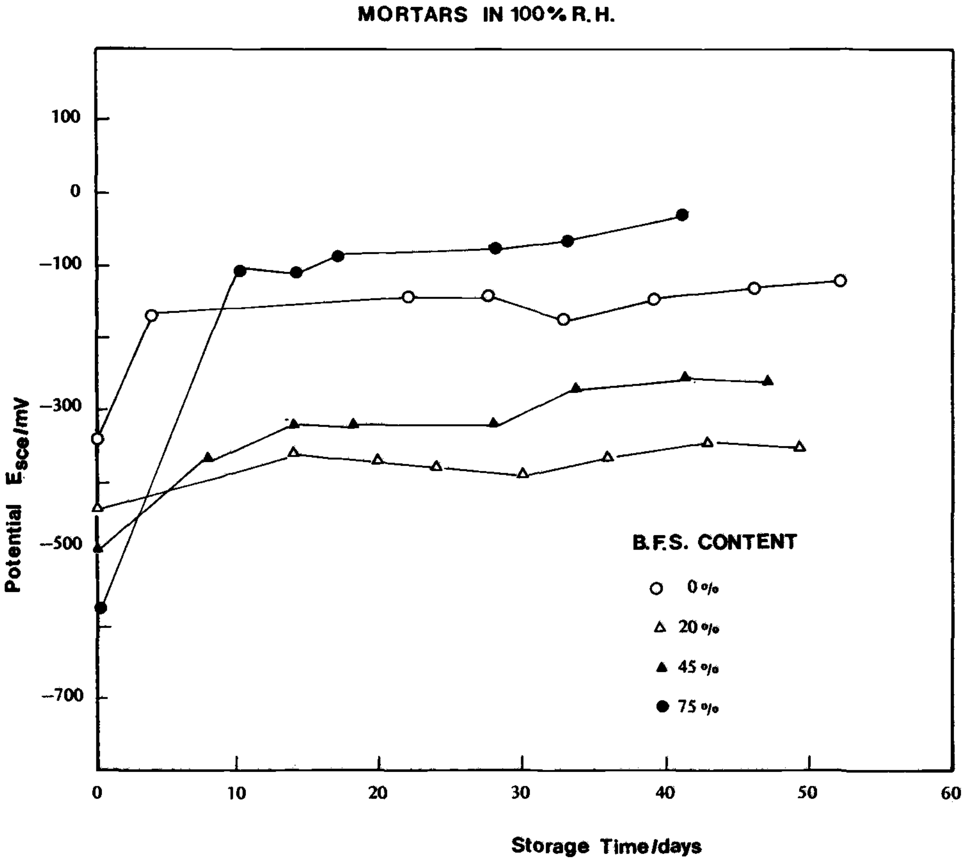

FIG. 6—*Variation of the corrosion potential of steel bars embedded in BFS cement mortars, 100% RH.*

Sulfide concentration in the pore solution does not have a constant value [*1*]. During the hydration period, sulfide is leached out in the pore solution, but there is a simultaneous disappearance due to both its oxidation and its solubility in the tetracalcium iron aluminate (C_4AF) phase [*9*]. The green patches observed near the rebar support the later mechanism. Moreover, even though the whole alkali content of the BFS mortars is lower than that of the pure cement mortar, the pore solution pH seems to be enough to maintain safe conditions. The fact that the SH^-/OH ratios calculated from the dates reported by Longuet [*1*], remain well below the safe value suggested by Salvarezza [*3*] would support that supposition.

The influence of the BFS content on the conductance, for the PI and 100% RH conditions (Fig. 10), could be related with the permeability decrease promoted by slag in blended mortars [*10*]. In the case of 50% RH condition, the conductance would be restricted by the less quantity of solution within the pores.

The unexpected diminution in current densities for the PI and 100% RH conditions on going from 20 to 75% BFS (Fig. 9) could be ascribed to the diminution in conductance discussed previously that would exist between microanodes and microcathodes. Conductance dependence was sketched in Fig. 9 to emphasize this supposition.

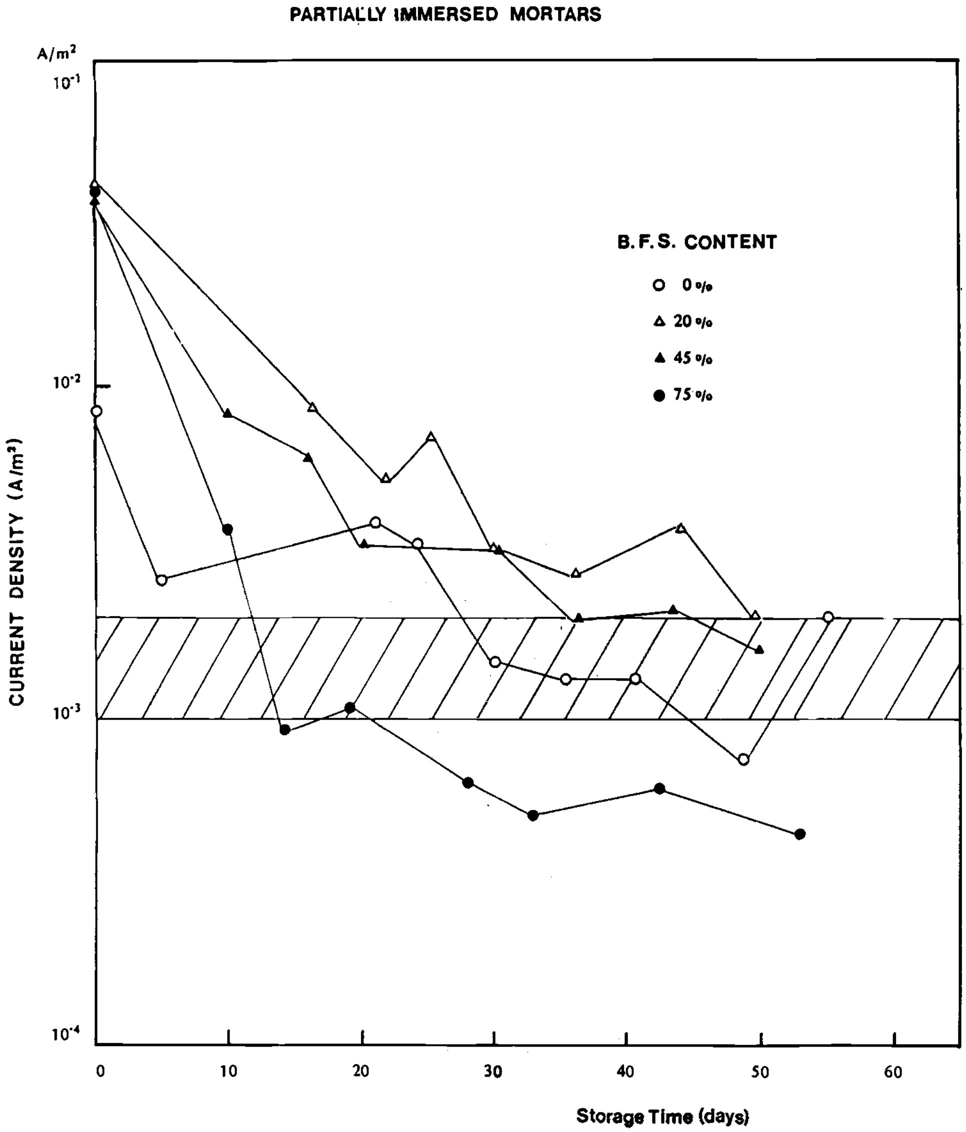

FIG. 7—*Variation of the corrosion intensity of steel bars embedded in BFS cement mortars, PI.*

Conclusions

Both corrosion currents and corrosion potentials show passivation trends for steel embedded in portland cement mortars whether blended or not with blast furnace slags up to 75%, in all tested conditions.

The corrosion current immediately after the curing period is independent of the amount of blast furnace slags (in the 20 to 75% range) and is about 10 times the current for pure portland mortar. This strong influence disappears with time. Then, laboratory tests performed on different ages of specimens could give contradictory results.

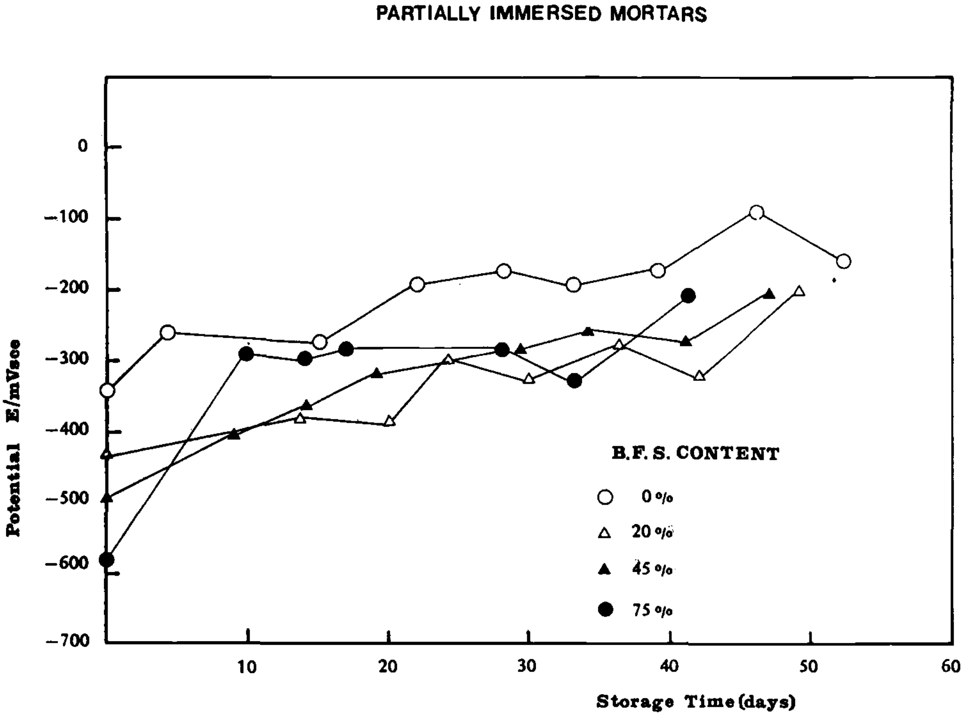

FIG. 8—*Variation of the corrosion potential of steel bars embedded in BFS cement mortars, PI.*

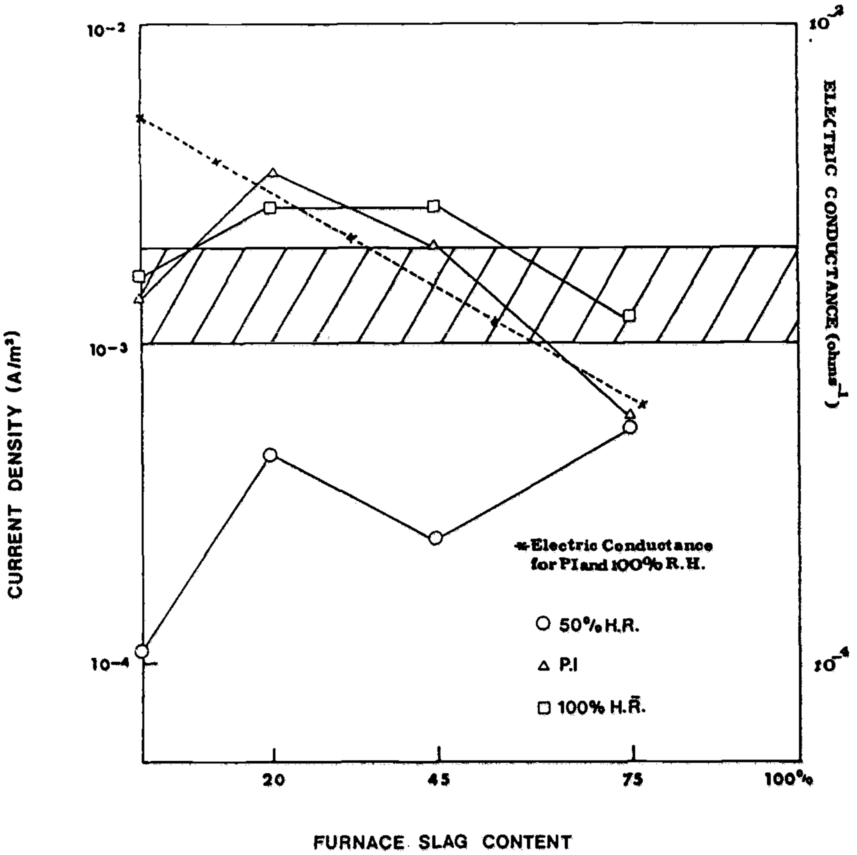

FIG. 9—*Current intensity of steel bars embedded in mortars with different BFS content. The dates correspond to the 40 days of storage life.*

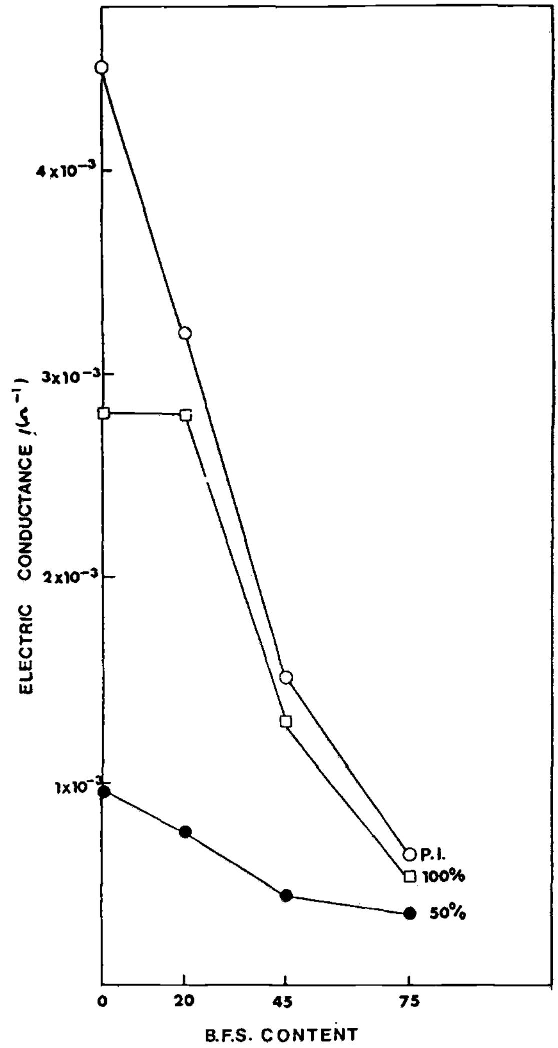

FIG. 10—*Conductance of mortars specimens with different BFS content. The dates correspond to the 40 days of storage life.*

Acknowledgments

We thank the Argentine Science & Technology Secretariat (SECYT) for partial financial support of this work. We also acknowledge Dra Maria del Carmen Andrade for helpful discussions and orientation.

References

[1] Longuet, P., *Silicates Industriels*, Vol. 7, No. 8, 1976, pp. 321–328.
[2] Tromans, D., *Journal of Electrochemical Society*, Vol. 127, No. 6, 1980, pp. 1253–1256.

[*3*] Salvarezza, R C , Videla, H A , and Arvia, A J , *Corrosion Science,* Vol 22, No 9, 1982, pp 815–829

[*4*] Vanden Bosh, V , *Silicates Industriels,* Vol 4, No 5, 1977, pp 145–149

[*5*] Batic, O R and Sota, J D , *Hormigon,* Vol 8, 1982, pp 23–30

[*6*] Alanis, I , Berardo, L , Moina, C , and Valentini, C , *Proceedings,* Jornadas Metalúrgicas 1987, SAM, Buenos Aires, Argentina, 11–15 May 1987

[*7*] Gonzalez, J A , Molina, A , Escudero, M L , and Andrade, C , *Corrosion Science,* Vol 25, No 10, 1985, pp 917–930

[*8*] Andrade, C and Gonzalez, J A , *Werkstoffe und Korrosion,* Vol 29, 1978, pp 515–519

[*9*] Vernet, C H , *Silicates Industriels,* 1982–1983, pp 85–89

[*10*] Bakker, F M , *Silicates Industriels,* 1982–1983, pp 91–95

[*11*] Andrade, C , Castelo, V , Alonso, M C , and González, J A , *Corrosion of Rebars in Cement, ASTM STP 906,* American Society for Testing and Materials, Philadelphia, 1986, pp 43–63

[*12*] Andrade, C and Macías, A , *Materiales de Construcción,* Vol 184, Oct–Nov–Dec 1981, pp 83–93

Carmen Andrade,[1] *Maria Cruz Alonso,*[1]
and José Antonio Gonzalez[2]

An Initial Effort to Use the Corrosion Rate Measurements for Estimating Rebar Durability

---

REFERENCE: Andrade, C , Alonso, M C , and Gonzalez, J A , **"An Initial Effort to Use the Corrosion Rate Measurements for Estimating Rebar Durability,"** *Corrosion Rates of Steel in Concrete, ASTM STP 1065,* N S Berke, V Chaker, and D Whiting, Eds , American Society for Testing and Materials, Philadelphia, 1990, pp 29–37

ABSTRACT: The approach presented here is an attempt to implement the values of corrosion intensity which have been measured in laboratory tests, in the framework of the service life prediction analysis for corroding structures First of all, the model on service life suggested by Tuuti was considered, and only the propagation period model has been analyzed in this paper

In order to expand the proposal, different steps were covered (1) the definition of an unacceptable level of deterioration, taking into consideration the levels suggested by the Comité Eurointernational du Béton (CEB) in its Bulletin No 162, in order to define the urgency of intervention in a damaged structure, (2) the reduction in bar diameter or bar section was taken as the determining parameter in failure risk, assuming that this decrease in section occurs either in a generalized form or in the zones of the structure in which the load-carrying capacity may be significantly affected, and (3) the ranges of possible corrosion intensity values were introduced in Tuuti's model for calculating the reduction in bar section in function of the life of the structure Some examples for bars of 10 and 20 mm ϕ were presented Finally, the limitations and the improvements of the proposal are discussed

KEY WORDS: residual service life prediction, corrosion intensity, deterioration levels, corrosion, steels, concrete

The unexpected, premature deteriorations in reinforced concrete structures have generated several theories and models in order to predict concrete service life [*1–4*], as a function of different sources of aggressive agents and of different rate-determining parameters

Service life prediction is a complex matter in which both technical topics and economical consequences are involved This concept has been expressed in different ways, an adequate one, perhaps, being the period in which a structure fulfills its structural requirements

Many aspects concerning nominal design life and residual service life remain unexplored In the case of failures due to rebar corrosion, some of the more key aspects are related to the deterioration rate of rebars and the acceptable limit of deterioration This is the maximum tolerable amount of corrosion corresponding to the condition of failure or that which may affect the load-carrying capacity of the structure

In this paper, a first attempt is presented on the prediction of the remaining service life

---

[1] Researcher, Institute of Construction and Cement "Eduardo Torroja"—CSIC, Madrid 28080, Spain
[2] National Center of Metallurgical Research, CSIC, Madrid 28040, Spain

of concrete structures being deteriorated by rebar corrosion. The approach has been made assuming that the "reduction in bar diameter or bar section" is the determining parameter in calculating the loss in load-carrying capacity of the structure.

Service Life Models

The most suitable scheme for modeling the service life of corroding structures is that presented by Tuutti [*5*], shown in Fig. 1. This model describes corrosion in two parts: (1) initiation period in which external aggressives enter into the concrete cover and (2) a propagation period which starts when the steel depassivates. The residual lifetime of the structure depends on the rate of deterioration. An unacceptable degree of corrosion, not quantified by Tuuti, is reached when a repair should be undertaken.

The quantification of this deterioration period becomes of crucial importance in the assessment of damaged structures.

Different laws of diffusion of chlorides and carbon dioxide (CO_2) have been proposed in order to calculate the time of corrosion initiation as a function of different parameters (cover quality, cover thickness, etc.). The length of this initiation period is not going to be a topic of discussion in this paper since other more documented authors [*6–8*] have suggested good models.

The propagation period, however, has received less attention, perhaps due to the scarce data offered by the literature on deterioration rates. In addition, the determination of an unacceptable level of corrosion has been described more philosophically than quantitatively.

For this propagation period model, three different steps need to be set out in order to calculate the residual service life of corroding structures: (1) a more accurate definition of the level or levels of deterioration which may affect the serviciability or the load-carrying capacity of the structure; (2) the election of the deterioration determining parameters, that is, the parameters that need to be measured to be able to quantify the damage; and finally, (3) the transformation of the experimental data of steel corrosion rates into a form applicable to the determining parameter. When introduced in Tuutti's model, the transformed data will allow the calculation of the residual service life.

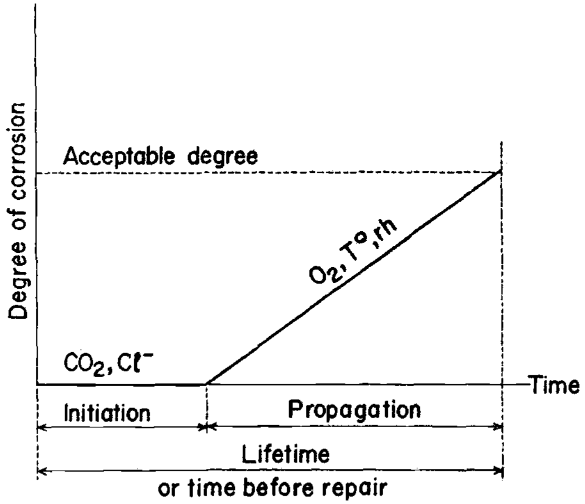

FIG. 1—*Tuuti's model of service life.*

TABLE 1—*Damage levels of reinforced concrete building elements subject to steel corrosion*.[a]

Visual Indications	Damage Levels A	B	C	D	E
Color changes[b]	rust stains	as in A	as in A	as in A	as in A
Cracking	some longitudinal	several longitudinal some on stirrups	extensive	as in C	as in C
Spalling		some	extensive	in some areas steel is no more in contact with concrete	as in D
Loss in steel-[c] section ($\Delta A_S/A_S$)		~5%	~10%	~25%	some stirrups broken main bars buckled
Deflections				possible	apparent

[a] A_S = bar cross section.

[b] Color modifications are not always present. Therefore, this indication is not a prerequisite for damage classification.

[c] Corresponding thickness of oxides $t_o \simeq a \cdot (\Delta A_S/A_S) \cdot \phi$, where ϕ = bar diameter, $a \simeq 0.5$ for plain oxides, and $a \simeq 1.0$ for oxides mixed with cementitious matter.

Levels of Deterioration

The proposal presented in Bulletin No. 162 of the Comité Eurointernational du Béton (CEB) for classifying the urgency of repairing or strengthening a structure after damage is an appropriate one for the purposes of this paper. In Table 1, we have just reproduced the levels of deterioration (A, B, C, D, and E) classified in the bulletin [9]. Combining these levels with the calculation of "capacity ratio" $\nu = R'/S'$ (R' being the load-bearing capacity and S' the action effect this system or element would be required to resist according National Codes), the residual stiffness may be approximately estimated. Thus, capacity ratio values lower than about 0.5 (see Table 2) [9] would require immediate repair action. Higher values of ν would allow up to 1 or 2 years before intervention and values about the unity would tolerate longer periods of time (10 to 20 years) before repairing.

Therefore, bearing in mind these principles, Levels C and D would be those which would require a rapid intervention, that is, the structure would have run out its residual service life, whereas Level B and A indicate a longer residual service life.

Determining Parameter of the Load-carrying Capacity Loss

In Table 1 five parameters (color changes, cracking, spalling, loss of steel section, and deflections) are used to define the level of deterioration. Among them, only cracking-spalling and steel section loss are going to be considered for discussion in this paper.

TABLE 2—*Pseudo-quantitative estimation of capacity ratio for building-elements after chemical attack*

Construction	R.C. Elements Damage Level A	B	C	D
New	0.95	0.80	0.60	0.35
Old	0.85	0.70	0.50	0.25

Cracks running parallel to the rebars are the common external sign of steel corrosion. Attempts have been made to calculate the stress needed to spall the cover by the generation of the oxides and, therefore, to design the bar diameter/cover ratio in order to avoid cracking if corrosion develops. Then, the cracking of the cover might be a rate-determining parameter in order to set the level of unacceptable deterioration.

However, when concrete reinforcements are corroding, the oxides generated may either crack the cover or may diffuse through the pore network producing brown spots on the concrete surface. This last situation often happens in very wet concrete and, although the steel corrosion may be high, no cracks can be observed in the concrete surface. Therefore, cracking has not been considered by the authors as a general indication of the corrosion level.

We have preferred to work with the reduction of the bar diameter or bar section (attack penetration) as the rate-determining parameter because in both cases (cracking or diffusion of the oxides through the pores), this reduction occurs as a consequence of the metal loss.

For the purposes of this paper, this reduction needs to be either generalized or to take place in the critical zones (from the mechanical point of view) of the structure in order to assume it affects the load-carrying capacity.

Therefore, referring to the previously suggested levels of deterioration, reduction in bar section between 10 to 25% in the critical zones of the structure will mean the depletion of its residual service life, whereas reduction of up to 5% (even with cracking and spalling) will indicate an early stage of deterioration with a remaining service life depending on the real corrosion rate of the steel.

Corrosion Intensity Ranges in Concrete Structures

The next step in predicting the remaining service life consists in calculating the number of years needed to reach the deterioration level previously described. This may be done once the real corrosion rates (attack penetration rate) of the steel bars embedded in concrete, are known.

Over a 20-year period, the authors have collected a large set of corrosion intensity values, i_{corr} [*10–12*], which were calculated using the electrochemical technique known as polarization resistance (R_p). Mortar and concrete specimens of different sizes were tested in the laboratory in order to monitor the corrosion intensity (by means of R_p values). Numerous variables were studied which might affect the corrosion rate of embedded steel such as: amount of chlorides in the mix, penetration of chlorides, humidity content in concrete, type of cement, etc.

Figures 2 and 3 are examples of the trend of the i_{corr} over time as a function of different variables. Figure 2 shows the case of steel bars embedded in mortar which was carbonated and held at different relative humidities, and Fig. 3 depicts the case of steel bars (1.5 and 7.5 cm cover) embedded in concrete immersed in seawater (using a B value in Stern's formula of 26 mV for active state and of 52 mV for the passive one).

Figure 4 summarizes the i_{corr} values which have been recorded in all the previously mentioned experiments. When the i_{corr} values measured are below 0.1 to 0.2 μA/cm^2 (1.1 to 2.2 μm/year), then either no corrosion products may be observed (passive state) or the attack is insignificant. Above 0.2 μA/cm^2 (2.2 μm/year) corrosion products may already be detected. The maximum i_{corr} measured in very aggressive environments is about 100 to 200 μA/cm^2 [*12*]. This maximum value also may be drawn up from Fig. 5 which shows the relationship found between i_{corr} and electrical resistance of carbonated mortar [*13*]. It is not the purpose of this paper to comment on the meaning of this figure, but only to emphasize that the i_{corr} values which correspond to the lower electrical resistance that can be measured

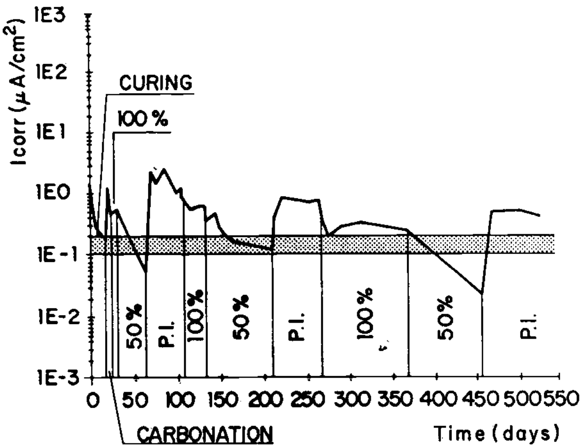

FIG. 2—*Evolution of* i_{corr} *values with time of bars embedded in carbonated mortar specimens fabricated with ordinary portland cement (OPC). The specimens were held in chambers with different relative humidities. The corrosion intensity values were calculated from polarization resistance,* R_p*, measurements.*

in uncracked concrete (between 50 to 100 Ω during setting) are about 100 to 200 μA/cm², which is the range limit previously mentioned.

Residual Service Life in Corroding Concrete Structures

The final step of the present approach consists in implementing all previous statements in Tuutti's model. Figure 6 represents such implementation as a first attempt to predict the

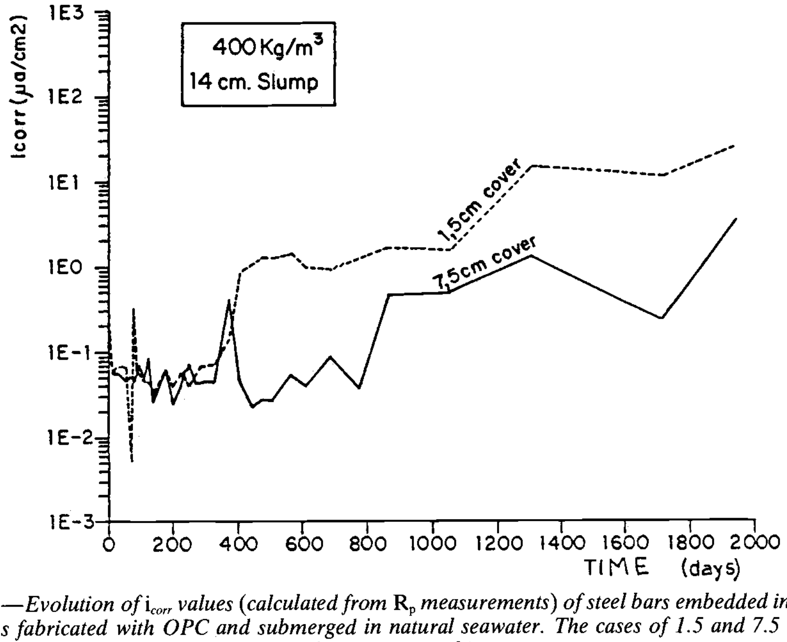

FIG. 3—*Evolution of* i_{corr} *values (calculated from* R_p *measurements) of steel bars embedded in concrete specimens fabricated with OPC and submerged in natural seawater. The cases of 1.5 and 7.5 cm cover are compared for a concrete with 400 kg of cement per cubic meter.*

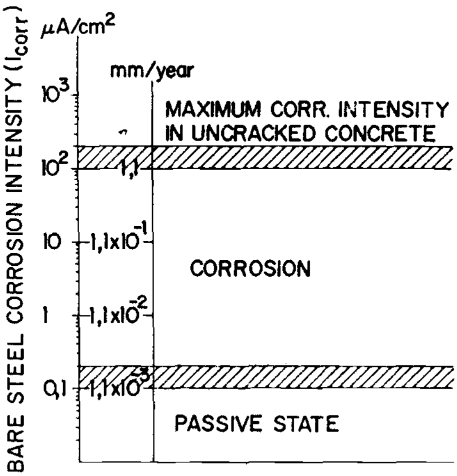

FIG. 4—*Values of corrosion intensity in* $\mu A/cm^2$ *and in mm/year which may be measured in concrete. Below the range 0.1 to 0.2* $\mu A/cm^2$ *the amount of corrosion is negligible. Between this range and until 100 to 200* $\mu A/cm^2$*, corrosion is active and brown oxides develop. Values above 100 to 200* $\mu A/cm^2$ *were never recorded in uncracked concrete.*

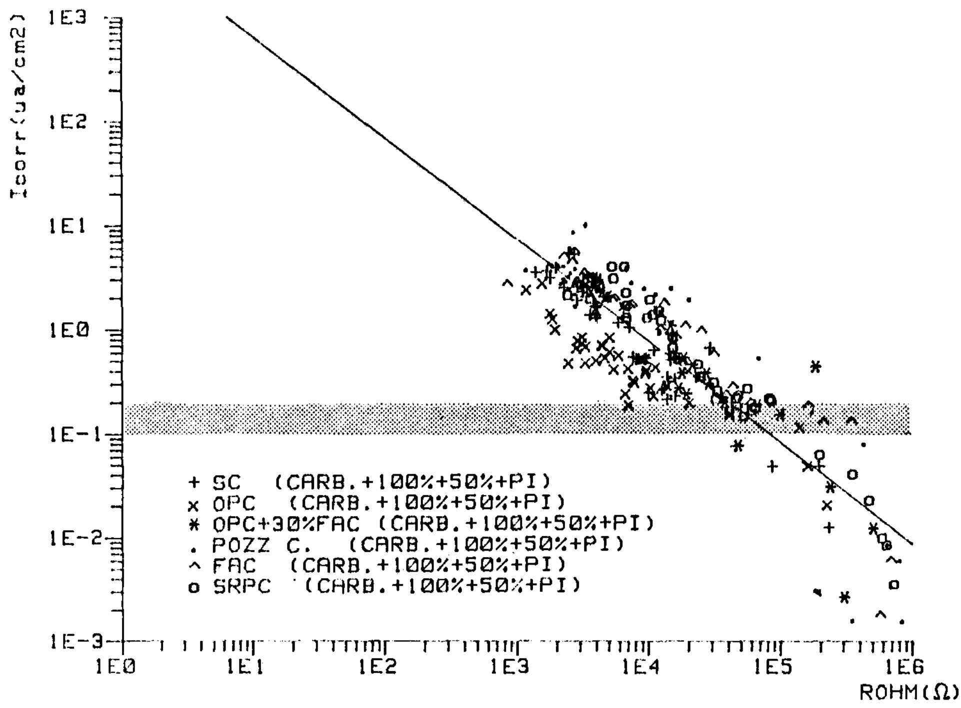

FIG. 5—*Values of* i_{corr} *(calculated from* R_p *measurements) measured in steel bars embedded in carbonated mortar in function of the ohmic resistance (calculated from the ohmic drop between working and reference electrodes) of the same mortars. Numerous environmental conditions were tested and are represented in the figure.*

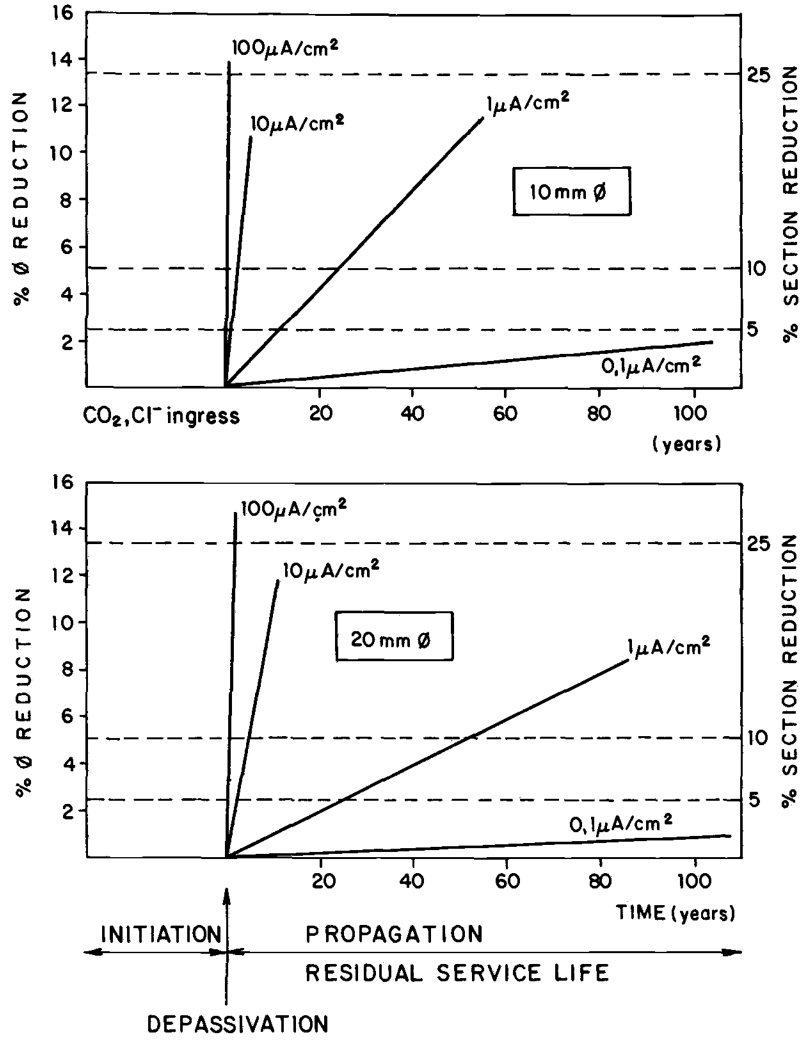

FIG. 6—*Examples of residual service life for bars of 10 and 20 mm* ϕ. *The reduction in bar section or diameter was represented in function of the number of years after depassivation.*

residual service life by a simple, and therefore practical, methodology. This figure has been arrived at by calculating the penetration attack in millimeters per year for bars of 10 mm in diameter (10 mm ϕ) and 20 mm ϕ, from the values of the possible corrosion rates. The i_{corr} values were transformed into percentage of reduction in bar diameter or bar section (1 $\mu A/cm^2$ is equivalent to about 11 μm/year). Therefore, assuming the corrosion rate remains constant, the prediction of the number of years to reach a deterioration level (either 5, 10, or 25%) is easily attained. So, for instance, if the corrosion rate is 5 $\mu A/cm^2$ (0.05 mm/year) a 25% reduction in bar section is reached in 12.5 years after depassivation for a bar of 10 mm ϕ and in 25 years in another 20 mm ϕ. Hence, the remaining service life would be the double for that of 20 mm ϕ (this example allows us to deduce that in a corroding structure, a few bars of large diameter seem safer than numerous thinner ones).

Final Considerations

The main difficulty of the proposal presented here is the estimation of the corrosion intensity in a corroding structure At the moment, no reliable methods exist which could be applied on-site, and thus, only indirect estimations may be used for implementation in Fig 6 Even though corrosion intensity values could be extrapolated from laboratory results, a high degree of uncertainty would remain Therefore, to predict the residual service life, only rough approaches are presently available such as (*a*) the estimation of the penetration attack from the real reduction of the bar section, assuming the life of the structure and its depassivation moment are known, or (*b*) using corrosion intensity values obtained from Fig 5 by means of the on-site measurement of the local ohmic resistance of the concrete

However, the reliability of the proposal to predict residual service life rests on the possibility of on-site measurement of the steel corrosion rate of damaged structures (a matter which the authors are also working on) and its further statistical treatment in order to take into consideration the fluctuations of i_{corr} due to environmental changes

Conclusions

The ideas set forth here are a first attempt to approach the prediction of the residual service life of corroding structures The authors have tried to advance previous suggestions by introducing a certain level of quantification in the schematic of existing service life models Future improvements are needed

(*a*) optimizing the assumptions made here,

(*b*) applying statistical treatment to the possible fluctuations of i_{corr} values during the structure life, and

(*c*) on-site monitoring of the corrosion intensity of damaged structures

Acknowledgments

The authors are grateful to Dr. J Rodríguez from the Architectural Faculty of Madrid and to Dr H. Reinhardt from Delft University, for their comments They are also grateful to the Comisión Asesora de Investigación Científica y Técnica of Spain which has supported this research

References

[*1*] Javor, T , Matériaux et Constructions, Rilem, Vol 19, No 113, 1986, pp 401–411

[*2*] Masters, L , Matériaux et Constructions, Rilem, Vol 19, No 114, 1986, pp 417–422

[*3*] Pommerrsheim, J and Clifton, J , Matériaux et Constructions, Rilem, Vol 18, No 103, 1985, pp 21–30

[*4*] Sneck, T , 3rd International Conference on the Durability of Building Materials and Components, Espoo, Finland, Aug 1984, Vol 4, pp 12–40

[*5*] Tuutti, K , *Corrosion of Steel in Concrete,* Swedish Cement and Concrete Research Institute, 1982, pp 17–21

[*6*] Bakker, R , Rilem, Committee 60-CSC—Corrosion of Steel in Concrete State of the Art Report, Matériaux et Constructions, in press

[*7*] Browne, R D , Geoghegan, M P , and Baker, A F , *Corrosion of Reinforcements on Concrete Construction,* A P Crane, Ed , Ellis Hordwood Ltd , London, 1983, pp 193–222

[*8*] Hamada, M , *Proceedings,* Fifth International Symposium of the Chemistry of Cement, Tokyo, 1968, Session III-3, Principal Paper, pp 343–409

[*9*] "Assessment of Concrete Structures and Design Procedures for Upgrading," CEB, Bulletin No 162, Aug 1983, pp 87–90

[*10*] Andrade, C and González, J A , *Werkstoffe und Korrosion,* Vol 29, 1978, pp 515–519
[*11*] González, J A , Algaba, S , and Andrade, C , *British Corrosion Journal,* Vol 15, 1980, pp 135–139
[*12*] Andrade, C , Jauregui, G , and González, J A , Eighth International Congress on Metallic Corrosion, Mainz, FRD, 1981, pp 1372–1377
[*13*] Alonso, C , Andrade, C , and González, J A , *Cement and Concrete Research,* Vol 18, No 5, 1988

Neal S. Berke,[1] Ding Feng Shen,[1] and Kathleen M. Sundberg[1]

Comparison of the Polarization Resistance Technique to the Macrocell Corrosion Technique

---

REFERENCE: Berke, N S , Shen, D F , and Sundberg, K M , **"Comparison of the Polarization Resistance Technique to the Macrocell Corrosion Technique,"** *Corrosion Rates of Steel in Concrete, ASTM STP 1065,* N S Berke, V Chaker, and D Whiting, Eds , American Society for Testing and Materials, Philadelphia, 1990, pp 38–51

ABSTRACT: Reinforced concrete structures are often subjected to chloride intrusion from deicing salts or marine environments or both The chloride ions disrupt the normal passivity of steel in concrete initiating corrosion The corrosion can lead to structural failure of the concrete due to the increased volume of the corrosion products which results in cracking and scaling Much work is underway to determine the corrosion rate of steel in concrete to determine the benefits of a particular protection system or to ascertain current condition of the steel

Polarization resistance can be used to compare different protection systems and to determine the corrosion rate at a given time The technique involves the use of a potentiostat or galvanostat, and ideally means to correct for ohmic resistance in the concrete Though relatively easy to perform, it requires a potentiostat with a means of correcting for ohmic resistance and occasionally a better than superficial understanding of corrosion theory

The Macrocell corrosion technique involves the measurement of the galvanic current passing between a layer of steel in a chloride rich top mat and a low chloride bottom mat which acts as a cathode A resistor is placed between the two mats, and the macrocell current is determined by measuring the voltage drop across the resistor This technique is most applicable when comparing corrosion protection systems in the laboratory

In this paper, we compare polarization resistance measurements to macrocell measurements on the same specimens Whenever the macrocell technique indicates severe corrosion is in progress, the polarization resistance technique also shows corrosion to be occurring However, the polarization resistance technique is able to determine localized corrosion in addition to the macrocell corrosion effect In several cases, this is present in the absence of a macrocell current Furthermore, even when the macrocell technique shows the presence of corrosion, rates can be significantly underestimated due to localized rates When calcium nitrite is present in the concrete, localized corrosion rates remain low

KEY WORDS: concrete corrosion, corrosion testing, polarization resistance, macrocell, calcium nitrite, inhibitors, reinforcing bars, concrete, corrosion, steels

Approximately half of the 500 000 plus bridges in the U S Highway system are in need of repair [*1*] The Strategic Highway Research Program (SHRP) pointed out that $450 to 500 million per year can be saved by correcting corrosion problems in current bridges [*2*]. In recognition of the problem of assessing the extent of corrosion damage, the SHRP program

---

[1] Senior engineering research associate, senior technical specialist, and assistant product manager, respectively, W R Grace, Construction Products Division, 62 Whittemore Ave , Cambridge, MA 02140

has allocated approximately $10 million to this problem [3] A good portion of this money is for electrochemical test methods

In addition to the field assessment of steel in concrete, one needs laboratory techniques that can be used to develop the field methods and to develop corrosion protection systems Two techniques that are widely used are macrocell corrosion [4–6] and polarization resistance [6–13]

In this paper, we compare corrosion rates determined by the macrocell corrosion and polarization resistance techniques Advantages of the macrocell technique are that it is simple to use and inexpensive The polarization resistance technique requires more sophisticated equipment and should correct concrete resistivity [14]

Test specimens consisted of control concrete with black steel, control concrete with galvanized steel, control concrete with aluminum conduit and these metals in concrete containing two levels of corrosion inhibitor The corrosion inhibitor used in this experimentation was a 30% calcium nitrite solution, one most commonly used in concrete structures Concrete cover was also varied Comparisons to other reported work on specimens with and without calcium nitrite are also given

It will be shown that corrosion in macrocell measurements is always detected by polarization resistance However, in several cases, corrosion was detected by polarization resistance, but not by the macrocell technique. Furthermore, rates determined by macrocell measurements do not reflect the total corrosion activity

Experimental

The purposes of the following experiments were to compare macrocell corrosion rates to those measured by polarization resistance, and to determine if calcium nitrite inhibits the corrosion of galvanized steel or aluminum in concrete The mix designs were chosen to help accelerate the corrosion process, and as such, have higher water-to-cement (w/c) ratios than recommended [15]. Concrete covers were also lower than recommended to accelerate the tests

Materials

An ASTM Specification for Portland Cement (C 150-86) Type 1 cement was used The coarse aggregate consisted of an ASTM Size 67 (19 to 4 75 mm) (¾ to ¼ in) trap rock The fine aggregate was a natural sand, which met the requirements of ASTM Specification for Concrete Aggregates (C 33-86) Calcium nitrite was added as a nominal 30% by mass solution (DCI corrosion inhibitor™)

A lignosulfonate-glucose polymer (Daratard-17[2]) retarder was added to the calcium nitrite mixes to offset set acceleration A vinsol resin (Daravair-M[2]) air entraining agent was used. Slumps ranged from 10 8 to 15 2 cm (4 25 to 6 in).

Concrete Design and Test Samples

The mix proportions and physical properties of the fresh and hardened concretes are presented in Table 1 The cement factor averaged 344 kg/m^3 (580 pounds per cubic yard (pcy)) and calcium nitrite solution was added at 0, 10, and 20 L/m^3 (0, 2, 4 gallons per yard (gpy)) This mix design is typical of concrete used in the field. The cement factor is high

---

[2] Registered trademark of W R Grace and Co , Cambridge, MA

TABLE 1—*Concrete mix designs and concrete properties*

Parameters	Control Sample	Inhibitor Dosage 1	Inhibitor Dosage 2
30% $Ca(NO_2)_2$ solution			
L/m^3	0	10	20
gallons/$yard^3$	0	2	4
Cement factor			
kg/m^3	348	343	343
pcy	587	578	578
Coarse aggregate			
kg/m^3	1044	1028	1028
pcy[a]	1759	1733	1732
Fine aggregate			
kg/m^3	736	725	724
pcy[a]	1240	1221	1220
Water/cement ratio	0.49	0.49	0.49
Air content, %	7.2	8.0	8.0
Slump			
mm	108	123	148
in	4.25	4.8	5.8
28-day compressive strength			
MPa	28.46	31.77	38.16
psi[b]	4128	4607	5535

[a] pcy = pounds per cubic yard
[b] psi = pounds per square inch

enough to be commonly found, but low enough to allow chlorides to penetrate at a reasonably rapid rate.

The concrete mixtures were prepared at 22°C (72°F). Samples for concrete mechanical testing were cast into 10.2 cm by 20.3 cm (4 in. by 8 in.) metal cylindrical molds. The cylinders were demolded at 24 h and cured at 22°C in a fog room. Compressive strengths are based on an average of two cylinders.

Corrosion samples were minislabs 22.9 cm by 11.4 cm by 15.24 cm (9 by 4.5 by 6 in.). Each minislab had a top and bottom reinforcing bar or, in the case of the aluminum samples, a conduit. The reinforcing bars were #4 bars (1.3 cm in diameter) and were either black steel, galvanized steel, or chromate-treated galvanized steel. The top bar was set at 1.9 cm (0.75 in.) or 3.5 cm (1.375 in.) from the top surface. The bottom bars were 2.54 cm (1 in.) from the bottom to ensure good access to oxygen. The aluminum conduit samples (2.54 cm outside diameter (OD) (1 in.)) were only tested at higher cover. Corrosion rate measurements are based on averages of three samples.

All the metal samples were taped with electroplater's tape to expose 17.8 cm (7 in.) of bar. A 5.1 cm (2 in.) high plastic dam with inside dimensions of 23 cm by 7.0 cm (9 in. by 2.75 in.) was caulked to the top. The four sides of the sample and top surface outside of the dam were coated with a concrete epoxy. Ground clamps were used to attach a 100 ohm resistor between the top and bottom bar.

Test Methods

Compressive strengths were determined in accordance with ASTM Test Method for Compressive Strength of Cylindrical Concrete Specimens (C 39-86). Total acid soluble chloride was determined as outlined in the Florida DOT Research Report 203 PB 289620 [16].

The minibeams were cyclically ponded with 3% sodium chloride (NaCl) solution The solution was applied for two weeks After two weeks of ponding, the solution was vacuumed off, and the minibeams were allowed to dry for two weeks The alternate wetting and drying similates normal exposures and allows oxygen into the beams Ponding procedures that allow rapid chloride ingress are used These practices are common and have been documented [*5*]

Corrosion rate measurements consisted of polarization resistance and macrocell corrosion techniques Both methods have been successfully used to measure corrosion rates of steel in concrete [*4–14*]

The polarization resistance method is a nondestructive means of determining the corrosion rate, and thus one can monitor corrosion rate as a function of time The technique uses a potentiostat to supply the current necessary to vary the potential between a reference electrode and the specimen away from the corrosion potential (typically ±20 mV) The voltage versus current curve is plotted on a linear scale

Polarization measurements were performed using a PAR Model 351 System with current interrupt The current interruption circuitry eliminates ohmic errors in the measurement of the polarization resistance These errors can be substantial and cause the calculated corrosion rate to be off by as much as 50% [*14*]

The polarization resistance values, R_p, are related to the corrosion rate by $i_{corr} = B/R_p$, where B is taken to be 26 mV [*8*] This value of B was in good agreement with actual observed corrosion on embedded rebars in concrete

Macrocell corrosion measurements were performed by measuring the voltage drop across the 100 ohm resistor connecting the top and bottom bars of the minibeams The macrocell currents were measured at the beginning of the second week of the ponding of each cycle The method is very simple and determines the galvanic corrosion susceptibility of a top salt rich metal mat coupled to a salt-free bottom mat with good access to oxygen

Results and Discussion

Compressive Strength

As can be seen in Table 1 and Fig. 1, calcium nitrite substantially improved 28-day compressive strengths The 20 L/m^3 addition (4 gpy) provided a 34% improvement

Corrosion Rates

After 14 and 24 months of cyclic ponding, corrosion rates on all low cover and aluminum conduit specimens were measured using polarization resistance in addition to the macrocell testing performed every four weeks The samples included minislabs containing black steel, galvanized steel, chromate-treated galvanized steel, and aluminum conduit The results for low concrete covers and aluminum conduit specimens are listed in Tables 2 to 5 Each type of metal was placed in concrete containing no calcium nitrite, as well as concrete containing either 10 or 20 L/m^3 (2 or 4 gpy) of calcium nitrite solution The steel embedded in concrete without calcium nitrite with 1 9 cm (0 75 in) of cover are corroding The steel samples with 3 5 cm (1 375 in) of cover have just begun to corrode after 24 months of ponding As will be shown later (Fig 10), the aluminum conduit samples with 3 5 cm cover began corroding after less than one month of ponding (Aluminum in concrete does not passivate as steel does as the result of the high pH of concrete Chlorides do not need to be present for aluminum corrosion to begin)

In many cases, there is a direct correlation between corrosion rates measured with each method Figure 2 displays the relationship between the methods for aluminum conduit in

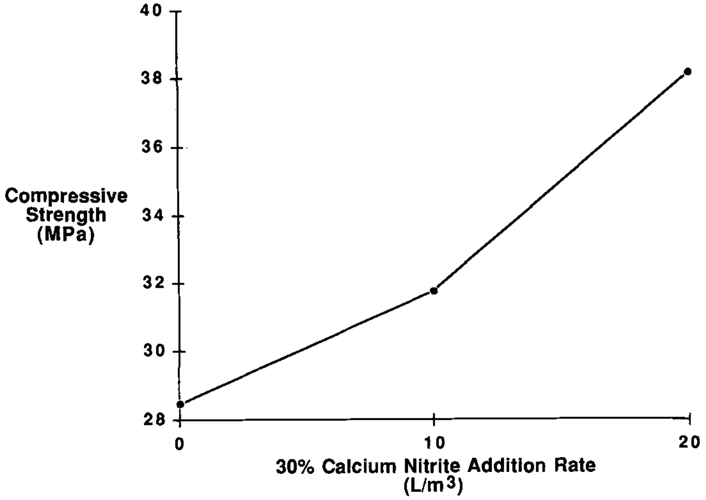

FIG. 1—*Compressive strengths as a function of calcium nitrite dosage.*

concrete after 14 months of ponding. The corrosion rates determined using the different methods are not equal. At the lowest corrosion rates, it is difficult to see a correlation. At slightly higher corrosion rates, however, both methods indicate the same trend in corrosion rates.

Figure 3 depicts the corrosion rates for several samples of black steel after 14 months of ponding. At the lowest corrosion rates, there is again little correlation between the different methods. At slightly higher corrosion rates, however, both methods show the same tendencies. After 24 months of ponding (Fig. 4), the trend continues to be the same, although polarization resistance indicates that the rate is much higher than the macrocell test suggests.

Although there are similarities between the two methods, there are several cases in which macrocell testing is not sufficiently accurate. Two of these cases are at very low corrosion rates and where both pieces of metal are presumably corroding. Note, visual observation showed severe corrosion of lower aluminum conduits, as well as the top conduits, when calcium nitrite was not added. This could account for the drop in macrocell currents. The variation between the test methods is more evident for the steel and aluminum samples that are at low corrosion rates. Another example is galvanized steel after 14 months of ponding

TABLE 2—*Corrosion currents of aluminum conduit after 14 months.*

Calcium Nitrite, L/m^3	Polarization Resistance, i_{corr}, μA/cm^2	Macrocell Testing, $i_{macrocell}$, μA/cm^2
0	2.22	0.23
10	0.013	0.005 to 0.001[a]
20	0.011	0.007 to 0.0[a]

[a] The first number is the average of the absolute values of all $i_{macrocell}$ values. The second is the average of actual $i_{macrocell}$ values. (Some samples had negative $i_{macrocell}$ values.)

NOTE—$i_{macrocell}$ is the current measured between the top and bottom bar. A positive number is used when the top bar is the anode.

TABLE 3—*Corrosion currents of steel rebar after 14 months*

Type of Steel	Calcium Nitrite, L/m^3	Polarization Resistance, i_{corr}, μA/cm^2	Macrocell Testing, $i_{macrocell}$, μA/cm^2
Black steel	0	0.510	0.508
	10	0.232	0.003
	20	0.061	0.004
Galvanized steel	0	4.33	0.212
	10	0.005	0.003
	20	0.006	0.002
Chromate treated galvanized steel	0	0.541	0.110
	10	0.191	0.004
	20	0.03	0.005

NOTE—$i_{macrocell}$ is the current measured between bottom and top bar. A positive number is used when the top bar is the anode.

(Fig. 5). After 2 years (Fig. 6), the corrosion rates of samples without calcium nitrite have increased, and there is less of a difference between the two methods.

Note that the galvanized steel samples in concrete with no calcium nitrite, under 1.9 cm of concrete cover, show signs of corrosion at about the same time as the black steel samples. Other studies have demonstrated the same results for galvanized steel [*17*]. However, the corrosion rates of the galvanized steel are about half that of the steel samples. (See Figs. 7 and 8.) Ten L/m^3 (2 gpy) of calcium nitrite solution reduced corrosion on the low-cover galvanized steel minislabs, but not as effectively as it did for the black steel. At 20 L/m^3 (4 gpy) of calcium nitrite solution, the galvanized samples are not corroding.

Once both the pieces of metal have begun to corrode, the macrocell test is inaccurate. Since the test monitors the difference between the two pieces, the experiment is only realistic when one acts as a reference. If both bars are corroding, the macrocell test will suggest that there is little activity on either rebar. Another limitation of the test is that as concrete resistivity increases, ionic current flow between the bars is reduced.

TABLE 4—*Corrosion currents of steel rebar after 24 months*

Type of Steel	Calcium Nitrite, L/m^3	Polarization Resistance i_{corr}, μA/cm^2	Macrocell Testing, $i_{macrocell}$, μA/cm^2
Black steel	0	1.575	0.831
	10	0.026	0.005
	20	[b]	0.001
Galvanized steel	0	0.722	0.041
	10	0.006	0.007 to 0.006[a]
	20	0.072	0
Chromate treated galvanized steel	0	1.091	0.035 to 0.025[a]
	10	0.325	0.005
	20	0.253	0.001

[a] The first number is the average of the absolute values of all $i_{macrocell}$ values. The second is the average of actual $i_{macrocell}$ values. (Some samples had negative $i_{macrocell}$ values.)

[b] Not available.

NOTE—$i_{macrocell}$ is the current measured between bottom and top bar. A positive number is used when the top bar is the anode.

TABLE 5—*Corrosion currents of aluminum conduit after 24 months.*[a]

Calcium Nitrite, L/m^3	Polarization Resistance, i_{corr}, $\mu A/cm^2$	Macrocell Testing, $i_{macrocell}$, $\mu A/cm^2$
0[b]	0.29	0.06
10	0.013	0.004
20	0.013	0.003

[a] The first number is the average of the absolute values of all $i_{macrocell}$ values. The second is the average of actual $i_{macrocell}$ values. (Some samples had negative $i_{macrocell}$ values.)

[b] Cracked beams removed, average based on three beams.

NOTE—$i_{macrocell}$ is the current measured between the top and bottom bar. A positive number is used when the top bar is the anode.

Polarization resistance, on the other hand, measures the corrosion rate of each bar individually. The accuracy of polarization resistance is confirmed by a good correlation with visual inspection.

The effects of corrosion of the lower mat of rebar are demonstrated in Fig. 4. Both methods yield approximately the same current until it reaches 1 $\mu A/cm^2$. At this point, polarization resistance indicates a much higher rate of corrosion. The lower $i_{macrocell}$ found using macrocell techniques indicates that the reference, or lower rebar, is corroding.

The changes in the corrosion rate of black steel with time are shown in Fig. 7. The rates are measured using macrocell tests. After 18 months of ponding, it appears that the corrosion rates are not increasing. Polarization resistance would indicate that both the top and bottom rebars are corroding at a faster rate.

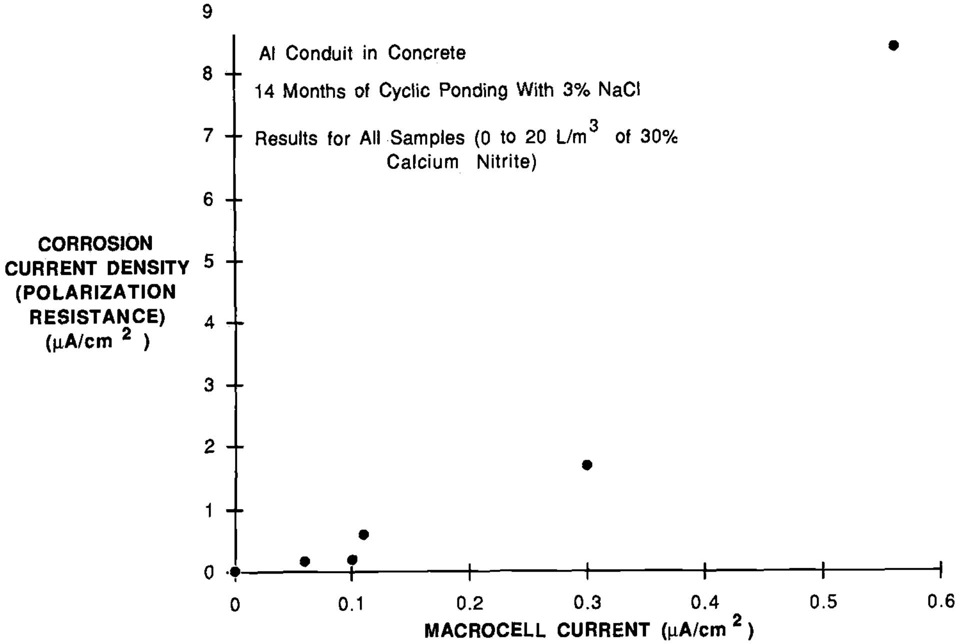

FIG. 2—*Comparison of macrocell and polarization resistance currents for aluminum conduit.*

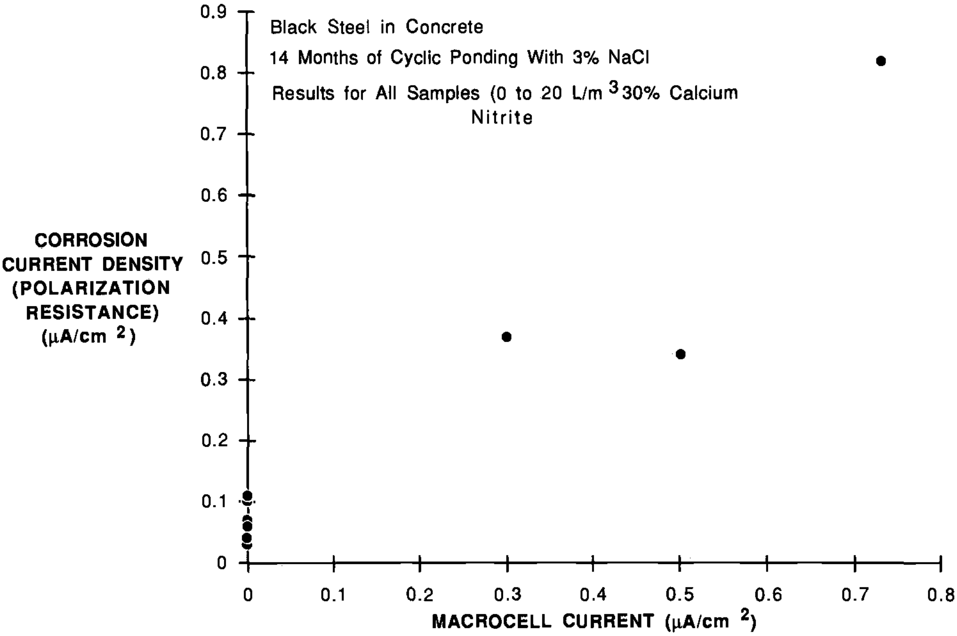

FIG. 3—*Comparison of macrocell and polarization resistance currents for steel—14 months.*

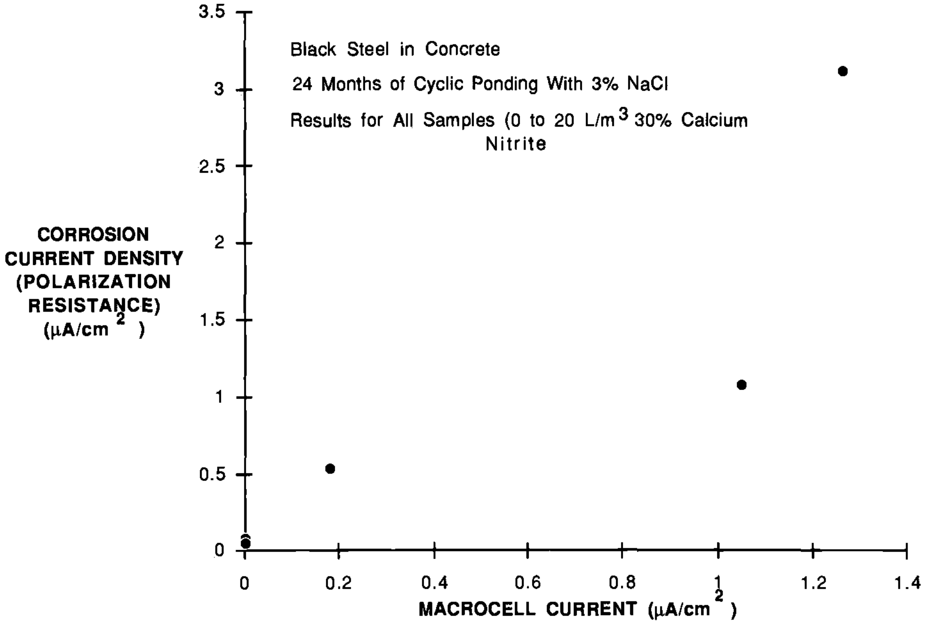

FIG. 4—*Comparison of macrocell and polarization resistance currents for steel—24 months.*

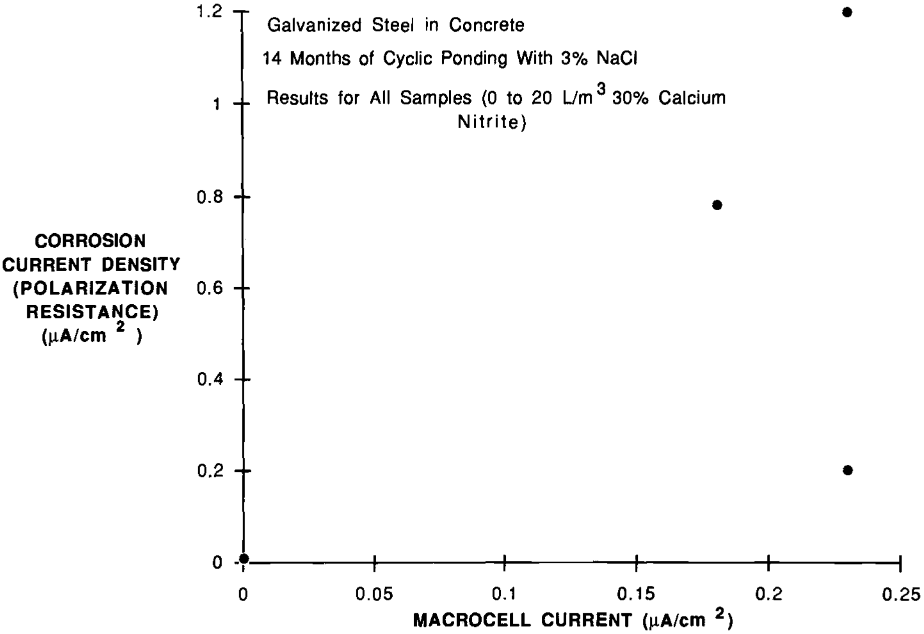

FIG. 5—*Comparison of macrocell and polarization resistance currents for galvanized steel—14 months.*

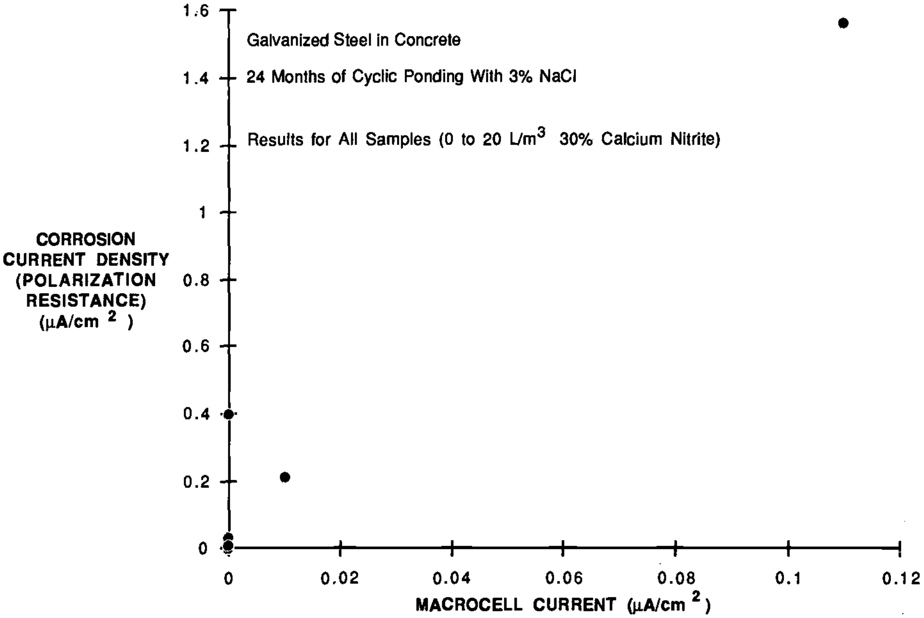

FIG. 6—*Comparison of macrocell and polarization resistance currents for galvanized steel—24 months.*

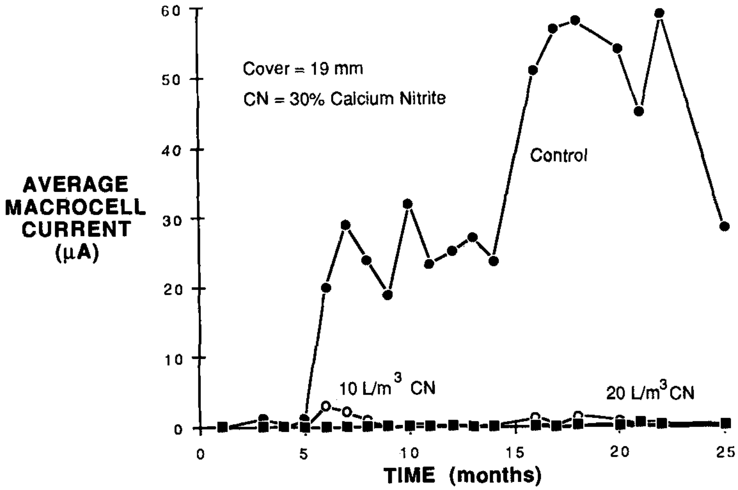

FIG. 7—*Average macrocell current as a function of time for black steel with 19 mm of cover.*

Figures 7 through 11 demonstrate the effects of calcium nitrite on the corrosion rates. In every case, both dosage rates have prevented the initiation of corrosion. Figures 7 and 11 show the wide fluctuations in measured rates using the macrocell method.

Chloride Analysis

Figure 12 shows the chloride profile at one year for concrete without calcium nitrite. Because chloride contents are significantly greater than 0.89 kg/m^3 (1.5 pcy) at the 1.9 cm

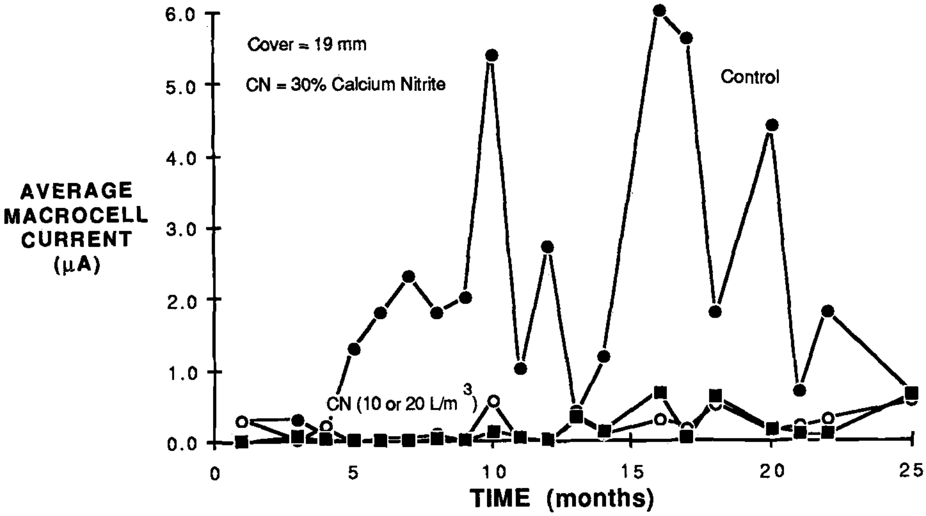

FIG. 8—*Average macrocell current as a function of time for chromated-galvanized steel with 19 mm of cover.*

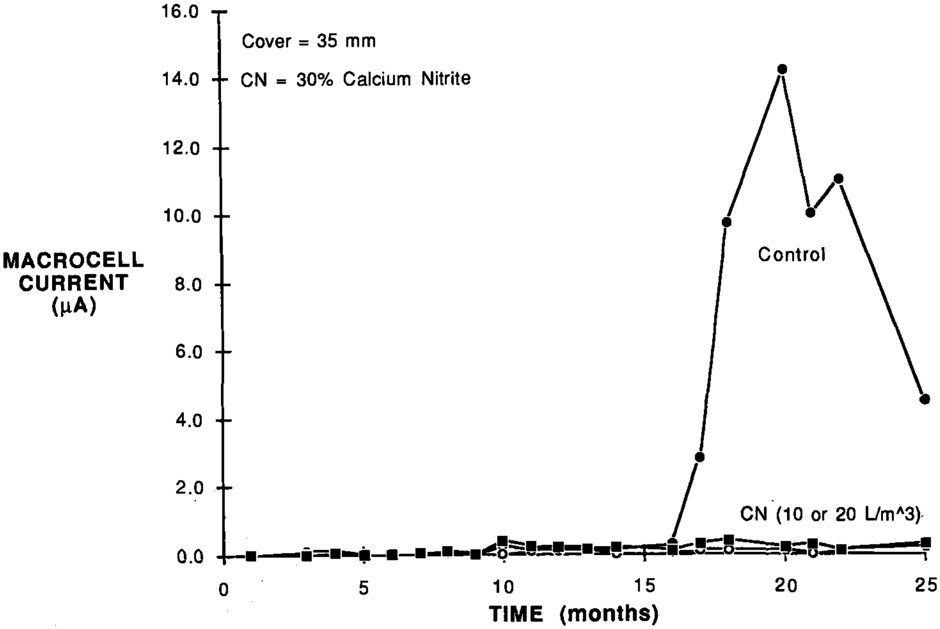

FIG. 9—*Average macrocell current as a function of time for black steel with 35 mm of cover.*

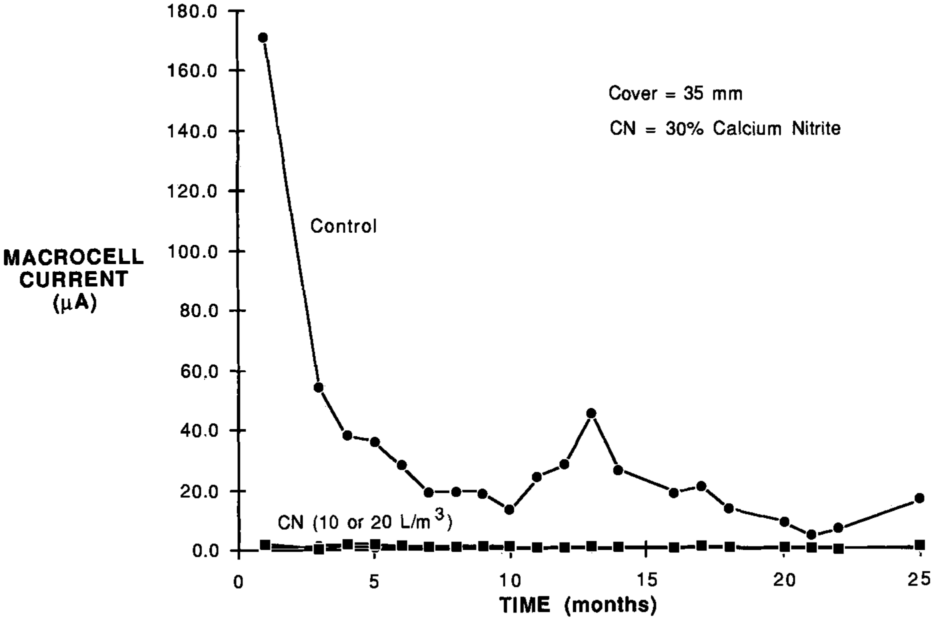

FIG. 10—*Average macrocell current as a function of time for aluminum conduit with 35 mm of cover.*

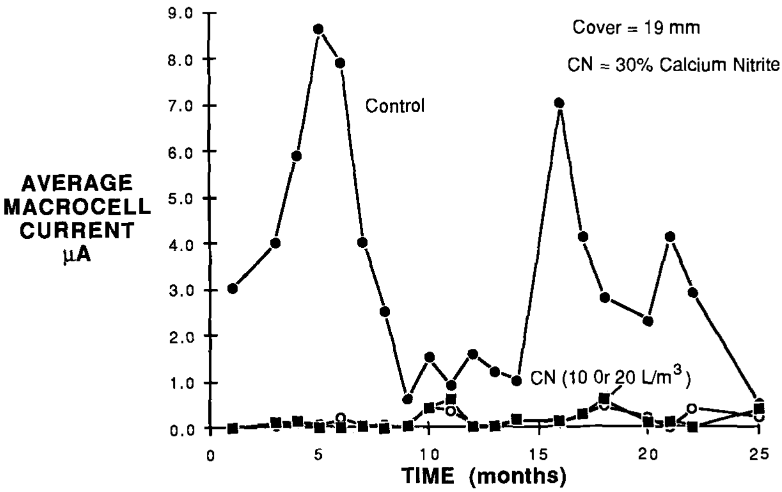

FIG. 11—*Average macrocell current as a function of time for galvanized steel with 19 mm of cover.*

(0.75 in.) reinforcement level, it is not surprising that the black steel samples were corroding rapidly before one year. The galvanized bars were also corroding rapidly before one year at low cover indicating that they offered little if any added protection in the presence of chloride.

Figure 12 also shows the predicted chloride profile based upon fitting the data to a one-dimensional diffusion model based on Fick's law. A nonlinear regression analysis was used to determine C_o and D_{eff} (surface concentration and effective diffusion coefficient). As can

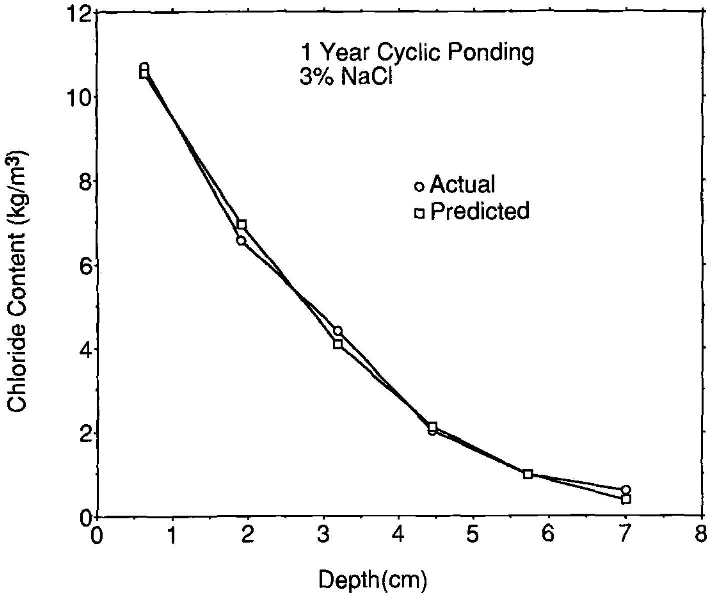

FIG. 12—*Actual chloride concentrations versus predicted.*

be seen, the data fit this model quite well The D_{eff} value was found to be 17 × 10^{-8} cm^2/s which is in relatively good agreement with other values determined in this laboratory for 0 48 w/c concrete [*18*], and by others [*12,19,20*]

Further Discussion

The improved corrosion resistance with calcium nitrite is in good agreement with previous studies measuring macrocell corrosion rates [*4,5,18*] Improvements with the galvanized steel are in general agreement with results reported in Ref *4* The reduced corrosion rates of the galvanized steel and aluminum conduit in the presence of calcium nitrite were significant and opens up the possibility of extending their use in concrete

The two test methods both measure currents indicating corrosion However, corrosion rates (currents) are higher when measured by the polarization resistance method We have noticed this trend in other experiments [*6,18*] Since the macrocell technique measures only the galvanic current, one would expect the rates measured by this technique to always be less than or equal to the total corrosion rate [*21*]

Both of these methods gave reasonable results during the early stage of corrosion in the laboratory. Currently, we are conducting experiments with embedded probes in field structures comparing both techniques However, in an already existing structure without embedded probes, macrocell tests would be difficult to perform

Conclusions

Based upon the results of this work, and comparisons to other studies, several conclusions concerning corrosion rate measurements and protection of steel in concrete can be made, namely

1. both macrocell and polarization resistance techniques can be used to determine corrosion rates of steel and aluminum in concrete in the laboratory until the lower mat of rebar (aluminum) begins to corrode,
2. the macrocell technique appears to underestimate the corrosion rate, sometimes by an order of magnitude;
3. calcium nitrite effectively delayed and reduced the corrosion of black steel, galvanized steel, and aluminum in concrete, and
4. unprotected galvanized steel corroded as early as black steel, but to a lesser extent

Acknowledgments

The authors wish to thank A J Dressler and P Toner for their assistance, American Hot Dip Galvanizers Association and Southern Galvanizing Company for providing the galvanized steel samples; and the management at W R Grace for allowing us to perform the studies and publish the results

References

[*1*] Strategic Highway Research Program, *Participant Workbook—National Workshop,* Strategic Highway Research Program Washington, DC, Sept 1985, p TRA 4-1

[*2*] *Focus,* Special Edition, Strategic Highway Research Program, Washington, DC, 18–20 Sept 1985

[*3*] Manning, D , "Bridge Component Protection, Final Report," Strategic Highway Research Program, Washington, DC, 18 Nov 1985

[4] Pfeifer, D W and Landgren, J R , "Protective Systems for New Prestressed and Substructure Concrete," Report No FHWA/RP-86/193, Federal Highway Administration, Washington, DC, April 1987

[5] Virmani, Y P , Clear, K C , and Pasko, T J , "Time-to-Corrosion of Reinforcing Steel in Concrete Slabs, Vol 5–Calcium Nitrite Admixture and Epoxy-Coated Reinforcing Bars as Corrosion Protection Systems," Report No FHWA/RF-83/012, Federal Highway Administration, Washington, DC, Sept 1983

[6] Berke, N S , "Microsilica and Concrete Durability," Paper No 870275, presented at 67th Annual Transportation Research Board Meeting, 11–14 Jan 1988, Washington, DC

[7] Berke, N S , "The Effects of Calcium Nitrite and Mix Design on the Corrosion Resistance of Steel in Concrete (Part 1)," Corrosion 85, Paper No 273, National Association of Corrosion Engineers, Boston, March 1985

[8] Berke, N S , "The Effects of Calcium Nitrite and Mix Design on the Corrosion Resistance of Steel in Concrete (Part 2)," Corrosion 87, Paper No 132, National Association of Corrosion Engineers, San Francisco, March 1987

[9] Berke, N S , "Corrosion Rates of Steel in Concrete," *Standardization News,* American Society for Testing and Materials, March 1986, p 57

[10] Wheat, H G and Eliezer, Z , *Corrosion,* Vol 41, No 11, 1985

[11] Andrade, C and Castelo, V , *British Corrosion Journal,* Vol 19, No 2, 1984, p 98

[12] Fischer, K P , Bryhn, O , and Aagaard, P , *Corrosion,* Vol 40, 1984, pp 358–366

[13] Dawson, J L , "Corrosion Monitoring of Steel in Concrete," *Corrosion of Reinforcement in Concrete Construction,* A P Crane, Ed , Ellis Horwood, Ltd , London, 1983, p 175

[14] Berke, N S , Shen, D F , and Sundberg, K M , "Comparison of Current Interruption and Electrochemical Impedance Techniques in the Determination of the Corrosion Rates of Steel in Concrete," presented at the ASTM Symposium on Ohmic Electrolyte Resistance Measurement and Compensation, Baltimore, 17 May 1988

[15] "Guide to Durable Concrete," ACI 201, American Concrete Institute, Detroit, MI

[16] Kessler, R and Browne, R D , "Determination of Low Levels of Chloride in Concrete and Raw Materials," Florida DOT Research Report No 203 PB 289620, July 1978

[17] Clear, K C , "Time-to-Corrosion of Reinforcing Steel in Concrete Slabs, Vol 4 Galvanized Reinforcing Steel," Report No FHWA/RD-82/028, Federal Highway Administration, Washington, DC, Dec 1981

[18] Berke, N S and Weil, T G , "Corrosion Protection Through The Use of Concrete Admixtures," *Proceedings,* Second International Conference on Performance of Concrete in Marine Environment, St Andrews by-the-Sea, New Brunswick, Canada, 21–26 Aug 1988

[19] Browne, R D , "Design Prediction of the Life for Reinforced Concrete in Marine and other Chloride Environments," *Durability of Building Materials,* Vol 1, 1982, pp 113–125

[20] Tuutti, K , *Corrosion of Steel in Concrete,* Swedish Cement and Concrete Research Institute, Stockholm, Sweden, 1982

[21] Mansfeld, F , Hengstenberg, R H , and Kenkel, J V , *Corrosion,* Vol 30, 1974, p 343

Harovel G. Wheat[1]

Corrosion Rate Determination on Repaired Reinforced Concrete Specimens

REFERENCE: Wheat, H G , "**Corrosion Rate Determination on Repaired Reinforced Concrete Specimens,**" *Corrosion Rates of Steel in Concrete, ASTM STP 1065,* N S Berke, V Chaker, and D Whiting, Eds , American Society for Testing and Materials, Philadelphia, 1990, pp 52-65

ABSTRACT: The repair and maintenance of reinforced concrete structures is becoming increasingly important as structures become older and the use of condition surveys becomes more extensive Although guidelines exist for repair methods, little is known about the corrosion behavior once repairs are made In this investigation, electrochemical tests typically used on reinforced concrete specimens were used on repaired specimens which were subjected to wet (3 5% sodium chloride (NaCl) solution) and dry cycling Repaired specimens made with a water/cement ratio of 0 6 and patched with a common repair material showed rust staining, severe delamination, and cracking after a number of cycles while the typical (control) samples did not Although both types of specimens had comparable corrosion potentials, linear polarization measurements showed that R_p was lower, and therefore corrosion rates in the repaired specimens were higher than in the control specimens

KEY WORDS: steels, concrete, corrosion, repair, linear polarization, a-c impedance

The normal corrosion protection afforded to reinforced concrete structures can be significantly compromised in chloride environments This is reflected in the deteriorated condition of many of the nation's bridges, which is caused at least in part by salt contamination through deicing salt application

Much progress has been made in terms of new bridge deck construction, because epoxy coated steel and corrosion inhibitors can be quite effective in retarding corrosion in many instances [*1*] Many other aspects of the corrosion of steel reinforcement in concrete construction, including the use of cathodic protection, have also been studied [*2*]. One of the problems which has surfaced involves the repair of steel-reinforced concrete structures Because the repaired concrete will involve a repaired portion and an unrepaired portion, increased galvanic action is possible Even in an ordinary steel-reinforced concrete sample, oxygen, pH, and microscopic surface differentials on the steel serve to cause galvanic corrosion [*3–7*] The situation will be more severe in the case of the repaired concrete since the steel—which will contain microscopic and macroscopic surface differences itself—will exist in two distinctly different environments simultaneously Although a number of guidelines are in existence for the repair of reinforced concrete structures [*8*], in many instances, the nature and extent of the repair are subjective

Moreover, little follow-up is carried out and the repair is considered successful unless another problem arises This paper addresses the evolution of the degradation of repaired specimens and the results from electrochemical testing are presented

---

[1] Assistant professor, Mechanical Engineering Department, The University of Texas, Austin, TX 78712

Procedure

Equipment

The electrochemical testing was carried out on a Model 350 corrosion measurement system and a Model 278 a-c impedance system (which consisted of a lock-in amplifier) from EG&G Princeton Applied Research. Both are microcomputer-controlled. Corrosion potential measurements were made using a saturated calomel electrode (SCE).

Specimen Preparation

Concrete prisms that were 5.08 by 5.08 by 30.48 cm (2 by 2 by 12 in.) were cast with a centrally located No. 4 (1.27 cm) bar of steel that was 27.94 cm (11 in.) long. Each bar had a piece of copper wire spot-welded to it, and the bottom cut face as well as the interface between the steel bar and the copper wire was covered with epoxy. The repair specimens were purposely cast with a specified area (approximately 2.54 cm or 1 in.) of the bar exposed. This was accomplished by casting the concrete using a foam insert which resulted in a hole when the foam was removed. A schematic representation of the specimen showing the resultant hole is shown in Fig. 1. Ten inches of the bar remained covered. The concrete was made with Type 1 cement and a water/cement ratio of about 0.6 to ensure relatively high permeability.

Procedure

Reinforced concrete specimens were prepared in two ways. The control specimens were cast without sponge inserts while the other specimens were cast with sponge inserts. Twenty four hours after casting, the specimens were demolded and sponge inserts were removed leaving a hole and exposing the steel underneath. The specimens were then cured for 28 days at 100% relative humidity, allowed to dry out in laboratory air for one month, and then placed in a solution of 3.5% sodium chloride (NaCl) and subjected to alternating wet and dry conditions (three days wet, four days dry). This lasted for two months and, by this time, severe deterioration had taken place along the exposed portion of the steel. The specimens were allowed to dry out again for one month. Some samples were broken open at this point to observe the extent of corrosion, and the extent of repair was based on observations made at that time. Some specimens were left un-repaired. Other specimens were prepared for repair. In those specimens which were repaired, the concrete was cut

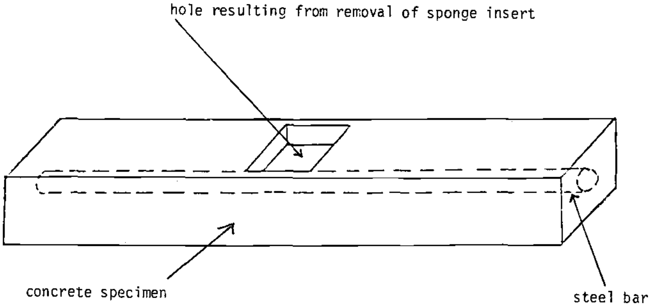

FIG. 1—*Schematic representation of a specimen showing the hole which resulted after removal of the sponge insert.*

back to ensure thorough cleaning by sandblasting the corroded area Following the sandblasting, the cleaned steel was covered with a common repair material known as Set-45 This product, which is made by Set Products, is composed of magnesia-phosphate powder and fine aggregate and is water activated The Set-45 was prepared according to package directions using 0 1 L of H_2O per kilogram of Set-45 Efforts were made to ensure good bonding of the repair materials with the specimens The repaired specimens were placed in a 3 5% solution of NaCl one week following repair and again subjected to wet-dry cycling This aggressive environment served to intensify the galvanic corrosion which resulted from the fact that the steel bar (which then contained the original surface and the cleaned surface) existed in two environments, namely, the old concrete and the repair material Electrochemical tests such as linear polarization and a-c impedance measurements were conducted on the third day of each cycle Linear polarization experiments which were conducted at a scan rate of 0 1 mV/s were started at 20 mV below E_{corr} and ended above E_{corr} A lock-in amplifier was used for a-c impedance measurements in the frequency range of 5 Hz to 100 kHz and a Fast Fourier Transform technique was used for the range 0 001 to 1 Hz Specimens were marked off in 2 54 cm (1 in) sections so that half-cell potential measurements could be determined according to the ASTM Test for Half Cell Potentials of Reinforcing Steel in Concrete (C 876-80).

Results and Discussion

Three control specimens (cast without inserts), three un-repaired specimens (visibly corroded but not repaired), and six repaired specimens have been observed through 16 cycles. Because of the high water/cement ratio, all repaired specimens exhibited active potentials (according to ASTM C 876-80) by the third day of the first cycle. The control specimens required several cycles before all of them had active E_{corr} values. The values of E_{corr} changed quite rapidly following immersion with the un-repaired specimens attaining active potentials within about 24 h By the second cycle, there was no significant difference in the corrosion potential in the twelve sections It was felt that there might be some marked difference between the patched area and the rest of the specimen, however, this was not observed It is possible that the high water/cement ratio resulted in such rapid intrusion of the NaCl that the differentials were quickly eliminated

After the first cycle, the average value of the polarization resistance, R_p, for the control specimens was 43 7 kΩ cm^2 while that of R_p for the repaired specimens was 6 1 kΩ cm^2 With continued cycling, R_p for the control and repaired specimens decreased until after 16 cycles they were 4 4 and 5.1 kΩ cm^2, respectively These values were determined using the linear polarization technique and the Model 350 corrosion measurement system

The a-c impedance data is often presented as a Nyquist plot in which the imaginary component of impedance (Z'') is plotted versus the real component of impedance (Z') for each excitation frequency It has recently been recommended [*10*], however, that Bode plots, which permit the examination of the absolute impedance $|Z|$ and the phase angle, Θ, be used as standard plots They show more clearly the characteristic features of the a-c impedance data, especially for an electrochemical cell involving more than one time constant

Initially, the control specimens and the repaired specimens showed Nyquist behavior similar to that predicted from a proposed equivalent circuit for the steel in concrete system A typical Nyquist plot and the proposed equivalent circuit are shown in Figs 2*a* and *b* [*9*] Actual a-c impedance data are shown in Figs 3*a*, *b*, *c*, and *d* While there is still some question as to how the actual data should be interpreted for the steel in concrete system, it is possible to make some inferences based on comparisons of the a-c impedance data

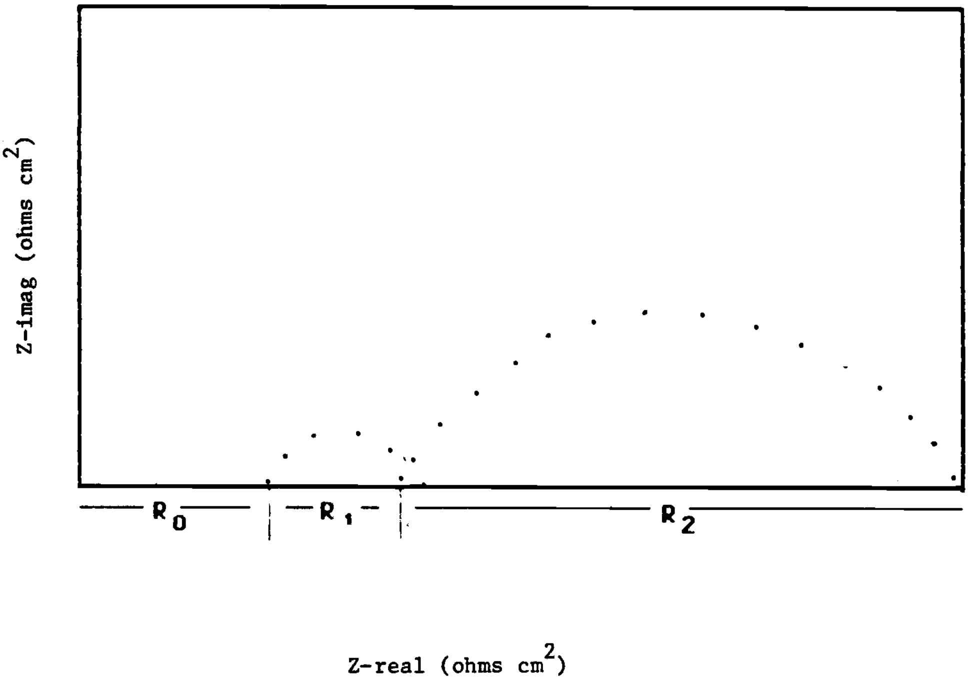

FIG. 2*a*—*Typical Nyquist impedance plot for steel in concrete.*

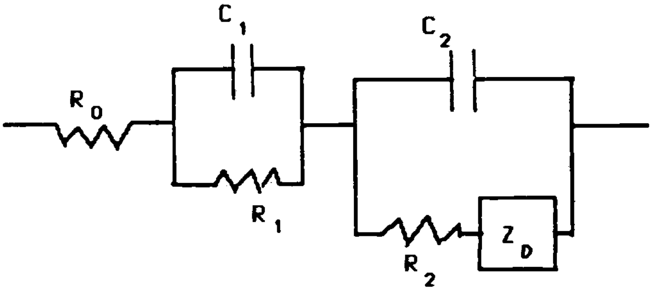

R_0 Concrete resistance (Ωcm^2)
R_1 Interfacial resistance (Ωcm^2)
C_1 Interfacial capacitance (F/cm^2)
R_2 Charge transfer resistance (Ωcm^2)
C_2 Double layer capacitance (F/cm^2)
Z_D Diffusion impedance (Ω/cm^2)

FIG. 2*b*—*Equivalent circuit used for steel in concrete.*

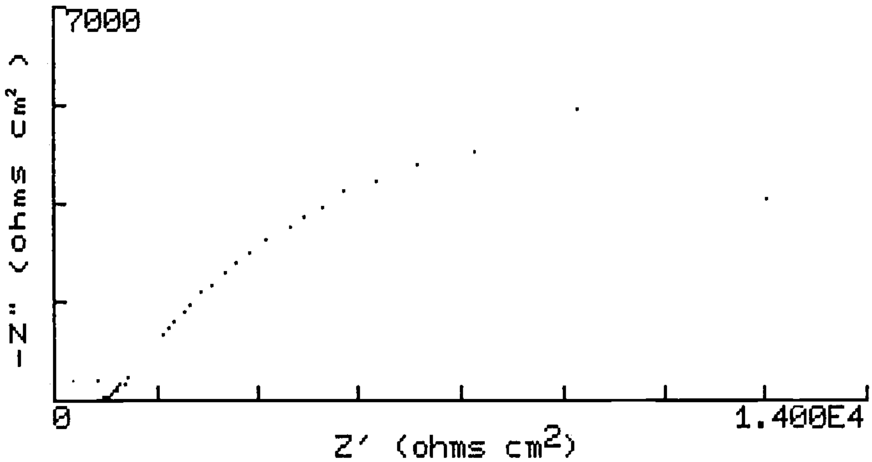

FIG. 3*a*—*Nyquist plot taken during Cycle 1 for a control specimen.*

taken during different times of salt exposure. Therefore, it can be seen that by Cycle 8, the behavior of the control specimens had changed somewhat. The Cycle 1 and Cycle 8 plots for a specimen are shown in Figs. 4*a* and *b*. The Cycle 8 plot clearly shows a depressed semicircle and thus a smaller value of R_2 and a higher corrosion rate during Cycle 8 than during Cycle 1.

The Nyquist and Bode plots for the un-repaired specimens were quite different from those

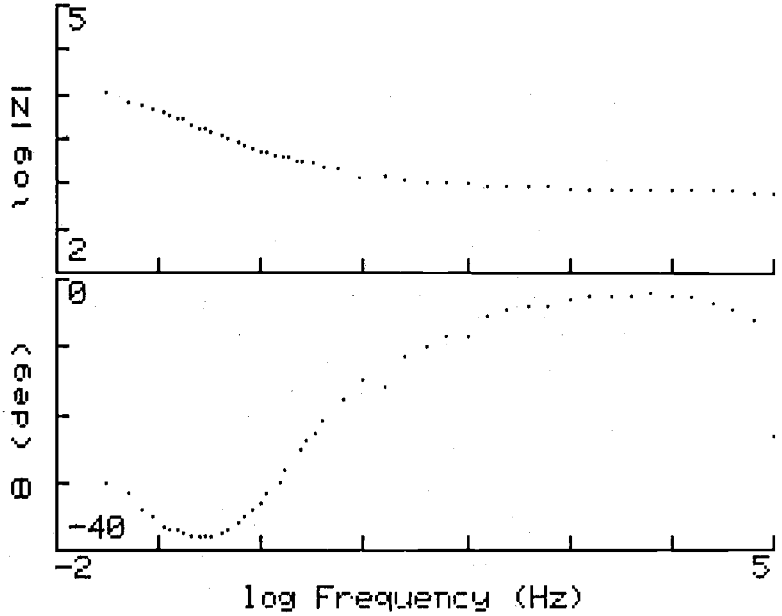

FIG. 3*b*—*Bode plot taken during Cycle 1 for a control specimen.*

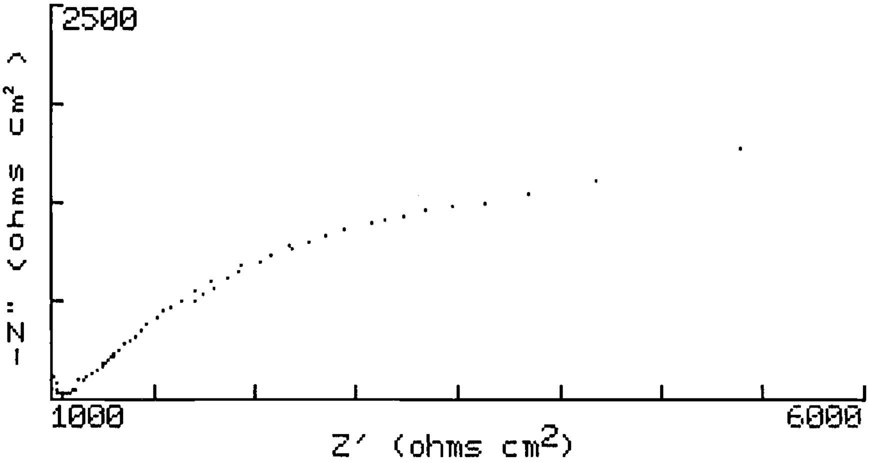

FIG. 3*c*—*Nyquist plot taken during Cycle 1 for a repaired specimen.*

for the control or the repaired samples in the early stages. Nyquist and Bode plots for an un-repaired specimen are shown in Figs. 5*a* and *b*, respectively. What is very remarkable, however, is that by the fifth cycle, the behavior of the repaired specimens was beginning to look more like that of the un-repaired specimens. Examples are shown in Figs. 6*a, b, c,* and *d*. Therefore, it appears that a-c impedance data can be used to follow the degradation of the steel in salt-contaminated concrete since definite changes can be observed as a function

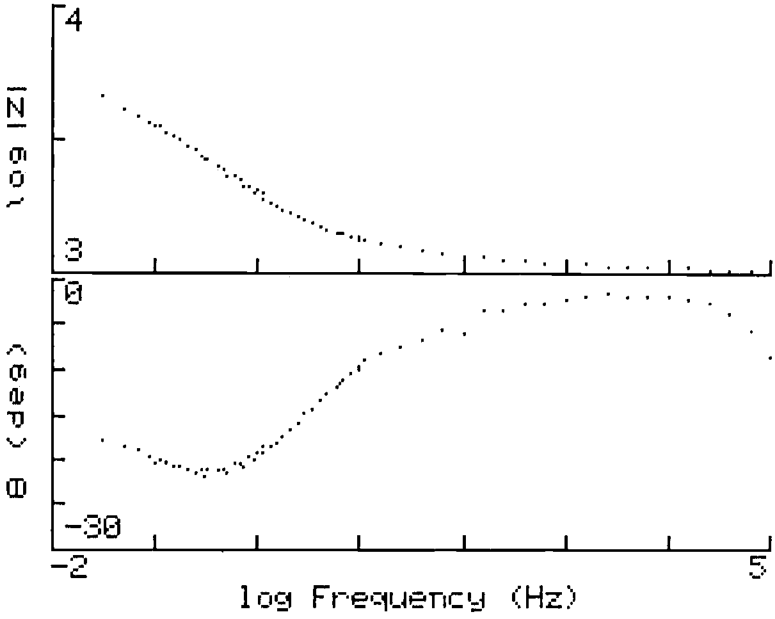

FIG. 3*d*—*Bode plot taken during Cycle 1 for a repaired specimen.*

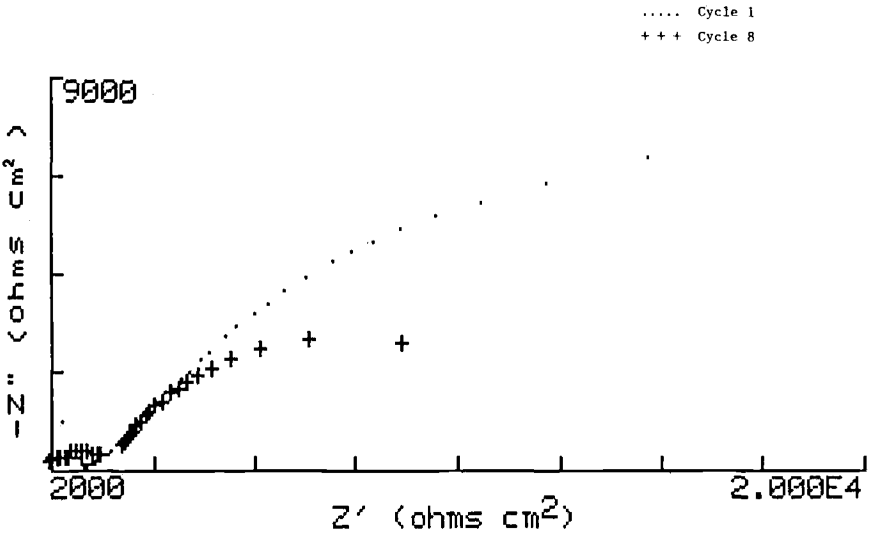

FIG. 4*a*—*Nyquist plot taken during Cycles 1 and 8 for a control specimen.*

of time. At the same time that the a-c impedance behavior was changing, rust stains and cracks were beginning to form on the repaired specimens. In some cases, the cracks were in the vicinity of the repair patch, but in other cases, the cracks extended the length of the top surface. Examples are shown in Fig. 7. Close up views are shown in Figs. 8*a* and *b*. A side view of the specimen in Fig. 8*a* is shown in Fig. 9. The rust staining and delamination are evident.

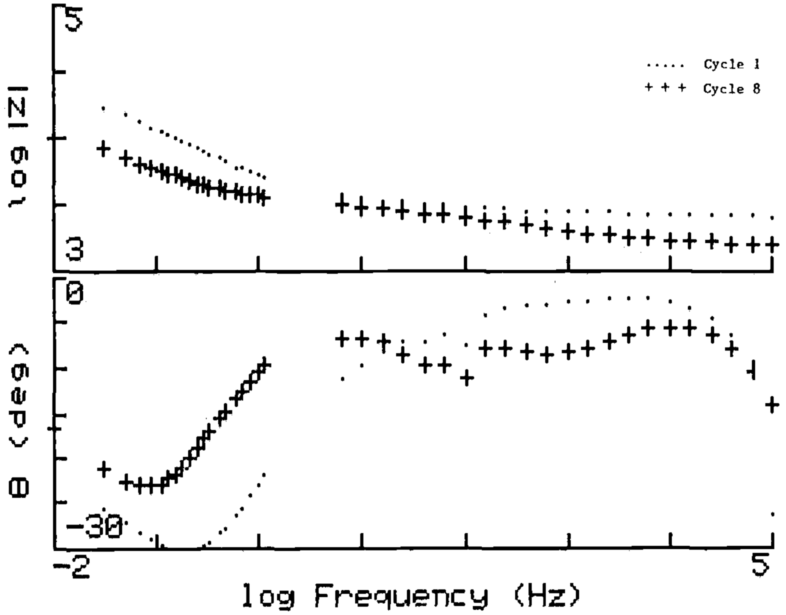

FIG. 4*b*—*Bode plot taken during Cycles 1 and 8 for a control specimen.*

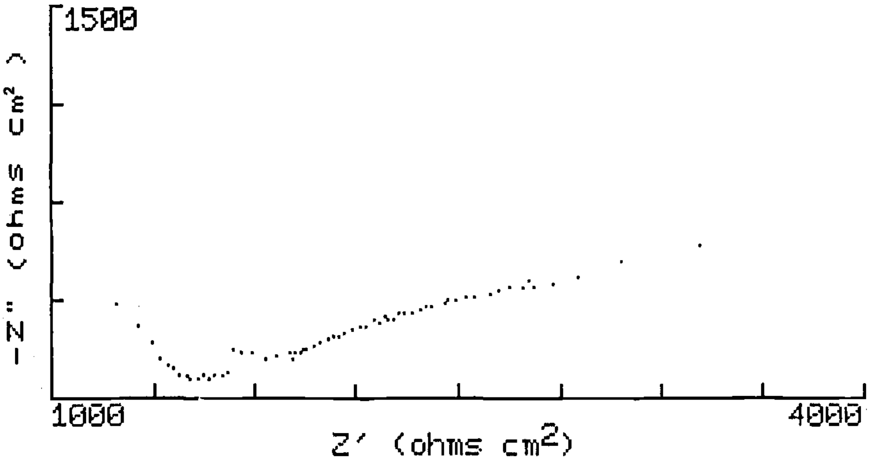

FIG. 5a—*Nyquist plot taken during Cycle 1 for an un-repaired specimen.*

While the corrosion potentials of the control, un-repaired, and repaired specimens were very similar, the corrosion behavior as determined from the a-c impedance technique was quite different and indicative of what was happening internally. To be sure, the results described here are for a relatively high water/cement ratio and so the initial quality of the concrete is already low. In addition, they are for a specific repair material which was prepared in a very small quantity. These two factors, namely, the quality of the concrete to be repaired

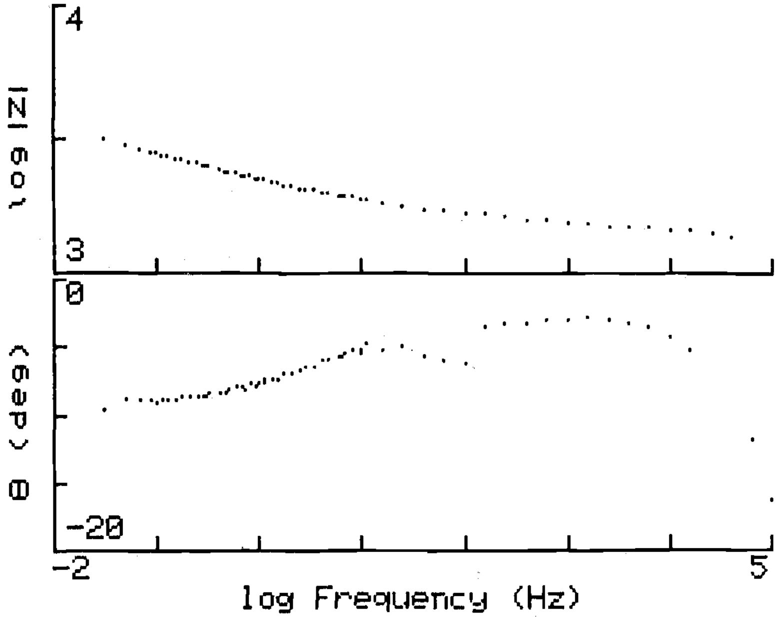

FIG. 5b—*Bode plot taken during Cycle 1 for an un-repaired specimen.*

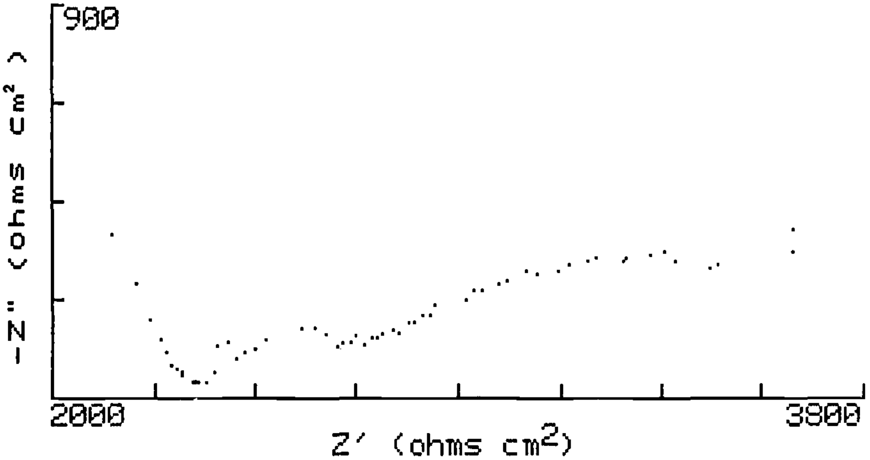

FIG. 6*a*—*Nyquist plot taken during Cycle 5 for a repaired specimen.*

and the mixing and placing procedures, have a tremendous effect on the corrosion behavior or the repaired structure. Therefore, the results show what can happen when repairs are made and the specimens continue to be exposed to chloride environments.

Efforts are under way to investigate at least three types of repair materials on larger specimens made with concrete having a lower water/cement ratio.

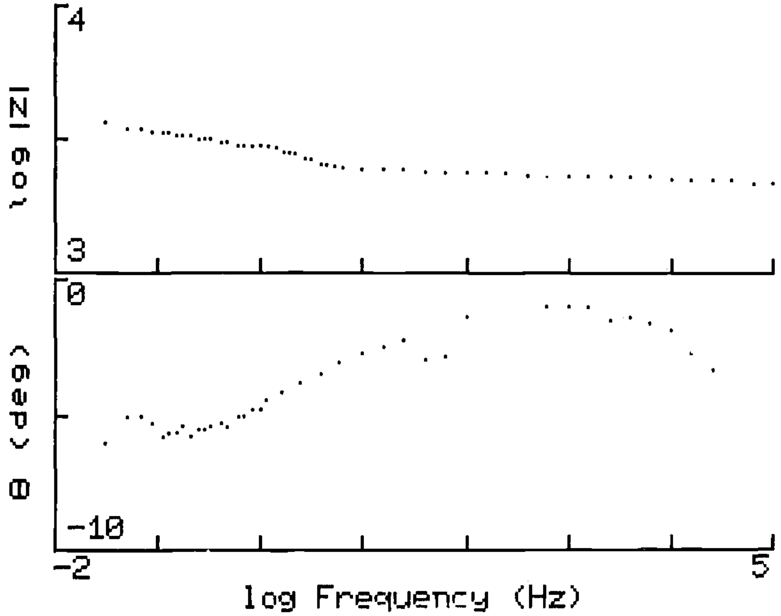

FIG. 6*b*—*Bode plot taken during Cycle 5 for a repaired specimen.*

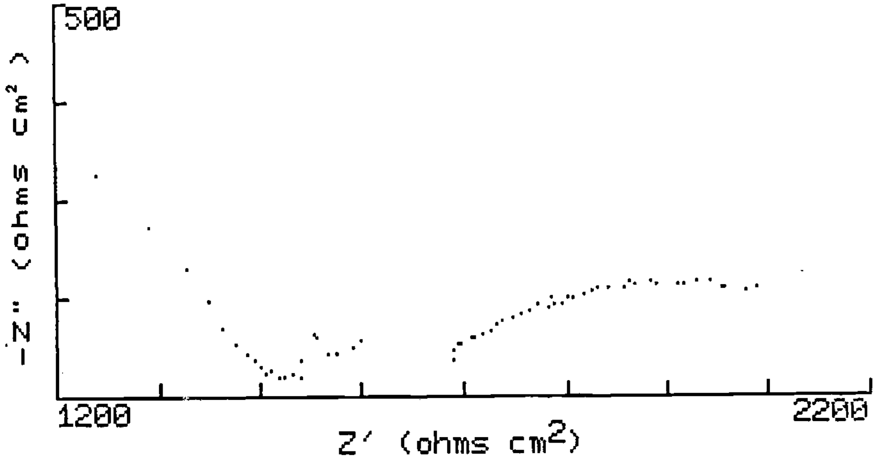

FIG. 6*c*—*Nyquist plot taken during Cycle 8 for a repaired specimen.*

Acknowledgments

This work was supported by a University Research Institute grant from The University of Texas at Austin. The author also wishes to thank David Whitney, Sam Holt, and Norman Williams for their valuable assistance in this project.

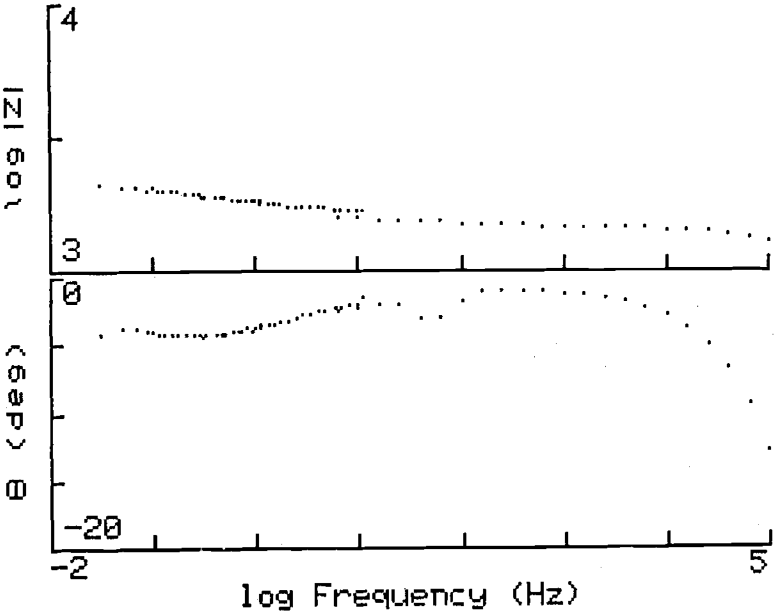

FIG. 6*d*—*Bode plot taken during Cycle 8 for a repaired specimen.*

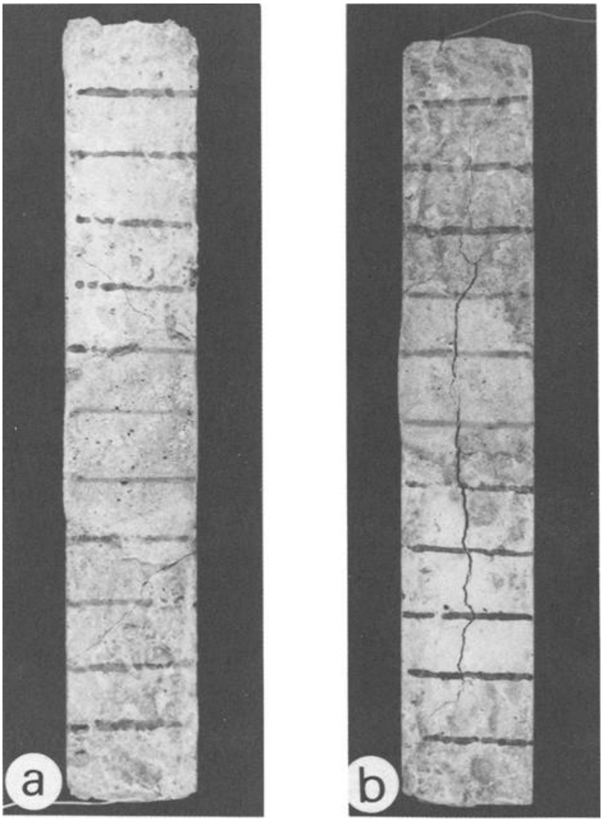

FIG. 7—(a) *Repaired specimen after eight cycles, cracks near patch.* (b) *Repaired specimen after eight cycles, cracks down center of specimen.*

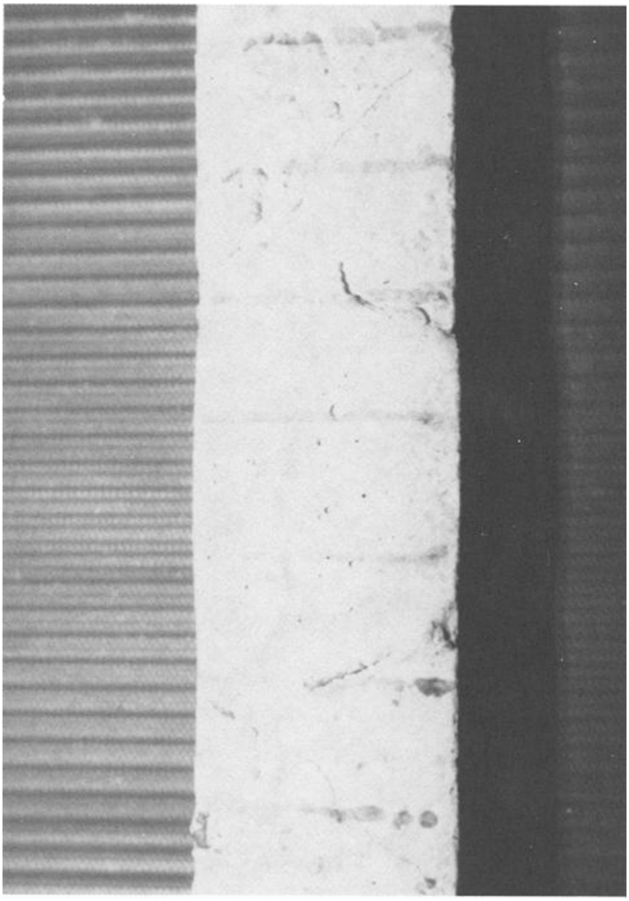

FIG. 8*a*—*Close up view of repaired specimens after eight cycles, cracks near patch.*

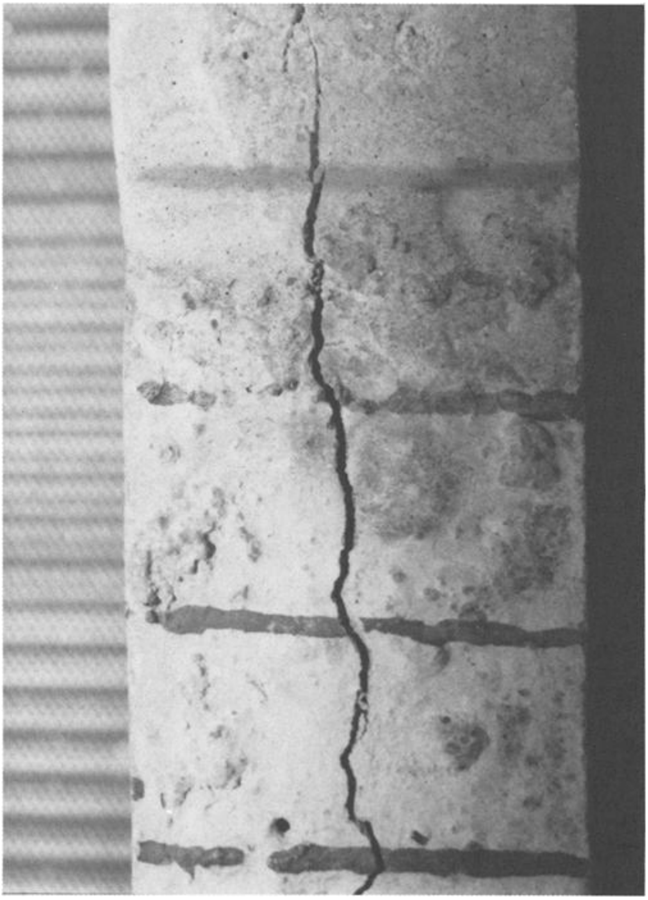

FIG. 8*b*—*Close up view of repaired specimens after eight cycles, cracks down center of specimen.*

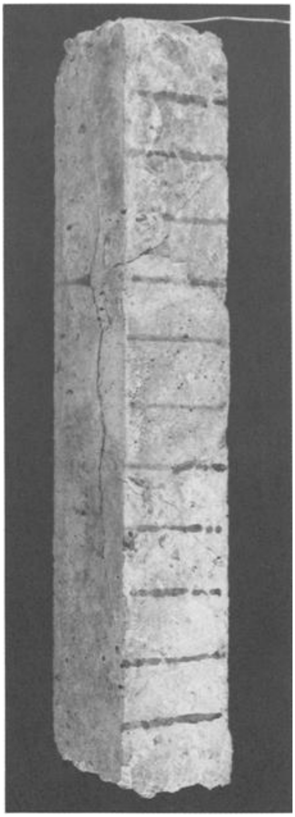

FIG. 9—*Side view of specimen which had cracks near the patch.*

References

[*1*] *Proceedings,* Corrosion/87 Symposium on Corrosion of Metals in Concrete, National Association of Corrosion Engineers, 1987.

[*2*] *Corrosion of Reinforcement in Concrete Construction,* A. P. Crane, Ed., Ellis Horwood Limited, London, 1983.

[*3*] Stratfull, R. F., *Corrosion,* Vol. 13, 1957, pp. 173 t–178 t.

[*4*] Lewis, D. A. and Copenhagen, W. J., *Corrosion,* Vol. 15, No. 4, July 1959.

[*5*] Gouda, V. K. and Mourad, H. M., *Corrosion Science,* Vol. 15, 1974, pp. 681–690.

[*6*] Gouda, V. K. and Mourad, H. M., *Corrosion Science,* Vol. 15, 1974, pp. 307–315.

[*7*] Gouda, V. K. and Mourad, H. M., *Corrosion Science,* Vol. 15, 1974, pp. 317–328.

[*8*] Browne, R. D., Geoghegan, M. P., and Baker, A. F. in *Corrosion of Reinforcement in Concrete Construction,* A. P. Crane, Ed., Ellis Horwood Limited, London, 1983, p. 194.

[*9*] John, D. G., Coote, A. T., Treadaway, K. W. J., and Dawson, J. L. in *Corrosion of Reinforcement in Concrete Construction,* A. P. Crane, Ed., Ellis Horwood Limited, London, 1983, p. 264.

[*10*] Mansfeld, F., *Corrosion,* Vol. 44, 1988, p. 558.

Alberto Aguilar,[1] *Alberto A. Sagüés,*[2] *and Rodney G. Powers*[3]

Corrosion Measurements of Reinforcing Steel in Partially Submerged Concrete Slabs

---

REFERENCE: Aguilar, A , Sagués, A A , and Powers, R G , **"Corrosion Measurements of Reinforcing Steel in Partially Submerged Concrete Slabs,"** *Corrosion Rates of Steel in Concrete, ASTM STP 1065,* N S Berke, V Chaker, and D Whiting, Eds , American Society for Testing and Materials, Philadelphia, 1990, pp 66–85

ABSTRACT: The corrosion of reinforcing steel in concrete partially submerged in salt water has been investigated using concrete slabs containing longitudinal rebars divided into elements with independent electrical connections Open circuit potential, interelement current, concrete conductance, and electrochemical impedance measurements have been conducted while specimens were exposed to water containing chlorides over a period of about one year Direct observations of corrosion and concrete characteristics were conducted at the end of the experiment Corrosion tended to initiate at the evaporation zone of the vertical slabs, where chlorides accumulated Once active corrosion started, a macrocell developed with the small portion of the bar below the water surface acting as an electron source Evaluations of the damage from macrocell current and electrochemical measurements were in rough agreement with direct estimates of sound metal loss based on after-exposure examination In bars where the separate elements were kept electrically isolated, corrosion proceeded at a higher rate at those elements near the evaporation zone The results have been used to propose a mechanism for corrosion initiation and propagation in partially immersed reinforced concrete members

KEY WORDS: corrosion, reinforcing, steel, rebar, concrete, piling, culverts, macrocell, chloride, measurement, partial submersion, culverts, impedance, evaporation, currents

The corrosion of steel reinforcing bars (rebars) in concrete is a result of depassivation of the steel surface [*1*] In uncontamined, freshly cured concrete the moisture in contact with the steel has a high pH (near 12) due to the presence of alkali hydroxides The metal acquires an open-circuit potential typically from 100 to −100 mV versus the saturated calomel electrode (SCE) and the surface exhibits passive behavior The breakdown of the passive film may occur because of the action of chlorides, once a threshold concentration of those ions has been reached at the metal surface The zone where passivity breakdown has occurred may become an anode in an electrochemical corrosion cell The anodic, metal dissolution reaction is matched by cathodic processes that can develop nearby or elsewhere on the rebar For structures in contact with air, oxygen reduction is the most likely expected cathodic reaction The severity of the deterioration and its evolution with time vary greatly from system to system

Reinforced concrete structures often encounter service under partial immersion in water containing chlorides These components are subject to a unique corrosion configuration

[1] Currently at Departamento de Ciencia de Materiales e Ingenieria Metalurgica, Universidad Complutense de Madrid, 28040 Madrid, Spain

[2] Associate professor, Department of Civil Engineering and Mechanics, University of South Florida, Tampa, FL 33620

[3] Materials Office, Florida Department of Transportation, Gainesville, FL 32602

[2,3]. Both the transport of chloride to the metal surface, and the factors determining the extent of the partial corrosion reactions after depassivation, are affected by the physical arrangement of the system. This is illustrated in Fig. 1 for a steel-reinforced column submerged in seawater. The portion of concrete below the water line is saturated with water, while regions near the top of the column will be relatively dry. This results in a moisture gradient with consequent upward transport of liquid. Water is removed by evaporation in the middle region. This process results not only in the transport of dissolved species (such as chloride) to the regions above the water line, but also in the accumulation of those species as residues in the region of evaporation. The accumulation can be so severe that chloride-rich effloresces can develop under stagnant conditions. The conditions for oxygen transport vary also as a function of position along the column. In the fully submerged region, the concrete pore network is filled with water and the effective diffusion coefficient of oxygen is smallest, comparable with that of oxygen in totally stagnant water (about 10^{-5} cm^2/s at room temperature [4]). Further up, the concrete pores are partially filled with water and transport of oxygen is easier. Effective diffusion coefficients of oxygen there can reach values that are orders of magnitude higher than those in the water-saturated zone [4]. The electrical conductivity of the concrete follows a trend generally opposite to, but more complicated than that of the oxygen diffusivity. The regions near the top of the column are dry and concrete resistivity can approach values typical of electrical insulators. The fully submerged region, saturated with seawater, has much lower resistivities, typically in the order of 1000 ohm · cm [5,6]. However, low resistivities may develop at the zone where chlorides accumulate, since some water is present there and the chlorides form a highly concentrated electrolyte with it.

The region above and close to the water line possesses then a severe combination of chloride concentration, oxygen availability, and electrolyte conductivity to promote corrosion. In marine structures, tidal action and sea spray, with concurrent wet-dry cycling, can

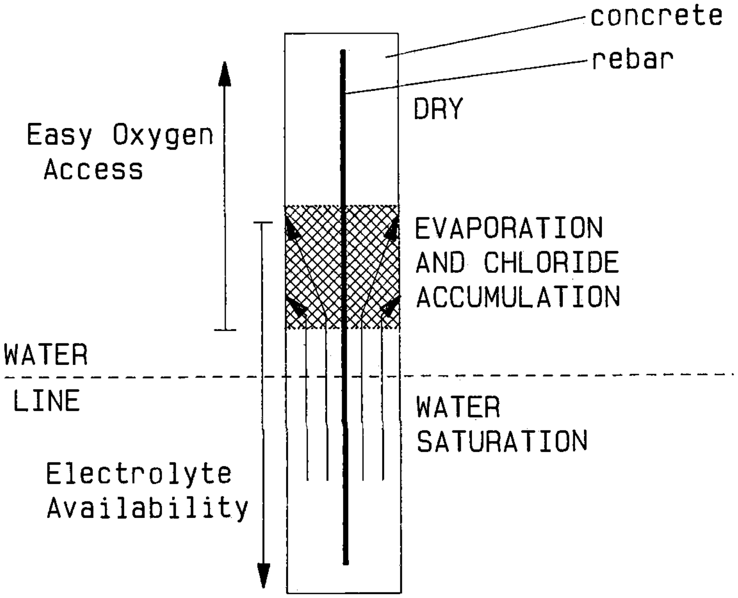

FIG. 1—*Conditions prevalent in a reinforced concrete component partially submerged in chloride-containing water.*

extend or aggravate those conditions over a larger portion of a piling member. Service experience confirms that corrosion damage appears normally above the water line, at or near the splash and tidal action area [*2,3,7,8,9*]. In warm parts of the country, where road deicing is not common, most corrosion damage of highway bridges is seen at substructure piling that is partially submerged in seawater [*10*]. While the problem is severe and widespread, many recent corrosion studies have concentrated on bridge deck structures, or concrete where chloride accumulation and moisture gradients result from a horizontal arrangement [*11,12*]. Investigations addressing the corrosion of partially immersed columns are less common. Among these, investigation of piling exposed in Tokyo Bay [*2*] demonstrated chloride buildup above the water line. The same work established by means of differential current measurements that corrosion tends to originate near the tidal area. Additional information on the operating mechanisms of deterioration is needed to develop reliable criteria for the durability of piling and other structures (such as drainage culverts) that experience partial submersion. An investigation to develop design life criteria for reinforced concrete culverts has been recently sponsored by the Florida Department of Transportation [*13,14*]. To this effect, corrosion measurements have been conducted in instrumented reinforced concrete columns with multiple-segment rebars, partially submerged in chloride-containing water. The results from the initial phase of this investigation are reported in the following sections.

Experimental

The majority of the test specimens were reinforced concrete slabs 5.1 cm (2 in.) thick, 15.2 cm (6 in.) wide, and 45.7 cm (18 in.) high. The steel reinforcement consisted of straight bars, either in one piece or divided into electrically separated segments. Sets of three slab specimens were exposed to each test environment. Figure 2 shows the configuration of the slabs, as well as the system used to designate the different specimens and elements within. Each rebar segment had its own external electrical connection. Wire connections were separated from the concrete environment by encapsulating the connection with epoxide metallographic mounting compound (Specimen Types 2 and 3) or an epoxy mix (Specimen Type 1). Different segments of each multi-element rebar were mechanically connected using metallographic mounting compound or epoxy mix (Types 2 and 3 and 1, respectively). Reference electrodes, made from activated Titanium wire (Elgard anode stock [*15*]), were embedded in the concrete as shown in Fig. 1. A connection box on top of each specimen allowed for electrical measurements. Switches in the box permitted closing or opening electrical contacts between different portions of the multi-element rebars.

The concrete used is described in Table 1. The various internal components of each slab

TABLE 1—*Concrete composition*

	Specimen Type	
	1, 2, and 3, typical	4, typical
Cement type	I	I
Composition (parts by weight of cement)		
Coarse aggregate[a]	3.36	3.33
Fine aggregate[a]	2.03	2.38
Water/cement ratio (w/c)	0.5	0.3
Slump (in.)	2.5	0

[a] Staturated surface dry conditions.

were precision-held in place during the casting procedure. Vibration and rodding were used to minimize voids and inhomogeneities. The slabs were cured in a moisture chamber for 28 days after casting. The steel used for the reinforcing bars was 10 mm (3/8 in.) wire meeting ASTM Specification for Steel Bars, Carbon, Cold-Finished Standard Quality (A 108-81). The carbon content was 0.04%. This material is used in welded cage reinforcements for concrete pipe culverts. The surface of the steel was sandblasted to a bare metal finish prior to casting the slabs.

In addition to the slabs, a 5.1 cm (2 in.) diameter cylindrical specimen was exposed in each environment (see Fig. 2). This cylinder contained the same type of rebar used in the slabs, but the concrete was dry-cast, with an effective water-to-cement ratio (w/c) of 0.3, representative of concrete commonly used in "dry-cast" concrete pipe.

The investigation involved determining the mechanism and extent of corrosion in reinforced concrete exposed to environments with various combinations of pH and liquid resistivity. This paper will address in detail the results from tests conducted using the test condition most resembling coastal water environments. The test liquid under consideration consisted of high purity water (with a resistivity of 30 000 ohm · cm, obtained from a high output reverse osmosis unit) with 9100-ppm chloride (added as sodium chloride) and 2570-ppm sulphate (added as sodium sulphate). The pH of the test solution in contact with the concrete was kept at a value of 8.5 by continuous renewal of the test solution with an automatic pumping system. The feed solution was made acidic with small additions of dilute hydrochloric acid (HCl) to keep the rate of renewal at a moderate level (typically 4 to 8 L/day). The resistivity of the liquid at the test container was 35 ohm · cm. Results from another, less aggressive medium will be briefly discussed for comparison.

After completion of the curing period, the specimens were placed in the test container. The specimens were submerged with the water line as shown in Fig. 2. Running tap water

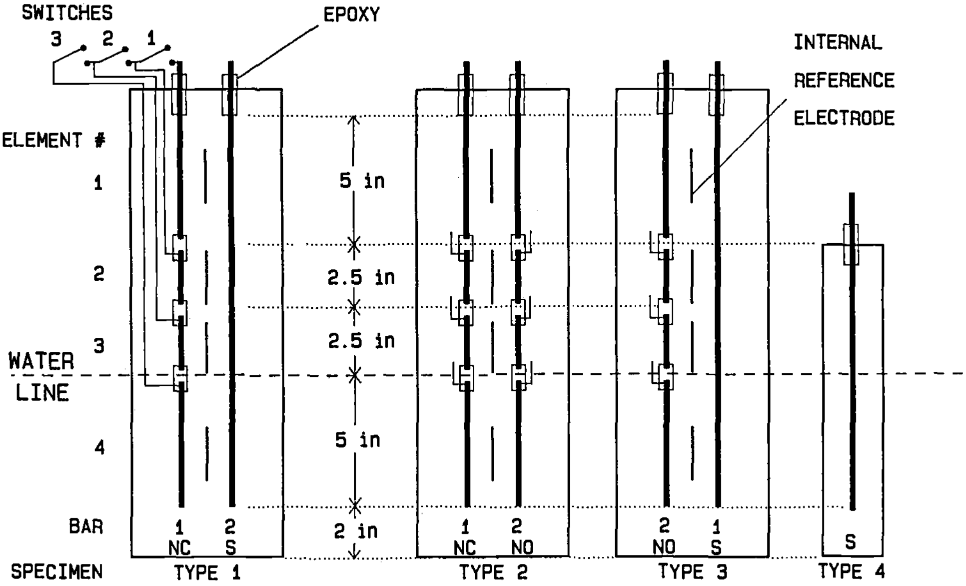

FIG. 2—*Test specimen configuration; S = single bars, NC = multi-element bars where switches were normally closed, and NO = multi-element bars where switches were normally open. For simplicity, external wire connections are shown only for bar elements in Specimen Type 1. The internal reference electrodes had individual external electrical connections (not shown) (1 in. = 25.4 mm).*

was used during the first week of exposure, after which regular exposure to the controlled test solution took place. Exposure times were on the order of one year.

Several parameters were monitored during the exposure time, using a computerized data acquisition system. These parameters included solution pH and resistivity, open circuit potential of rebar, current between electrically coupled rebar segments, electrochemical impedance of rebar, and electrical conductance between parallel rebar segments. The open circuit potential measurements were conducted with respect to the internal reference electrodes and converted to values with respect to an external SCE electrode immersed in the liquid. Intersegment currents were measured with a zero resistance ammeter (ZRA) for the two segmented bars that were kept normally electrically continuous. Electrochemical impedance measurements were conducted with a computerized system [*16*] at periodic intervals, using the internal electrodes as reference and with a graphite counter electrode immersed in the liquid. The electrical conductance between similar parallel rebar elements within a given slab (as in Specimen Type 2, Fig. 2) was measured by momentarily isolating both elements and using a low-amplitude a-c bridge or current source/potential test combination. For segments facing a continuous bar (as in Specimen Type 1, Fig. 2) the segment was isolated and the conductance between element and bar was determined as just indicated.

After about one year of exposure, one of the concrete slabs (Specimen Type 3, Fig. 2) was split open for direct observation of corrosion, concrete condition, and chloride and moisture gradients.

Results

Open Circuit Potentials

Figure 3 shows the typical open circuit potential behavior, as a function of exposure time, of electrically continuous (single and multi-element) rebars in slabs. Additional potential

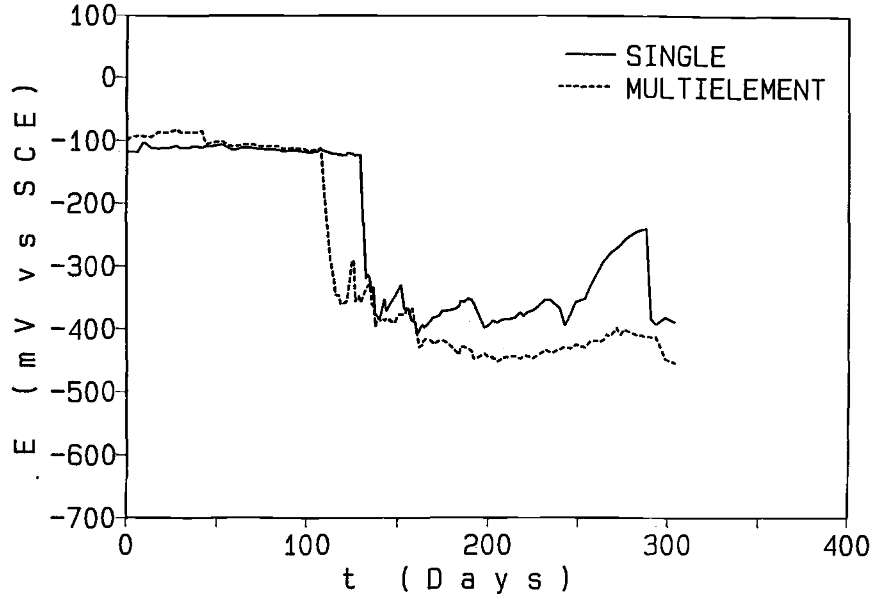

FIG. 3—*Electrode potential versus time for a single bar (Bar 2, Specimen Type 1) and a normally electrically continuous bar (Bar 1, Specimen Type 1).*

versus time results for a multi-element, electrically continuous bar are presented later in Fig. 13. The potentials remained high (within 100 mV of the SCE) for about 100 days until a sudden drop to −250 mV versus SCE, or lower, took place. The time for that initial drop was longer for the rebar in the cylindrical, dry cast specimen. After the initial drop, potential fluctuations took place occasionally, but large negative values were eventually resumed. Figures 4 and 5 show the open circuit behavior observed in each electrically independent element of the two rebars that were kept electrically discontinuous during the test. Where short-term potential fluctuations took place, the main trends are similar in both bars. The No. 1 elements (the highest) remained at a high potential through the test. The No. 3 elements, just above the water line, experienced a potential drop the earliest. The No. 4 elements, in the fully immersed zone, showed the largest potential drop, but took the longest time to evolve. The No. 2 elements showed a behavior comparable to that of the No. 3's, but the potential drops took place at a later date. The time for the first potential drop in the No. 3 elements were comparable to the times observed in the electrically continuous bars in slabs. These trends are summarized in Table 2.

Interelement Currents

The elements in Bar 1 of Specimen Types 1 and 2 were kept normally electrically connected. Interelement currents were measured periodically with the ZRA. Except for a few isolated instances at low current levels, the current was such that electrons flowed from a given element to the element above. This permitted displaying the results by plotting the logarithm of the absolute value of the current as a function of current, as shown in Figs. 6 and 7. In these figures, Levels 1, 2, and 3 correspond to the electronic current flowing through Switches 1, 2, and 3, respectively in Fig. 2. Interelement currents were typically less than 0.1 μA when the potential of the continuous bar was high; the first drop of potential

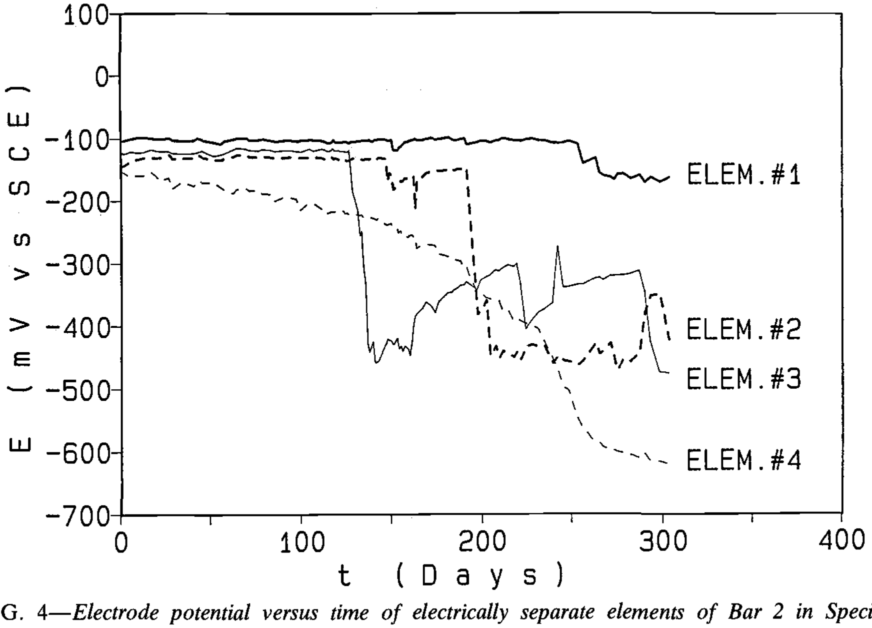

FIG. 4—*Electrode potential versus time of electrically separate elements of Bar 2 in Specimen Type 2.*

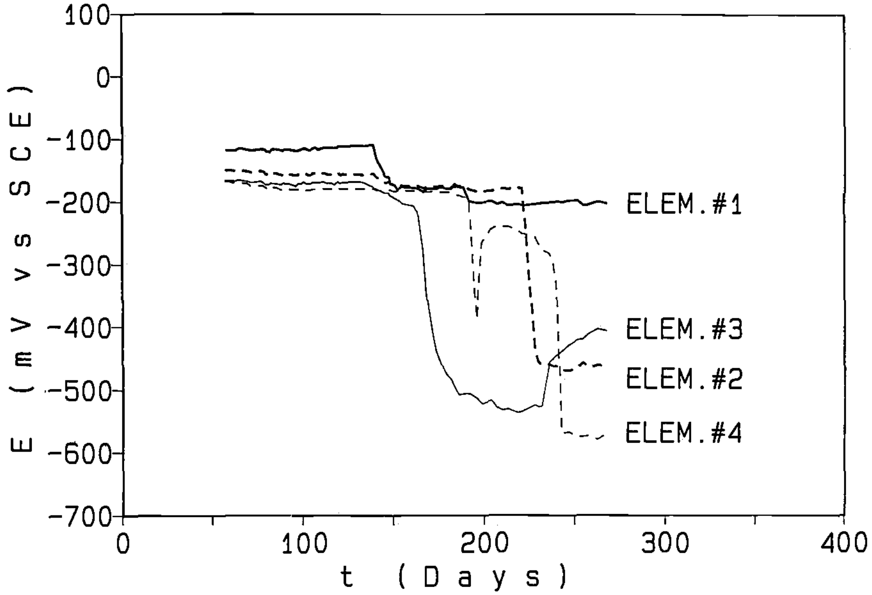

FIG. 5—*Electrode potential versus time of electrically separate elements of Bar 2 in Specimen Type 3.*

of the bar coincided with the first current with a value of 0.3 μA or higher. Interelement currents reached values on the order of 10 μA when corrosion was fully underway.

Interelement Conductance

Figure 8*a* shows the electrical conductance between parallel elements at four different levels of Specimen Type 1. Figure 8*b* shows similar data obtained in an identical slab specimen, but exposed in a low chloride test where the liquid conductivity was maintained at 1000 ohm · cm (chloride content 400 ppm; pH = 4.5 [*14*]). Initially in that test, the values of the concrete conductance were relatively high, due to the moisture conditions from the wet chamber. The initial, high values were roughly maintained during the test at those levels corresponding to portions of the specimen submerged in water or just above the water line. Higher up in the slab, the conductance values followed the drying trend of the concrete, decreasing and stabilizing at relatively low values. The specimens exposed to the high chloride

TABLE 2—*Time to first potential drop.*

Specimen Type	Bar	Element No.	Time (days)
1	1	All	110
1	2	(Single)	130
2	1	All	150
3	1	(Single)	125
3	2	3	130
2	2	3	160
4	...	(Single)	235

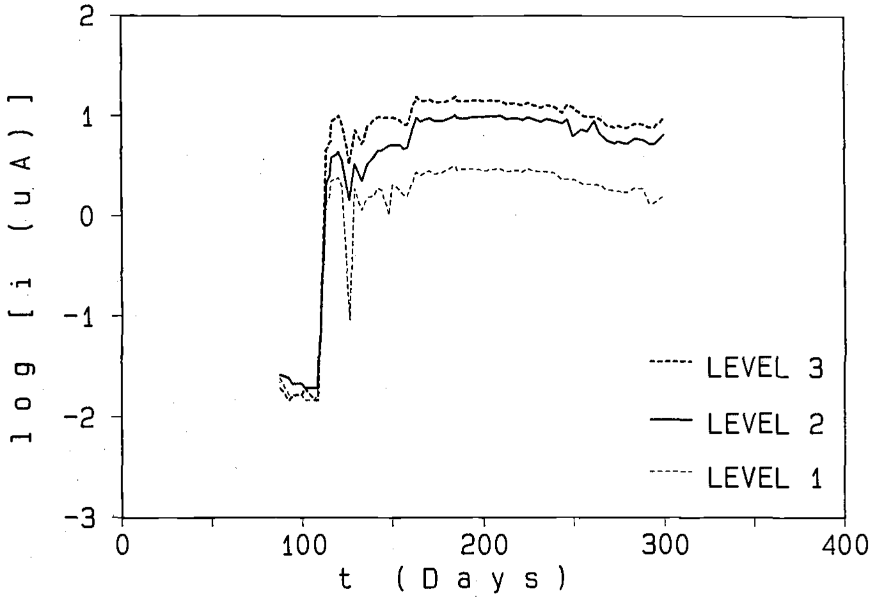

FIG. 6—*Interelement electronic currents versus time at the multi-element, electrically continuous Bar 1 of Specimen Type 1. Levels 1, 2, and 3 correspond to the positions of Switches, 1, 2, and 3, respectively, in Fig. 2.*

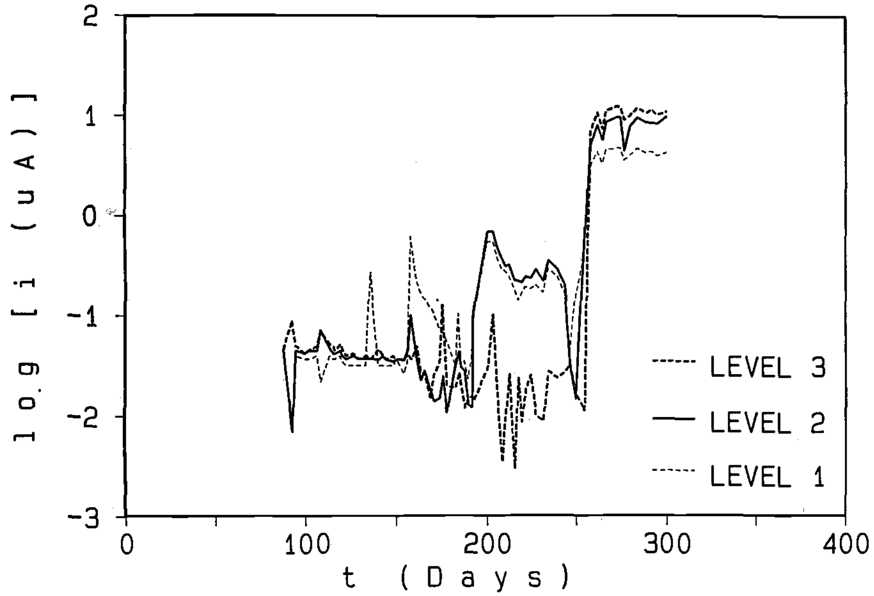

FIG. 7—*Interelement electronic currents versus time at the multi-element, electrically continuous Bar 1 of Specimen Type 2. Levels 1, 2, and 3 correspond to the positions of Switches 1, 2, and 3, respectively, in Fig. 2.*

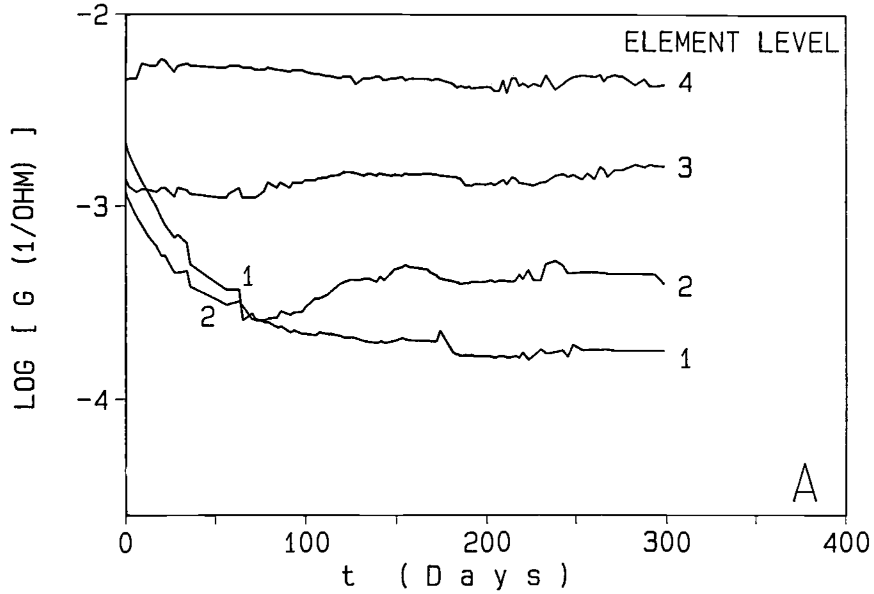

FIG. 8a—*Electrical conductance, G, between pairs of elements at four different levels (keyed as in Fig. 2, with element Level 1 at the top), for Specimen Type 2. Note that elements at Levels 1 and 4 are twice as long as elements at Levels 2 and 3.*

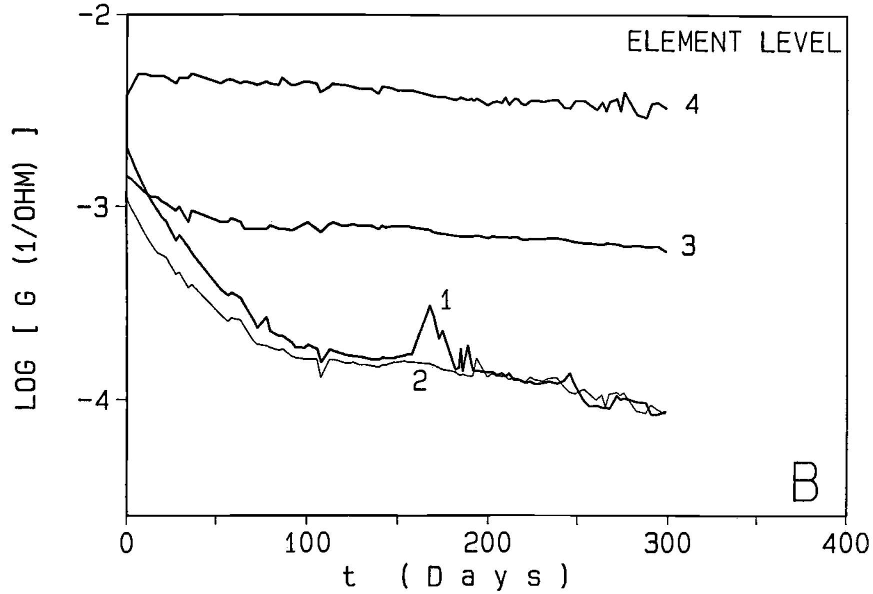

FIG. 8b—*Electrical conductance for a specimen configured identically to that of Fig. 8a, but exposed to a low chloride (1000 ohm · cm) liquid under the same immersion conditions.*

environment considered in this paper showed similar drying-induced trends, except for Level 3 where the trend experienced a reversal After an initial decrease, the conductance at that level increased and roughly stabilized after 150 days of exposure, at around $5 \, 10^{-4}$ ohm^{-1}

Electrochemical Impedance Measurements

Figure 9 (Specimen 3, Bar 1) illustrates the typical impedance behavior observed in electrically continuous bars as the time of exposure progressed At short exposure times, when the open circuit potential was high, the impedance diagram approximated the behavior expected from a resistor-capacitor (R-C) parallel circuit with a very high value of R After the initial potential drop, the impedance diagram evolved as in Figs 9*b* and *c*, toward a closed, somewhat depressed semicircle Figure 10 (Specimen Type 3, Bar 2) shows the impedance behavior of each element of a bar that was kept electrically discontinuous during the test, at day 260 (see Fig 5 for potentials of each element at that time) Different elements show significantly different impedance behavior Elements 2 and 3, above and near the water line, show an impedance diagram resembling that of the electrically continuous bar (Fig 9) at the latest stages of evolution Element 1, in the dry zone, has a diagram characteristic of the early stages of exposure of the continuous bar

Post-Exposure Tests

Figure 11 shows the moisture and chloride content profiles obtained from the post-exposure examination of Specimen Type 3 The chloride content corresponds to drilled-out specimens from the inside of the slab, in the area between the parallel steel elements The moisture is free water (weight change following 48 h at 60°C) of bulk samples (full cross section) obtained from different heights of the slab.

Visual examination of the continuous bar (Bar 1) in Specimen Type 3 revealed that corrosion proceeded only in a zone of about 1 5 cm^2 on the side of the lowest end of the bar The corrosion products were black The average corrosion penetration in that area was estimated to be ~0 2 mm. In the multi-element, electrically discontinuous bar of the same specimen (Bar 2) deterioration appeared to be concentrated at some of the zones where the epoxide coating of the junction between elements joined the metal However, the deterioration did not appear to travel deep into the micro-crevice area. The region showing the highest corrosion occurred in the upper side of the joint between Elements 2 and 3, whereas no evidence of deterioration was observed in Element 1 or in Element 4 The overall extent of visible corrosion in this bar with multiple, isolated elements was much less than that seen in Bar 1 (single construction) of the same slab

Discussion

The open circuit potentials displayed in Figs 3 to 5, and 13 are given with respect to an external SCE submerged in the test liquid The values were obtained by measuring the difference of potential of each element with respect to its closest internal reference electrode, and adding the difference of potential between the internal reference electrode and the SCE The internal and external reference electrodes were typically within ±100 mV of each other This difference showed little variation throughout the test, except when macrocell action (discussed later) developed elsewhere in the slab In those cases (see, for example, the curve for Element 1, Fig 5), a small potential step (typically less than 100 mV) would develop in the potential versus time curve These potential steps take place when macrocell current begins circulating along the longitudinal slab resistance The magnitude of the steps

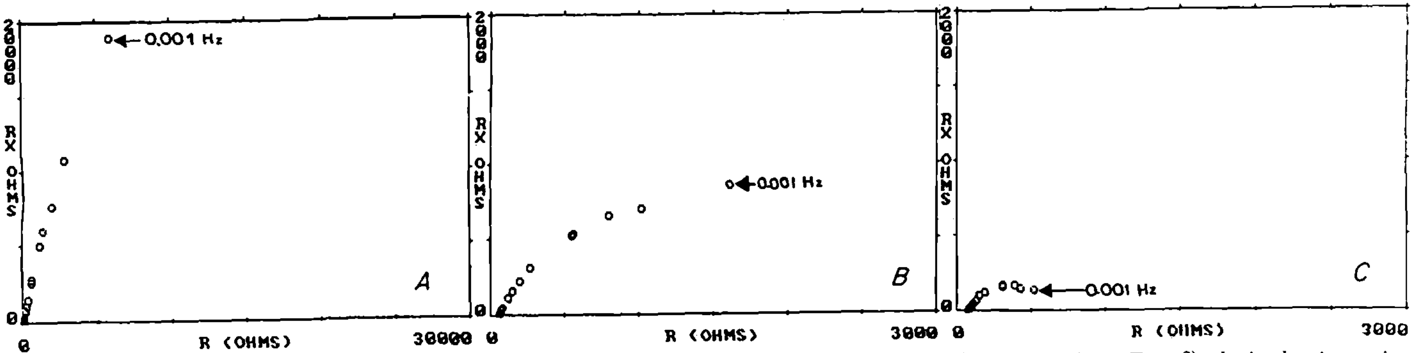

FIG. 9—*Electrochemical impedance diagrams (negative reactance versus resistance) of a single bar (Bar 1, Specimen Type 3) obtained at increasing times of exposure. A = 30 days, −100 mV versus SCE; B = 225 days, −450 mV versus SCE; and C = 298 days, −500 mV versus SCE.*

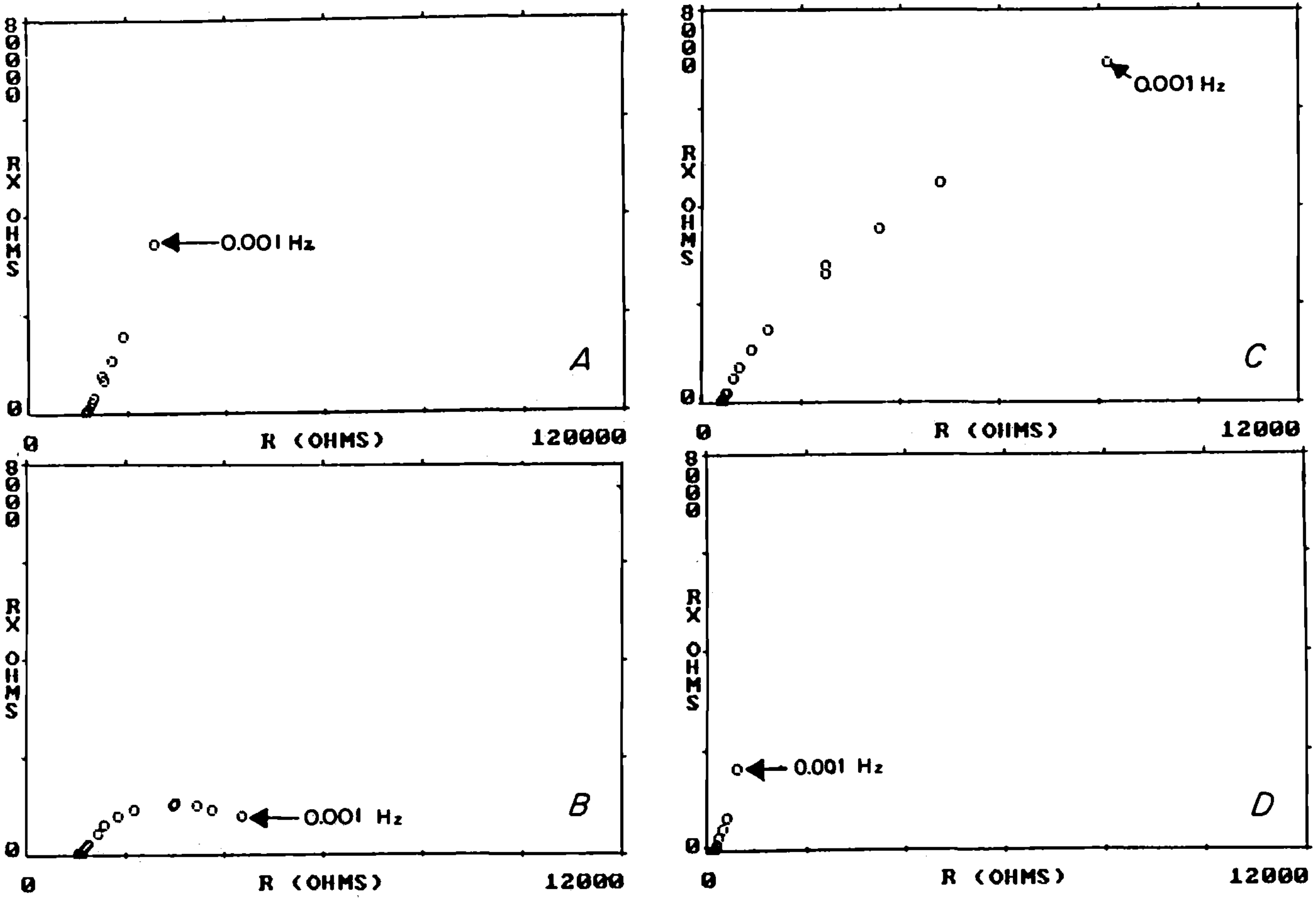

FIG. 10—*Electrochemical impedance diagrams of the different elements of Bar 2, Specimen Type 3 at Day 260. A through D correspond to Elements 1 through 4, respectively.*

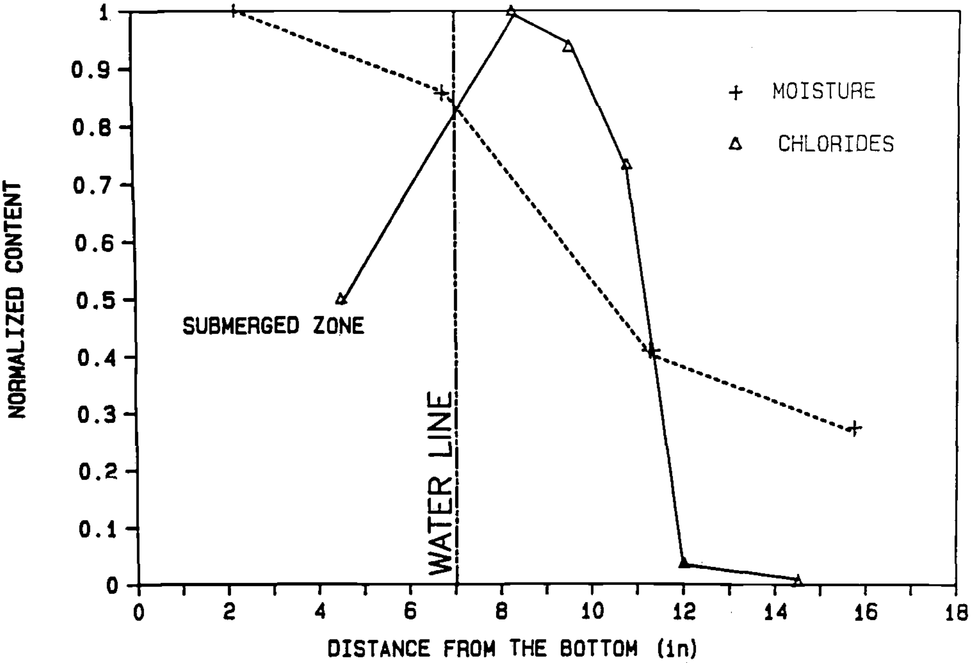

FIG. 11—*Normalized moisture and chloride concentration profiles obtained from Specimen Type 3 after 310 days of exposure, Maximum moisture content measured: 5.95%. Maximum chloride content measured: 26 pounds of chloride per cubic yard of concrete (1 in. = 25.4 mm and 1 pound per cubic yard = 0.594 kg/m^3).*

is small because the slab dimensions are small and the concrete resistivity over most of the slab is moderate. For the same reason, only small potential differences appeared along electrically continuous bars even after local depassivation took place. Consequently, the potential of electrically continuous bars has been represented by a single value, chosen to correspond to the fully submerged portion.

The open circuit potential is often an approximate indicator of the corrosion state of steel in concrete. For steel placed so that oxygen access is not severely limited, and in conditions not very different from highway structures, the criteria described in ASTM Test for Half-Cell Potentials of Uncoated Reinforcing Steel in Concrete (C 876-87) may be applicable. A corrosion behavior transition from passivity to activity is expected under those circumstances when the open circuit potential of the steel reinforcement drops from values near ±100 mV (SCE) to values below −300 mV (SCE). Based on that, the potential trends shown in Figs. 3 and 13, and Table 2, suggest that active corrosion began somewhere in the electrically continuous bars within 100 to 150 days of exposure for the slabs (0.5 w/c) and 235 days for the dry-cast cylinder (0.3 w/c). The ratio of these time values is in agreement with empirical correlations between mixing water content and time to corrosion [*17*].

The potential evolution trends for isolated rebar segments (Figs. 4 and 5) indicate that the regions to experience depassivation first were on the second element above the waterline. Figure 11 shows that, after one year, the concentration of chloride above the waterline reached a value about twice that encountered in the fully submerged region. Thus, this agrees with the observation of early depassivation in that region as well as with the concrete conductance measurements The data in Fig 8 indicate that the interelement conductance at Level 2 begins to deviate significantly from that of a low-chloride test at around Day 100, which is the time of the early potential transitions The conductance data can be converted to approximate conductivity values by considering the element dimensions and their separation A simplified calculation yields a value of 3×10^{-3} ohm^{-1} cm^{-1} for the average conductivity at Level 2 after 300 days of exposure This value is representative of moist, cured concrete [*5*,*6*] The conductance results are affected by shunting effects from adjacent elements and from the salt water in contact with the slab The presence of a moisture gradient in the slab introduces further complications Because of these factors, a quantitative estimate of the chloride concentration distribution from conductance data is not straightforward Nevertheless, the results show that the interelement conductance is an additional useful indicator of conditions leading to corrosion

Once depassivation has taken place in a portion of the rebar, the subsequent behavior is affected by the presence or absence of macrocells The a-c impedance diagrams of rebar elements that were kept normally disconnected from each other (as in Fig 10) show that corrosion proceeds at a faster rate in those elements where depassivation started first This is also in agreement with the visual observations of corrosion at Elements 2 and 3 at the end of the exposure period, in Specimen Type 3 where the elements were kept normally isolated However, in bars where the elements were kept normally interconnected, the interelement currents suggest a different trend The electronic currents move upward, and are of different magnitude at different levels The data in Figs 6 and 7 can be processed to determine whether a given element is a net producer or net consumer of electrons In a simplified macrocell scheme, metal oxidation could be visualized as taking place at one of the elements (the electron generator) while oxygen reduction is taking place at other elements (electron consumers) Calling I_{L1}, I_{L2}, and I_{L3} the electronic currents flowing through the switches at Levels 1, 2 and 3, respectively, the net electronic currents I_i generated at each Element i can be calculated as

$$I_1 = 0 - I_{L1} \tag{1}$$

$$I_2 = I_{L1} - I_{L2} \tag{2}$$

$$I_3 = I_{L2} - I_{L3} \tag{3}$$

$$I_4 = I_{L3} - 0 \tag{4}$$

These currents have been calculated and plotted in Figs 12 and 13 for the two normally electrically continuous bars used in the experiment Figure 12 shows that the potential drop of one of those bars was accompanied by the onset of fairly large interelement currents Element 4 (completely submerged) was a net electron generator once corrosion started The other elements, with one brief exception, were net electron consumers once corrosion started The interelement currents reflected variations on the overall bar potential For example, the small potential spike at approximately Day 120 (Fig 3, dashed line) was paralleled by a momentary decrease in interelement current activity

Figure 13 offers a better opportunity of studying the development of corrosion in another electrically continuous bar, when the process takes some time to evolve In this particular bar, the potential fluctuated before reaching a stable low value (Fig 13*a*) These fluctuations probably reflect the switching back and forth between active and passive behavior, as a result of small variations in environmental conditions, or the formation and breakup of

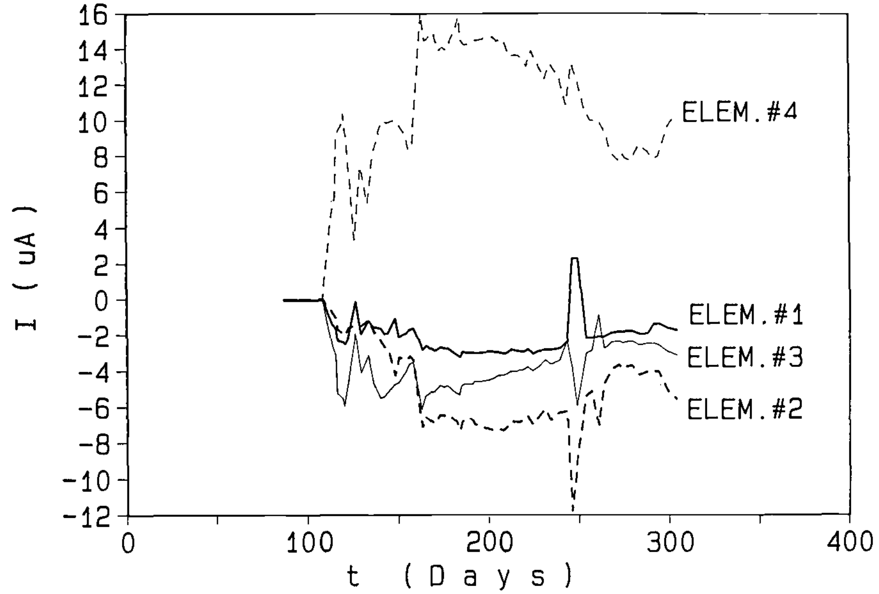

FIG. 12—*Net electronic currents generated (positive) or consumed (negative) during the exposure period by the elements of the electrically continuous multi-element bar (Bar 1) in Specimen Type 1.*

corrosion products at the microscopic level [*18*]. The first potential drop, at around Day 150, was attended by the development of small currents between Elements 2 and 1. The potential then recovered, to fall again near Day 200 when larger currents developed, this time between Elements 3 and 1. At around Day 250, the potential reached values near −500 mV versus SCE and much larger interelement currents developed. Element 4 then showed measurable current activity for the first time, and the overall current levels resembled those documented in Fig. 12.

The currents observed early in Elements 2 and 3 (Fig. 13*b*) indicate that these elements were initially net electron generators. Assuming that cathodic and anodic reactions are restricted to opposite ends of the macrocell, the current measurements suggest that corrosion developed first at Elements 2 and 3. This deduction is in good agreement with the open-circuit potential trends observed in the multi-element, electrically discontinuous bars, where depassivation was observed first at those same elements. While in the electrically discontinuous bars, those two elements continue to show the highest corrosion at later stages, in the electrically continuous bars, corrosion appears to shift to a lower region. In Fig. 13*b*, the current reversal near Day 250 at Element 3 (from net electron generation to net consumption) and the abrupt onset of net electron generation at Element 4 is suggestive that the latter element has begun corroding at a considerable rate, while the upper elements are being the site of oxygen reduction reactions. In the bar of Specimen Type 1 (Fig. 12), corrosion may have started first at Element 3, but if so the transition to high corrosion at Element 4 was very fast. Macrocell action can be very complex and net electron generation does not necessarily imply the predominance of anodic, metal dissolution reactions. However, this interpretation of current trends for electrically continuous bars is supported by the direct observation of considerable corrosion at the bottom of Bar 1 in Specimen Type 3, and by the a-c impedance and corrosion morphology observations in the electrically discontinuous bars.

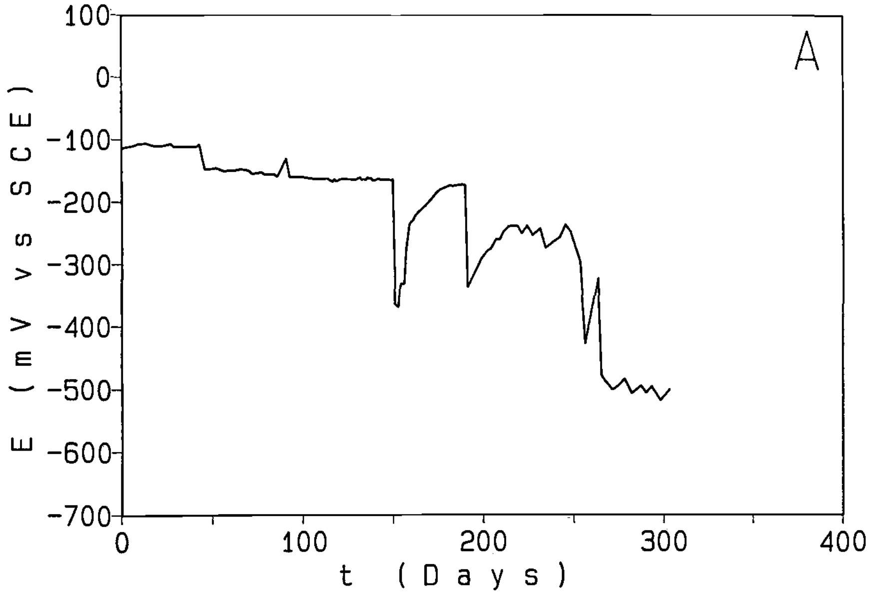

FIG. 13*a*—*Electrode potential versus time for the multi-element, electrically continuous bar* (*Bar 1*) *in Specimen Type 2.*

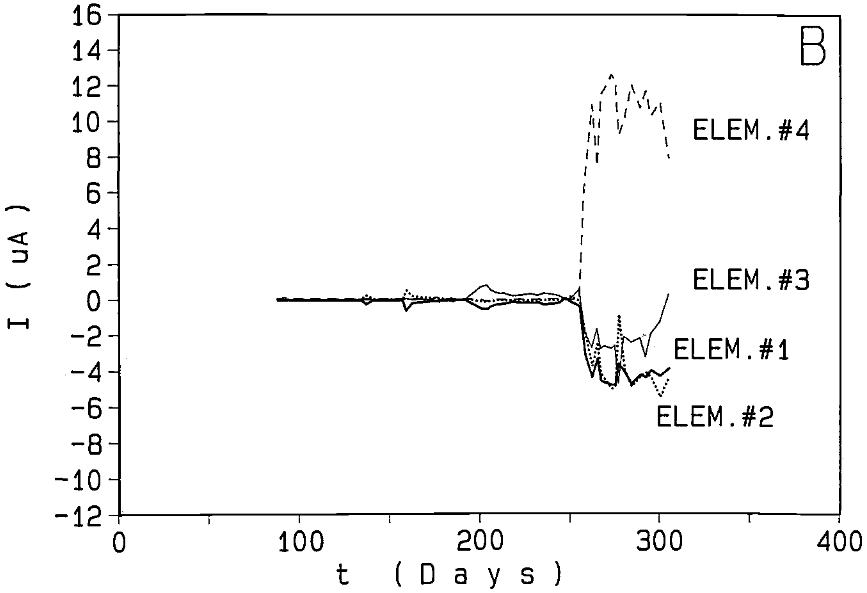

FIG. 13*b*—*Net electronic currents generated* (*positive*) *or consumed* (*negative*) *by the elements of the bar.*

The observations just described can be used to advance the following sequence of events describing the progression of corrosion on an electrically continuous bar When a freshly cured slab is partially submerged in water, the upper parts begin to dry and a moisture concentration gradient is established This results in upward transport of chloride-rich water and evaporation at an intermediate level above the water line (somewhere near the level of Elements 2 or 3) Chlorides begin to accumulate in that area, possibly first near the surface of the slab and then further inside As indicated by the post-test examination, chloride levels can be higher than those in the fully submerged area The critical chloride level for depassivation is reached at the accumulation region, prior to other areas in the slab At that moment, iron begins to oxidize in that region, which becomes an electron source for the rest of the electrically continuous bar The potential of the whole bar is shifted downward by an appreciable amount Other portions of the rebar in contact with high chloride concentrations will also enter the active corrosion regime This could happen immediately (as in the case of Fig 12), or after some time to allow for reaching a higher chloride concentration at the metal surface (Fig 13) The zone observed to undergo this transition is the submerged portion, probably because of its considerable chloride concentration and low-resistance electrolytic path connection with Element 3 Once corrosion starts in this region, it is likely to take place with less anodic polarization because of the easy availability of electrolyte Since the conductance of the concrete is appreciable, the cathodic reaction can take place in the upper regions without excessive ohmic polarization and taking advantage of easier oxygen transport than in the fully submerged zone These conditions result in the formation of a macrocell with electron transport through the metal from the lower to the upper portions of the bar With these assumptions, the macrocell should be relatively stable and corrosion will take place preferentially on the lower portion of the bar over an extended period of time

The proposed mechanism describes the conditions prevalent in a short, electrically continuous rebar spanning the area around a fixed water line For a long rebar, extending several feet above and below the waterline, the zone of highest corrosion is not likely to be at the bottom of the bar Once active corrosion begins at the evaporation zone, the potential drop is expected to be limited to a relatively small portion of the rebar. Since longer resistive paths are involved, the ohmic polarization is no longer small except for a zone close to the waterline In an actual marine environment, tidal and spray action will aggravate chloride accumulation in the area above and below the average water line by introducing wetting-evaporation cycles Under those conditions, corrosion may be conspicuous even above the tidal portion. This is in agreement with numerous observations of piling deterioration in semi-tropical environments [*10*]

In addition to providing mechanistic information, the tests offered an opportunity to compare different ways of evaluating the severity of corrosion Large electrode potential fluctuations, especially if they take place over a short time interval, appear to be reliable indicators of the onset of active corrosion However, the potential measurements cannot provide an indication of the rate of corrosion, or provide a reliable indication of where localized corrosion is taking place in the short rebars used here Dividing the rebar into elements with individual connections has provided a means of studying the location of first corrosion initiation, and the shift of the position of highest corrosion with time Measurement of the interelement currents provides a quantitative indication of differential corrosion activity However, the differential currents cannot be converted into absolute rates of deterioration unless simplifying assumptions are made about the corrosion state of some of the electrodes For example, when interpreting the results from Figs 12 and 13, one can propose that since Elements 1, 2, and 3 are under partial moisture conditions, then the primary electrochemical reaction taking place there is oxygen reduction Making the complementary assumption that Element 4 is the site of only metal oxidation, then a metal oxidation rate can be calculated for that element assuming an oxidation state and using the net current of electrons leaving the element

$$dw/dt = I_4 \quad M_w/n \quad F \tag{5}$$

where dw/dt is the iron oxidation rate expressed in grams per second, M_w is the molar weight of iron in grams, n is the oxidation state (assumed to be +2), and F the Faraday constant Using Eq 5 and an average value for I_4 of 12 μA (Figs 12 and 13*b*), a rate of oxidation of approximately 0 3 mg/day is obtained

The impedance measurements offer an alternative way of evaluating the rate of deterioration Because sizable interelement currents complicate greatly the evaluation of impedance diagrams, this analysis will be limited to normally isolated rebar elements, or to whole electrically continuous rebars The diagrams shown in Fig 9 for a single, continuous bar are typical of steel in moist concrete exposed to ambient air, at increasing stages of deterioration [*19*] The impedance diagram in Fig 9*a* can be approximated by a segment of semicircle, centered close to the real axis, with a diameter on the order of hundreds of kilo-ohms This is characteristic of rebar in the passive state, with a negligible corrosion rate [*19*] Figures 9*b* and *c* show diagrams that can be roughly approached by semicircles (centered below the real axis) with diameters of about 3000 and 600 ohms, respectively A nominal corrosion current can be obtained by assuming that the diameter of the semicircle is equivalent to the polarization resistance and applying the Stern-Geary equation

$$I_{\text{corr}} = B/R_p \tag{6}$$

where I_{corr} is the corrosion current, B is the corrosion constant (assumed to be about 26 mV for active iron [*19*]), and R_p is the polarization resistance Application of Eq 6 to Fig 9*c*, and conversion of the resulting current into an oxidation rate by means of Eq 5, yields a value of approximately 1 3 mg/day

Individual elements of a discontinuous bar produce impedance diagrams corresponding generally to the stage of corrosion evolution of each element, following generally the pattern established in Fig 9. Thus in Fig 10, Elements 2 and 3, which had experienced early potential transitions, show impedance diagrams suggestive of relatively high corrosion rates Element 1, at a still high potential, shows a diagram characteristic of passive material Element 4, while displaying a low open circuit potential, shows a primarily capacitive response which suggests a large nominal polarization resistance This element is isolated and, because of its being fully submerged, subject to a limited supply of oxygen The impedance and potential behavior is consistent with that expected from an element in the active state, but corroding at a very low rate due to the limited extent of the cathodic reaction If the elements were short-circuited, it is easy to visualize that Element 4 would begin to corrode at a greater rate while supplying electrons to the upper elements which in turn would corrode at lower rates than before This is in agreement with the expectations of the corrosion evolution sequence discussed earlier The impedance diagrams in Fig 10 were obtained by placing a counter electrode in the liquid and using the internal reference electrodes nearest to each element tested Taking into consideration the dimensions of the reference electrode and the distance to the elements tested, the high frequency intercept of each impedance diagram can be used to evaluate the conductivity of the concrete between the electrodes The results were in reasonable agreement with the values reported in Fig 8 [*14*]

Another rough estimate of the rate of metal loss can be attempted from the post-exposure examination of Bar 1 in specimen Type 3 From the dimensions of the deteriorated area (1 5 cm^2, average depth of loss 0 2 mm), an estimated volume of metal consumed of 0 03 cm^3 is obtained Taking into account the density of steel and that the bar showed corrosion activity for about 125 days, the nominal rate of metal loss calculated by this method turns out to be approximately 2 mg/day

The rates of deterioration estimated earlier, 0 3, 1 3, and 2 mg/day, are concordant values obtained, by three different methods, from two different bars embedded in similar concrete slabs and exposed to the same environment Keeping in mind the limitations of the underlying assumptions and the sample variability expected in these systems, the values are in reasonable agreement The techniques described appear to provide useful tools to diagnose the state of corrosion of a partially submerged reinforced concrete structure

Conclusions

1 Corrosion initiation in rebars within partially immersed concrete slabs takes place at the region where chlorides accumulate This region develops above the water line as a result of capillary transport and evaporation of water

2 Concrete conductance measurements could be correlated with direct observations of chloride accumulation in the evaporation zone of the test specimens

3 Differential current measurements show that after its initiation, corrosion proceeds by the formation of macrocells Metal dissolution tends to take place in regions of greater electrolyte availability Oxygen reduction occurs preferentially where the concrete is not saturated with water

4 In isolated rebar segments, where macrocell currents are limited, corrosion is most extensive above the water line, in the area of chloride accumulation and fast oxygen transport Short segments under complete immersion tend to corrode at a relatively low rate after depassivation takes place

5 Electrochemical impedance and differential current measurements of corrosion show quantitative, order of magnitude agreement with a direct observation of damage Simultaneous electrode potential, differential current, electrochemical impedance, and concrete conductivity measurements provided a coherent set of observations for the determination of corrosion development in the system tested

Acknowledgments

Funds for this investigation were provided by the Florida Department of Transportation (FDOT) The opinions, findings and conclusions expressed in this document are those of the author and not necessarily those of the FDOT

The authors are indebted to Rick Kessler (FDOT) for many helpful discussions, and to the personnel of the Corrosion Research Group, FDOT, for their assistance in preparation of the test specimens

References

[1] Slater, J E , *Corrosion of Metals in Association with Concrete, ASTM STP 818,* American Society for Testing and Materials, Philadelphia, 1983

[2] Makita, M , Mori, Y , and Katawaki, K , "Marine Corrosion Behavior of Reinforced Concrete Exposed at Tokyo Bay," *Performance of Concrete in Marine Environments,* ACI Publication SP-65, V M Malhotra, Ed , American Concrete Institute, Detroit, 1980, p 271

[3] Geymayr, G , "Repair of Concrete in Tropical Marine Environment," *Performance of Concrete in Marine Environment,* ACI Publication SP-65, V M Malhotra, Ed , American Concrete Institute, Detroit, 1980, p 527

[4] Tuuti, K , *Corrosion of Steel in Concrete,* Swedish Cement and Concrete Research Institute, Report CBI 10 4 82, Stockholm, 1982

[5] Buenfeld, N and Newman, J , *Cement and Concrete Research,* Vol 16, 1986, p 511

[6] Lay, P , Lawrence, P , Wilkins, N , and Williams, D , *J Applied Electrochemistry* Vol 15, 1985, p 755

[7] Popovics, S , Simenov, Y , Bozhinov, G , and Barovsky, N , "Durability of Reinforced Concrete in Sea Water," *Corrosion of Reinforcement in Concrete Construction,* A Crane, Ed , Ellis-Horwood, Ltd , Chichester, UK, 1983, p 19

[8] Aziz, M and Mansur, M , "Deterioration of Marine Structures with Special Emphasis on Corrosion of Steel and its Remedies," *Corrosion of Reinforcement in Concrete Construction,* A Crane, Ed , Ellis-Horwood, Ltd , Chichester, UK, 1983, p 91

[9] Leeming, M , "Corrosion of Steel Reinforcement in Offshore Concrete-Experience from the Concrete-in-the-Oceans Programme," *Corrosion of Reinforcement in Concrete Construction,* A Crane, Ed , Ellis-Horwood, Ltd , Chichester, UK, 1983, p 59

[10] Powers, R , "Corrosion Control of Marine Structures," presented at the NACE SE Region Meeting, National Association of Corrosion Engineers, Panama City, FL, 19–22 Oct 1987

[11] Locke, C and Boren, M , "The Effect of CMA on Corrosion of Reinforcing Steel in Portland Cement Concrete," Paper 129, Corrosion/87, National Association of Corrosion Engineers, Houston, 1987

[12] Wyatt, B and Irvine, D , *Materials Performance,* Vol 26, Dec 1987, p 12

[13] Sagüés, A , "Corrosion Measurements of Reinforcing Steel in Concrete Exposed to Various Aqueous Environments," Paper 118, Corrosion/87, National Association of Corrosion Engineers, Houston, 1987

[14] Aguilar, A , "Corrosion of Reinforcing Steel in Partially Submerged Concrete," M S thesis, College of Engineering, University of South Florida, Tampa, 1988

[15] Martin, B and Bennet, J , "An Activated Titanium Mesh Anode for the Cathodic Protection of Reinforcing Steel in Concrete," Paper 147, Corrosion/87, National Association of Corrosion Engineers, Houston, 1987

[16] Sagüés, A , "A System for Electrochemical Impedance Corrosion Testing Using a PC With Isaac-Cyborg Interface," Paper 104, Corrosion/88, National Association of Corrosion Engineers, Houston, 1988

[17] California Test Method No 532-A, California Department of Transportation, 1967

[18] John, D , Eden, D , Dawson, J , and Langford, P , "Corrosion Measurement on Reinforcing Steel and Monitoring of Concrete Structures," Paper 136, Corrosion/87, National Association of Corrosion Engineers, Houston, 1987

[19] Gonzalez, J , Molina, A , Escudero, M , and Andrade, C , *Corrosion Science,* Vol 25, 1985, pp 518 and 917

Edward Escalante[1] *and Satoshi Ito*[2]

Measuring the Rate of Corrosion of Steel in Concrete

REFERENCE: Escalante, E and Ito, S , **"Measuring the Rate of Corrosion of Steel in Concrete,"** *Corrosion Rates of Steel in Concrete, ASTM STP 1065,* N S Berke, V Chaker, and D Whiting, Eds , American Society for Testing and Materials, Philadelphia, 1990, pp 86–102

ABSTRACT: A study on the relationship of pH, chloride concentration, and oxygen concentration shows that a drying cycle, which locally concentrates chloride and oxygen, initiates the corrosion of steel in concrete Once corrosion is initiated, the pH at the anodic areas decreases allowing corrosion to proceed more easily Oxygen controls the rate of corrosion, but chloride affects the number of sites where corrosion initiates

Using a small portable computer system that applied the technique of polarization resistance with current interruption for elimination of iR error, the voltage measurement error generated when current flows through a resistive media, the corrosion of steel in concrete was measured in the laboratory The portable system was then used to perform preliminary rate of corrosion measurements on reinforcing steel in three bridge decks in Frederick County, Maryland

KEY WORDS: bridge deck deterioration, chloride concentration, corrosion of steel, corrosion rate measurement, effect of pH, iR error, oxygen concentration, polarization resistance, reinforcing steel in concrete, corrosion, steels, concrete

A literature search made at the beginning of the program revealed that many of the studies on the corrosion of steel in concrete were directed at determining the effect of chloride ion and concrete mixture design on the corrosion process [*1*] Only two references considered the effect of oxygen, and none were found on the corrosion of steel in an alkaline environment [*2,3*] On the basis of this, our first effort was directed at learning more about the role of oxygen concentration, chloride concentration, and pH on the corrosion of steel in alkaline environments [*4*] These initial experiments were carried out in solutions, sand, and mortar The second phase of this study was directed at controlling the corrosion of steel in a concrete environment and developing a portable computer system to measure the corrosion rate of steel in the concrete using a nondestructive electrochemical technique [*5*] The third and final phase was to use this portable system to measure the corrosion of reinforcing steel in three bridge decks in Frederick County, Maryland

Procedure

Preliminary Measurements—Phase 1

Coupons in Solution—Coupons of steel (AISI 1018 steel) were cut from 1 mm sheet to 2 by 10 cm and weighed before and after exposure The top portion of the specimen,

---

[1] Metallurgist, National Bureau of Standards, Gaithersburg, MD 20899

[2] Research scientist, Nippon Steel Corporation, Kawasaki, Japan

extending through the electrolyte/atmosphere interface, was coated. These steel specimens were placed in an environmental matrix of cells containing solutions of calcium hydroxide in which the oxygen content was controlled by bubbling an oxygen-nitrogen mixture through the solution and in which pH and chloride content were controlled. Concentration of oxygen was maintained at 0.5, 2, 3.5, and 8 ppm, pH ranged from 10.5 to 12.5, and chloride was maintained at concentrations of 1 × 10^{-4} to 6 mol/L using sodium chloride. A selective ion electrode was used to measure oxygen concentrations. Exposure times of up to 600 h were used.

Coupons in Sand—To evaluate the effect of moisture, coupons were imbedded in a sand mixture of 72% sand, 14% calcium hydroxide, and 14% sodium chloride held in small perforated ceramic crucibles in an atmosphere of flowing air with controlled moisture content. In one series of experiments, steel specimens were imbedded in a sand mixture saturated with sufficient distilled water to fill the voids between the sand particles and then exposed to flowing moisture saturated air for the entire period of exposure. In a second series, steel coupons were placed in a dry sand mixture which was then exposed to moisture saturated flowing air. Eventually the moisture content of this initially dry sand mixture increased to saturation. Once saturated, the wetting cycle was reversed by placing the crucibles in a desiccating atmosphere (above a desiccant of calcium chloride). Changes in mass of the steel coupons were measured by gravimetric means.

Coupons in Mortar—The effects of varying moisture and chloride content in mortar on corrosion of steel were evaluated. Mortar mixtures (cement:sand:water = 2:4:1) with a chloride concentration range from 0.1 to 1.2% were cast around steel coupons (0.5 by 10 by 65 mm) resulting in a mortar cover of 4 mm. Twenty-four hours after casting, the coupons were exposed in two sets. One set was immediately immersed in calcium hydroxide-sodium chloride solutions, and the other set was allowed to dry for one week before immersion. After immersion, the polarization resistance for each specimen was measured periodically. This measurement was made by polarizing the specimens from −10 to 10 mV using potentiostatic control with positive feedback iR compensation and a scan rate of approximately 4 mV/min. Measurements of coupon mass loss were also made.

Measurements in Concrete—Phases 2 and 3

Preliminary studies indicated that corrosion of steel in concrete can be measured by polarization methods [*4*]. Field measurements on other systems, using manually controlled equipment, revealed that this manual approach is slow, tedious, and not suitable for rapid measurements necessary on a bridge deck. Furthermore, eliminating iR error, the voltage measurement error generated when current flows through a resistive media, is always difficult and, at times, questionable with these manually controlled methods. Details of this portion of the study have been described previously, and the following is a general overview of the use of a portable, battery powered computer system applying the techniques of polarization resistance and current interruption as a means of measuring the corrosion of steel in concrete [*6, 7*].

Laboratory—The computer controlled device operates by modulating the current applied between the working electrode (WE) and the counter electrode (CE), so as to maintain a potential difference, ΔE, between the WE and the reference electrode (REF) which is 10 mV less than the same potential difference at open circuit. The voltage measurement, however, is taken during a brief period while the current is interrupted, so that the potential due to the iR drop is absent, but soon enough (75 ms) after the interruption of the current that the potential due to polarization of the WE has not yet decayed significantly

Briefly, the measurement sequence occurs in two stages as follows Immediately after the open circuit potential is measured, the first stage, called the "setting" stage, begins, and it is during this period of time that the WE electrode is polarized to $\Delta E = -10$ mV Once the computer senses that the preselected target voltage of -10 mV is reached, it enters the second stage, called the "holding" stage, where the applied current is controlled to maintain the WE potential at -10 mV for a preselected period of time (3 min) The open circuit potential (versus a saturated calomel electrode) and the series of readings of polarized potential and applied current, taken during the holding stage, are stored in memory and used to calculate corrosion current An example of the potential and current traces as observed with a digital oscilloscope during a measurement sequence are shown in Fig 1*a* Figure 1*b* is an idealized drawing of the oscilloscope trace identifying the setting and holding stages Not easily visible in this figure is the current interruption taking place during the measurement

By magnifying the wave forms of current and potential, the details of current interruption events can be readily examined The idealized wave forms of current and potential are illustrated in Fig 2, showing their relationship as a function of time, and also showing that the duty cycle is 2 2 s with the current on and 0 4 s with the current off Applied current is measured at the end of the current decay curve, just before the current is turned off As indicated earlier, the current is modulated during the "holding" stage in order to maintain the polarized potential at the target voltage of $\Delta E = -10$ mV

Figure 2a illustrates the response of the WE potential to the applied current, showing the instant change in potential (iR) as current is applied, followed by a time dependent change as the WE is polarized during the 2 2 s of current application When the applied current is turned off, the iR component of potential is eliminated and the polarized potential of the WE can be measured This iR-free measurement of potential, identified as V3 occurs 75 ms after the current is turned off The cycle is then repeated 0 4 s later as illustrated

Initial measurements were all made in the laboratory as the software and hardware were in the stages of development. Cleaned and weighed steel rods 1 3 cm in diameter and 15 2 cm long encased in cast concrete cylinders were used for laboratory measurements Concrete mixes with and without chloride added were used The steel in concrete specimens were immersed in simulated pore solution (0 6 *M* potassium hydroxide (KOH), 0 2 *M* sodium hydroxide (NaOH), 0 001 *M* calcium hydroxide ($Ca(OH)_2$)), simulated pore solution saturated with sodium chloride, or saturated solution of sodium chloride as listed in Table 1 [*8*] Some specimens were continuously immersed while others were immersed 2 h a day and allowed to air dry the remaining 22 h Specimens were exposed for a total period of 115 to 148 days, and measurements were made on each specimen once a day, five days a week Mass loss measurements were carried out in accordance to ASTM Standard Practice for Preparing, Cleaning, and Evaluating Corrosion Specimens (G 1-81) (Chemical Designation C 3 1)

Field—Three bridges in Frederick County, Maryland, were chosen for the study on the basis of age, known history, and condition Thus, Bridge No 10029 was a 54-year-old structure with fine cracks scattered over the surface of the deck, but otherwise in good condition Bridge No 10100, along a major interchange, was 17 years old and appeared to be in excellent condition The newest bridge, No 10059, was 13 years old and also in good condition, but cracks are beginning to appear along the rebar positions Deicing salts for snow removal are used on all three decks

The procedure for measurements in the field was essentially identical to that used in the laboratory The differences were mostly physical For example, the configuration of the

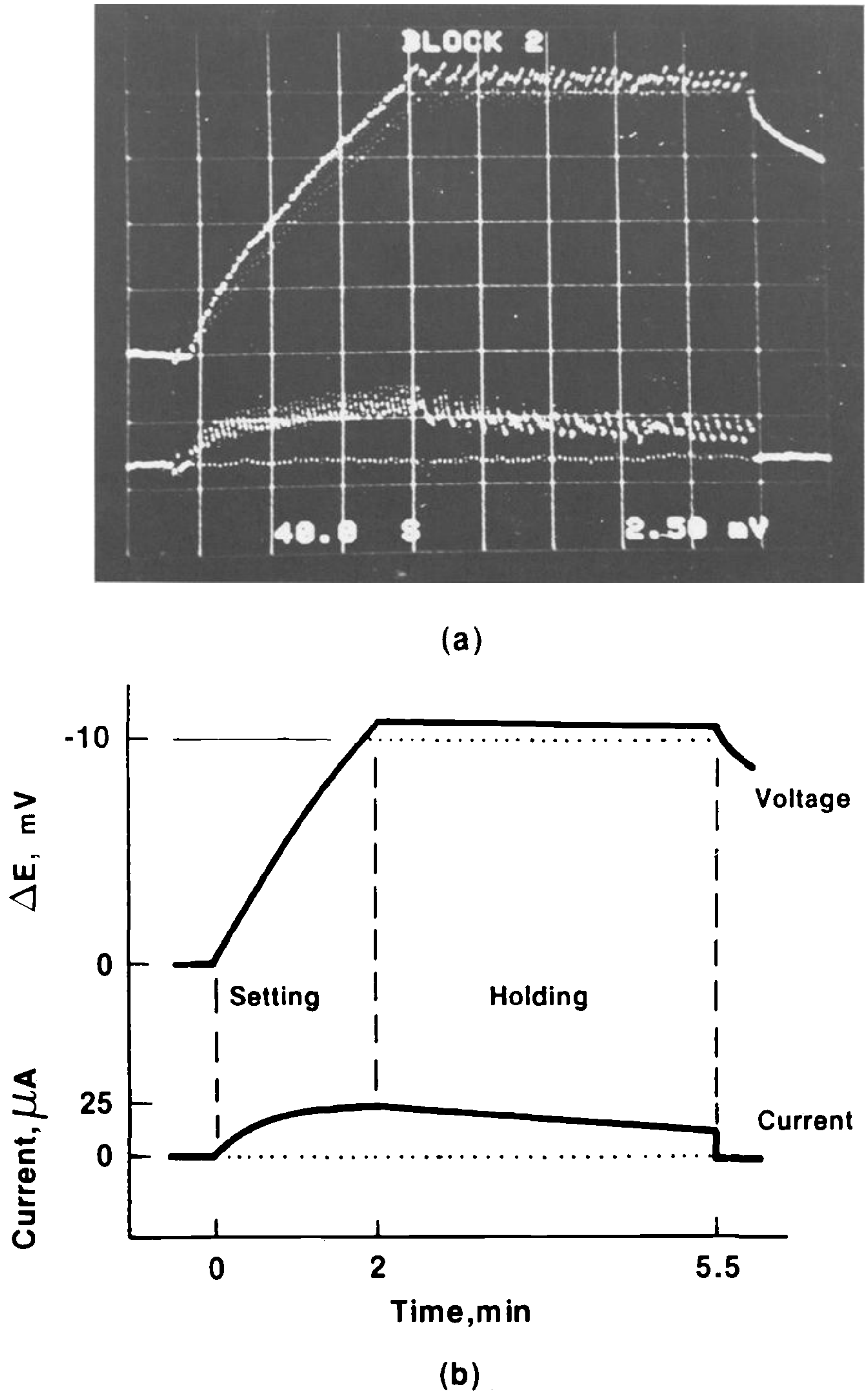

FIG. 1—(a) *Digital oscilloscope traces of potential and current versus time during measurement sequence.* (b) *Idealized traces of potential and current versus time during measurement sequence.*

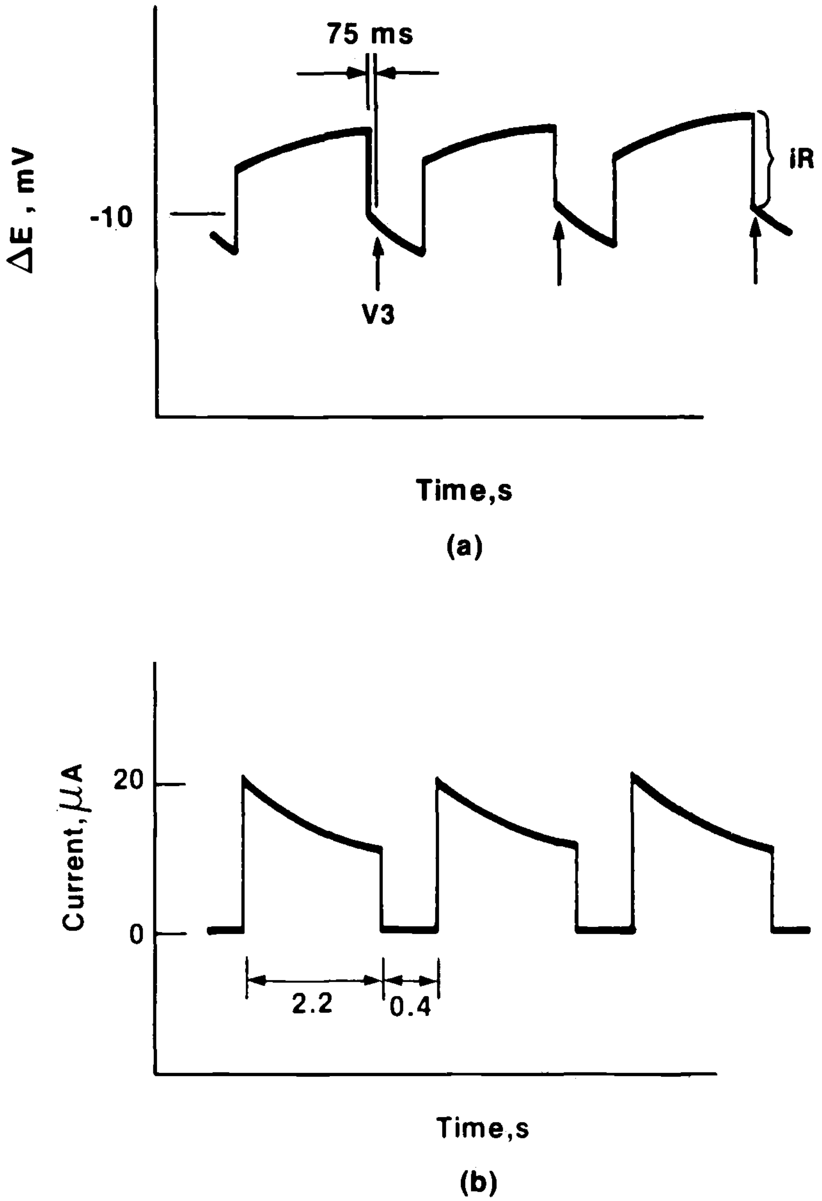

FIG. 2—(a) *Details of potential versus time illustrating effects of current interruption.* (b) *Details of current versus time illustrating current interruption wave form.*

electrodes in the field was as illustrated in Fig. 3 showing the use of a copper-copper sulfate reference electrode, a lead (Pb) ring for a counter electrode, and steel reinforcing bar in the concrete bridge deck as the working electrode. Note that the CE and the REF are on a wetted absorbent material (towel or sponge) and are supported by a clear plastic holder that facilitated alignment of the electrodes. A 1% solution of liquid detergent in tap water was used as a wetting agent. Scrubbing of the concrete surface with a wire brush to break-

TABLE 1—*Conditions of exposure*

Specimen No	Type of Immersion	Condition
1	alternate	Cl free concrete Cl free pore solution
2	continuous	Cl free concrete Cl free pore solution
3	alternate	Cl free concrete Cl in pore solution
4	continuous	Cl free concrete Cl in pore solution
5	continuous	Cl in concrete Cl in pore solution
6	continuous	Cl in concrete Cl in pore solution
7	alternate	Cl in concrete Cl in pore solution
8	alternate	Cl in concrete Cl in pore solution
9	continuous	Cl in concrete Cl in distilled water
10	continuous	Cl in concrete Cl in distilled water
11	alternate	Cl in concrete Cl in distilled water
12	alternate	Cl in concrete Cl in distilled water

up the oil film on the surface proved useful As a precaution, a small area of concrete (15 by 15 cm) was removed to expose the reinforcing bar for making good contact to the WE. One problem encountered was that of eliminating electrical noise, and unfortunately, this process was time consuming One such elusive noise problem manifested itself in irreproducibility of the WE potential Lengthy investigation revealed that corrosion of the steel counter electrode originally used was generating an electric current that seriously affected the potential measurement By trial and error, it was discovered that a lead (Pb) CE reduced or eliminated the effect Another serious problem encountered in the field measurements was electronic equipment damage resulting from mechanical vibration generated during transportation Using a dummy cell, the equipment and cables were checked before and after every series of measurements Three measurements were made on each bridge span every two weeks over a four month period during the summer The location of each measurement was permanently marked on the bridge deck surfaces so that the measurements could be repeated at the same location each time

Only a small area of rebar was polarized during the measurement process. Based on earlier current distribution measurements, it was determined that current from the CE to

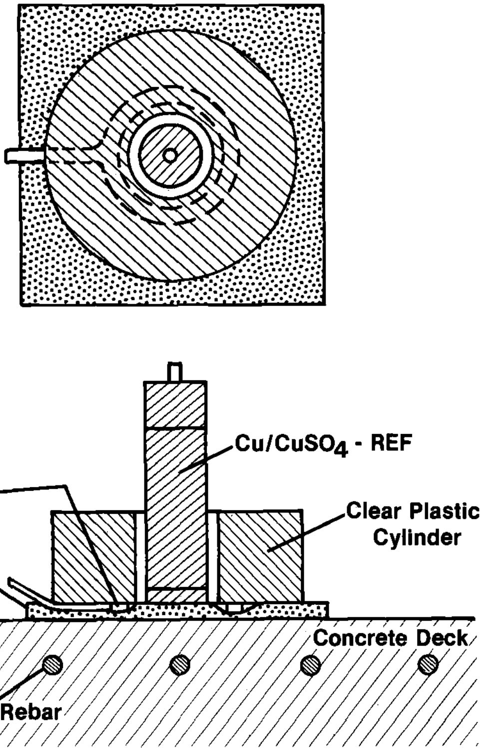

FIG. 3—*Configuration of electrodes on bridge deck during field measurements.*

the WE is limited to a small area of the rebar [5]. Calculations of corrosion rate on the bridge decks were based on an area of the rebar twice the area of projection from a 6-cm-diameter CE on a 1.6-cm rebar, and a Tafel slope of 150 mV, obtained through polarization measurements.

Results and Discussion

Preliminary Measurements

Coupons in Solutions—The solution experiments revealed several interesting results as will be described. For example, it was found that even in the absence of chloride ions, pH controls the initiation of corrosion of steel. Figure 4 is a plot of the mass loss of steel as a function of time at various pH levels and an oxygen concentration of 8 ppm, showing that in the period of exposure of this experiment, the corrosion of steel was negligible at a pH of 12.5 (saturated calcium hydroxide solution). However, as the environment is made slightly less alkaline (pH = 11.5 to 12), corrosion initiated in approximately 240 h. At a pH of 10.5, corrosion is initiated immediately on immersion as the data show. Thus, as the pH is reduced from a level of 12.5, corrosion initiation time is reduced.

The same experiment was repeated in the presence of chloride ions as illustrated in Fig. 5, and it was found that corrosion did not occur at a pH of 12.5. When pH was reduced to

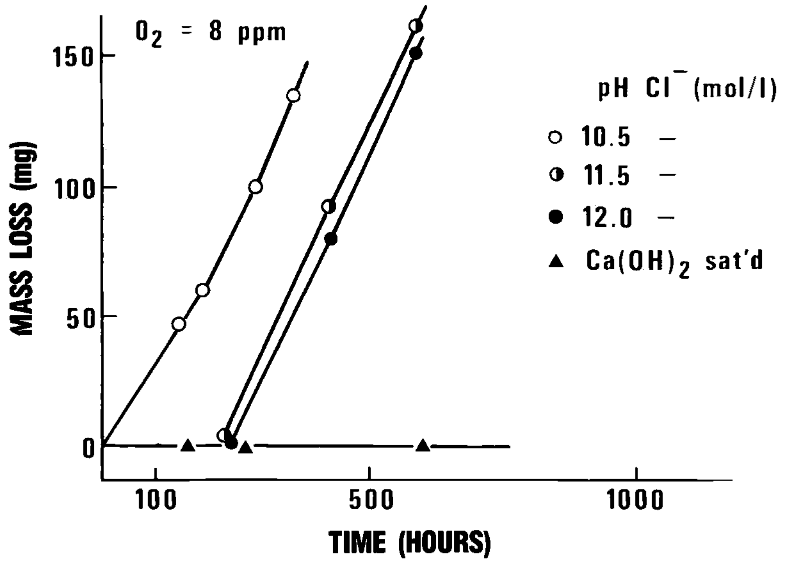

FIG. 4—*Plot of mass loss versus time for steel in calcium hydroxide solutions showing effect of pH on corrosion initiation.*

12, corrosion initiated in slightly over 500 h, and at a pH of 11.5, corrosion initiated in about 50 h. At a pH of 10.5, as before, corrosion started spontaneously on immersion as shown. The data show that chloride had a limited effect on time of corrosion initiation as compared to the effect of pH. Corrosion initiation depends not only on environmental conditions, but also on the condition of the metal surface. Though all specimens were treated

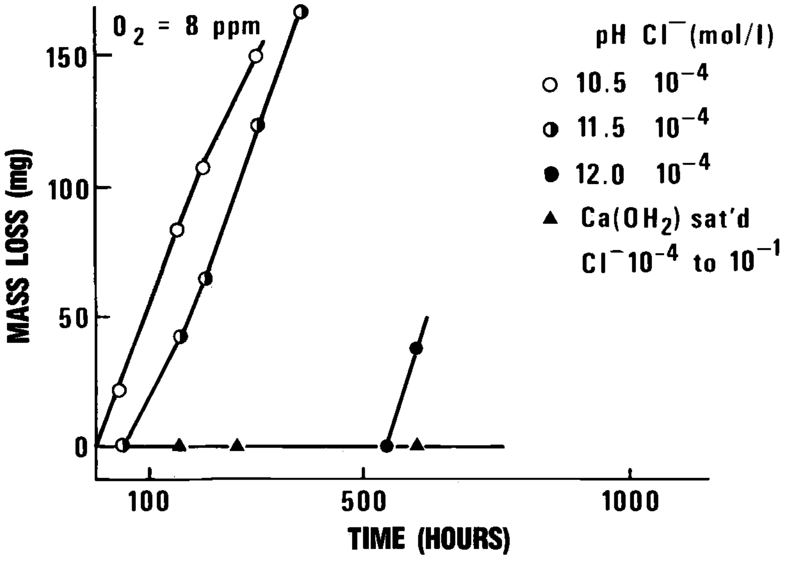

FIG. 5—*Plot of mass loss versus time for steel in calcium hydroxide solutions showing effect of pH and chloride ions on corrosion initiation.*

in the same way before exposure, surface imperfections such as inclusions and other surface inhomogeneities, outside of the scope of this study, also influence corrosion initiation time.

As expected, the effect of oxygen concentration on the rate of corrosion was dramatic. Figure 6 is a plot of the mass loss of steel as a function of time at different concentrations of oxygen in the presence of chloride and a pH of 10.5. With an oxygen concentration of 0.5 ppm corrosion was negligible, but as the oxygen concentration was increased from 2 to 3.5 to 8 ppm, the rate of corrosion increased by over two orders of magnitude.

A summary of all the data, much of which is not shown in the previous figures, of the corrosion of steel in solutions as a function of pH, oxygen concentration, and chloride concentration is illustrated in Fig. 7. This is a plot depicting a three-dimensional envelope within which corrosion will not initiate. Outside of this envelope, however, conditions will cause steel to corrode. This figure shows that under special conditions, even at a pH of 12.5, corrosion will occur. For example, at oxygen concentrations above 3 ppm and chloride concentrations greater than 1 mol/L, corrosion will initiate. At lower pH values, corrosion initiation can take place at even lower concentrations of oxygen and chloride.

Coupons in Sand—The effect of moisture on the corrosion of steel in a sand environment is shown in Fig. 8. This figure shows the mass loss of steel as a function of time for two conditions of moisture. Under conditions of continuous moisture saturation, corrosion did not occur during 800 h of exposure. However, the coupons initially imbedded in a dry sand then exposed to moisture saturated air began to corrode as soon as the moisture was introduced. As the degree of moisture in the sand increased to saturation, the rate of corrosion decreased, and when moisture was reintroduced, the corrosion rate began to increase again. Moisture has a very important effect on corrosion by affecting the transport of oxygen.

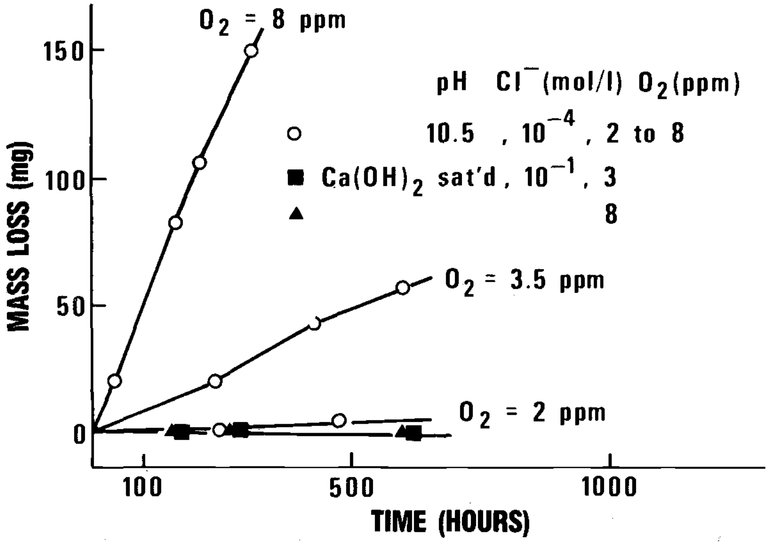

FIG. 6—*Plot of mass loss versus time for steel in calcium hydroxide solutions showing effect of oxygen concentration on corrosion rate.*

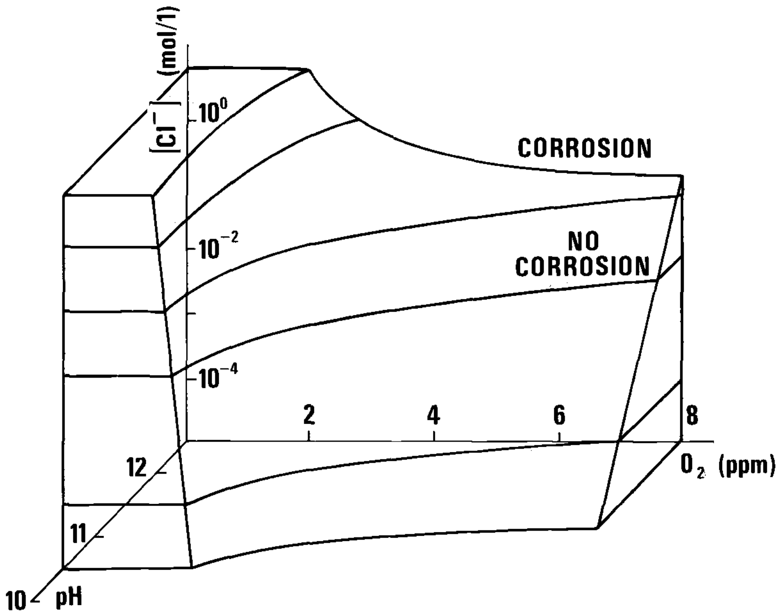

FIG. 7—*Three dimensional plot of oxygen concentration, chloride concentration, and pH illustrating regions of corrosion and no corrosion for steel.*

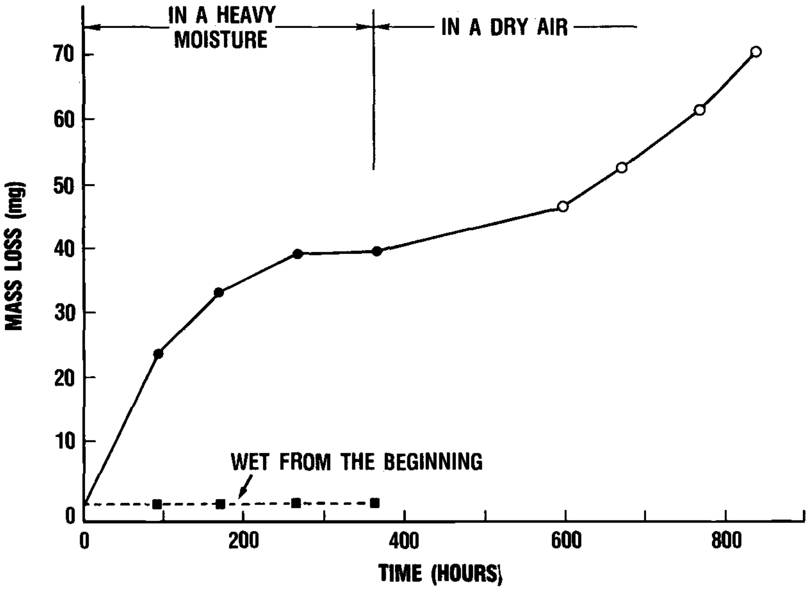

FIG. 8—*Plot of mass loss versus time showing the effect of moisture on the corrosion of steel in sand.*

Coupons in Mortar—As described earlier, one set of mortar covered specimens was immersed in calcium hydroxide-sodium chloride solutions and the second set was dried for seven days before immersion. Illustrated in Fig. 9 are the effects of immersion on the corrosion of steel as a function of time. The mortar covered coupons kept continuously wet displayed negligible corrosion for the entire period of exposure, and those that were immersed after drying showed a high corrosion rate which decreased with time as shown. This result is similar to that observed in the sand environment. After exposure, the specimens that were initially in dry sand and had undergone some degree of corrosion were broken out of the mortar, cleaned, and weighed. Figure 10 is a plot of the mass loss of steel as a function of chloride content indicating that mass loss increased with increased concentration of chloride in the mortar. At first glance, this result appears to be a contradiction of the solution experiment which showed that corrosion rate was independent of chloride concentration and dependent only on oxygen concentration, once corrosion was initiated. Closer consideration of the events taking place shows that the solution experiments are valid and can help explain this apparent discrepancy. It is important to recognize that the corrosion of steel in mortar is not uniform, and the number of sites and intensity of corrosion are controlled by two factors already described. First, increasing the chloride concentration increases the number of sites on the coupon where corrosion initiates resulting in a larger total area of corrosion. Second, increased chloride content reduces initiation time for the onset of corrosion resulting in the steel being active during the initial stages of exposure when oxygen concentration is highest in the conditions of this experiment. These two effects result in an increase in mass loss with increased chloride concentration for the specimens in mortar.

The preliminary experiments revealed that pH and chloride play a critical role in the initiation of corrosion, but once initiated, oxygen concentration controls the rate of corrosion of the steel in concrete. The process of corrosion of steel in concrete is believed to occur

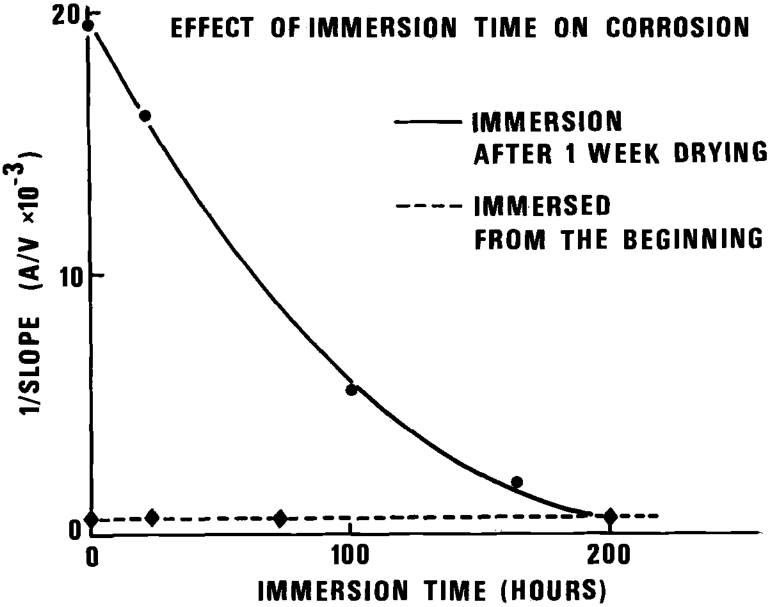

FIG. 9—*Plot of mass loss versus time showing effect of immersion time on the corrosion of steel in mortar.*

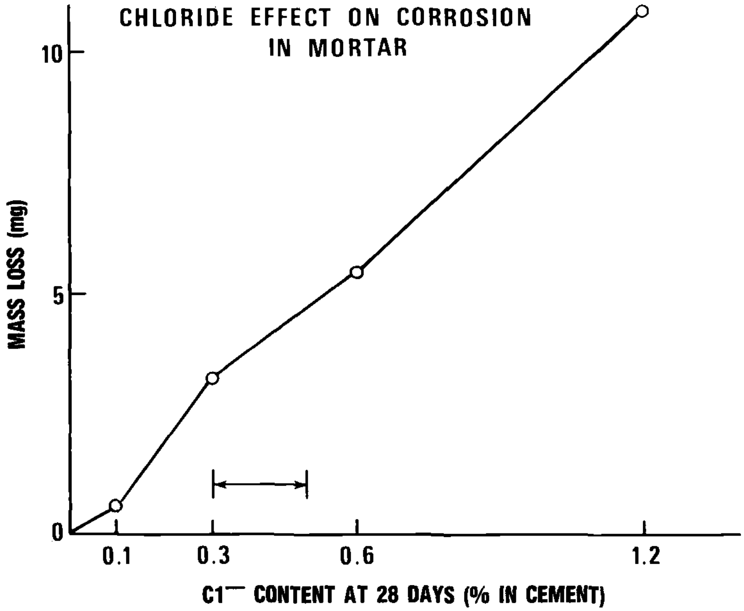

FIG. 10—*Plot of mass loss versus chloride content for steel in mortar.*

in the following way, and it is further believed that this activity takes place in voids in the concrete. Immediately after casting of concrete, the pH of the concrete environment is very high and of the order of 12.5 or more, and the concentrations of chloride and oxygen are well within the region of "no corrosion" of Fig. 7. However, as the concrete cures and dries, chloride concentration increases, and oxygen diffusion increases leading to conditions that move the concrete environment out of the "no corrosion" region and into the "corrosion" region as illustrated in Fig. 11 (arrow). Figure 12 illustrates this process as it might occur adjacent to a steel surface. Moisture saturated concrete is depicted in Fig. 12*a* showing a solution-filled void containing low concentrations of chloride and oxygen. As the concrete dries, however, the salts concentrate and precipitate on the walls of the void as illustrated in Fig. 12*b*. Air diffuses into the concrete replacing the moisture, thereby, increasing oxygen concentration in these voids. This wetting and drying process takes place continuously in a bridge deck, but it is only after chloride ions become available that breakdown of the normally protective oxide on the steel occurs. Once corrosion is initiated by this drying process, pH is decreased at the anodic areas by the reaction

$$Fe^{++} + 2H_2O \longrightarrow Fe(OH)_2 + 2H^+$$

These anodic areas now exist at pH levels below 12.5, and as a result, subsequent re-initiation of corrosion occurs much more easily in future moisture cycles when oxygen is available.

Results and Discussion

Measurements in Concrete

Laboratory—As an example of the results obtained on a day to day basis, the calculated corrosion rates of three specimens (Nos. 1, 3, and 7) are plotted on a logarithmic scale as

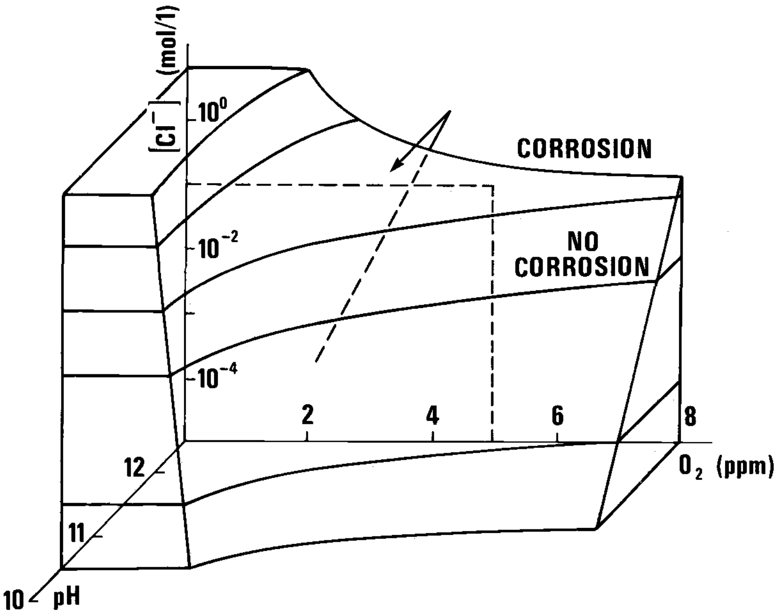

FIG. 11—*Three dimensional plot of oxygen concentration, chloride concentration, and pH with arrow illustrating changes in the environment as concrete drys.*

a function of time and illustrated in Fig. 13. Specimen No. 1 was exposed to chloride-free conditions, and displayed the lowest corrosion rate throughout the entire period. Specimen No. 7 underwent the most severe corrosion, as expected, since it was cast in chloride-containing concrete and alternately immersed in a chloride-containing solution. A corrosion rate between the two extremes was displayed by Specimen No. 3 that was cast in a chloride-free concrete but alternately immersed in a chloride-containing solution. After the exposure period, the concrete was broken and the specimens removed. Using pH paper, it was observed that the pH at the corroded areas was 3 to 5. Once removed, the steel rods were cleaned and weighed. These gravimetric mass loss data are compared to the mass loss calculated from the polarization data, and the results shown in Fig. 14.

Field—The first 90 days of the four month period were spent in improving the equipment and developing our ability to make the measurements in the field. After this initial period, measurements were continued, and the results, summarized in Table 2, show that the 54-year-old bridge, No. 10029, exhibited the lowest average corrosion rate (0.5 mdd) (milligrams/dm^2 d) of the three bridges. The 17-year-old bridge, No. 10100, had an average corrosion rate of 1.1 mdd, and the 13-year-old bridge, No. 10059, exhibited the highest average corrosion rate of 1.9 mdd. However, it is difficult to assess the reliability or accuracy of these data obtained through these preliminary field measurements. Examination of the reinforcing steel by borings was not done because the limited amount of data collected did not warrant such a destructive action. However, the results can be compared to the visual appearance of the bridge deck surfaces in the immediate vicinity of the measurements. On this basis, the following observations can be made. The 54-year-old bridge, though it has

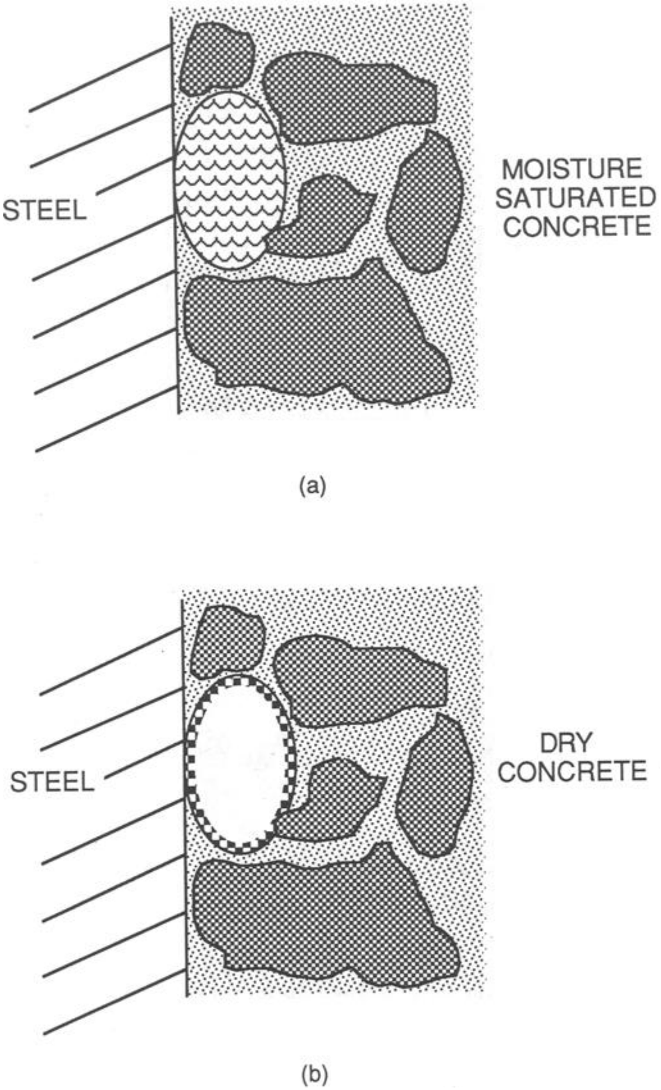

FIG. 12—(a) *Illustration of idealized concrete void adjacent to steel containing a solution of low concentrations of salts and oxygen.* (b) *Illustration of idealized concrete void adjacent to steel showing concentration of salts on walls of void during drying cycle.*

suffered wear and tear through the years, is in surprisingly good condition with small cracks randomly scattered over the surface of the deck. The 17-year-old bridge appears to be relatively crack-free with little evidence of wear to the surface. The 12-year-old bridge, in general, looks good, but close examination of the surface reveals cracking of the concrete above and in line with many of the reinforcing steel bars. This crack alignment is not evident on the other two bridges. Thus, the visual appearance of the bridge surfaces tends to support the electrochemical data.

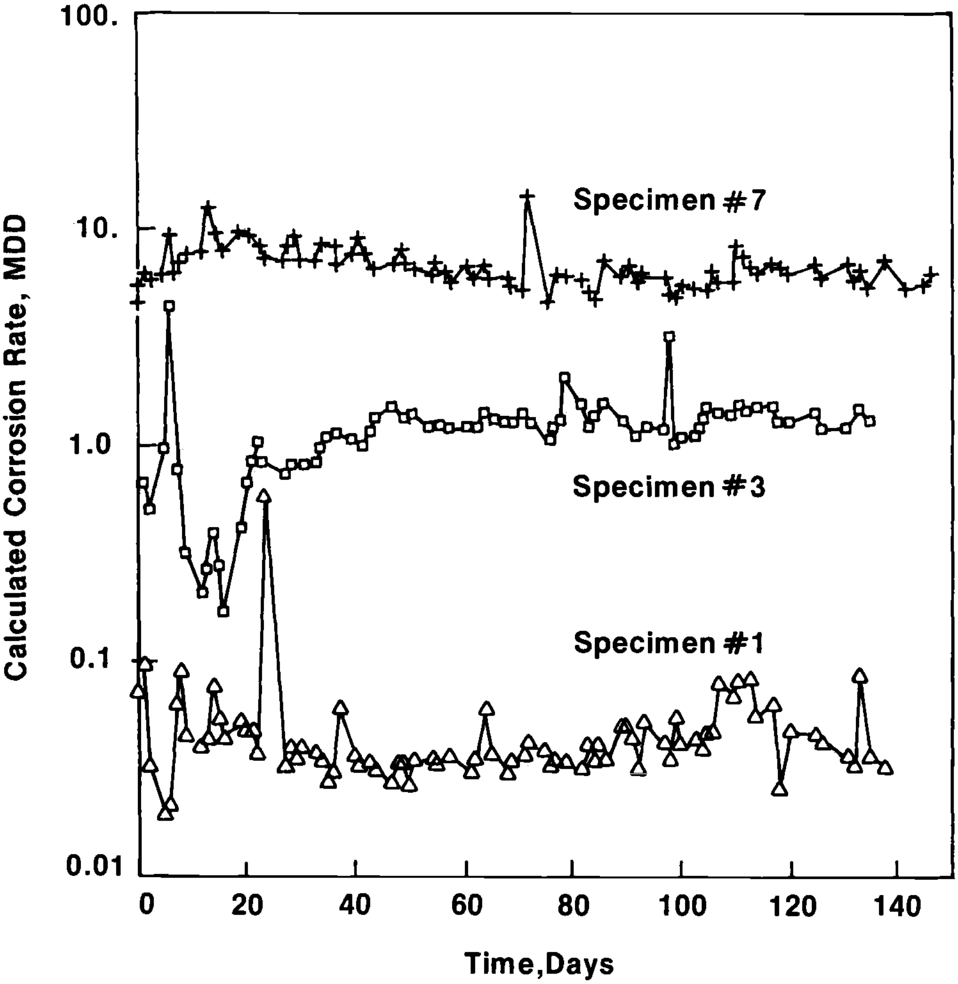

FIG. 13—*Plot of corrosion rate versus time for steel in three conditions of concrete.*

Summary and Conclusions

The preliminary study has shown that a drying cycle in the presence of oxygen and chloride will initiate corrosion of steel in concrete, and once initiated, the pH of the anodic areas decreases making it easier to re-initiate corrosion in subsequent moisture cycles.

Oxygen controls the rate of corrosion of steel in concrete, but the concentration of chloride affects the number of sites where corrosion initiates.

Using a portable computer system for control, the technique of polarization resistance coupled with current interruption for iR compensation has been used successfully to measure the rate of corrosion of steel in concrete in the laboratory, and preliminary measurements in the field indicate that the portable computer system can be applied to measuring the corrosion of reinforcing steel in bridge decks.

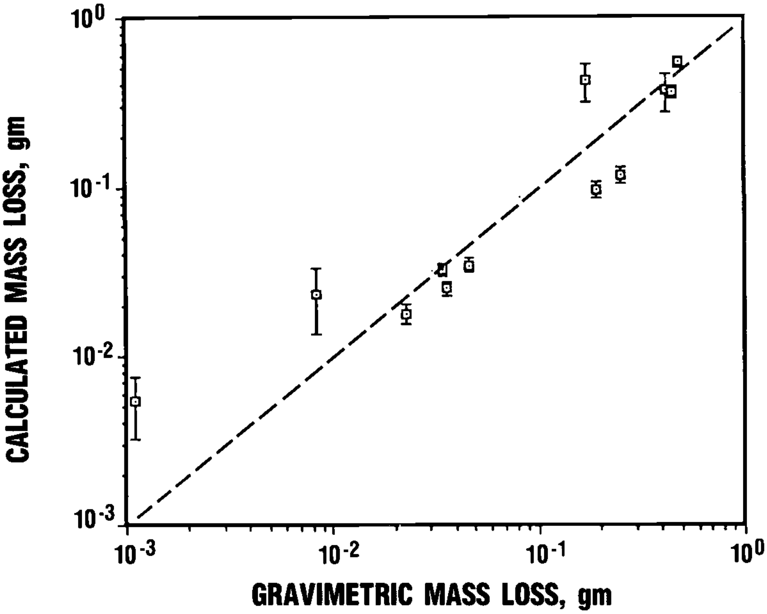

FIG. 14—*A plot comparing gravimetric to calculated mass loss of steel in concrete.*

TABLE 2—*Calculated corrosion rate, mdd, at six positions on three bridges.*

	Span 1			*Span 2*		
	Position			*Position*		
Date	*A1*	*A3*	*A4*	*B1*	*B3*	*B4*
Route 28 Bridge (1931) No. 10029						
Oct 8	...	...	...	...	...	...
Oct 23	0.6	0.3	...	0.8	0.3	0.6
Nov 6	(bridge under floodwater)					
Average corrosion rate = 0.5						
Route 15 Bridge (1968) No. 10100						
Oct 8	0.4	3.2	0.5	1.3	2.6	1.7
Oct 23	0.8	0.5	1.3	1.3	1.0	0.6
Nov 6	...	0.8	1.0	...	0.9	0.2
Average corrosion rate = 1.1						
Route 80 Bridge (1972) No. 10059						
Oct 8	3.6	2.8	2.3	...	...	...
Oct 23	3.5	1.3	1.2	0.7	0.8	2.1
Nov 6	3.1	2.1	2.6	0.6	1.2	1.0
Average corrosion rate = 1.9						

References

[*1*] Escalante, E and Ito, S, *A Bibliography on the Corrosion and Protection of Steel in Concrete,* NBS SP 550, National Bureau of Standards, Gaithersburg, MD, Aug 1979

[*2*] Hausmann, D A, "Steel Corrosion in Concrete, How Does it Occur," *Materials Protection,* Vol 6, No 11, 1967

[*3*] Gjorv, O E, Vennesland, O, et al, "Diffusion of Dissolved Oxygen Through Concrete," *Corrosion/76,* 22–26 March 1976, Paper 17, National Association of Corrosion Engineers, Houston, TX, 1976

[*4*] Escalante, E, Ito, S, and Cohen, M, *Measuring the Rate of Corrosion of Reinforcing Steel in Concrete,* NBSIR 80-2012, National Bureau of Standards, Gaithersburg, MD, March 1980

[*5*] Escalante, E, Cohen, M, and Kahn, A H, *Measuring the Rate of Corrosion of Reinforcing Steel in Concrete,* NBSIR 84-2853, National Bureau of Standards, Gaithersburg, MD, April 1984

[*6*] Escalante, E, Whitenton, E, and Qiu, F, *Measuring the Rate of Corrosion of Reinforcing Steel in Concrete—Final Report,* NBSIR 86-3456, National Bureau of Standards, Gaithersburg, MD, Oct 1986

[*7*] Escalante, E, "Eliminating iR Error in Measurements of Corrosion in Concrete," *The Measurement and Correction of Electrolyte Resistance in Electrochemical Tests, ASTM STP 1056,* L L Scribner and S R Taylor, Eds, American Society for Testing and Materials, Philadelphia, 1988

[*8*] Wheat, H G and Eliezer, Z, "Some Electrochemical Aspects of Corrosion of Steel in Concrete," *Corrosion,* Vol 41, No 11, 1985

Kazumi Matsuoka,[1] *Hiroshi Kihira,*[1] *Satoshi Ito,*[1] *and*
Tomomi Murata[2]

Corrosion Monitoring for Reinforcing Bars in Concrete

REFERENCE: Matsuoka, K , Kihira, H , Ito, S , and Murata, T , **"Corrosion Monitoring for Reinforcing Bars in Concrete,"** *Corrosion Rates of Steel in Concrete, ASTM STP 1065,* N S Berke, V Chaker, and D Whiting, Eds , American Society for Testing and Materials, Philadelphia, 1990, pp 103–117

ABSTRACT: To monitor accurately the corrosion rate of rebars in a concrete structure using electrochemical techniques, the area of the rebar surface to be measured should be well specified by taking into account the wide-spreading distribution of the polarization current For this purpose, the double-counter electrode method proposed by some investigators is projected to be one of the most accurate methods However, there have been few actual studies on its accuracy Therefore, the aim of this study is to establish the basis of accuracy for the double-counter electrode method, using numerical simulation by the two-dimensional finite element method The obtained results indicate that the corrosion rate of rebars can be accurately monitored by the double-counter electrode methods, and that its accuracy is mainly affected by the degree of confinement of the longitudinal current distribution related to the concrete cover and the polarization resistance Finally, a graphic method to correct the raw *a-c* impedance data obtained by the double-counter electrode method to arrive at the true impedance data is presented in this paper

KEY WORDS: steels in concrete, corrosion monitoring, *a-c* impedance techniques, double-counter electrode, numerical simulation, finite element method, steels, corrosion, concrete

Electrochemical corrosion monitoring techniques for reinforcing bars in concrete structures have been developed to meet corrosion potential mapping methods as described in ASTM Test for Half-Cell Potentials of Uncoated Reinforcing Steel in Concrete (C 876-87). This practice is very convenient in estimating the probability of the corrosion of rebars in structures. However, it is still limited to qualitative measurement of the degree of corrosion attack, and may even be misleading since corrosion potential depends upon the surrounding environmental conditions Therefore, there is a strong need to develop a more quantitatively accurate on-site monitoring method

Until now, some techniques to quantify the corrosion of rebars in concrete, such as the polarization resistance method, the *a-c* impedance method, and so on, have been studied in the laboratory by many researchers [*1–6*], and some researchers have reported the applicabilities for field corrosion monitoring [*4–6*]

In applying the methods just mentioned to field monitoring, some difficult issues are introduced because one must deal with larger areas of reinforcement than in the laboratory

---

[1] Research engineer, research chemist, and senior research chemist, respectively, R & D Laboratories-1, Nippon Steel Corporation, 1618 Ida, Nakahara-ku, Kawasaki 211, Japan

[2] General manager, New Materials Division, Nippon Steel Corporation, 6-3, Otemachi 2-chome, Chiyoda-ku, Tokyo 100-71, Japan

The most difficult issue is that one cannot directly obtain the true values of the electrochemical parameters, such as the polarization resistance and the impedance at each position to be measured. This difficulty occurs because the degree of polarization of the rebar surface, induced by the overpotential applied at corrosion potential, gradually decreases with the distance from the counter electrode.

Recently, some attempts have been made to analyze the data obtained by a single-counter electrode method that is a usual laboratory method, using a current distribution model, such as a transmission line [*7–9*]. However, the results still give us an average corrosion resistance over the whole measured area, which may vary over a wide range (occasionally more than one order) due to the variation in the reinforcement geometry, the resistive characteristics of concrete, surface films, and so on. This order of magnitude variation makes an average value meaningless and also means the corrosion rate cannot be estimated accurately at each position of rebar.

Then, the double-counter electrode method has been proposed [*10,11*] to obtain corrosion resistance directly from a confined area. The main concept of this method is to polarize the rebars in concrete by a central counter electrode (CE) together with an additional surrounding counter electrode (SE), obtaining only the corrosion resistance from the well-confined area under the central counter electrode. We have developed a sensor using a circular type of a double-counter electrode and its impedance measurement system. A schematic illustration of this system is shown in Fig. 1. Using this system, the typical impedance data

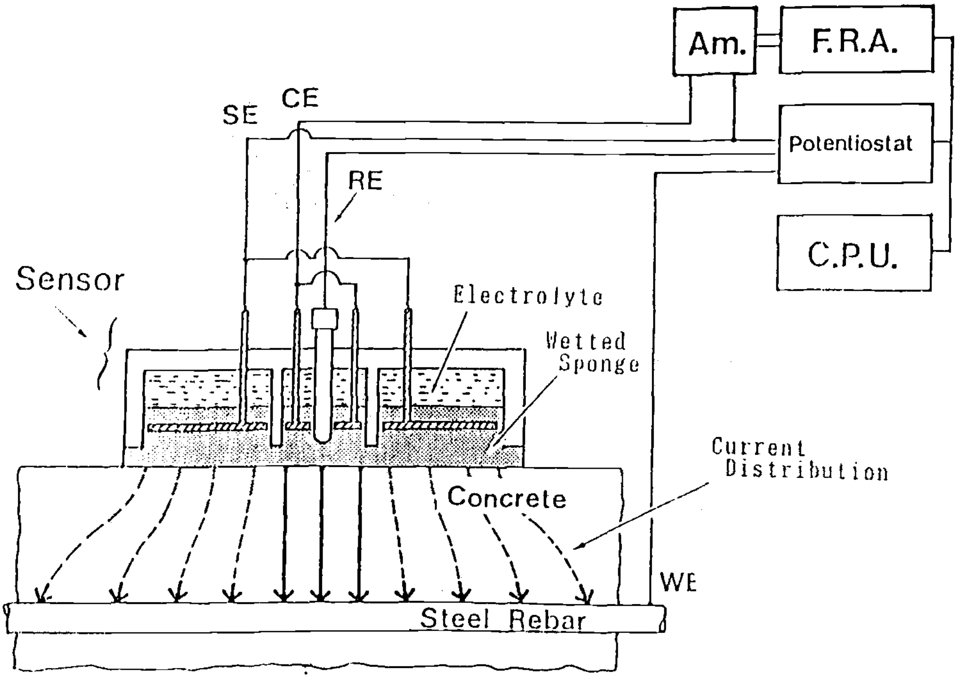

RE = reference electrode
CE = central counter electrode
SE = surrounding counter electrode
WE = working electrode

FIG. 1—*On-site corrosion monitoring system utilizing double-counter electrode method.*

obtained on a laboratory test block containing a rebar 500 mm long and 20 mm in diameter are shown in Fig. 2*a*. Figure 2*b* shows the impedance data with the same specimen by the single-counter electrode method. The single-counter electrode method gives us a very small impedance, while the double-counter electrode method gives results which are similar to those published previously [*3*], as shown in Fig. 3. This similarity is one reason that the double-counter electrode method is considerably more effective for field corrosion monitoring. Even so, the degree of accuracy still depends on distributing the polarizing current in the same way as for the single-counter electrode method. In other words, the accuracy of both methods, more or less, varies not only with the geometry and the dimensions of

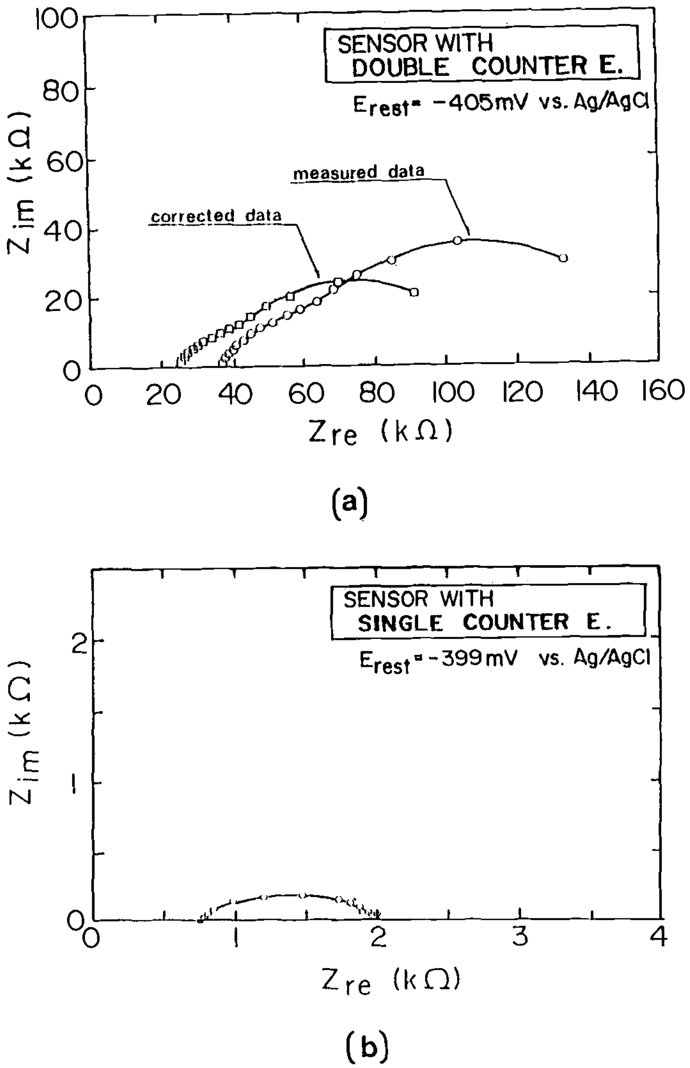

FIG. 2—*Experimental data from a concrete beam:* (a) *double-counter electrode method and* (b) *single-counter electrode method.*

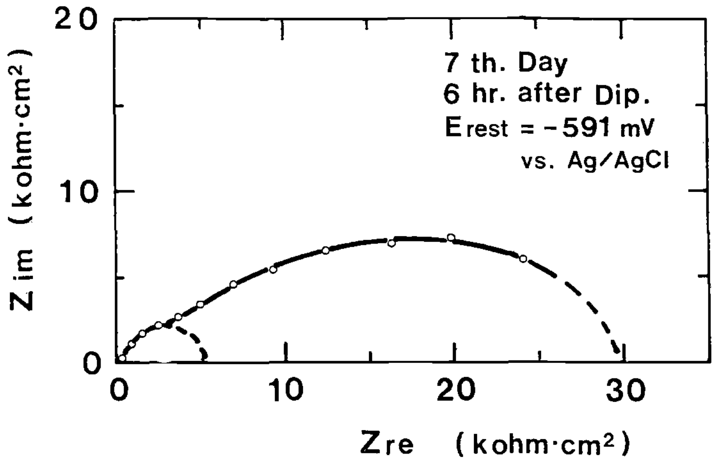

FIG. 3—*Experimental data from a small mortar sample.*

reinforcement but also with resistivity (R_s) of concrete and the resistive characteristics (R_f) of the surface film having the frequency dependency as shown in Fig. 4.

If the characteristics of both methods would be studied in detail, first, it would be possible to establish a quantitative on-site corrosion monitoring method. Second, it would be possible to relate many useful results collected in the laboratory and also in the field in the near future. In this paper, therefore, we present a fundamental study of both the single-counter electrode method and the double-counter electrode method by numerical simulation.

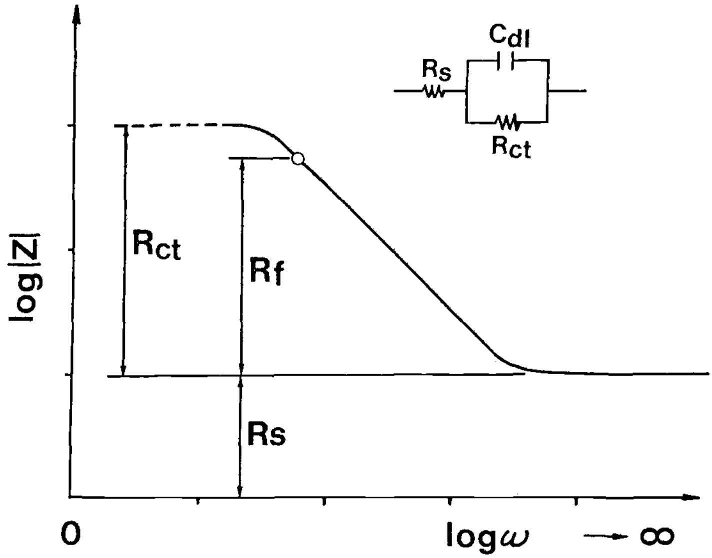

FIG. 4—*Typical bode diagram.*

Numerical Simulation

Simulation Model

In general, real concrete structures are three-dimensionally reinforced with several types of rebars However, in this simulation, the model consists of a round reinforcing bar embedded in a concrete beam The electrochemical measurement is assumed to be potentiostatically controlled, such as by *a-c* impedance measurements The schematic illustration of the on-site monitoring model (beam model) using the double-counter electrode method is shown in Fig 5*a* For comparison, Fig 5*b* shows a laboratory monitoring model (cubic model) by which one can evaluate the characteristics of the true impedance to be compared with that of the model in Fig 5*a* The "true" impedance means the impedance defined per unit steel area without the spreading phenomenon of the polarization current In this figure, ΔE is the overpotential applied at the corrosion potential, and ΔI_s, ΔI_c are the resulting currents of the surrounding counter electrode and center counter electrode, respectively

In this simulation, the following two items are assumed.

1 The electrical properties of the concrete and steel are expressed purely by the resistivities (ρ_c, ρ_s, respectively, but that of steel is negligible)
2 The characteristics of the impedance of the steel/concrete interface including the Faraday impedance (Z_f) and the double layer capacitance (C_{dl}), which gradually increases with the frequency, are approximated by changing the resistivity (ρ_f) of the thin surface film as shown in Fig 6

Under these modeling conditions, if the resulting currents (ΔI_s, ΔI_c, ΔI) were in any way given, the impedance moduli for both the models could be easily calculated

Numerical Evaluation Procedure

In general, this kind of problem can be mathematically modeled by the Laplace equation under the constant potential boundary condition. In order to solve the preceding equation and calculate the potential/current distribution, some different approaches are feasible such as (1) the analytical solution technique and (2) the numerical solution technique Analytical approaches are limited to cases of simple geometry and boundary conditions, and generally invoke cumbersome descriptions. In this study, therefore, the two-dimensional finite element method (FEM), a numerical solution technique, is employed for the longitudinal section and cross section of the beam model The employed element is a so-called isoparametric rectangular element with eight nodes and is characterized by giving an adequate solution despite a small number of elements (a more detailed description related to this can be found in Ref *12*) Though a three-dimensional FEM is more exact, it would add little to the points which we wish to make clear.

The examples of the mesh arrangement, which we employed in the FEM analysis for the longitudinal section and cross section of the rebar, are shown in Figs 7*a* and *b*, respectively The electrical nature of the surface film around the rebar was approximated by a thin layer of the element with the thickness (ℓ_f) and the resistivity (ρ_f) In these figures, d is concrete cover, D is diameter of rebar

From the FEM analysis, the polarization current (ΔI_s, ΔI_c) resulting from the applied overpotential (ΔE) can be calculated by the numerical integration as shown in Eq 1

$$\Delta I_s = 2\int_{r_c}^{r_s} i \quad dr, \; \Delta I_c = 2\int_{0}^{r_c} i \cdot dr \tag{1}$$

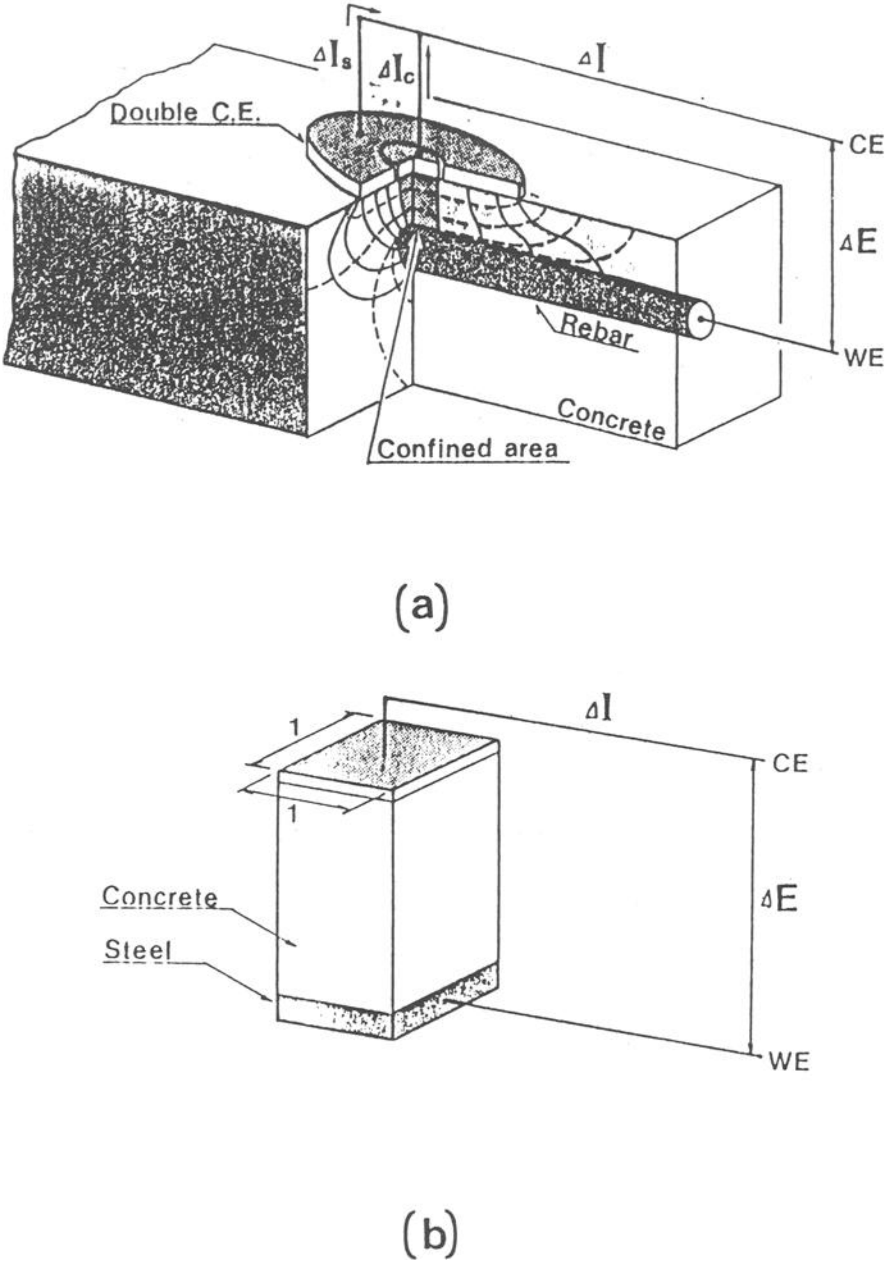

FIG. 5—*Simulation model for corrosion monitoring:* (a) *on-site monitoring model* (*beam model*) *and* (b) *laboratory monitoring model* (*cubic model*).

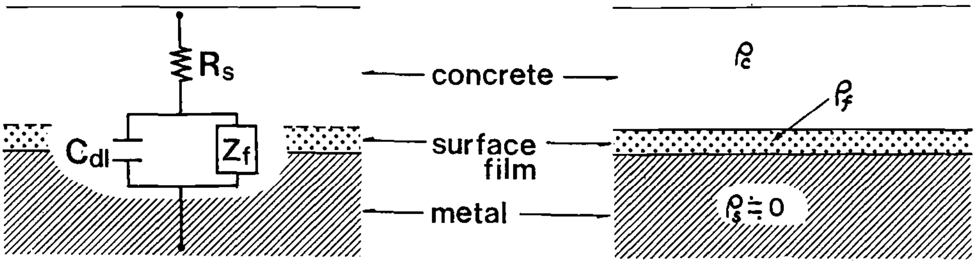

FIG. 6—*Interface model in numerical simulation.*

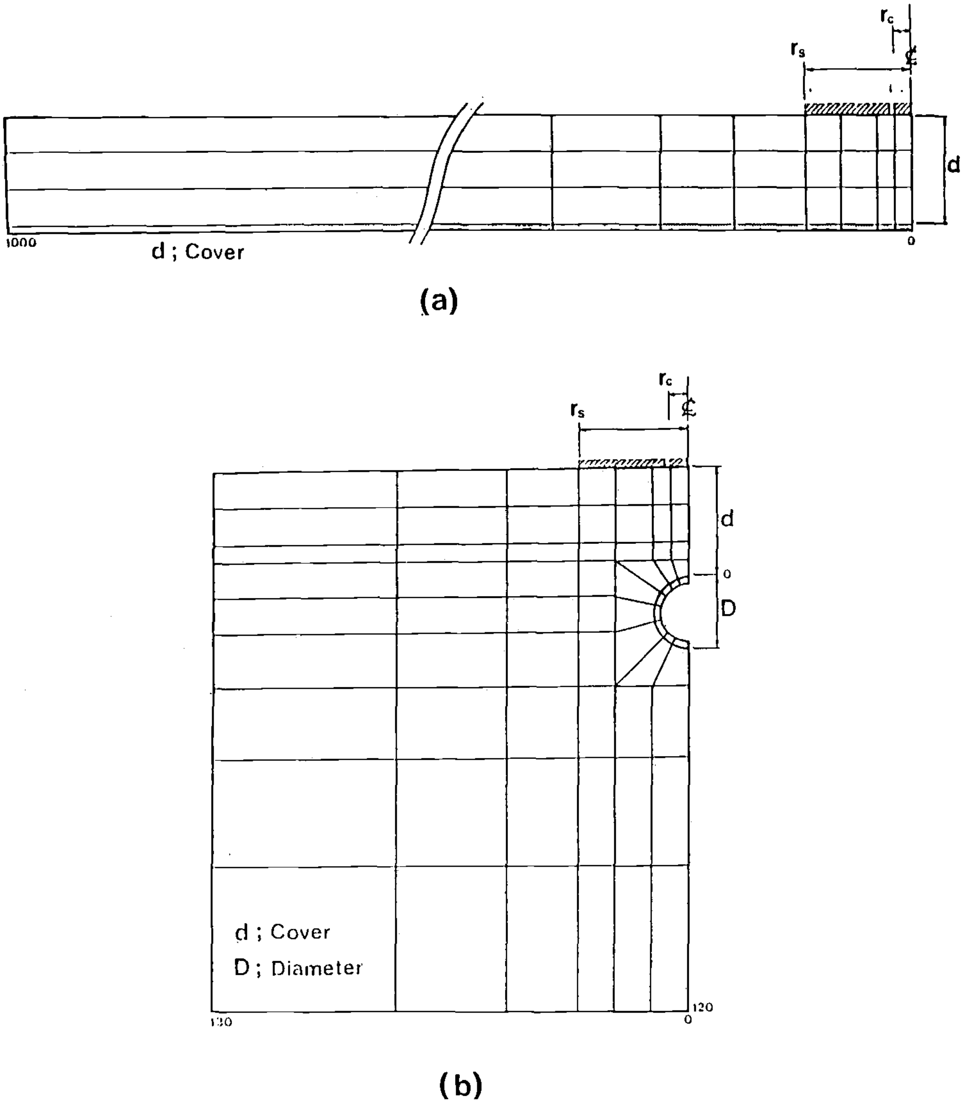

FIG. 7—*Mesh arrangement of finite element method (FEM):* (a) *longitudinal mesh arrangement and* (b) *cross-sectional mesh arrangement.*

where r_s, r_c = outer radius of surrounding counter electrode, and outer radius of the central counter electrode, respectively, and i = current density The current density values were calculated in four elements in contact with the surrounding counter electrode and the central counter electrode Accordingly, the impedance modulus obtained by the double-counter method can be evaluated as follows

$$|Z_d| = \Delta E/\Delta I_c \tag{2}$$

and the impedance modulus by the single-counter method can be evaluated in the same way in Eq 3.

$$|Z_s| = \Delta E/(\Delta I_s + \Delta I_c) \tag{3}$$

On the other hand, for the cubic model, which has concrete cover (d) with the resistivity (ρ_c) and surface film thickness (ℓ_f) with the resistivity (ρ_f), the impedance modulus is evaluated by the following simple equation

$$\begin{aligned} |Z_t| &= R_s + R_f \\ &= R_s\,(1 + R_f/R_s) \end{aligned} \tag{4}$$

where $R_f/R_s = (\ell_f/d) \times (\rho_f/\rho_c)$

In this parametric study, the outer radii (r_s, r_c) were constantly set to be 30 and 5 mm The other analysis parameters employed for the longitudinal section and the cross section were, presented in Tables 1 and 2, respectively For each combination of the geometrical parameters (d, ℓ_f) in Table 1 and (d, ℓ_f, D) in Table 2, the surface film thickness (ℓ_f = 1 mm) was employed, the resistivity of concrete (ρ_c) was set to be a constant value (1 $K\Omega$cm), and the ratio (ρ_f/ρ_c) was varied in the range 1 to 10^5 In the case of $\rho_f/\rho_c = 1$, the impedance moduli evaluated with Eqs 2 through 4 approximately correspond to the impedance moduli measured at such a high frequency that the solution resistance mainly dominates In the case of $\rho_f/\rho_c > 1$, the impedance moduli correspond to the impedance moduli at the frequency where the interfacial impedance of steel/concrete dominates in comparison with the solution resistance

Results and Discussion

Potential/Current Distribution

The typical patterns of potential/current distributions in concrete obtained from FEM analysis for both sections of the beam model (10 mm cover and 20 mm diameter) are shown in Figs 8 and 9, respectively The overpotential (ΔE) is 100 mV, and equipotential lines (----) are drawn by 10-mV pitch The current lines (——) can be estimated by the fact that the equipotential line and the current line cross at right angles

In the longitudinal section, the equipotential lines line up almost horizontally beneath the central counter electrode and rise up gradually under the outer edge of the surrounding counter electrode The slopes of the equipotential lines under the outer edge increase rapidly with the increment of the ratio (ρ_f/ρ_c) For instance, in the case of $\rho_f/\rho_c = 10^2$, the equipotential lines almost line up vertically This trend indicates that the current distribution in the low frequency range spreads widely along the rebar.

TABLE 1—*Analysis parameters for longitudinal direction of rebar*

	CONCRETE
Cover	d = 5, 10, 20, 30, 40, 50 mm
Resistivity	ρ_c = 1 K Ω cm
	SURFACE FILM
Thickness	ℓ_f = 1 mm
Resistivity	ρ_f = 1 K, 10 K, 100 K, 1 M, 10 M, 100 M Ω cm

On the other hand, in the cross section, the distribution pattern of the equipotential lines hardly changes, even in the case of $\rho_f/\rho_c = 10^5$ Consequently, the current distribution is expected to be a settled pattern

Impedance Characteristics

To compare the impedance characteristics of the double-counter method with that of the single-counter method, all the impedance moduli evaluated for the beam model and the cubic model were normalized by the solution resistance ($R_s = d \times \rho_c$) of the cubic model and plotted in Figs. 10 and 11 In these figures, all the x-axes indicate the normalized values ($|Z_t|/R_s$) of the true impedance moduli for the cubic model, and both the y-axes in Figs 10*a* and 11*a* indicate the normalized values ($|Z_d|/R_s$) of the impedance moduli by the double-counter method Both the y-axes in Figs 10*b* and 11*b* indicate the normalized values ($|Z_s|/R_s$) of the impedance by the single-counter method In these figures, the vertical deviation of the plotted points from the diagonal lines (----) shows how accurate each method is quantitatively

From the comparison of the results in Fig 10 along the longitudinal section of the rebar, it can be found that the double-counter method gives us more accurate impedance data than does the single-counter method For instance, the data points for a concrete cover of 10 mm in Fig 10*a* almost coincide to the diagonal line in the wide range ($|Z_t|/R_s$ = 1 to 10^3) On the other hand, the data points for the same cover in Fig 10*b* are plotted lower than a sixth of the true data This means that the double-counter method is effective for specifying the measuring area of the rebar surface However, in other cases, all the data gradually tend to shift with the increment of the concrete cover and with the ratio (ρ_f/ρ_c) corresponding to the decrement of frequency ($\omega \rightarrow 0$) This indicates that the spreading manner of the current distribution along the longitudinal direction of the rebar is the most significant factor to be considered in the development of an accurate on-site monitoring method

TABLE 2—*Analysis parameters for cross-section of rebar*

	CONCRETE
Cover	d = 5, 10, 20, 30, 40, 50 mm
Resistivity	ρ_c = 1 K Ω cm
	SURFACE FILM
Thickness	ℓ_f = 1 mm
Resistivity	ρ_f = 1 K, 10 K, 100 K, 1 M, 10 M, 100 M Ω cm
	REBAR
Diameter	D = 10, 15, 20, 25 mm

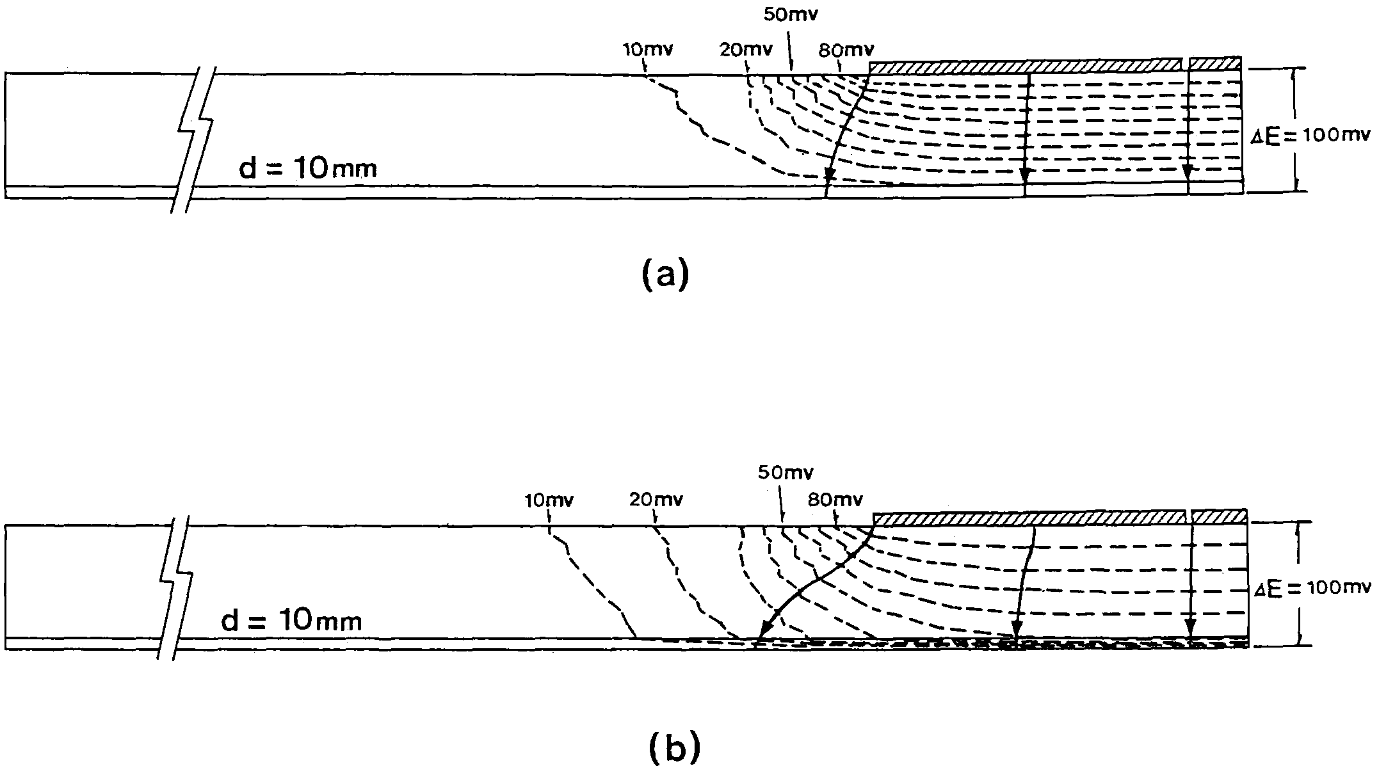

FIG. 8—*Current distribution of longitudinal section of reinforced concrete. (10 mm cover):* (a) ρ_f/ρ_c = *1.0 and* (b) ρ_f/ρ_c = *10.*

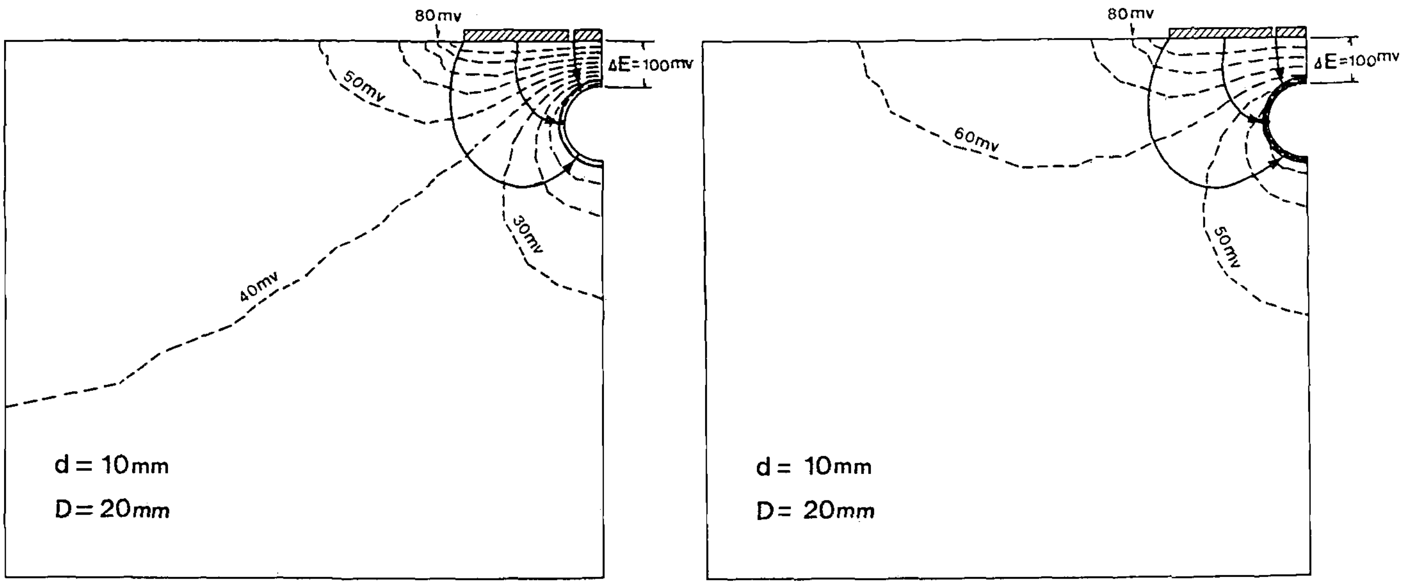

(a)

(b)

FIG. 9—*Current distribution of cross-section of reinforced concrete (10 mm cover):* (a) ρ_f/ρ_c = *1.0 and* (b) ρ_f/ρ_c = *10.*

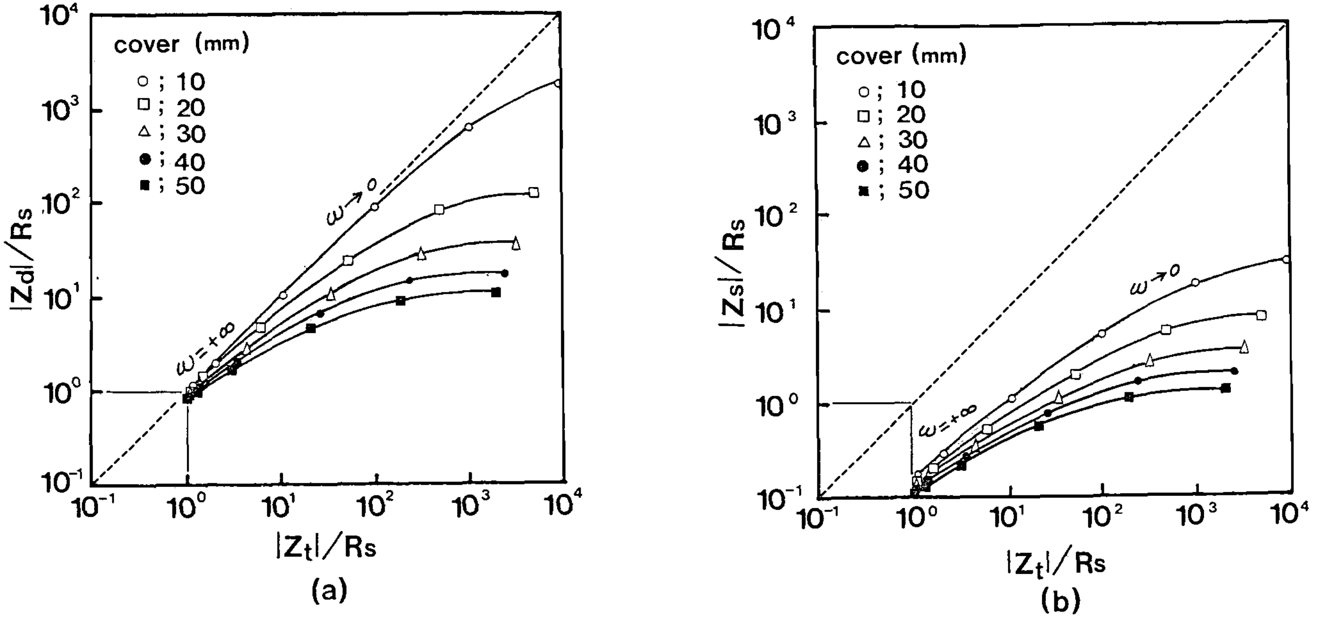

(a)

(b)

FIG. 10—*Comparison between the impedance characteristics for the longitudinal section of reinforced concrete:* (a) *double-counter electrode method and* (b) *single-counter electrode method.*

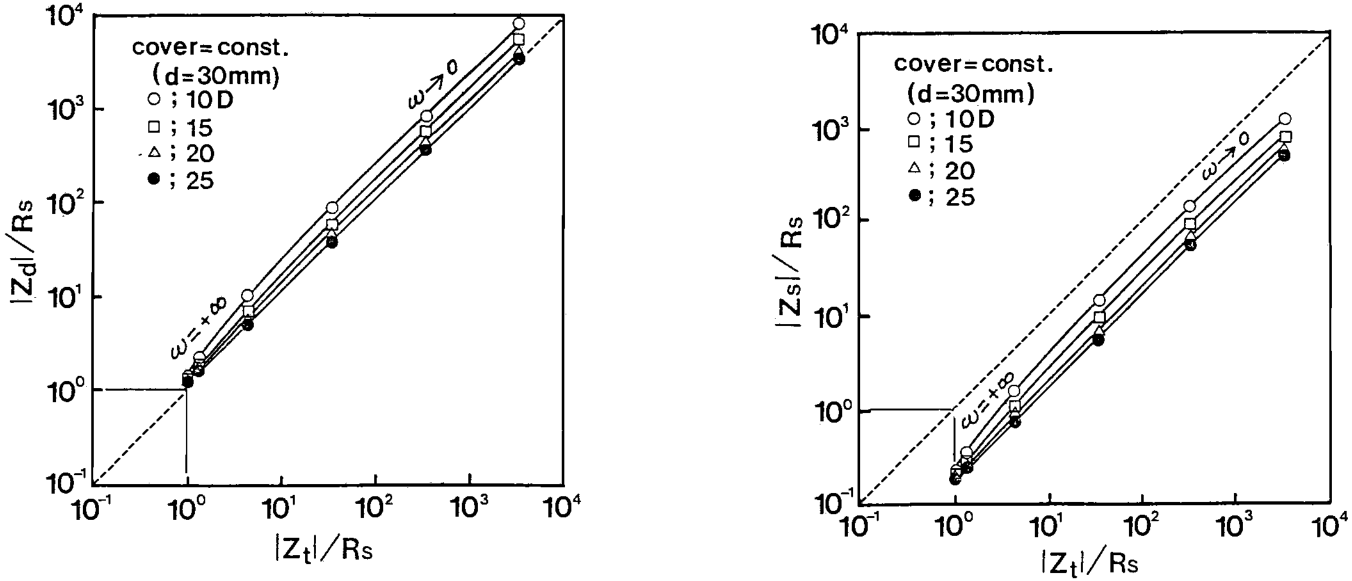

(a)

(b)

FIG. 11—*Comparison between the impedance characteristics for the cross-section of reinforced concrete:* (a) *double-counter electrode method and* (b) *single-counter electrode method.*

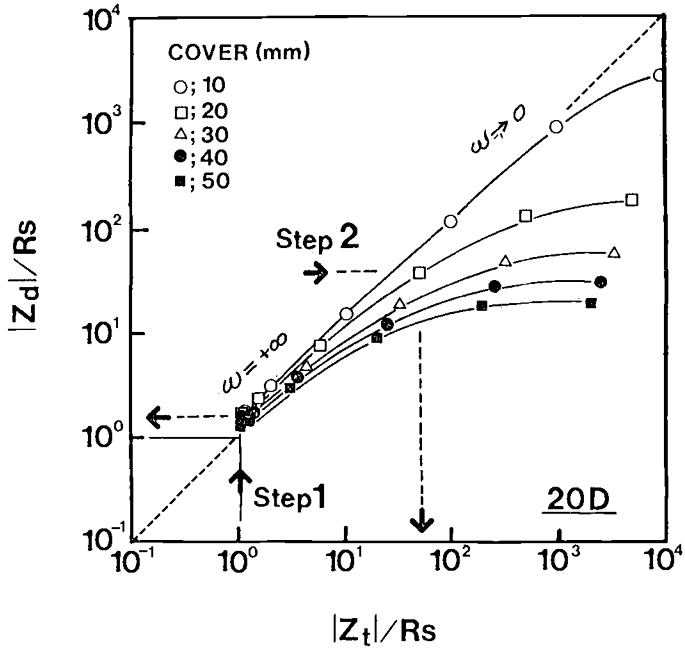

FIG. 12—*The graph for the correction of a-c impedance data (20 mm diameter).*

For the comparison for the cross section, the typical data evaluated under the condition that the concrete cover (d = 30 mm) and the rebar diameter (D = 10, 15, 20, 25 mm) are shown in Figs. 11*a* and 11*b*. In this case, the deviation of the double-counter method from the diagonal line is a little less than that of the single-counter method, and this deviation scarcely changes even if the frequency decreases. From this comparison, it was found that the main significant factor is the diameter of rebar rather than the frequency or the concrete cover.

Correction Method

As the results of the preceding comparisons indicate, in cases of thicker covers or larger corrosion resistances ($\fallingdotseq R_{ct}$), one cannot avoid getting erroneous data even if using the double-counter method. However, this difficulty can be easily solved by the following method. As mentioned previously, the vertical deviation of the plotted points from the diagonal line (----) in Figs. 10*a* and 11*a* represents the quantitative accuracy for both the longitudinal section and the cross section of the rebar. In other words, it is nothing but an indicator relating to the confined area of the rebar surface polarized by central counter electrode. Additionally, the configuration of the confined area can be practically assumed to be an ellipse. Accordingly, the confined area on the rebar surface, as shown in Fig. 5*a*, can be numerically estimated from these figures. Using these confined areas (for example, testing area) data of double-counter measurement and its true impedance data, the graph to correct the raw impedance moduli from the double-counter method to match its true impedance moduli can be prepared for each case of rebar diameter and concrete cover, as shown in Fig 12 The method for using this graph is as follows

Step 1—First, read the ordinate that corresponds to $|Z_t|/R_s = 1$, and then calculate the true R_s value by dividing the impedance modulus ($|Z_d|$) by the ordinate, where $|Z_d|$ is the measured value in such a high frequency range that the solution resistance mainly dominates

Step 2—Calculate the ratio ($|Z_d|/R_s$) of the impedance modulus ($|Z_d|$) measured at each frequency to the true R_s value in Step 1, and read the abscissa of the point having this ratio on the correction curve Multiply the abscissa by the R_s, and the product is the true impedance modulus Figure 2*a* shows an example of the corrected data using this procedure With this procedure, it will be possible to correct any *a-c* impedance data measured by the double-counter method and evaluate the true corrosion resistance for the confined area of the rebar surface

Conclusions

In this study, the current distribution under double-counter electrode system was numerically simulated by the finite element method, then compared to that under single-counter electrode system It may be concluded that

1 the double-counter electrode method more effectively confines polarizing current flow into the constant area than does the single-counter electrode method,
2 the current distribution along the longitudinal direction of the rebar has a more significant effect on the corrosion resistance data than on the cross-sectional one, and
3. a methodology is established to obtain the true corrosion resistance from the measured raw data by using the conversion graph

References

[*1*] Dawson, J L , et al , *Corrosion/78,* National Association of Corrosion Engineers, Paper 125

[*2*] Andrade, C , Castelo, V , Alonso, C , and Gonzalez, J , "The Determination of the Corrosion Rate of Steel Embedded in Concrete by the Polarization Resistance and AC Impedance Method", *Corrosion of Rebars in Concrete, ASTM STP 906,* V Chaker, Ed , American Society for Testing and Materials, Philadelphia, 1984, pp 43–63

[*3*] Matsuoka, K , Kihira, H , Ito, S , and Murata, T , *Corrosion/87,* National Association of Corrosion Engineers, Paper 121

[*4*] Tamura, H and Yosida, M , American Concrete Institute SP-82, 1984, pp 689–702

[*5*] Matsuoka, K , Oka, T , Kihira, H , and Ito, S , 32th Fushoku-Boushoku, Japan Society of Corrosion Engineers, 1985, pp 267–269

[*6*] Escalante, E , Whitenton, E , and Qiu, F , NBS Report NBSIR 86-3456, National Bureau of Standards, Gaithersburg, MD, Oct 1986

[*7*] Macdonald, D , Mckubre, M C H , and Macdonald, M U , *Corrosion/87,* National Association of Corrosion Engineers, Paper 120

[*8*] Wenger, F , Zhang, J , Galland, J , and Lemoine, L , *Proceedings,* 10th International Congress on Metallic Corrosion, 1987, pp 1539–1546

[*9*] Feliu, S , et al , *Corrosion/87,* National Association of Corrosion Engineers, Paper 145

[*10*] Matsuoka, K , Kihira, H , Ito, S , and Murata, T , *Annual Report 1987,* R&D Activities at Nippon Steel, 1987, p 11

[*11*] John, D G , Eden, D A , Dawson, J L , and Langford, P E , *Corrosion/87,* National Association of Corrosion Engineers, Paper 136

[*12*] Togawa, H , "Finite Element Method Analysis by Using Micro-Computer" (in Japanese), Baifukan, 1987, pp 117–149

L. Lemoine,[1] *F. Wenger,*[2] *and J. Galland*[2]

Study of the Corrosion of Concrete Reinforcement by Electrochemical Impedance Measurement

---

REFERENCE: Lemoine, L , Wenger, F , and Galland, J , **"Study of the Corrosion of Concrete Reinforcement by Electrochemical Impedance Measurement,"** *Corrosion Rates of Steel in Concrete, ASTM STP 1065,* N S Berke, V Chaker, and D Whiting, Eds , American Society for Testing and Materials, Philadelphia, 1990, pp 118–133

ABSTRACT: Electrochemical impedance measurement is a convenient method to analyze the corrosion phenomena of steel in concrete A data analysis method is used on the basis of an equivalent circuit correlated to the properties of concrete and electrochemical mechanisms The different parts of the diagram versus frequency allow characterization of the concrete cover, the presence of a film at the surface of steel, the transfer resistance connected to the anodic reaction, and some other relaxation phenomena Some agreement has been obtained with mass losses

A mathematical model has been developed in order to analyze the results on large concrete beams with a small-size auxiliary electrode Particular emphasis is given to the spatial location of an active area in order to demonstrate the feasibility of such a method either on large specimens or on real structures For this application, the principle of an alternative method was developed An auxiliary electrode is used with an electrical guard At low frequencies (<10 Hz), the first experimentation gives encouraging results

KEY WORDS: Reinforced concrete, electrochemical impedance plot, corrosion, mathematical model, steels, concrete

Reinforced concrete is used widely to build large projects like bridges, tunnels, and offshore structures It is now recognized that the corrosion of rebars is an important problem to be solved in order to increase the reliability of the structure and to reduce maintenance costs

In concrete, steel is in a passive condition This fact is due to the high level of pH (12 5 to 13 7) of the solution contained in the pores of the concrete The corrosion of rebars can occur when this passivation is destroyed by the penetration of chloride ions at the metal concrete interface and by a decrease of pH as a result of the action of various phenomena such as carbonation The rate of corrosion is mainly controlled by the diffusion of dissolved oxygen through the concrete cover The corrosion products formed at the surface of rebars introduce tension stresses in the material causing the cracking and spalling of the concrete Therefore, the mechanical strength is reduced

Many laboratory studies and site inspections are carried out to analyze this phenomenon or to detect an attack as soon as possible In order to face these problems, a method of analysis of the corrosion mechanisms is required Considering the nature of the phenomenon,

[1] Materials Department, Infremer, DITI BP70, 29280 Plouzané, France
[2] Ecole Centrale Paris, Paris, France

electrochemical methods are often used The most widely used method consists of measurement of the electrode potential of the rebars which, in some cases, allows differentiation between the active and passive states of the steel

Potential mapping is a convenient tool to localize the corroded parts on large structures exposed in the atmosphere But, this method cannot give any information on kinetics, and the correlation between electrode potential and the probability of corrosion can be erroneous [*1*]

Therefore, more sophisticated methods like A-C techniques have been chosen for the study of the corrosion of steel embedded in concrete [*2,3*] With these methods, it is possible to detect the initiation of the corrosion, but the complete analysis of the data is more difficult to perform In a Nyquist plane, the shape of the a-c plots sometimes does not allow operation of the models generally adopted for the study of simple electrochemical systems equivalent circuits, mechanisms of electrochemical reactions At the initiation step of corrosion, the surface of the steel consists of either anodic or cathodic areas As the first point of this study, we propose a method for data analysis on small specimens of concrete or mortar In a second part, results are presented from tests which have been performed on large concrete beams in order to study the feasibility of such a measurement on a real structure. Two different approaches are proposed the first one consists of the development of a mathematical model, the second one is based on the use of an electrical guard in order to restrict the surface of the reinforcement measurement

Small Specimens

Experimental Procedures

Our first impedance measurements with the steel-concrete system were carried out in and after 1979. We used cylindrical mortar (sand + cement + water) specimens, containing a small mild steel rod (Fig 1) Some of the specimens were deliberately contaminated with chlorides (mass of chlorides/mass of cement = 2%), in order to initiate immediate corrosion of the steel rod After the setting of the mortar, all specimens were cured for 29 days in water saturated air at 20°C

The impedance plots were obtained with the specimens dipped in an alkaline electrolyte (sodium hydroxide solution 0 1 N) contained in a test cell, the pH of which being close to the pH of the interstitial pore solution. A classical three electrode potentiostatic set up was used .The reference electrode was saturated calomel electrode (SCE) and the counter electrode was a stainless steel grid The potentiostat was a 1186 Solartron electrochemical interface, and impedance measurements were carried out by a 1172 Solartron frequency response analyzer, in a wide range of frequencies (10^4 to 10^{-4} Hz), on the basis of five frequencies to a decade

$$f_n = 10^{0\,2n} \quad (n = 20, 19 \;\;.\;\;, -20)$$

Results

Nyquist impedance plots obtained without and with chlorides, at the rest potential, are given in Fig 2 Without chlorides, steel is passive, and with chlorides, steel is locally corroded The influences of the thickness and the porosity of the mortar cover, were also studied Furthermore, the alterations of the plots of the corroding samples were observed over a two year period In any case, the corrosion rate and the corroded areas of the steel

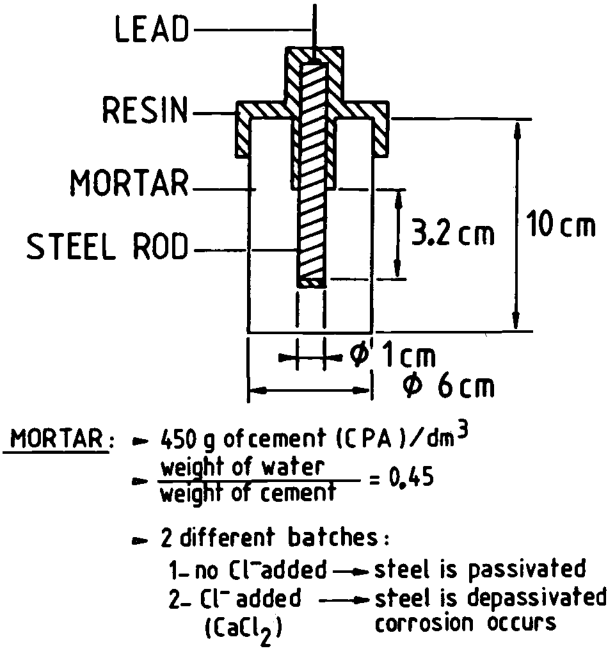

FIG. 1—*Reinforced mortar specimens.*

rod increased continuously. From these experiments, the interpretation of impedance plots could be stated precisely.

The capacitative arc of a circle obtained between 10^4 and 10 Hz is correlated to a thin precipitate of calcium hydroxide which grows slowly on the steel surface after the setting of the mortar. This interpretation was given by John et al. [*2*], who first noticed this arc in the impedance plots obtained with reinforced concrete specimens. This interpretation seems to be reasonable because we showed that the features of this arc did not depend either on the electrochemical state of the reinforcement (passive or corroded) or on an imposed anodic or cathodic overvoltage.

Moreover, we showed that the influence of the dielectric properties of the mortar cover itself appears at frequencies higher than 10^4 Hz [*4*]. The resistance of R_0 of the concrete cover is given by the high frequency limit of the arc on the real axis. The resistance of the film, R_1, is given by the length of the chord obtained at the intersection of the extrapolated arc of a circle with the real axis.

The low frequency range (10 to 10^{-4} Hz) gives precisely the electrochemical state of the steel in mortar: when the steel is passive, only on capacitative arc of a circle is visible (Fig. 2*a*) and when steel is depassivated and corroded, two arcs can be seen (Fig. 2*b*). One month after the setting of the mortar, these general features of the plots no longer change. Only the sizes and relaxation frequencies of the capacitative arcs change when the corroded area increases.

An analysis of the impedance plots of the specimens with a passive reinforcement by numerical methods, shows that the single capacitative arc is the result of more than one relaxation process.

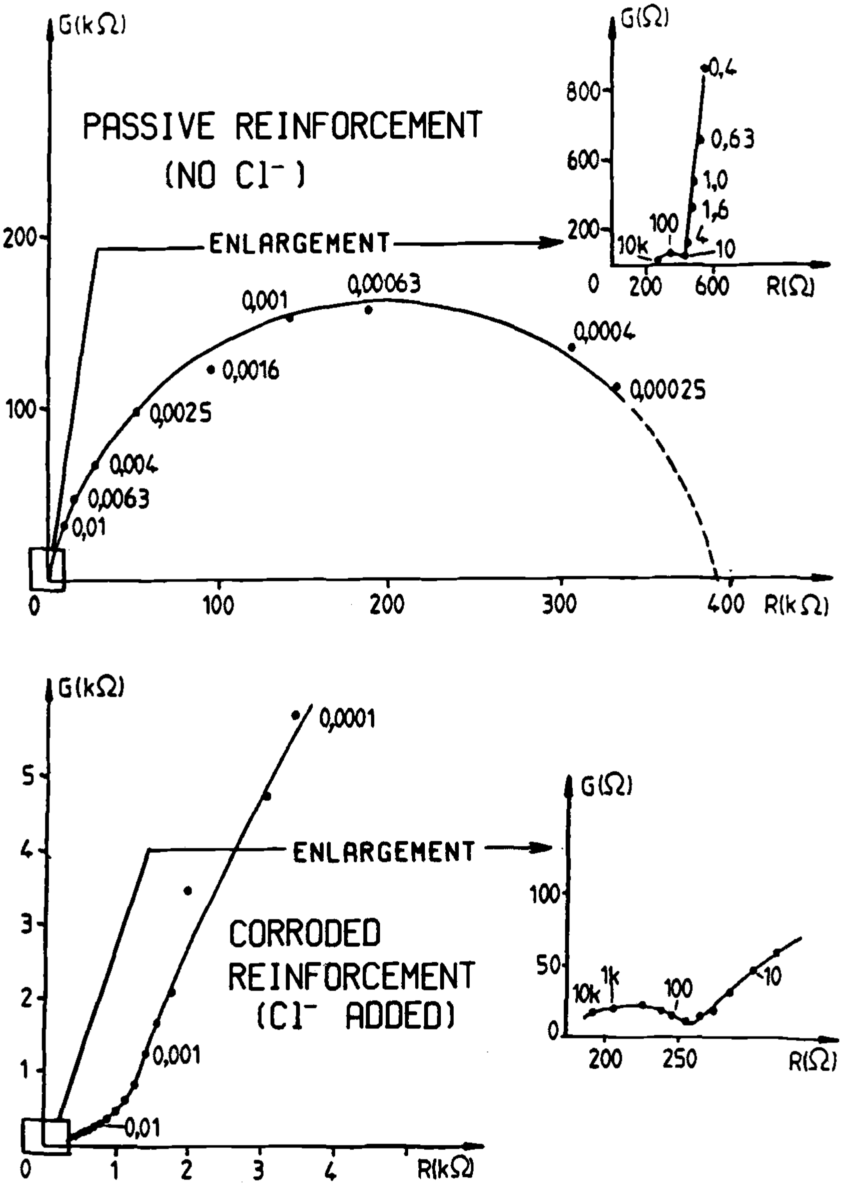

FIG. 2—*Impedance plots of the mortar specimens* (*frequencies in Hz*) *at the rest potential:* (a) *passive reinforcement and* (b) *depassivated reinforcement.*

The plots of all specimens could be explained by coupling of two relaxation processes:

1. relaxation of the double layer capacity in parallel with the transfer resistance and
2. relaxation of the surface concentration of the passivating species.

With the corroded specimens, the coupling is low enough and both arcs are visible.

Very High Frequency Measurement

In order to plot the impedance diagram at very high frequencies another frequency response analyzer was chosen: a 1255 Solartron. It allows for the reaching of frequencies up to 10 MHz. Considering the performance of the electrochemical interface (Solartron 1286), at these high frequencies, it was not possible to use a classical set up with a potentiostat. The generator of 1255 was directly connected to the specimen and to an auxiliary electrode. The voltage signal was measured between the rebar and a metallic electrode by the 1255. The current signal was obtained by measuring the ohmic drop in a calibrated resistor in series with the auxiliary electrode.

The high frequency limit is virtually equal to zero (resistance of the electrolyte). The length of the chord obtained by the intersection of the arc with the real axis gives the resistance of the concrete cover (Fig. 3).

These results have been compared to the classical set up with a 1286 Solartron interface which permits levels up to 10^5 Hz. Up to these frequencies the results are similar. But more tests are needed in order to analyze the value of capacitance.

Model of Equivalent Circuit

A model of electrical circuit (Fig. 4), equivalent to the steel-concrete systems, was developed in order to improve the analysis of the experimental Nyquist impedance plots: the circuit contains resistances R_i and capacities C_i ($i = 0, 1, 2, 3$).

1. R_0 and C_0 represent the resistive and dielectric properties of the concrete cover, and R_1 and C_1 the resistive and dielectric properties of the lime layer.
2. R_2 may be identified with the transfer resistance and C_2 with the double layer capacity.
3. The circuit R_3-C_3 represents the influence of a surface concentration relaxation (may be the concentration of the passivating species).

A numerical analysis of the impedance plots by a least squares method shows that the center of all capacitative arcs is under the real axis.

If R_1 and C_1 are pure resistances and capacitances, the centers must be on the real axis. We show in Eq 4 that the experimental diagrams can be simulated by an empirical formula

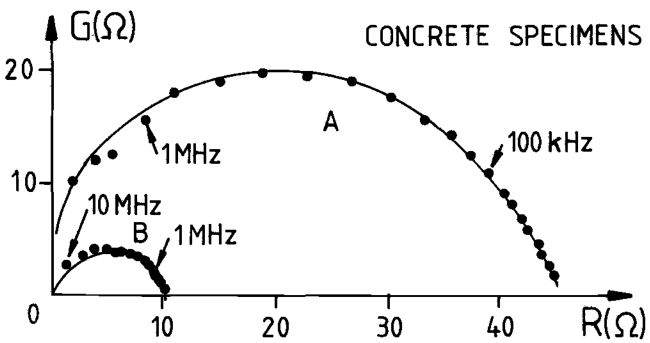

FIG. 3—*Very high frequency part:* (a) *cover thickness = 5 cm of cement content = 400 kg/m³ and* (b) *cover thickness = 2.5 cm of cement content = 350 kg/m³.*

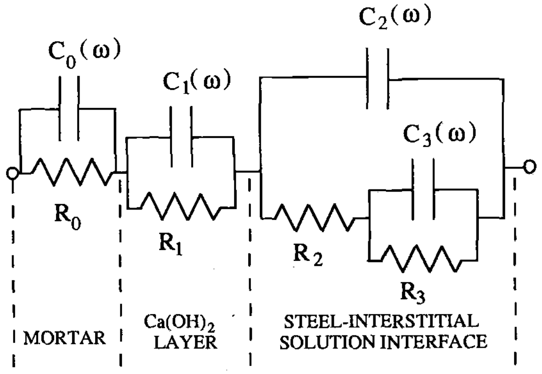

FIG. 4—*Electrical circuit, equivalent to the mortar specimens.*

to describe the frequency dependence of the complex impedance along the capacitative arc corresponding to a single relaxation process

$$Z = \frac{A_i}{1 + (j\,\tau_{0i}\,\omega)^{(1-\alpha_i)}} \tag{1}$$

where A_i, τ_{0i}, α_i are real; A_i is a resistive term (difference between the "high frequency" and "low frequency" limit if of Z); τ_{0i} is a relaxation constant; α_i is a number between 0 and 1; and ω is the pulsation of the sinusoidal signal (ω) is related to frequency (f) by the formula

$$\omega = 2\,\pi\,f$$

Equation 1 is similar to the formula of Cole and Cole [5], giving the complex dielectric constant of solid and liquid materials as a function of frequency. A formula as Eq 1 has already been used in order to analyze electrochemical impedance plots.

If the center of the capacitative arcs are under the real axis, the equivalent circuit of Fig. 4 can be used to calculate the impedance plot, but R_i and C_i are no longer real values which depend on the frequency. If we compare Eq 1 and

$$Z_i = \frac{R_i}{1 + j\,R_i\,C_i\,\omega} \tag{2}$$

giving the impedance of a parallel R_i C_i circuit, we may take

$$A_i = R_i \text{ and } C_i = \frac{{\tau_{0i}}^{1-\alpha_i}}{R_i} - \alpha_i \left(\cos\frac{\alpha_i\pi}{2} - j\sin\frac{\alpha_i\pi}{2}\right) \tag{3}$$

The analysis of the impedance plots by the least squares method gives the values of R_i, C_i, τ_{0i}. Then the impedance plot of the equivalent circuit is calculated. This model matches the experimental plots (Fig. 2) well.

According to our assumptions, R_2 is the transfer resistance. If we consider that the corrosion process may be described by the following simplified mechanisms

$$\mathrm{Fe} \rightarrow \mathrm{Fe}^{2+} + 2e^- \ (\mathrm{Fe}^{2+} \rightarrow \mathrm{rust})$$

$$\frac{1}{2}\mathrm{O}_2 + \mathrm{H_2O} + 2e^- \rightarrow 2\ \mathrm{OH}^-$$

The corrosion current, I_{corr}, is given by

$$I_{\mathrm{corr}} = \frac{K}{R_2} \tag{4}$$

The theoretical value of K depends on the number of steps in the anodic and cathodic reactions, and on the Tafel slopes of the rate constants of these steps

This assumption seems to be valid because in the low frequency range the modulus of the impedance of a corroding area is much smaller than the modulus of the impedance of a passive area (Fig 2) It means that impedance Z_p of the passive area is short circuited by the impedance Z_c of a corroding area which is in parallel with Z_p

The value of K is obtained by comparing impedance measurements and mass losses

Comparison with Mass Losses

Accelerated corrosion tests were used These tests consist of different periods of immersion of the samples in a chloride solution of 35 g/L and drying in atmosphere at 50°C The duration of the wetting period is three days and the drying period, four days The diagrams are plotted during the immersion After a certain number of cycles, three specimens were broken, the mass losses and the surface of corroded areas were measured The electrode potential is stored in a data logger versus time

Potential measurements show that the steel is depassivated after two cycles and that the corrosion remains active The potential is between -500 and -600 mV/SCE Diagrams are plotted at each cycle for 18 weeks for the duration (t_i) of the experiment Values of transfer resistance (R_t) are obtained by using the model formerly presented

After obtaining a diagram, the specimen is broken and the mass loss (ΔP_{1i}) is obtained Transfer resistance can be correlated to corrosion current I_{corr}

Using Faraday's law, it is possible to obtain the mass loss, ΔP_{2i}, after the duration, t_i, as follows

$$\Delta P_{2i} = \frac{KM}{4F}\, \Sigma_{n=0}^{i}\, \tau_i \left(\frac{1}{R_j} + \frac{1}{R_{j+1}}\right) (\tau_{j+1} - \tau_j) \tag{5}$$

M = mere atomic weight of iron

In plotting for different τ_i values of ΔP_{1i} versus ΔP_{2i}, we obtain different points If we try to draw a straight line starting from the origin, we obtain a value of K equal to 35 mV But taking into account the fact that the corrosion rate is not constant during the different periods of wetting and drying, and that the corrosion is not uniform, this value cannot be used to determine an instantaneous corrosion rate (Fig 5)

After breaking the sample, the measurement of the corroded area of the steel bar is not very accurate but gives interesting information on the propagation of corrosion We consider that the corrosion rate on the active surface is quite constant and that the transfer resistance decreases with an increase of the active surface

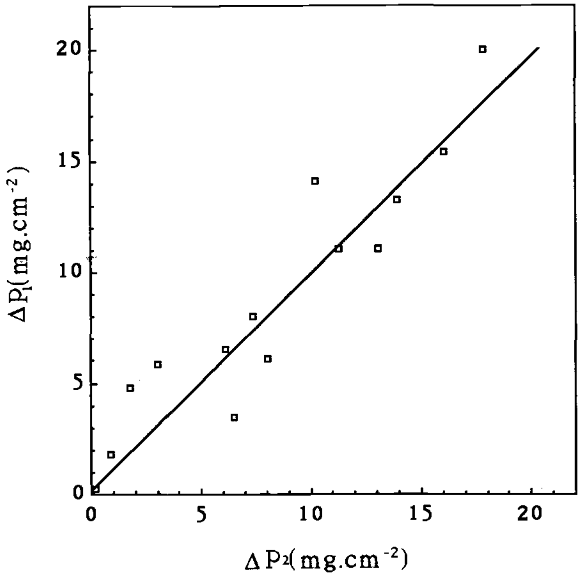

FIG. 5—*Results of an accelerated corrosion test of reinforced concrete specimens. Comparison of the experimental mass losses* (ΔP_l) *with the mass losses* (ΔP_2) *calculated from impedance plots by Eq 4 with* K = *35 mV.*

Large Scale Tests

Feasibility of Impedance Measurements

We thought that electrochemical impedance measurements could be carried out on large reinforced concrete structures to detect and analyze the local corrosion of the reinforcement.

Impedance plots of big reinforced concrete beams (Fig. 6) were obtained with beams in seawater and out of water. The measurement setup was the same as the one used with small specimens. The working electrode was the whole reinforcement (bars, frames, pins). The counter electrode was a small (10 by 10 cm) platinized titanium sheet, and the reference electrode was a saturated calomel electrode. These two electrodes were put in a small open

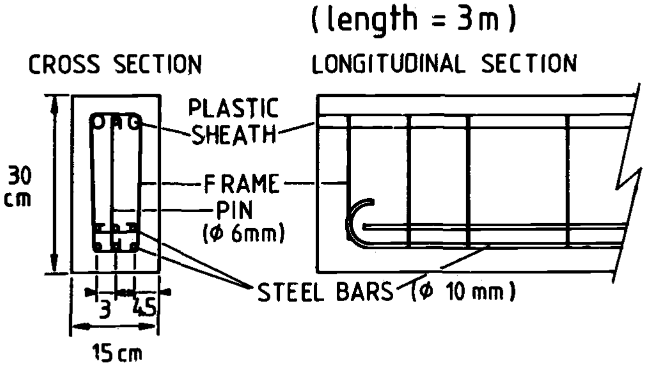

FIG. 6—*Reinforced concrete beams.*

box which was simply dipped in seawater near the beam. When the beam was out of water, the open gasket-lined side of the box was pressed on the concrete and the box was filled with a 0.5 *M* potassium chloride solution. Before the impedance measurements, the beams were cracked by cyclic loading and subject to cyclic dipping in seawater.

Two beams were tested. We cannot describe damage on these two beams, but we can specify that Beam *A* presented wide cracks and some rust spots at the surface of the concrete. On the Beam *B*, the cracks were very few and narrow and no rust spots were visible.

The impedance plots of the beams in seawater are given in Fig. 7. Their main features do not depend on the location of the probe (cell containing the counter and reference electrodes) near the beam. This fact is due to the conductivity of seawater which is higher than the conductivity of concrete. Differences appear in the low frequency range of the plots. With the severely corroded Beam *A*, a straight line appears below 0.01 Hz, that makes an angle of 45° with the real axis. With Beam *B*, the low frequency range, below 0.1 Hz, is an arc of circle, the center of which is under the real axis, and the diameter is approximately 300 ohm. In the high frequency range, a small capacity arc of circle is found, similar to the arc obtained with mortar specimens, which is explained by the precipitation of a lime layer on the steel surface.

When the beams are out of water, the features of the impedance plots depend on the placement of the probe on the surface of the beam. The diagram in Fig. 8 was obtained with the probe near a wide crack of Beam *A*. A large "high frequency" arc, and a "low frequency" straight line are found.

These experiments proved that impedance measurements are feasible with large reinforced structures dipped in water or out of water, and proved that the detection of corroded structures can be done by these measurements. In seawater, the impedance plot does not depend on the place of the "probe" (reference electrode + counter electrode) near the beam. In this very conductive medium, which acts as a short circuit, the share of a little steel area of a bar, in the beam impedance, depends only on the electrochemical state of the steel, and not on the position of the area on the bar. In these conditions, the whole corrosion current could be obtained from impedance plots. However, the location of the corroded area cannot be found.

By contrast, in the open air, the only conductive medium (the mortar itself) has a low conductivity, and we note that the impedance plots depend on the location of the probe on the beam surface to a large extent. In this case, the shape of the impedance of each element of area depends also on the distance between the probe and the element.

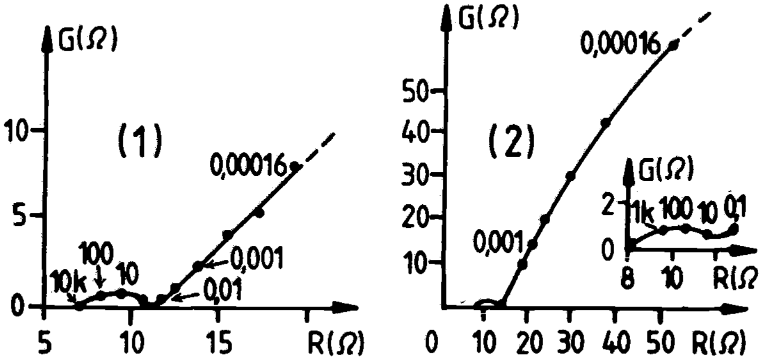

FIG. 7—*Impedance plots of reinforced concrete beams dipped in seawater:* (1) *Beam A = severely corroded and cracked and* (2) *Beam B = lightly cracked, no corrosion evidence.*

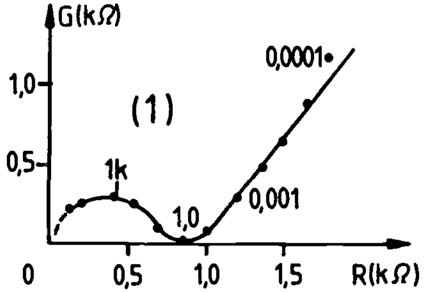

FIG. 8--*Impedance plot of a reinforced concrete beam (Beam* A *out of water). Impedance plot recorded near a crack.*

The difficulties that arise concerning the interpretation of the impedance plots are the result of the unusual experimental conditions:

1. the big length of the steel bars (longer than the counter electrode used for the measurements),
2. the complicated geometry of the working electrode (reinforcement), and
3. the galvanic corrosion cells encountered in the corrosion of the locally depassivated reinforcement.

We first analyzed the problems related to the big length of the reinforcing bars, and the occurrence of local corrosion, in the case of measurement out of water.

Theoretical and Experimental Models

Our model was developed to describe the one-dimensional instance of a long reinforcing bar embedded in concrete. The steel bar is the working electrode; the concrete, containing the pore solution, is an electrolyte; the reference electrode and the counter electrode are in a cell containing an electrolyte and lying on the concrete surface what we call "the probe." The dimension of the counter electrode is supposed to be much smaller than the length of the bar. Under these conditions, that are represented in a simplified version on Fig. 9*a*, every unit area of the bar (for example, 1 on Fig. 9*a*) being separated from the probe (A)

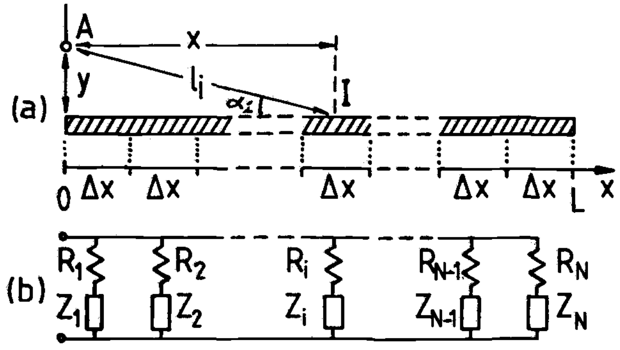

FIG. 9—*Academic model.*

by a concrete layer, the electrical resistance of which (R_i) depending on its thickness (L_i). The current lines are supposed to be the straight lines, AI. The corresponding electrical model is given on Fig. 9*b*. In this model, Z_i is the impedance of the metal-electrolyte interface in series with the resistance, R_i, which means that several unit Randles circuits are in parallel. The resistance, R_i, is supposed to be given by the formula

$$R_i = \frac{\rho L_i}{\Delta S_i \sin \alpha_i} \tag{6}$$

where ρ is the resistivity of the electrolyte, α_i is the angle AIO, ΔS_i is the area of I.

The total electrochemical impedance can be calculated from

$$\frac{1}{Z} = \Sigma_i \left(\frac{1}{R_i + Z_i}\right) \tag{7}$$

When the electrochemical state of the bar is uniform (for example: completely passive or completely active and no d-c potential applied), an analytical calculation of the total impedance is possible.

Test of the Model with an "Academic" Electrochemical System

This theoretical model was tested in simplified experimental conditions [7]. A 1-m-long stainless steel bar (304L) has been dipped in a 0.1 N sulfuric acid (H_2SO_4) solution. The steel is in a uniform passive state. The impedance measurements were carried out in experimental conditions corresponding to the model (Fig. 9*a*). The experimental and calculated, Eq 7, impedance plots are represented on Fig. 10. Only the "high frequency" part of the plots was given, in order to show the distortion of the curve, which clearly appears, as a result of the geometry of the system.

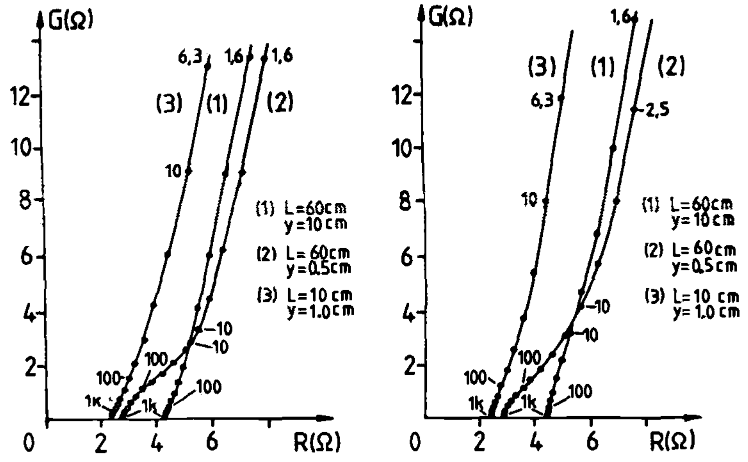

EXPERIMENTAL PLOTS CALCULATED PLOTS

FIG. 10—*Experimental results.*

In the simulation, the specific interfacial impedance is only a double layer capacity in parallel with a transfer resistance. To attribute the distortion to a coupling of two different relaxation processes would be a serious misinterpretation.

When the local depassivation and corrosion occur on a long steel bar, the total impedance cannot be calculated by Eq 7 because the specific impedance distribution is actually unknown. But the probe can be used to detect the corroded area, and sometimes to measure the corrosion current on this area [*4,6*]. The value of current density needs to know the active surface. Generally, the specific impedance of a depassivated area is much smaller in the low frequencies range than the specific impedance of a passive area. In a way, the impedance of the corroded area tends to make a short circuit in the circuit of Fig. 9*b*. The most effective short circuit is obtained when the resistance, in series with the impedance of the corroded area, has the minimum value. If Distance *y* is fixed (see Fig. 9*a*), this condition is obtained when the probe is straight above the corroded area.

In 0.1 *N* H_2SO_4, a mild steel rod (5-cm-long) was inserted in the stainless steel bar. The passive stainless steel and the corroding mild steel made a galvanic cell. The probe was shifted parallel to the bar, from one end to the other, and impedance plots were recorded in different places. The results are gathered in Fig. 11. The analysis of the changes of the plots gives a very accurate detection of the corroded area location: the size of the plot is

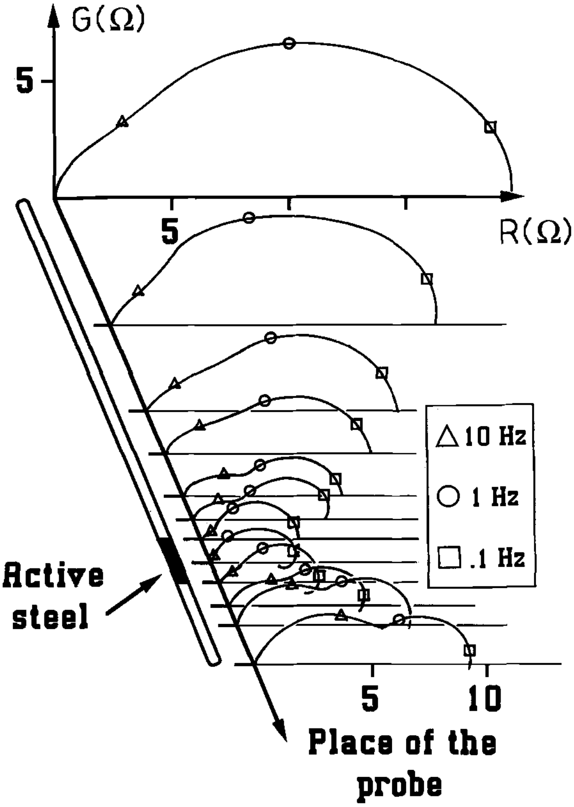

FIG. 11—*Detection of a corroded mild steel zone (active steel) in a passive (304L steel) bar (1 m long), dipped in 0.1* N H_2SO_4.

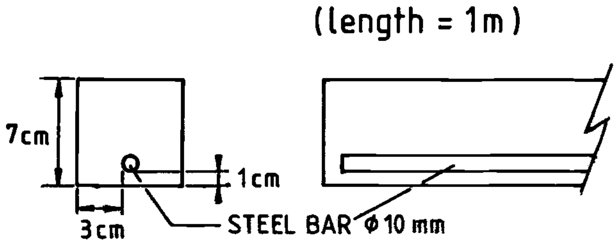

FIG. 12—*Reinforced mortar beam.*

minimum when recorded above the middle of the mild steel rod. We showed [*8*] that this plot was virtually identical to the impedance plot of the steel rod alone, when polarized at the galvanic cell potential and we succeeded in calibrating the relationship between the transfer resistance and the corrosion rate of the steel rod in acid. We now make the same calibration for the steel in concrete using mass losses.

Test of the Model of a Mortar Beam

The validity of our model was tested on a small (7 cm by 7 cm by 100 cm) reinforced mortar beam (Fig. 12). The reinforcement was made of one single mild steel bar. No chlorides were added to the mortar, and the bar was in a uniform passive state. Experimental impedance plots are given on Fig. 13 and show the distortion, predicted by the model, which appears here in the low frequency range.

The shape of the distortion depends on the placement of the probe along the surface of the beam, as predicted by the model.

Experiments must now be carried out with a mortar beam, the reinforcing bar of which is locally depassivated and corroded. Such an experiment will prove the capacity of the model to interpret the experimental plots obtained with long structures and will give the basis of experimental procedures to detect and analyze the local corrosion of the reinforcing bars.

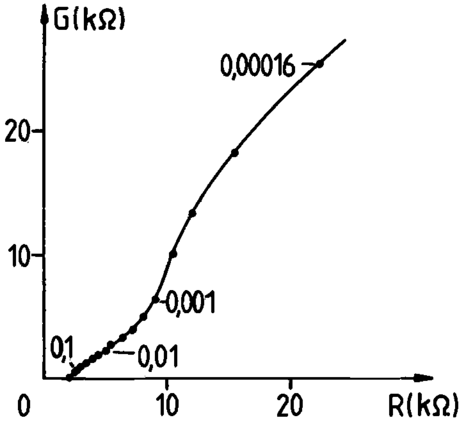

FIG. 13—*Impedance plot (low frequency range) of a mortar beam (out of water with passive reinforcement). The probe is at one end of the beam.*

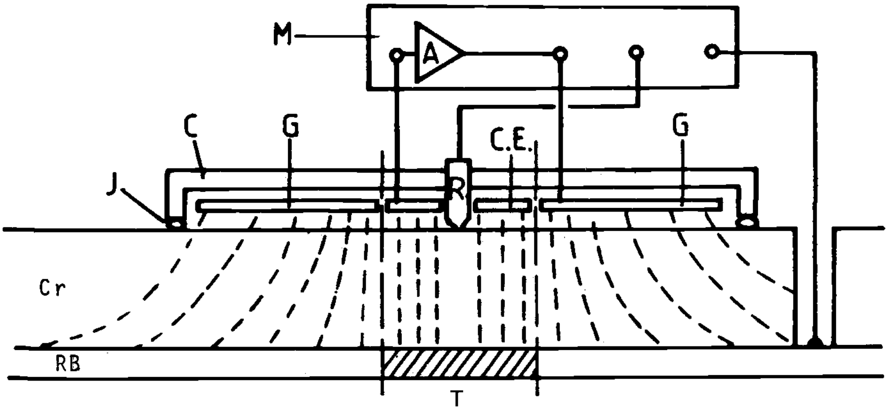

Cr : Concrete
RB : Reinforcing bar
M : Measurement device
A : Current amplifier (measurement of the current flowing through the CE)
CE : Counter electrode
G : Electrical guard
C : Cell (contains a conductive solution)
R : Reference electrode
J : Sealing gasket
T : Area the impedance of which is measured.
\- - - - - - : lines of current

FIG. 14—*Setup with an electric guard.*

Setup with an Electrical Guard

It is possible to avoid the spatial distribution of impedance versus the frequency by using a specific auxiliary electrode with an electrical guard. This setup allows measurement of only the current flowing from the surface of rebars in front of the auxiliary electrode (Fig. 14).

In order to obtain accurate and worthwhile data, it is necessary to maintain the auxiliary electrode and its guard at the same potential versus different frequencies. Therefore, a specific electronic device was developed and integrated in a classical three electrode setup with a potentiostat and a frequency response analyzer. These measurements were performed on concrete beams in the atmosphere. The reference and auxiliary electrodes are put in water box allowing an electrolyte junction between the surface of the concrete and the electrodes (Fig. 14).

Experiments were carried out on 1.5-m-long concrete beams containing two reinforcing steels. The cover thickness is 4 cm. The cement content is 300 kg/m^3. The water to cement ratio (w/c) is 0.55. The results obtained are presented in Fig. 15. The influence of the electrical guard is clearly shown. At low frequencies, a good agreement is obtained between data gathered on the whole concrete beam and data acquired from the electrical guard setup, taking into account the ratio of surface.

At high frequencies, some scatter is obtained due to the difficulty of maintaining the same potential at the auxiliary electrode and of its guard. The low currents that were measured need the use of an amplifier with a very high gain. Its performance at high frequencies is not good enough to avoid any phase shift disturbing the measurements. We consider that the concept of this measurement is adapted, but some technical problems have to be solved in order to obtain good data at high frequencies.

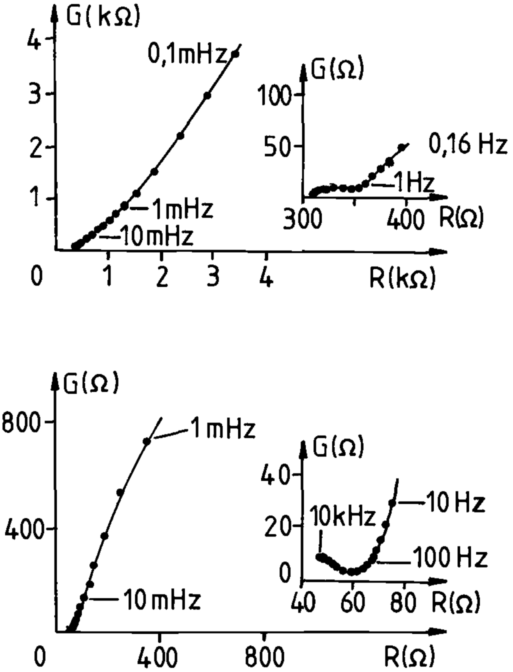

FIG. 15—*Tests on large concrete beams:* (top) *with electrical guard and* (bottom) *without electrical guard.*

Conclusions

Electrochemical impedance plots allow the characterization of the different mechanisms of corrosion of steel embedded in concrete. The developed model using an equivalent circuit is in good agreement with the obtained data. Different parameters (capacitance and resistance) were correlated with different phenomena including effect of cover thickness, film at the steel concrete interface, transfer resistance, etc. This method can be used to benefit the study of the durability of reinforced concrete considering different environmental parameters and various concrete compositions (cement content, w/c, etc.).

But considering the fact that the corrosion of concrete is not uniform, this model does not allow the obtaining of a quantitative value of the corrosion rate in the first step of the propagation.

Some new interpretations have to be found, in order to try to measure the real corrosion rates on the anodic surface.

This method used on large specimens is feasible. The results show that it is possible to detect an active surface taking into account the shape of the diagram and a specific model.

This method can certainly be a useful tool to detect corrosion on real structures. However, some further research is needed in order to obtain more quantitative data.

References

[*1*] Lemoine, L., Tache, G., and Raharinaivo, A., "Corrosion du beton arme en environnement marin: methodologies d'inspection," 8e Congres Europeen de corrosion, Nice, 1985.

[2] John, D. C., Searson, P. C., and Dawson, J. L., *British Corrosion Journal*, Vol. 16, No. 2, 1981, p. 102.

[*3*] Wenger, F and Lemoine, L , "Etude de la corrosion de l'acier doux dans le beton par les methodes electrochimiques," 9th International Congress on Metal Corrosion, 1984

[*4*] Wenger, F , "Etude de la corrosion de l'acier dous dans le beton par les methodes electrochimiques Application au controle des ouvrages de genie France Civil," No 3158, Thesis, Universite Paris Sud, 91 Orsay, 1987

[*5*] Cole, K S and Cole, R H , *Journal of Chemical Physics*, Vol 19, 1984, p 1951

[*6*] Zhang, J , Wenger, F , and Galland, J , *Controle de l'etat local de corrosion de structures metalliques de grands dimensions par les mesures d'impedance electrochimiques*, C R Academie Sc , Paris, Serie II, No 14, 1987, p 304

[*7*] Zhang, J , Wenger, F , Jerome, M , and Galland, J , "Controle de la corrosion par la mesure de l'impedance electrochimique pb des structures de grandes dimensions," C R A C A D S C , Paris, Serie II, No 14, 1985, p 995

[*8*] Zhang, J , "Etude de la corrosion de structures metalliques de grandes dimensions par les mesures l'impedance electrochimiques Application au controle de l'etat de corrosion des armatures de beton," thesis, Ecole Centrale de Paris, 92 Chatenay Malabry, Paris, France, Dec 1987

Carmen Andrade,[1] *Angeles Macias,*[1] *Sebastian Feliu,*[2] *Maria Lorenza Escudero,*[2] *and José Antonio González*[2]

Quantitative Measurement of the Corrosion Rate Using a Small Counter Electrode in the Boundary of Passive and Corroded Zones of a Long Concrete Beam

---

REFERENCE: Andrade, C , Macias, A , Feliu, S , Escudero, M L , and González, J A , **"Quantitative Measurement of the Corrosion Rate Using a Small Counter Electrode in the Boundary of Passive and Corroded Zones of a Long Concrete Beam,"** *Corrosion Rates of Steel in Concrete, ASTM STP 1065,* N S Berke, V Chaker, and D Whiting, Eds , American Society for Testing and Materials, Philadelphia, 1990, pp 134–142

ABSTRACT: Recently, in CORROSION-87, one paper was presented which, assuming the electrical model of the "transmission line" to represent the nonuniform distribution of the current in a concrete beam, demonstrated the calculation of the instantaneous corrosion rate by unit of length of the rebar through mathematical equations

In the present contribution those equations are used in order to determine whether the equations enable distinction between the corroded zones of a rebar and those which remain passive A concrete beam was fabricated, half of it by mixing chlorides with the cement (and therefore inducing a corrosion in the rebars) and the other half without admixtures (passivated zones of the rebars) The apparent polarization resistance was measured along the beam using a small counter electrode Through the equations previously proposed, the corrosion rate was calculated

The results obtained confirm that the boundary between corroded and passivated zones can be clearly identified using these formulae Finally, some comments are given on the relative activity of galvanic macrocells compared with the corrosion microcells

KEY WORDS: steel in concrete, polarization resistance measurements, on-site corrosion rate, macrocell action, steels, corrosion, concrete

The direct measurements of the corrosion rate in real structures would be the ideal method for monitoring the structures' behavior However, only in few cases was this possible and the laboratory reproduction of the system metal/environment has been the usual method for determining the corrosion performance of big structures Monitoring situations in concrete structures is especially complicated because of the difficulties that concrete poses when using nondestructive measurement techniques Concerning the corrosion of reinforcements, the only measurement technique employed successfully has been, up to now, the potential mapping whose most important limitation is its qualitative character In recent papers [*1–4*], the authors have tried to offer a new approach in order to estimate electrochemically the corrosion rate of reinforcements in beams and slabs.

---

[1] Researchers, Institute of Construction and Cement "Eduardo Torroja," CSIC, Madrid 28080, Spain

[2] Researchers, National Center of Metallurgical Research, CSIC, Madrid 28040, Spain

In big structures, the main difficulty arises from the impossibility of using an electrode the same size as the structure itself. If small electrodes are used, then the electrical signal vanishes in accordance with the distance up to a critical length, as Fig. 1*a* shows.

As the electrical signal is not uniformly sprayed, the polarization resistance (Stern's formula) cannot be directly applied because of the ratio between the applied signal and the current or potential response: $R_p = \Delta E/\Delta I$. The surface area reached is unknown and the value of signal varies with the distance.

If the distribution of the signal was uniform (Fig. 1*b*) through an electrode of the same size as the structure, then the difficulty would disappear as was mentioned.

In the aforementioned paper [*1*], mathematical formulae assuming the transmission line as equivalent circuit (Fig. 2) to model the concrete/steel system, were proposed in order to solve these limitations. The results obtained showed there was a good agreement between the corrosion rates calculated when a uniform distribution of the signal (Fig. 1*b*) is guaranteed and those rates obtained from the mathematical formulae presented. Beams fabricated without admixtures (passivated steel) and with 3% of calcium chloride ($CaCl_2$) in the mix (active corrosion) were used for the experiments.

In the present communication, beams containing active and passive zones in the same reinforcement were fabricated (half beam contaminated with chlorides and other half without admixtures). Formulae aforementioned [*1*] are employed here for checking their validity to identify active/passive boundaries. Moreover, the action of galvanic macrocells was investigated.

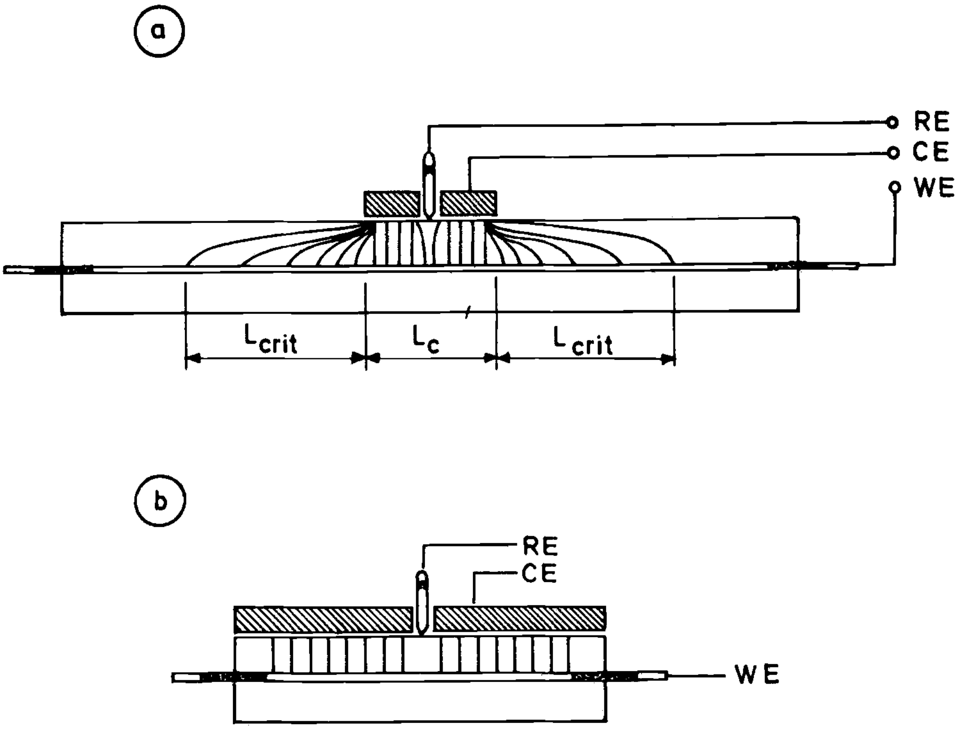

FIG. 1—*Distribution of electrical signal as a function of counter electrode size:* (a) *non-uniform one and* (b) *uniform one.*

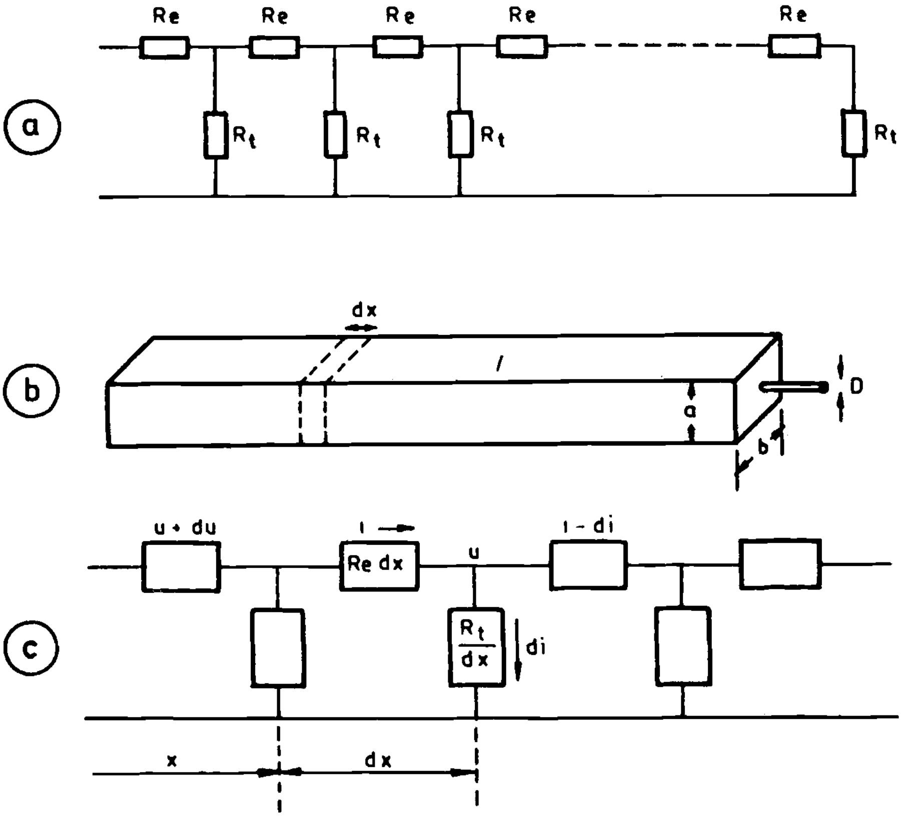

FIG. 2—*Equivalent circuit for interpreting the response of the reinforcement to a small-amplitude electrical signal:* (a) *model in "transmission line,"* (b) *and* (c) *flow of the current through and infinitesimally small beam element.*

Materials

The experimental work was carried out on beams of 160 cm length and 6 by 10 cm^2 cross section. The beams have 350 kg of cement per m^3 of concrete. Half beam was fabricated without admixtures and to the other half 3% $CaCl_2$ by weight of the cement content was added in the mix (Fig. 3).

Three steel bars of 0.7 cm in diameter were embedded in the beams as Fig. 3 also shows. The disposition of the bars was such that two identical ones were on contact either with the concrete without admixtures (thus being passivated) or with that contaminated by chlorides (thus actively corroding). Their exposed length was 70 cm each. The other bar was in contact throughout the two halves (with and without chlorides) of the beam. Its exposed length was 140 cm.

As a counter electrode, a small cylinder 4.5 cm in diameter was used. A hole of 0.8 cm in diameter allowed the placement of the reference electrode in its center.

Procedure

For evaluating the corrosion rate of each bar, the distribution of the electrical signal in the bars is assumed to follow the transmission line model [*1*], Fig. 2*a*. Taking into account

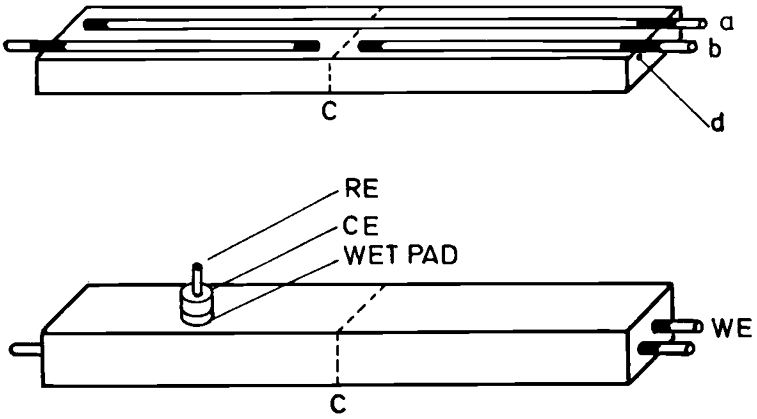

FIG. 3—*Representation of the beam type used:* (a) *continuous rebar,* (b) *half-bar,* (c) *boundary between the concrete with and without chlorides, and* (d) *insulating tape.*

the differential equations for an infinitesimal element of the model (Figs. 2*b* and *c*), the following mathematical solution may be obtained [*1*].

$$R_t = 4(R_p')/Re \tag{1}$$

$$R_t = Re/\alpha^2 \tag{2}$$

which gives the true polarization resistance values by unit of beam length, R_t, as a function of the apparent polarization resistance, R_p', also by unit of length (R_p' is the value directly obtained by the ratio between applied polarization and current response $R_p' = \Delta E/\Delta I$) or as function of the coefficient α, estimated by the attenuation of the potential with the distance from the counter electrode. *Re* is the ohmic resistance of the concrete by unit of slab length.

The coefficient, α, in the case of a beam, may be calculated through Eq 1

$$\alpha = \frac{1}{x_2 - x_1} \ln \frac{u(x_1)}{u(x_2)} \tag{3}$$

Where $u(x_1)$ and $u(x_2)$ are the potential values of the rebar at the distances x_1 and x_2 from the counter electrode when a step of potential ΔE (here, 100 mV) is applied.

In order to calculate R_t through one of the two methods mentioned, the estimation of *Re* is needed. As was previously described, *Re* may be calculated in different ways, one of which is through the known expression $\rho = 2RD$, where D is the counter electrode diameter, ρ is the concrete resistivity, and R is the ohmic resistance compensated by the potentiostat.

TABLE 1—*Values obtained from a step of potential of 10 mV in beams slightly wet.*

E_{corr}, mV	ΔI, μA	R_p', ohm	R, ohm	Remarks
−348	66	151	500	bar divided into two and concrete with chlorides
−108	4.1	2440	1500	bar divided into two and concrete without chlorides

TABLE 2—*Attenuation of the potential with the distance along the beam from the counter after applying a step of potential of 100 mV*

Distance, cm	E_1, mV	E_2, mV	ΔE, mV	Remarks
2 5	−351	−325	26	bar divided into two and concrete with chlorides
5	−373	−360	13	
10	−383	−375	8	
15	−370	−364	6	
5	−129	−88	41	bar divided into two and concrete without chlorides
10	−126	−91 3	34 7	
15	−121 6	−91 6	30	
20	−123 8	−98 1	25 7	

The values of R_T (ohm cm^2) obtained by these "indirect" measurements were finally compared with those obtained with an extended counter electrode which completely covers the beam Through this arrangement an uniform distribution of the signal is guaranteed (Fig 1*b*) and R_T may be directly calculated from the measurement by Stern's formula

Results

Although numerous experiments were carried out, only one set of them is represented here It corresponds to the cases in which the beams were maintained slightly wet or partially immersed in water

In Table 1, the values of E_{corr}, ΔI, R_p' and R_{ohm} obtained from direct measurement are given In Table 2, the values corresponding to the attenuation of potential method are also shown Finally, in Table 3, the R_T values are presented, which correspond to the two previous methods and to that using an extended counter electrode

The R_T values for the case of maintaining the beam partially immersed in water are presented in Table 4

Concerning the action of galvanic macrocell in the case of the longest rebar (half passivated and half actively corroding), Table 5 gives the values of the different parameters as a function

TABLE 3—*Comparison between the* R_T *(ohm cm^2) values obtained from the indirect measurements (Eqs 1 and 2 in the text, Methods A and B, respectively) and those obtained from the direct determination using and extended counter of the same size as the beam (Method C) Beam slightly wet*

Conditions	E_{corr}	R_T Values		
		A	B	C
CONCRETE WITHOUT CHLORIDES				
Continuous bar	−216	300 000	154 000	187 000
Bar divided into two	−108	273 000	380 000	250 000
Rebar divided into two and short-circuited	−217	235 000	123 000	136 000
CONCRETE WITH CHLORIDES				
Continuous bar	−316	4 500	5 100	4 800
Bar divided into two	−366	2 900	2 100	7 100
Bar divided into two and short-circuited	−348	4 500	9 700	6 500

TABLE 4—*The same comparison as in Table 3, but for a beam partially submerged in water*

Conditions	E_{corr}	R_T Values		
		A	B	C
	CONCRETE WITHOUT CHLORIDES			
Continuous bar	−334	75 000	53 000	83 000
Bar divided into two	−101	303 000	284 000	300 000
	CONCRETE WITH CHLORIDES			
Continuous bar	−468	900	3 100	2 300
Bar divided into two	−487	1 100	4 700	3 400

of the distance along the beam The R_T values were calculated through the Apparent R_p method The effectiveness of the method for distinguishing the boundary between active and passive is high whereas the corrosion potential values method is not effective

The action of the galvanic macrocell may also be followed by externally short-circuiting the smaller rebars Figure 4 shows the changes in the individual E_{corr} measured after short-circuiting the bars In the figure, the evolution of the macrocell current, measured through a zero resistance ammeter (ZRA), is also shown

The E_{corr} values of the active rebar are slightly affected by the macrocell action However, the E_{corr} of the passivated bar moves about 100 mV or more in the negative direction depending on the moisture conditions

It may be also observed from Tables 3 and 4 that the R_T values for a concrete without chlorides in the longest bar are lower (i_{corr} is higher) than in the smaller ones (not suffering

TABLE 5—*Evolution of the* R_T (*ohm cm*^{2}) *values with the distance to the interface between chloride contaminated and non-admixed parts of the continuous* (*longest*) *rebar The* R_T *values were obtained through Eq 1 in the text*

Distance, cm	E_{corr}, mV	ΔI, μA	R_p'	R, ohm	R_T, ohm cm^2
		3% CALCIUM CHLORIDE			
70	−182	73	137	500	2 600
60	−194	70	143	420	3 300
50	−210	71	141	410	3 300
40	−221	63	159	380	4 600
30	−226	51	196	320	8 200
20	−218	59	170	440	4 500
10	−216	45	222	540	6 300
0	−200	11 5	870	770	67 000
		WITHOUT CHLORIDE			
10	−178	6 2	1 610	730	244 000
20	−173	6 2	1 610	680	262 000
30	−176	5 8	1 720	680	300 000
40	−193	5 7	1 750	1 300	162 000
50	−191	4 6	2 170	840	385 000
60	−209	3 3	3 030	840	751 000
70	−181	4 6	2 170	1 600	202 000

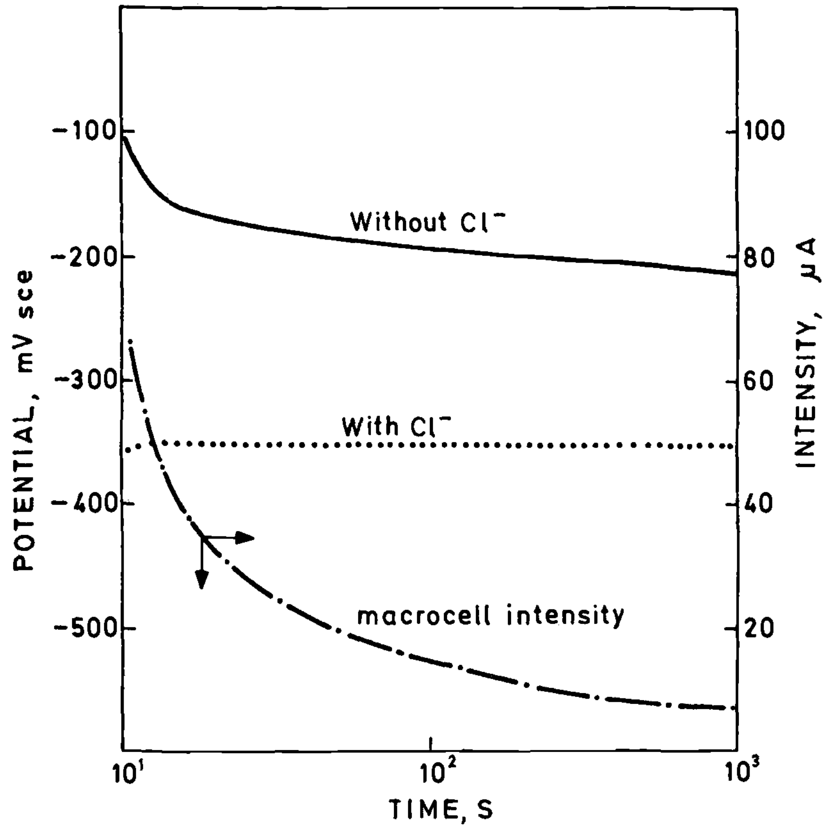

FIG. 4—*Evolution of* E_{corr} *and macrocell current with time of the smaller bars just after being externally short-circuited.*

macrocell action). Apparently, the passivated zones of a bar suffering macrocell action are three or four times more active than in the case in which no macrocell is established. Further work is needed to clarify this unexpected inconsistent result. On the other hand, the galvanic macrocell does not appear to play an important role in the chloride contaminated part of the beam.

Discussion

The possibility of using formulae previously proposed by Feliu et al. [*1,2*] in order to distinguish active and passive zones on the same rebar is experimentally justified here.

The results offered enable this differentiation because the i_{corr} values obtained differ by one or two orders of magnitude between passivated zones and those which are actively corroding. On the other hand, in slightly wet conditions the potential mapping leads to erroneous conclusions since the E_{corr} values do not differ significantly.

Another important advantage of the proposed measurement methods is the possibility of studying the real effect of galvanic macrocells. Numerous comments were previously stated [*5,6*] concerning the importance of this effect, but the experimental contributions are rather limited, and based only on the galvanic current measurements, because no other method of measurement of the corrosion rate was available.

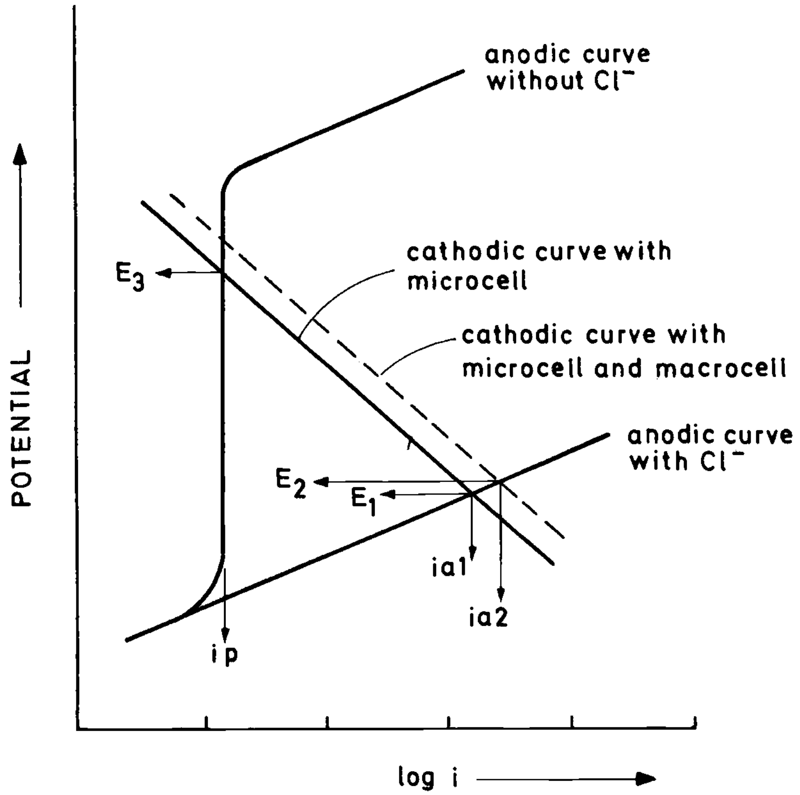

FIG. 5—*Evans' diagram representing the galvanic macrocell. In the active zones,* E_l *and* i_{al} *represent the values before short-circuiting the smaller bars and* E_2 *and* i_{a2} *after short-circuiting them. In the passive zones, the influence appears to be much higher in* E_{corr}*, moving* E_3 *to* E_2*, but lower on the* i_{corr} *values.*

In the present paper, a first attempt of comparing the contribution of the current of the galvanic macrocell with the total corrosion current, is presented. From the results obtained some interesting deductions and some contradictory evidence arise. Regarding Evans diagram in Fig. 5, the facts may be interpreted as follows:

1. The macrocell only slightly polarizes the actively corroding zones. Almost no difference in the R_T values may be found in the isolated rebars compared with the longest one.
2. The macrocell highly polarizes the passive zones in spite of the low galvanic current value detected (Fig. 4). In this situation, perhaps the R_T calculated is not correct as other authors have previously stated [5]. This point needs further investigation.

Conclusions

It is confirmed that the methods of measuring R_T in concrete structures previously proposed by the authors enable:

1. the measurement of the time corrosion rate in big real concrete structures (The results show a good agreement with those obtained when a uniform distribution of the electrical signal is guaranteed.),

2 the delimitation and distinction between active and passive zones in the same rebars, and

3 the study of the galvanic macrocell action

Acknowledgments

The authors are grateful to the "Comisión Asesora de Investigación Científica y Técnica" (CAICYT) of the Ministry of Education and Science of Spain which supports this research

References

[*1*] Feliu, S, González, J A , Andrade, C , and Feliu, V , Corrosion/87, Paper No 145, San Francisco, CA, March, 1987

[*2*] Feliu, S , González, J A , Andrade, C , and Feliu, V , *Materials and Structures (RILEM) Corrosion,* Vol 22, 1989, pp 199–205

[*3*] Feliu, S , González, J A , Andrade, C , and Feliu, V , *Corrosion Science,* Vol 29, No 1, 1989, pp 105–113

[*4*] González, J A , Feliu, S , Escudero, M L , Andrade, C , and Macias, A , "Measurements and Testing in Civil Engineering," Intern Conference, Lyon, Sept 1988

[*5*] Slater, J E , in *Corrosion of Metals in Association with Concrete, ASTM STP 818,* American Society for Testing and Materials, Philadelphia, 1983, pp 40–43

[*6*] Schiessl, P , *Betonwerk Fertigteil Technik,* Vol 52, No 10, 1986, pp 626–635

Bernhard Elsener[1] *and Hans Böhni*[2]

Potential Mapping and Corrosion of Steel in Concrete

REFERENCE: Elsener, B , and Bohni, H , **"Potential Mapping and Corrosion of Steel in Concrete,"** *Corrosion Rates of Steel in Concrete, ASTM STP 1065,* N S Berke, V Chaker, and D Whiting, Eds , American Society for Testing and Materials, Philadelphia, 1990, pp 143–156

ABSTRACT: The results of potential mapping surveys of bridge decks of the Swiss highways, using a new eight-wheel electrode measurement system, are reported here A comparison of the state of corrosion of the rebars (obtained by visual inspection after removing the concrete cover), including the potential fields in addition to theoretical considerations, clearly demonstrates that an absolute potential value (that is, −350 mV copper sulfate electrode (CSE) as proposed in ASTM Test for Half-Cell Potentials of Uncoated Reinforcing Steel in Concrete (C 876-80) for the identification of active corrosion of steel in concrete does not exist Combining the local potential gradient on the surface with information on the electrical resistivity of the concrete (measured with the four-point method or a-c impedance) allows determination of a rough estimate of the corrosion rate in a single macrocell Impedance spectroscopy, well suited for studying corrosion mechanisms in the laboratory, was found to be too time consuming and difficult to interpret in field measurements Instead, a very rapid new technique—using galvanostatic pulse measurements—was tested successfully on site It gives clear, unambiguous results on the corrosion state of the rebars, when half-cell potential measurements are uncertain

KEY WORDS: corrosion, steel in concrete, potential mapping, survey, a-c impedance, galvanostatic pulse technique, steels, concrete

Corrosion of reinforcing steel is a worldwide problem as evidenced by the source of the papers at this conference In Switzerland, with a highway system involving nearly 3000 bridges (generally elegant, post-tensioned constructions with a membrane and asphalt cover on the concrete), the increasing use of deicing salts has resulted in severe localized corrosion of the reinforcement In addition to the damage of the bridge decks, other parts of bridge structures, piers, beams, and pilings suffer by salty runoff or salt-containing snow Deicing salts are carried on automobiles into all the tunnels and have resulted in chloride concentrations in the concrete up to 4% by weight of cement and severe damage to these structures, too

The precise cost of the corrosion-induced damage of reinforced concrete structures is not known The Swiss Federal Highway Administration calculates annual costs of about 80 million Swiss Franks for survey and maintenance of bridge decks only [1] The repair and replacement of deficient bridges demand even greater expenditures A great problem is

---

[1] Materials scientist, lecturer, and researcher, Departments of Materials and Civil Engineering, Swiss Federal Institute of Technology, Zurich, Switzerland

[2] Professor, Departments of Materials and Civil Engineering, Swiss Federal Institute of Technology, Zurich, Switzerland

adequately defining which areas of bridges require repair. The usual method of inspection of concrete structures is too limited:

(*a*) relying on a *visual inspection* only, damage is detected too late, when it manifests at the concrete surface and
(*b*) the exact results of laboratory tests on *core sampling* (that is chloride penetration) are not representative for the whole structure.

The main problem, the corrosion of the reinforcing steel, cannot be detected before extensive damage occurs. In this paper, the results and experience of potential surveys of bridge decks of the Swiss Highways, using a new eight-wheel electrode measuring system, are reported. Attempts to overcome the "gray zone" of half-cell measurements and to calculate the corrosion rate in a particular macrocell are reported and discussed.

Location of Corroding Rebars—Potential Mapping

The potential mapping technique has been used since the early 1970s to locate corroding rebars in concrete structures [*2–3*]. Its use and interpretation are described in ASTM Test Method for Half-Cell Potentials of Reinforcing Steel in Concrete (C 876-80). Use of this technique has been increasing for several years in Switzerland [*4,5*].

Electrochemical Fundamentals

The electrochemical nature of corrosion processes of steel in concrete is well known [*6*]. A characteristic feature is the development of corrosion cells, that is, the coexistence of passive and corroding areas on the same rebar (Fig. 1) forming a short-circuited galvanic element with the corroding area as anode and the passive surface as cathode. The cell voltage

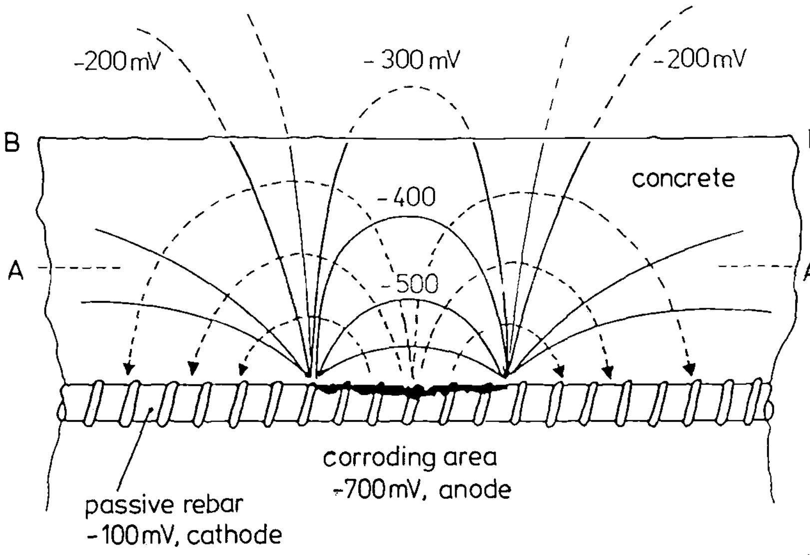

FIG. 1—*Schematic view of the electric field and current flow of an active/passive macroelement on steel in concrete: ---- current path and —— potential line.*

ΔU in this macroelement equals the potential difference between active and passive steel and may reach up to 0.5 V. The resulting current flow I

$$I = \frac{\Delta U}{R_E + R_A + R_C} \tag{1}$$

where

I = current flow, mA,
ΔU = cell voltage in the macro element, mV,
R_E = electrical resistance of concrete, Ω,
R_A = anodic reaction resistance, Ω, and
R_C = cathodic reaction resistance, Ω.

is determined by the electrical resistance of the concrete and the anodic and cathodic reaction resistance.

This current flow in the concrete is coupled with an electric field $\varphi(x,y)$: the change in electric potential from anode to cathode is continuous. This electric field can be measured at the concrete surface, resulting in equipotential lines (potential field) that allow the location of corroding zones at the most negative values.

Factors Affecting the Potential Field

When surface potentials are taken, they are essentially remote from the reinforcement due to the concrete cover. The potentials thereby measured are, in fact, mixed potentials. Several factors, discussed in the following paragraphs, can have a significant effect on the potential measurements.

Concrete Cover Depth—The concrete cover depth has a direct effect on the measured potential values as is schematically shown in Fig. 2. With increasing concrete cover, the potential values of active corroding and passive steel become similar. At infinite distance, a uniform potential value results. Thus, the location of small corrosion spots gets more difficult with increasing cover depth.

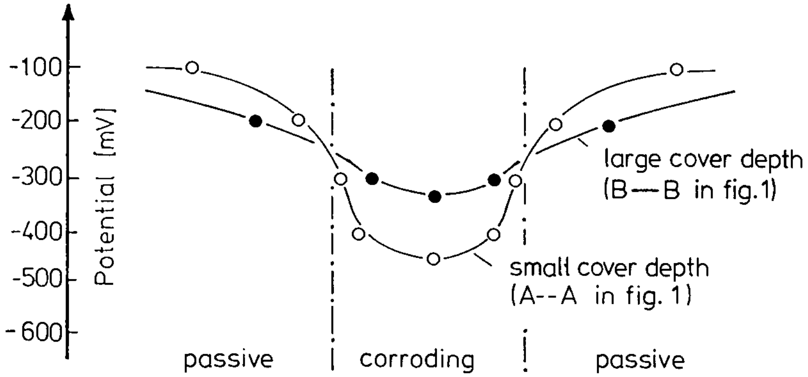

FIG. 2—*Schematic view of the influence of concrete cover depth on the potential field at the surface (depth A . . . A, B . . . B) for the macroelement in Fig. 1.*

Electrical Resistivity of the Concrete—The concrete humidity and the presence of ions in the pore solution affect the electrical resistivity of the concrete. According to Eq 1, decreasing electrical resistance, R_E, increases the current flow in the corrosion cell. This does not change the potential difference measured, but the absolute values are shifted up to ±50 mV [7].

High Resistive Surface Layer—A high-resistance surface layer enhances the effect of cover depth, as the macrocell current paths tend to avoid the highly resistive concrete (Fig. 3). The measured potentials at the surface become more positive (compare with Fig. 1) and thus corroding areas could be masked and not detected [*8,9*].

Polarization Effects—Steel in concrete structures immersed in water or in the earth often has a very negative potential due to the restricted oxygen access [*10*]. In the transition region of the structure (splash zone or above ground) negative potential values can be measured due to the galvanic coupling with the immersed rebars. These negative potential values are not related to corrosion, so interpreting potential surveys of these types of structures requires great care [*8,9*].

This short summary of the most important effects on potential measurements on the concrete surface shows that, despite the simple measuring procedure, the results of potential mapping need careful interpretation. It becomes obvious that a fixed potential value for the evaluation of half-cell potential data are not applicable.

Procedure

The procedure for measuring half-cell potentials at the concrete surface is comparatively straightforward and several commercial instruments are on the market. One or several half-cells (generally copper/copper sulfate ($Cu/CuSO_4$) electrodes) are placed on the concrete and connected to a high input impedance voltmeter. The low impedance pole is connected to the reinforcement. Care must be taken to have a very good electrical connection to the rebars (that is, by drilling a hole and mounting a screw). The half-cell should be put on a wet sponge on the concrete.

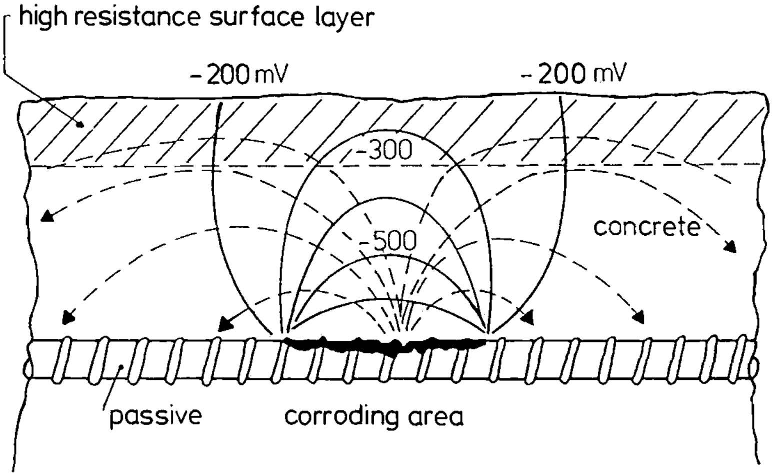

FIG. 3—*Effect of a high resistive surface layer on the current paths in concrete (schematic). The measured potentials at the surface become more positive.*

To facilitate the potential survey of large bridge decks, walls, or parking decks, the IBWK (Institute of Materials Chemistry and Corrosion, Swiss Federal Institute of Technology, Zurich) developed an eight-wheel electrode measuring system [*4,5*] (Fig. 4). This system allows one to survey 200 m^2/h with grid dimension of 15 cm using computer assisted data acquisition and storage.

Interpretation and Results

The interpretation of the potential readings is usually performed according to ASTM C 876-80. The potential values indicating corrosion were fixed on the basis of both laboratory measurements and bridge-deck inspection in the United States [*11*]. Recent practical experience has shown, however, that for different conditions (that is, concrete cover, humidity, chloride content) different potential values indicate corrosion. The upper limit of the potential for corrosion can range from −200 to −570 mV (bridge deck Morbio versus column in seawater, Fig. 5). Two examples of our recent work are presented in the following paragraphs.

Cugniertobel Bridge II—Potential mapping of this bridge deck (450 m^2, built in 1962) was performed during the replacement of the asphalt cover and other restoration work in the summer of 1986. In Fig. 6, a part of the potential field is shown. The numerous small "corrosion spots" are typical for the very severe localized corrosion attack due to chlorides. A visual inspection of the concrete surface revealed only two points with corrosion products. After the potential survey, the concrete cover was removed and the top mat of the reinforcement was visually inspected. Localized corrosion attack was found in all the areas with

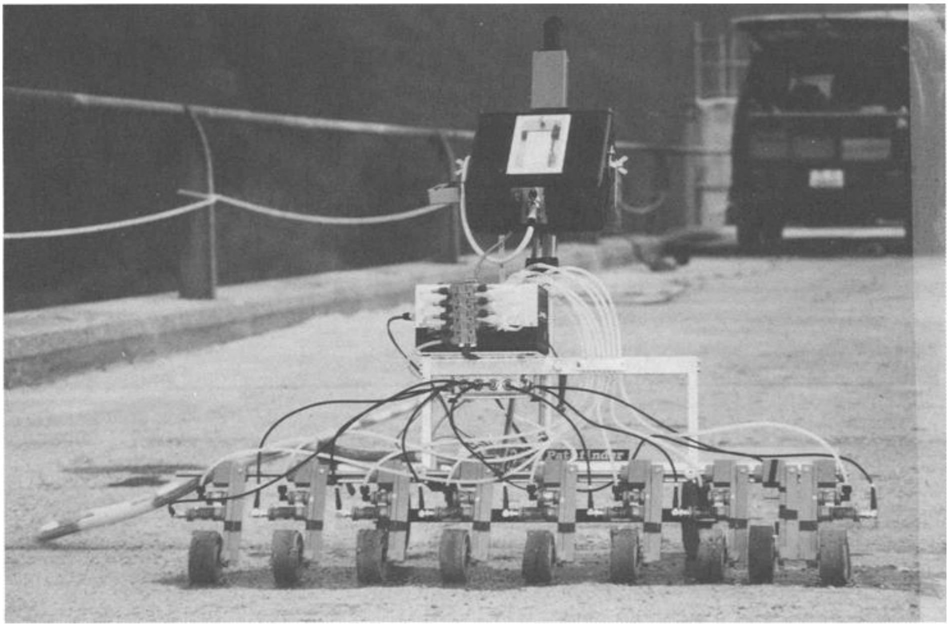

FIG. 4—*The eight-wheel electrode measuring system developed at the institute of materials chemistry and corrosion (ETH Zurich) for potential surveys.*

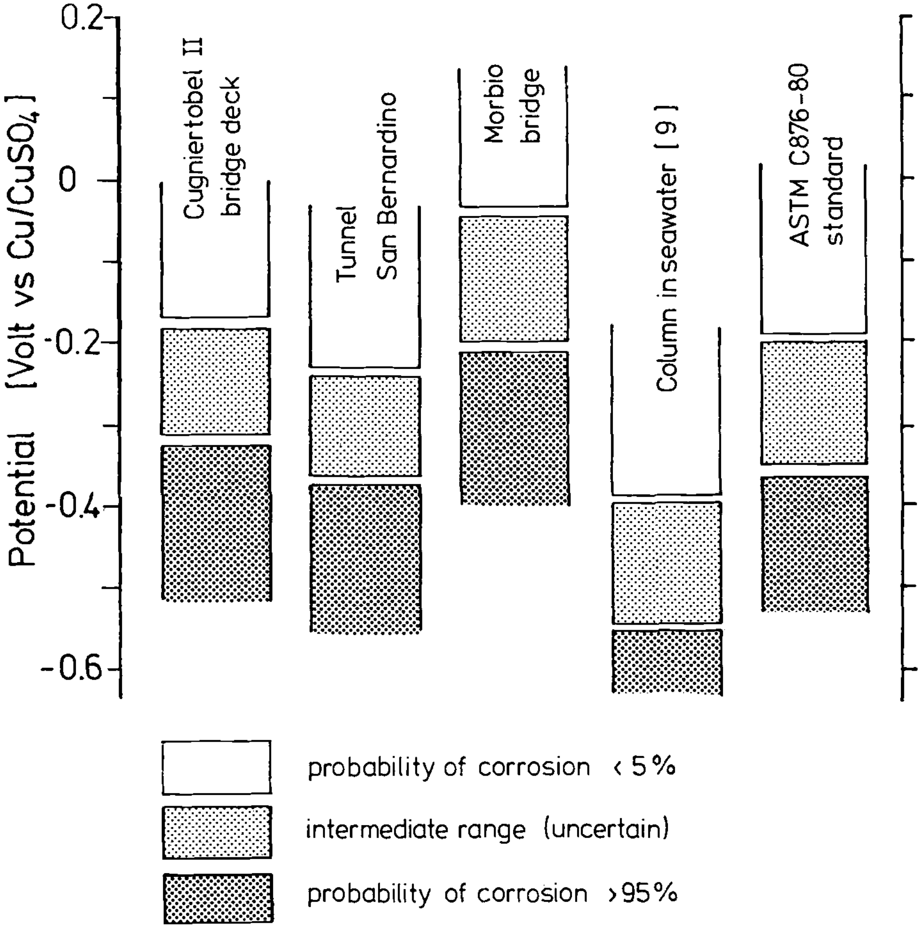

FIG. 5—*Comparison of the experimentally determined potential range indicating corrosion with the ASTM C 876-80 standard.*

a potential negative of more than ≤300 mV $CuSO_4$. Using the ASTM C 876-80 criteria of ≤350 mV $CuSO_4$, more than 70% of all the corrosion sites would not have been detected. In addition, this example shows that a grid dimension of 15 cm or less must be used to detect all the small areas of localized corrosion.

San Bernardino Tunnel—The San Bernardino tunnel, built 1967, is 6.6 km long and constructed as a "bridge in a tunnel." The riding deck, 20 cm reinforced concrete covered with asphalt, is divided in sections of 25 m to allow contraction and expansion of the concrete (due to day/night temperature differences of up to 30°C). These main dilatation sections (DF) are subdivided every 2.5 m to avoid uncontrolled cracking of the deck (SF). The potential survey of the deck has been performed from the underside (channel for fresh air supply) on eight different areas of 125 m^2 each. A part of the computer generated contour plot is shown in Fig. 7. It is obvious that corrosion is found only near the dilatation joints.

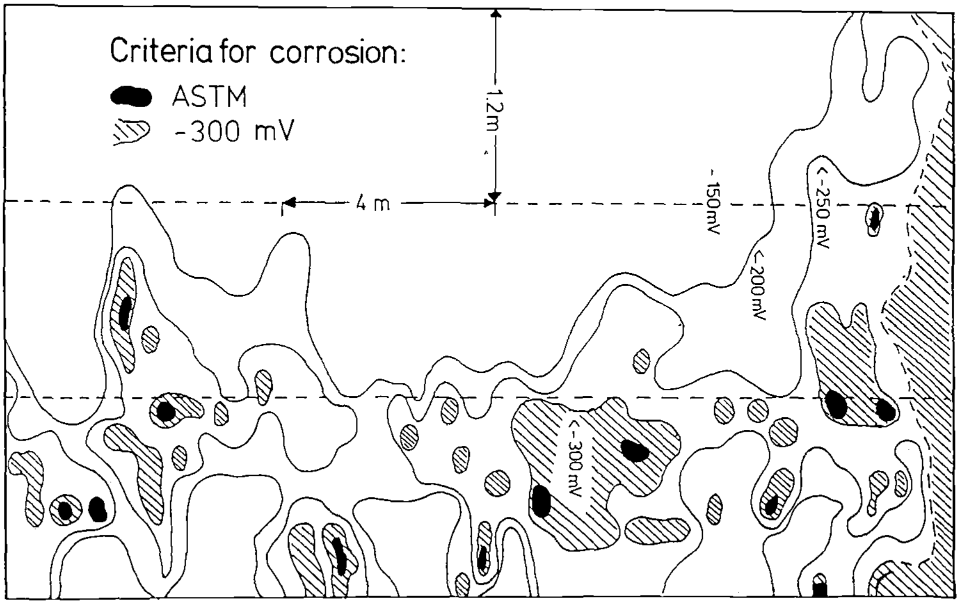

FIG. 6—*Part of the measured potential field of the bridge deck "Cugniertobel II" (concrete cover 2 to 3 cm, temperature 24°C). Equipotential lines millivolts $CuSO_4$.*

To check the state of corrosion of the rebars, the concrete has been removed at several points. The ASTM C 876-8D criteria ≤350 mV in this case detected all corrosion, even the beginning corrosion reactions. Compared to the visual inspection, the corroding zones located with the potential survey were about 30% bigger [5].

Summarizing our experience with potential surveys, the interpretation of the potential field, that is, the location of corrosion, cannot be based on an absolute value as proposed by ASTM C 876-80. The examples presented (among numerous others [9]) show that the structure of the potential field and the local potential gradient are better ways to identify the type of corrosion and to locate corroding rebars.

Corrosion Rate

The potential mapping technique has provided a useful, nondestructive means of delineating areas of corrosion. It is an early warning system which can assess the magnitude of the problem of corrosion and follow the extent of the anodic area as it changes with time. In conjunction with data from other tests such as resistivity or chloride ion content, the technique can be used to assess the corrosion status of a structure. For assessing the remaining service life of existing bridges and for evaluating materials and procedures for protection and rehabilitation of bridge components, a method to measure the rate of corrosion of embedded reinforcement is needed [*12–14*].

Potential Gradient

The electric field $\varphi(x,y)$ over a single active/passive macrocell (Fig. 1) is determined by the geometry of the system and by the cell voltage ΔU. This cell voltage and the current

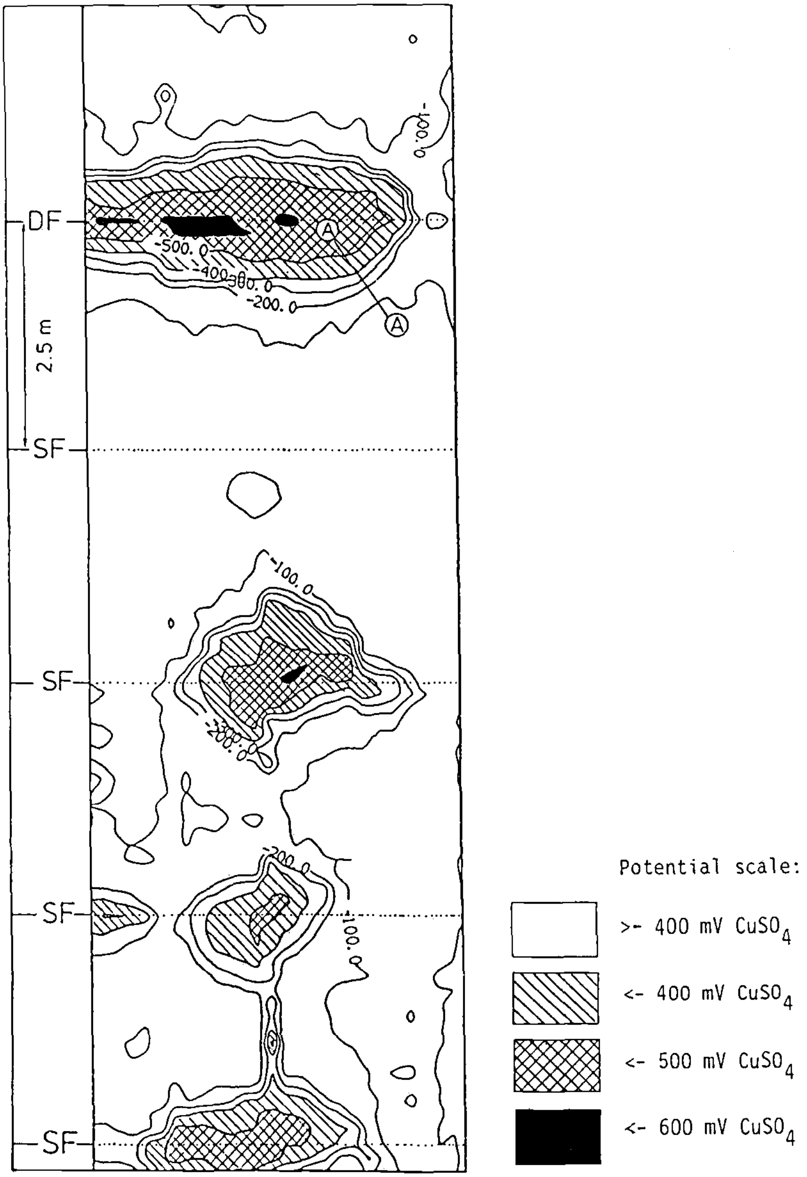

FIG. 7—*Part of the computer generated contour plot of potential mapping at the underside of the riding deck (San Bernardino tunnel). Equipotential lines millivolts $CuSO_4$.*

flowing in the macro cell can be calculated with the experimentally measured potential gradient at the concrete surface.

The potential field at the concrete surface for a small corrosion cell (typical for chloride induced corrosion of rebars) can be written as [*15*].

$$\varphi(x,y = d) = \frac{I \cdot \rho}{2\pi \cdot \sqrt{x^2 + d^2}} \qquad (2)$$

where

I = cell current, mA,
ρ = specific concrete resistivity, Ωcm,
d = cover depth, cm, and
x = horizontal distance from corrosion site, cm

The potential difference at the surface between the two points $x = 0$ and x is calculated to

$$\begin{aligned}\Delta\varphi_x &= \varphi(x,d) - \varphi(0,d)\\ &= \frac{I\ \rho}{2\pi} \cdot \frac{\sqrt{d^2 + x^2} - d}{d\ \sqrt{d^2 + x^2}}\end{aligned} \tag{3}$$

The current, I, in the cell results in

$$I = \frac{2\pi\ \Delta\varphi x}{\rho} \cdot \frac{d\ \sqrt{d^2 + x^2}}{\sqrt{d^2 + x^2} - d} \tag{4}$$

For the distance $x \cong 3d$, one gets approximately

$$I \cong \frac{2\pi\ \Delta\varphi}{\rho}(x = 3d) \cdot \frac{3d}{2} \tag{5}$$

$$\cong \frac{9d \cdot \Delta\varphi(x = 3d)}{\rho} \tag{6}$$

For the experimentally determined cover depth, d, and the measured potential difference, $\Delta\varphi$ $(x = 3d)$ (potential gradient), the cell current, I, can easily be calculated. For the example of the Cugniertobel bridge with typical values of $d = 2.5$ cm, a potential gradient of 5 mV/cm, and a concrete resistivity of 10 000 Ωcm, a current, I, of about 80 μA is calculated. For a typical localized corrosion spot of 1 cm^2, this current corresponds to a corrosion rate of 0.8 mm/year, a value which is in reasonable agreement with practical experience.

Impedance Measurements

Impedance spectroscopy makes it possible to obtain information on the electrical resistivity and the dielectrical properties of the concrete cover, and on the corrosion rate and mechanism of small steel bars in mortar or concrete. Since the early work of Dawson [*16*], this technique is frequently used to study the corrosion of steel in concrete in the laboratory [*17–19*]. Laboratory experiments of the present authors [*20,21*] have shown a close relationship between the corrosion rate (determined by weight loss measurements and visual inspection) and the calculated values from the impedance measurements for different chloride contents and environmental conditions.

On attempting to measure the corrosion rate on large slabs of reinforced concrete (with a large working electrode and a small counter electrode) special problems arise which were not found in the small-scale laboratory experiments. The interpretation of the impedance spectra is required to consider the spatial distribution of the impedance. Several models of equivalent circuit [*22*] and transmission line analysis [*23*] were proposed to overcome these difficulties. An important consequence of this analysis is that the measured apparent polarization resistance beyond a critical length of the working electrode bar becomes independent of the length. Typical values for this critical length were found to be 20 to 50 cm [*23*].

Procedure—Our experiments with the impedance technique were performed on large concrete slabs (1 m by 1 m by 0.2 m) to simulate a part of a bridge deck. All the rebars were electrically isolated and could be coupled externally. The top mat of the reinforcement was in chloride-containing concrete (1% chloride/weight of cement), the bottom mat in chloride-free concrete. The impedance spectra were measured at the corrosion potentials in potentiostatic mode with 20 mV sinusoidal amplitude in a frequency range from 10 mHz to 10 kHz, using Solartron 1250 TFA (Transfer Function Analyzer) and 1286 potentiostat (more details are given in ref. [*20*]).

The counter electrode (Fig. 8) was put on the concrete surface, as working electrodes one, three, or seven parallel steel bars (length 1 m, distance from bar to bar 0.12 m) were used.

Results—The resulting impedance spectra in the complex plane representation are shown in Fig. 9. The main difference between active (Fig. 9*a*) and passive rebars (Fig. 9*b*) was the slope of low frequency part of the complex impedance plots in agreement with other work [*18,24*]. Increasing the working electrode surface (that is, the number of rebars) did change the shape of the curves markedly only from Curve 1 to 2, thus confirming that the size of the counterelectrode determines the impedance [*23*].

The same type of measurements with the same equipment were performed on-site, on

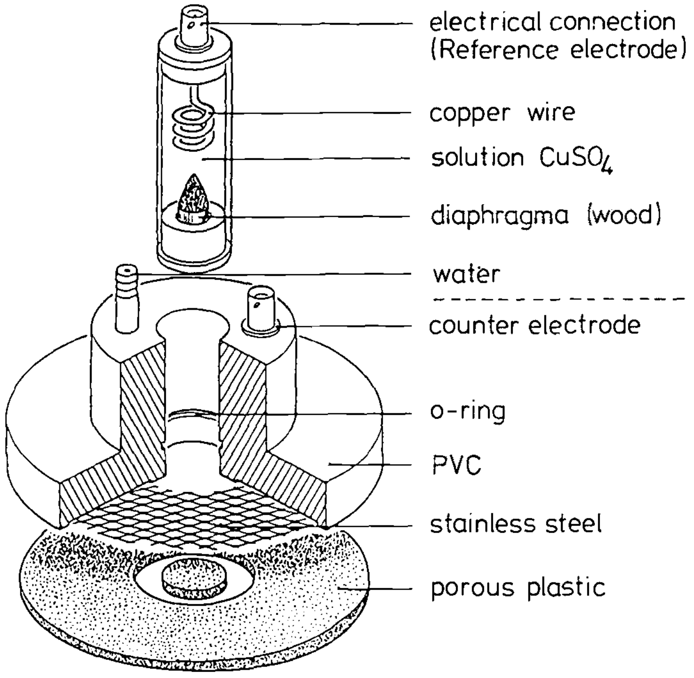

FIG. 8—*Combined counter/reference electrode for electrochemical measurements on steel in concrete (diameter 10 cm).*

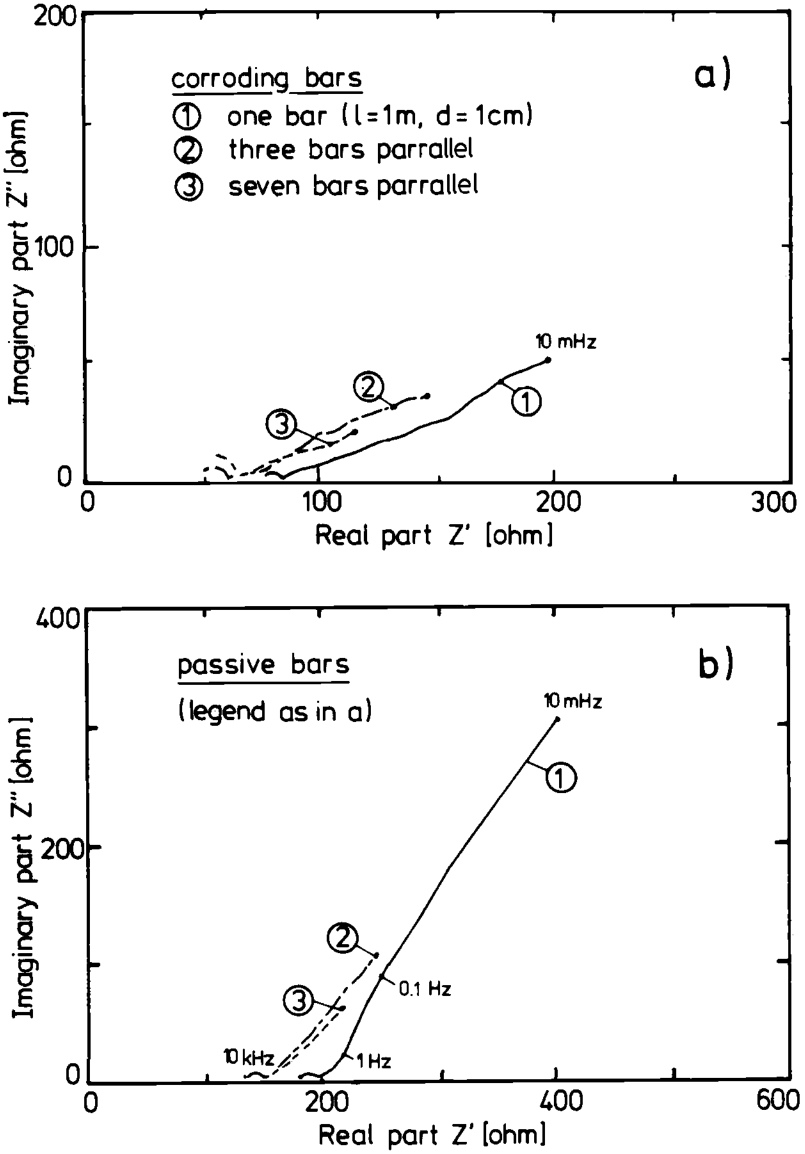

FIG. 9—*Impedance spectra at the corrosion potential of parallel steel bars in concrete measured against a small counter electrode. Laboratory,* $\Delta\varepsilon = 20$ *mV,* f = *10 mHz . . . 10kHz.* (a) *actively corroding bars,* $\varepsilon_{korr} = -480$ *mV* $CuSO_4$. (b) *passive bars,* $\varepsilon_{korr} = -220$ *mV* $CuSO_4$.

real structures in regions with active corrosion (chloride contaminated) and with a passive state of the rebars. The resulting impedance spectra were similar to Curve 3 in Fig. 9*a*. In laboratory and field measurements, no quantitative information concerning the corrosion rate could be obtained so far. Taking into account the long measuring time of 45 min for each spectra, the impedance spectroscopy does not seem to be promising for measuring corrosion rates of steel in concrete on site.

Galvanostatic Pulse Technique

As discussed in the section on potential mapping, the potential readings taken at the concrete surface are mixed potentials and can not always be interpreted in a straightforward manner Negative potential values due to polarization effects may lead to misinterpretations The galvanostatic pulse measurement method is a rapid, nondestructive technique to obtain unambiguous information on the corrosion state of the reinforcement

Procedure—A short-time anodic current pulse is imposed in galvanostatic mode onto the reinforcement from a small counter-electrode (Fig 8) on the concrete surface and the resulting potential change is recorded The same equipment as for the impedance measurements was used Typical duration of the current pulse is 3 s, the intensity 100 μA

Results—From the experimentally measured potential/time curve, two main pieces of information can be obtained (Fig 10*b*)

1 The slope $\Delta\epsilon/\Delta t$ at longer times A nearly horizontal line indicates that the reinforcement is corroding Due to the steep current/potential curve in the case of localized corrosion, the rebars can be polarized only a few millivolts with the small current pulse ΔI A continuous increase of potential ($\Delta\epsilon/\Delta t$ high) instead indicates passive state of the rebars

2 The initial jump in potential at $t = 0$ is the ohmic potential drop $\Delta\epsilon_\Omega$ of the system An apparent ohmic resistance, R_Ω, can be calculated with the known current

$$R_\Omega = \Delta\epsilon_\Omega/\Delta I \tag{7}$$

where

$\Delta\epsilon_\Omega$ = ohmic potential drop, mV and
ΔI = current pulse, mA

For a constant cover depth, this ohmic resistance is directly proportional to the concrete resistivity Thus information on the concrete humidity or salt content can be obtained, which allow location of areas with high corrosion risk [*6,8*]

The results of galvanostatic current pulse measurements, taken at the riding deck of the San Bernardino tunnel along the line A-A (see Fig 7), are shown in Fig 10 Figure 10*b* shows the potential response to a 100-μA current pulse at four different points along the line A-A From these individual curves, the slope $\Delta\epsilon/\Delta t$ and the apparent ohmic resistance R_Ω (according to Eq 7) are determined and plotted against the measuring position (Fig 10*c*) As can be seen, the slope $\Delta\epsilon/\Delta t$ gives unambiguous information on the corrosion state of the rebar, independent of the value of the corrosion potential In addition, it can be seen that areas with active corrosion show a much lower ohmic resistance than the concrete over passive zones Compared to the corrosion potentials in the transition from corroding to passive rebars (Fig 10*a*), a more precise location of the corroding zones is possible

The galvanostatic pulse measurements are a rapid, nondestructive technique that allows gathering of information on the concrete resistivity and on the corrosion state of the reinforcement without the risk of misinterpretation A more detailed analysis of galvanostatic pulse measurements on steel in concrete has been published recently [*25*]

Summary

The results of field applications of nondestructive electrochemical techniques to access the corrosion of rebars in concrete are reported here

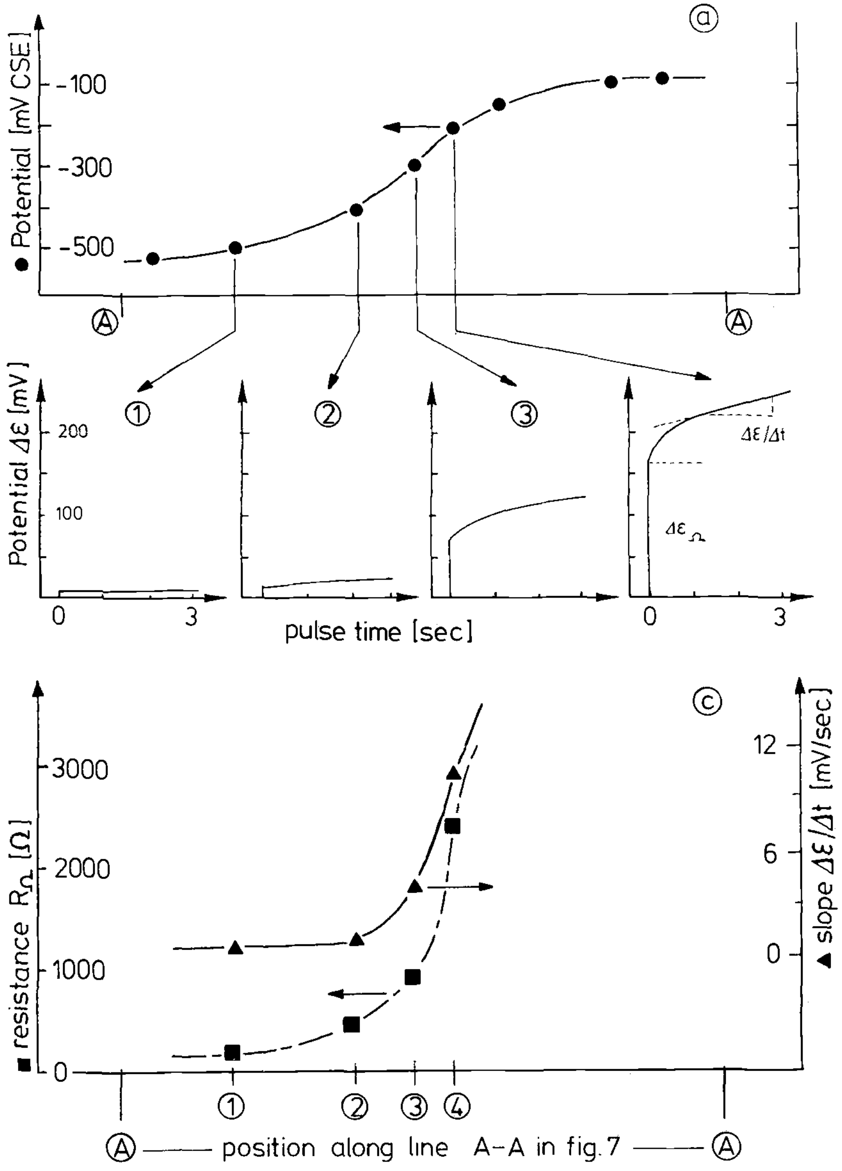

FIG. 10—*Galvanostatic pulse measurements, experiments performed on-site at the riding deck of the San Bernardino tunnel (line A-A, Fig. 7):* (a) *corrosion potentials in the transition from corroding to passive reinforcement (line A-A),* (b) *potential response to a current pulse* $\Delta I = 100\ \mu A$ *at four different points along the line A-A, and* (c) *graph of the slope* $\Delta\varepsilon/\Delta t$ *and the apparent ohmic resistance along the line A-A.*

1. The *potential mapping* is an easy technique. Due to the concrete cover, only mixed potentials can be measured. It is shown in this paper that an absolute potential value for the location of corrosion as proposed in ASTM C 876-80 is not applicable.

2. Our experience with *impedance spectroscopy* has shown that this technique is too time-consuming for on-site application. In addition, the difficulties with the spatial distribution

of the electrical signals do not allow interpretation of the impedance spectra with respect to the corrosion rate

3 The *galvanostatic pulse technique,* proposed in this paper, overcomes the difficulties in interpreting potential measurements At the same time, information on the concrete resistivity is obtained This technique is a promising new and rapid monitoring technique for reinforced concrete structures

References

[1] Menn, C , *Schweizerischer Ingenieur und Architekt,* Vol 105, 1987, p 1253

[2] Stratfull, R F , *Corrosion,* National Association of Corrosion Engineers, Vol 13, 1957, p 173t

[3] Stratfull, R F , "Half Cell Potentials and the Corrosion of Steel in Concrete," *Highway Research Record,* 1973, Vol 433, p 12

[4] Elsener, B and Bohni, H "Elektrochemische Methoden zur Bauwerksuberwachung," *Schweizerischer Ingenieur und Architektenverein,* SIA-Doc D 020, Zurich, 1988

[5] Elsener, B and Bohni, H , *Schweizerischer Ingenieur und Architekt,* Vol 105, 1987, p 528

[6] ACI-Committee 222, "Corrosion of Metals in Concrete," ACI 222R-85, American Concrete Institute, Detroit, 1985

[7] John, D G , Eden, D A , Dawson, J L , and Langford, P E , *Proceedings,* CORROSION/87, Paper No 136, National Association of Corrosion Engineers, Houston, 1987

[8] Browne, R D , Geoghegan, M P , and Baker, A F in *Corrosion of Reinforcement in Concrete Constructions,* Society of Chemical Industry, London, 1983, p 193

[9] Baker, A F , "Potential Mapping Techniques," Seminar on Corrosion in Concrete—Monitoring, Surveying and Control by Cathodic Protection, London Press Centre, 13 May 1986, Paper No 3

[10] Popovics, S , Simeonov, Y , and Bozhinov, G in *Corrosion of Reinforcement in Concrete Constructions,* Society of Chemical Industry, London, 1983, p 19

[11] Van Deever, J R , *Journal,* American Concrete Institute, Vol 12, 1975, p 697

[12] "TRA 4 Detailed Planning for Research Bridge Component Protection," Final Report, Strategic Highway Research Program, April 1986

[13] Hansson, C M , "A Critical Assessment of Methods of Measuring the Rate of Corrosion of Steel in Reinforced Concrete," Ontario Ministry of Transportation and Communication, 1986

[14] Escalante, E , Whitenton, E , and Qiu, F , "Measuring the Rate of Corrosion of Steel in Concrete, Final Report," National Bureau of Standards Interagency Reports, 86-3456, Gaithersburg, MD Oct 1986

[15] Baeckmann, W and Schwenk, W , *Handbuch des Kathodischen Korrosionsschutzes,* Verlag Chemie Weinheim, 1971, p 384

[16] Dawson, J L , Callow, L M , Hladky, K , and Richardson, J A , *Proceedings,* Corrosion/78, Paper No 125, National Association of Corrosion Engineers, Houston, 1978

[17] Wenger, F , Lemoine, L , and Galland, J , *Proceedings,* 9th International Congress on Metallic Corrosion, Toronto, 3–7 June 1984, Vol 2, p 349

[18] Andrade, C , Castelo, V , Alonso, C , and Gonzalez, J A , "The Determination of the Corrosion Rate of Steel Embedded in Concrete by the Polarization Resistance and AC Impedance Methods," *Corrosion of Rebars in Concrete, ASTM STP 906,* V Chaker Ed , American Society for Testing and Materials, Philadelphia, 1986, p 43

[19] Dawson, J L , in *Corrosion of Reinforcement in Concrete Construction,* Society of Chemical Industry, London, 1983, p 175

[20] Elsener, B and Bohni, H , *Materials Science Forum,* Vol 8, 1986, Trans Tech Publications Switzerland-UK-USA, p 363

[21] Elsener, B and Bohni, H , *Proceedings,* European Congress of Corrosion, 19–21 Nov 1985, Nizza, Vol 1, p 1

[22] Wenger, F and Galland, J , *Proceedings,* EUROCORR'87, Karlsruhe, Vol 6 -10 4 87, p 625

[23] Feliu, S , Gonzales, J A , Andrade, M C , and Felin, V , *Proceedings,* Corrosion/87, National Association of Corrosion Engineers Houston 1987, Paper 145

[24] John, D G , Coote, A T , Treadaway, K W , and Dawson, J L , in *Corrosion of Reinforcement in Concrete Construction,* Society of Chemical Industry, London, 1983, p 263

[25] Newton, C J and Sykes, J M , *Corrosion Science,* Vol 28, 1988, p 1051

J. P. Broomfield,[1] P. E. Langford,[2] and A. J. Ewins[2]

The Use of a Potential Wheel to Survey Reinforced Concrete Structures

REFERENCE: Broomfield, J P, Langford, P E, and Ewins, A J, **"The Use of a Potential Wheel to Survey Reinforced Concrete Structures,"** *Corrosion Rates of Steel in Concrete, ASTM STP 1065*, N S Berke, V Chaker, and D Whiting, Eds, American Society for Testing and Materials, Philadelphia, 1990, pp 157–173

ABSTRACT: The design, construction, and use of a Potential Wheel is discussed Its application for determination of corrosion of steel in concrete is explained with brief case histories Laboratory tests of reproducibility and temperature effects are presented

KEY WORDS: corrosion, corrosion of steel in concrete, chloride, potentials, half-cells, steels, concrete

The corrosion of reinforcing steel within reinforced concrete is a growing and major worldwide problem In the United States alone, it is estimated that some 300 000 bridge decks are suffering from corrosion due to deicing salt attack The cost of repair is estimated at over US $100 000 000 000 In the United Kingdom, approximately $900 000 is being spent annually on surveying buildings and civil engineering structures suffering from deterioration, or requiring statutory surveys

A number of destructive and nondestructive techniques are used to survey reinforced concrete structures for signs of deterioration Among the nondestructive techniques used is the measurement of the corrosion potential of the rebar (reinforcing steel) within the concrete The Potential Wheel is a new instrument for carrying out rapid acquisition of potential data collected during deterioration surveys of reinforced concrete structures

Corrosion Potentials

Corrosion potentials are measured by placing a half-cell, such as copper/copper sulfate, in contact with the surface of the concrete A full electrical cell is thus created and an electrical potential can be measured between the rebar within the concrete and the copper rod of the half-cell

The magnitude of this corrosion potential can be related to the probability that the rebar is in a corroding state The fact that there are two dissimilar electrolytes (the concrete and the copper sulfate) adds a small, but insignificant, voltage to the overall corrosion potential measured The technique is illustrated in Fig 1. By taking discrete corrosion potential measurements at regular intervals across the surface of the structure being investigated, the extent of any corrosion problem can be mapped prior to more detailed examination and

---

[1] Senior corrosion engineer, Taywood Engineering Ltd, Southall, Middlesex, UK presently at Strategic Highway Research Program, Washington, DC 20006

[2] Corrosion engineer and senior instrumental engineer, respectively, Taywood Engineering, Southall, Middlesex, UK

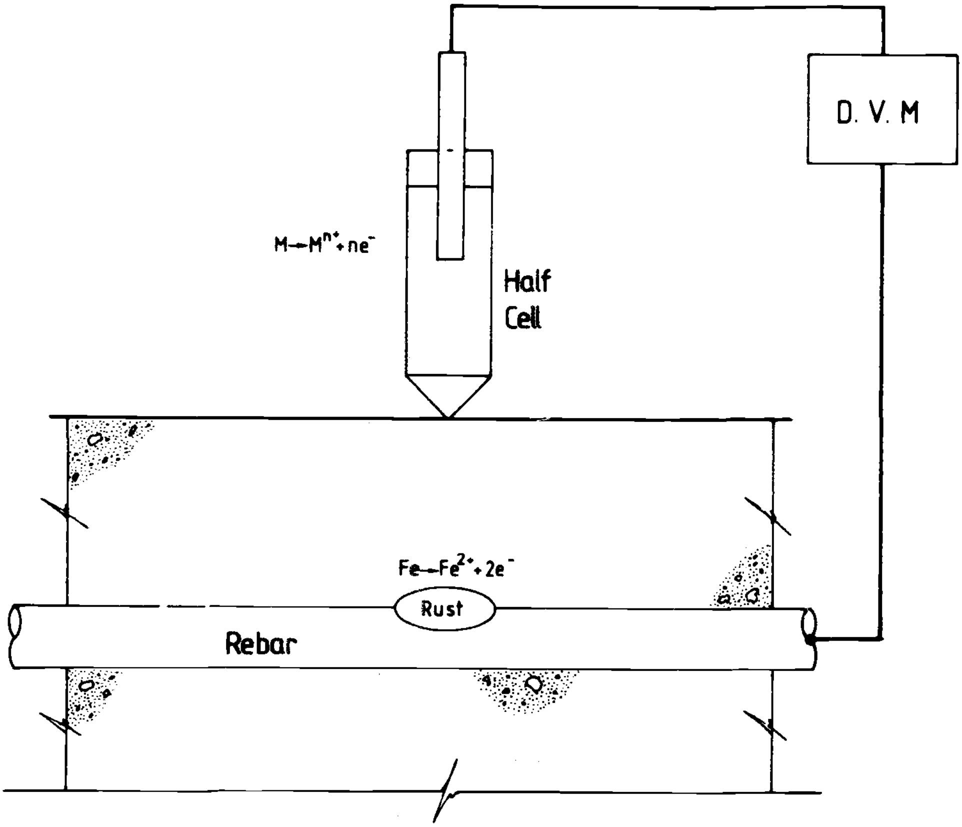

FIG. 1—*The potential measurement.*

repair. The ASTM Test for Half-Cell Potentials of Uncoated Reinforcing Steel in Concrete (C 876–87) [*1*], gives a method for taking, displaying, and interpreting these readings.

The use of electrochemical potentials to determine areas of corrosion risk is well established in the cathodic protection industry. The application of this technique to reinforcing steel in concrete was pioneered in the United States on bridge decks suffering from deicing salt attack and resulted in the acceptance of the empirical criteria of Van Daveer [*2*], now in slightly modified form in the ASTM standard.

The potential survey technique is frequently used in the early stages of examining a reinforced concrete structure for sign of deterioration due to rebar corrosion. As an initial survey tool, it is required to examine as much of the structure as possible, both thoroughly and quickly. However, the more thorough the examination the slower and more costly the exercise. The Potential Wheel has been invented to produce an instrument that will do a thorough investigation speedily, and hence, inexpensively.

Corrosion of Steel in Concrete: Mechanisms

The problems of corrosion of steel in concrete are different from those encountered by most corrosion engineers. Concrete is a porous medium which retains and transmits oxygen, moisture, and aggressive species to the steel surface. However the alkalinity of the pore water reduces the corrosion rate to a negligible level by the formation of a passive layer in favorable conditions.

The passive layer is ordinarily maintained at pH 9 or more but can be broken down by three major factors.

1. Lack of oxygen to maintain the passive film.
2. Carbon dioxide reducing concrete alkalinity (carbonation).
3. Chloride attack of the passive film.

The first case can lead to very large potentials, −800 to −1100 mV with respect to silver/silver chloride (Ag/AgCl), but a negligible corrosion rate due to the limited oxygen supply. This phenomenon has been studied for reinforced concrete immersed in seawater [3].

The second and third cases lead to problems either due to loss of structural strength or to concrete spalling due to internal stresses built up by the large volume of corrosion product compared with the volume of metal consumed.

The aim of potential measurements is to map anodic (corroding) and cathodic areas (Fig. 2) and to determine the extent of corrosion. As potential measurement is a thermodynamic process, no information on corrosion rates is available. However, if assumptions are made about the form of the mixed potential and the potential gradients between anodic and cathodic macrocells, then areas of high corrosion risk (but not rate) can be identified, as per the ASTM criteria.

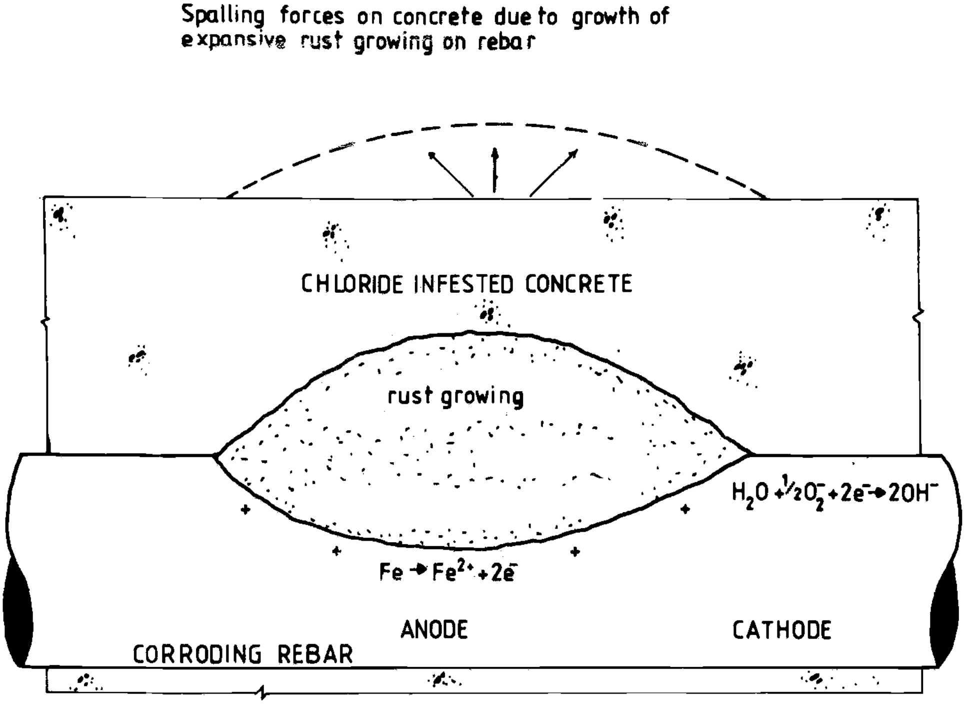

FIG. 2—*The corrosion of steel in concrete.*

While the criteria for corrosion of bridge decks suffering from deicing salt attack are applicable in a wide range of circumstances they do not always apply, especially if corrosion is due to carbonation. It is not intended to review the technique in detail here as it has been covered in some detail elsewhere [*4*,*5*].

The Potential Wheel

The Potential Wheel is simply a half-cell with a wheel for a tip and some sophisticated logging electronics for capturing the corrosion potentials and storing them for subsequent examination and analysis. The half-cell/wheel assembly is known as the Wheel and the logging electronics as the Data Bucket. A schematic of the Potential Wheel measurement system is shown in Fig. 3*a*.

In operation, the water-saturated, foam-rubber tired rim of the Wheel is placed in contact with the surface of the concrete structure under examination, and rolled along. With an

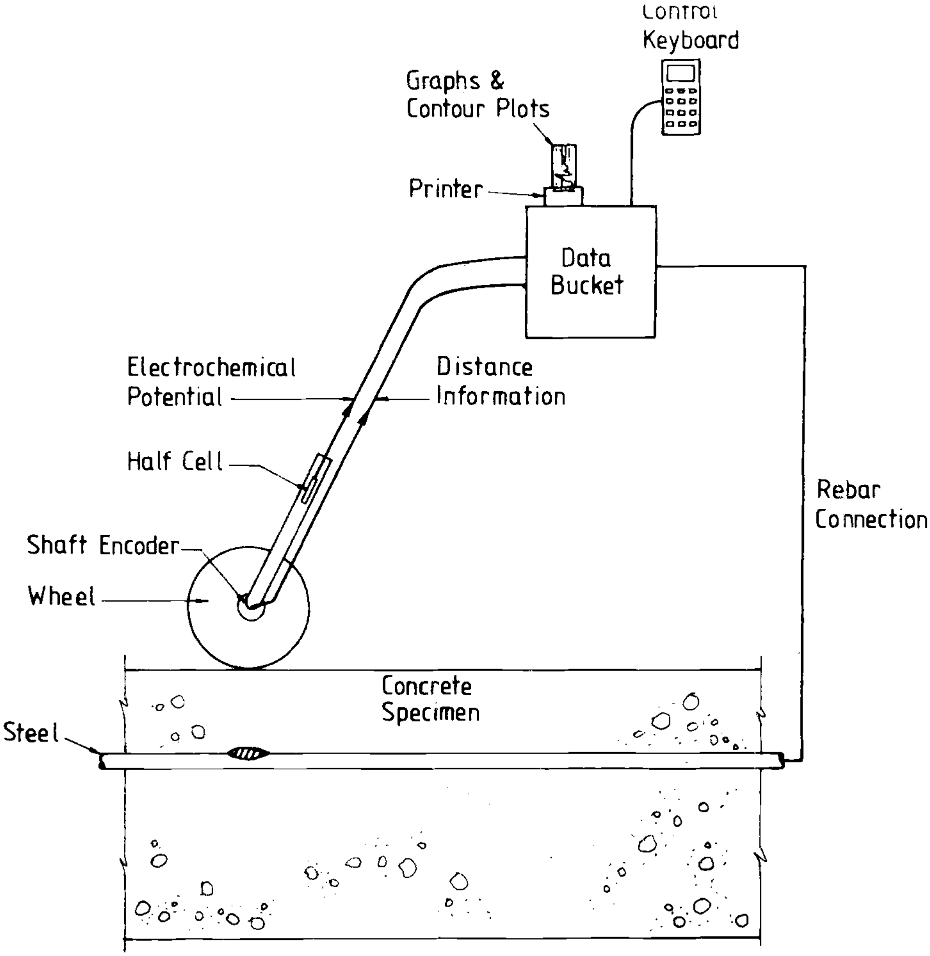

FIG. 3a—*A schematic of the Potential Wheel.*

electrical connection between the rebar and the Data Bucket, the corrosion potentials are automatically measured and stored within the Data Bucket as the Wheel is rotated A single data gathering traverse of the Wheel across the surface of the concrete is called a scan

The corrosion potential measurement process is initiated by a shaft-encoder coupled to the Wheel For every 5 mm of travel of the Wheel's rim, the shaft-encoder generates a pulse, which instructs the electronics within the Data Bucket to convert the instantaneous value of the analogue corrosion potential into a digital value and record it in a memory store Each value of the stored corrosion potential is thus directly related to the distance traveled by the Wheel

The Wheel

The Wheel is essentially the revolutionary part of the device In order to provide a half-cell with a rotating tip, a number of design problems have had to be overcome.

Cell

Firstly, a suitable choice of half-cell had to be made The conventional copper/copper sulfate was considered undesirable on two grounds

1 it has a fairly slow response time in providing a stable output voltage when contacted to the concrete surface, and
2 it used a liquid electrolyte-copper sulfate

The slow response time was thought to be a possible limiting factor to the speed with which the Wheel could be drawn across the surface of the concrete The use of a liquid electrolyte also posed an interface problem between the concrete surface and the copper rod of the copper/copper sulfate half-cell

Before ruling out the use of a copper/copper sulfate half-cell the design of a hollow wheel, to contain the copper sulfate, with a copper electrode internally connected to the hub, was considered This possible solution then posed further problems with respect to the control of the flow of the copper sulfate through the periphery of the wheel, the maintenance of a saturated solution of copper sulfate, and electrical connection to the copper electrode It was thought that such a solution would also result in the depositing of large quantities of copper sulfate over the surface of the concrete While this is an accepted fact with conventional copper/copper sulfate half-cells, the amount deposited is small and of little consequence Large quantities deposited by a wheel in continuous contact would be unsightly on visible concrete of certain types of structures and could aggravate a corrosion problem since copper sulfate is a corrosion agent

A silver/silver chloride half-cell was eventually chosen because of its much faster response time, its greater stability with respect to time and temperature and because its use of a "solid" electrolyte allowed more flexibility in interfacing it to the concrete surface The design of a suitable interface between the silver chloride tip of the half-cell and the concrete surface has become, in fact, the novel feature of the Wheel's design

In order to provide an electrical path between the silver-chloride tip of the half-cell and the concrete surface, some sort of ionic fluid is necessary that will not contaminate the reinforced concrete Ordinary tap water is normally used to improve the ionic contact between a half-cell and the concrete surface However, if tap water is used to surround the silver chloride of the half-cell, its slow dissolution can be expected and the half-cells performance will be degraded Ideally, the silver chloride tip needs to be surrounded by a chloride solution in order to maintain the half-cell stability. Although potassium-chloride can be used, it is still desirable to prevent direct contact of the potassium chloride solution with the concrete's surface. A satisfactory response to the problem is arrived at by allowing the use of water in contact with the concrete, a solution of potassium chloride in contact with the silver-chloride, and by designing a porous membrane between the two liquids.

The Half-Cell/Concrete Junction

Figure 3*b* illustrates the construction of the Potential Wheel. The Ag/AgCl half-cell is mounted in a plastic bush (8) which push-fits into the main body (9) of the wheel. The tip of the silver rod (1) protrudes into the back chamber (10) where it makes connection to a high-input impedance, unity gain, buffer-amp in chamber (11) via the leaf-spring (12) on back-plate (13).

The silver-chloride tip of the half-cell (2) makes contact with the potassium chloride in the chamber (3). An absorbent nylon rod (4) provides an ionic path from the chamber to a foam-rubber tip (5) outside the chamber and in contact with a perforated slipper-plate (6) against which the foam-rubber rim (7) of the wheel makes rotational contact. The foam-rubber rim (7) is wetted with water to provide an ionic path to the surface of the concrete when the wheel is rolled across its surface. The full-cell so created is formed thus: silver rod, silver chloride, potassium chloride, water, concrete, rebar.

The output from the buffer-amplifier, plus electrical pulses from the wheel's shaft-encoder (14), is fed via multicore cable to the Data Bucket, to which is also made the rebar connection. The potential of the full-cell is thus measured. Note that water path around the rim of the wheel can contribute a small potential of a few millivolts, to the overall potential measured, if the wheel's rim is allowed to become less than wet, that is damp but not dry.

Dilution of the Potassium Chloride

There is no evidence to suggest that the potassium chloride (KCl) becomes dilute with the possible ingress of water from the wheel's rim into the KCl chamber. On the contrary, as the wheel's rim is dry for longer than it is wet, during periods of nonuse, it is believed that the KCl maintains its saturated state by evaporation of the water from the chamber.

In practice, it has been found only necessary to "top up" the chamber, containing the KCl, from time to time as the level decreases due to evaporation. Occasionally, the KCl has been entirely replaced when overhaul of the wheel has been carried out. Periodic checks of the half-cell's potential, by placing another standard half-cell in contact with the wheel's wet rim and connecting the metal electrode to the rebar input of the Data Bucket, has shown no significant change in its value over a number of years.

There is no doubt that no significant change in the saturation level of the KCl is likely to take place over the period of a day's usage. Complete replacement of the KCl, daily, during use will therefore guarantee its saturation level should this be thought desirable.

Distance Measurement

The second problem that had to be overcome was the design of a distance measuring device coupled to the rotation of the wheel, relating distance measurement to the analogue measurement of the corrosion potential.

An obvious solution to the measurement of distance was the use of shaft-encoder. Such devices are readily commercially available and, generating a number of pulses per revolution, can simply be coupled to an electronic counter to provide distance measurement information.

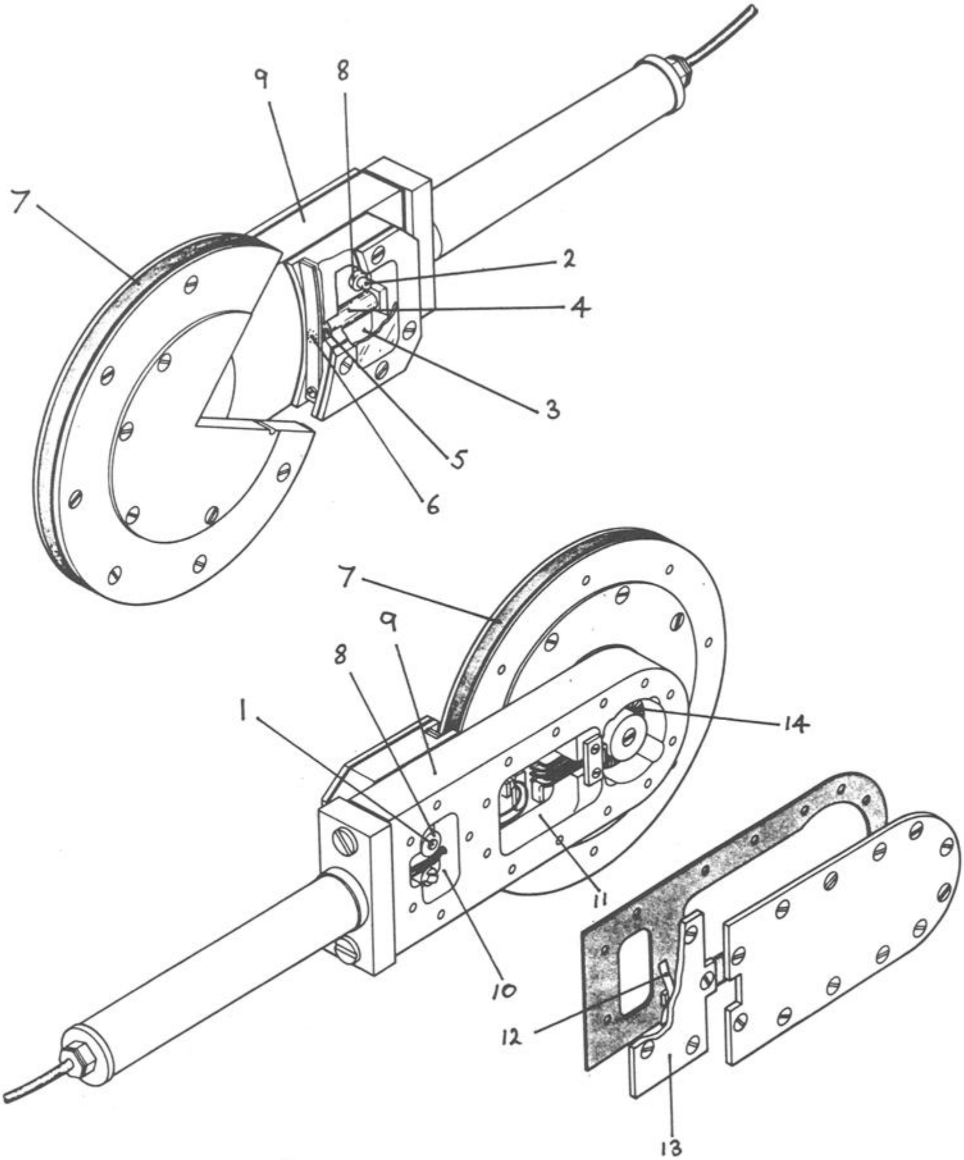

FIG. 3b—*Schematics of the wheel assembly. See text for description.*

Early experiments at producing voltage versus distance measurement plots were carried out with a prototype wheel and a chart recorder, the time axis of the chart recorder (the chart paper drive) being driven by the pulses from the shaft-encoder. Once it was decided to develop a logger from storing the corrosion potentials, it was a logical step to use the shaft-encoder pulses to initiate the storage process. Having built early prototype wheels with commercially available shaft-encoders, a simpler, lighter, and much less power consuming shaft-encoder was specifically developed for later versions.

High Input Resistance

Finally, a high input resistance stage for the voltage measurement is essential because the full-cell created by the reference half-cell and the reinforced concrete can have a very high internal resistance In order to provide such an input stage, and to provide a low output impedance signal source from the Wheel to the Data Bucket, a simple operational amplifier integrated circuit with very low input bias current was used This high input impedance "buffer" amplifier, together with the electronics of the shaft encoder, is incorporated in the main body of the Wheel

The Data Bucket

The Data Bucket is battery operated, making the complete Potential Wheel a portable instrument suitable for site use A number of prototypes of the Data Bucket were built at various stages and the instrument is designed to be as robust and as weatherproof as practically possible

The Data Bucket uses well-known electronic microprocessor techniques Apart from tailoring the electronic hardware of the Data Bucket to operate specifically with the Wheel, its uniqueness mainly lies in the controlling software This provides the means for storing the values of the corrosion potentials and examining them by a number of different programs A built-in impact printer enables the stored data to be plotted out on site according to the controlling software A calibration potentiostat enables the half-cell to be checked and an offset put in to convert the readings to a copper/copper sulfate ($Cu/CuSO_4$) reading from the Ag/AgCl readings produced by the Wheel

Table 1 lists the programs available to the user of the Data Bucket One program enables voltage versus distance plots to be obtained, for each scan recorded, via the built-in impact printer Another program enables a number of scans to be printed out, side-by-side, using variable density characters to represent five voltage ranges of the corrosion potential, a potential contour map is thus produced Figure 4 shows typical plots of single scans and contour maps, with a computer generated three-dimensional image of the same data A contour map enables an operator on site to get very fast feed-back of the data he has gathered, enabling him to make on the spot decisions about its validity This feature is considered very desirable when time spent on site costs money, and a return to site, to remeasure incorrectly gathered data, is even more expensive

Other programs within the Data Bucket enable the operator to examine the data collected, visually, via a liquid crystal display, to down-load the collected data to another computer for more detailed analysis, and to erase scans of incorrectly gathered data One final program

TABLE 1—*Programs for control of the data bucket functions*

There are seven controlling programs within the Data Bucket, plus one to turn the printer ON and OFF They are listed here

1	STORE	enables parameters to be set and data stored
2	V/PLOT	produces voltage versus distance plots of each scan
3	C/PLOT	produces equi-potential contour plots of a number of scans
4	VISUAL	scan data may be viewed via the pocket terminal
5	D/DUMP	stored data may be dumped to another microcomputer
6	ERASE	individual/groups of scans may be erased in reverse order
7	DIST	enables the wheel to be used to measure distance
8	PRINTER ON/OFF	

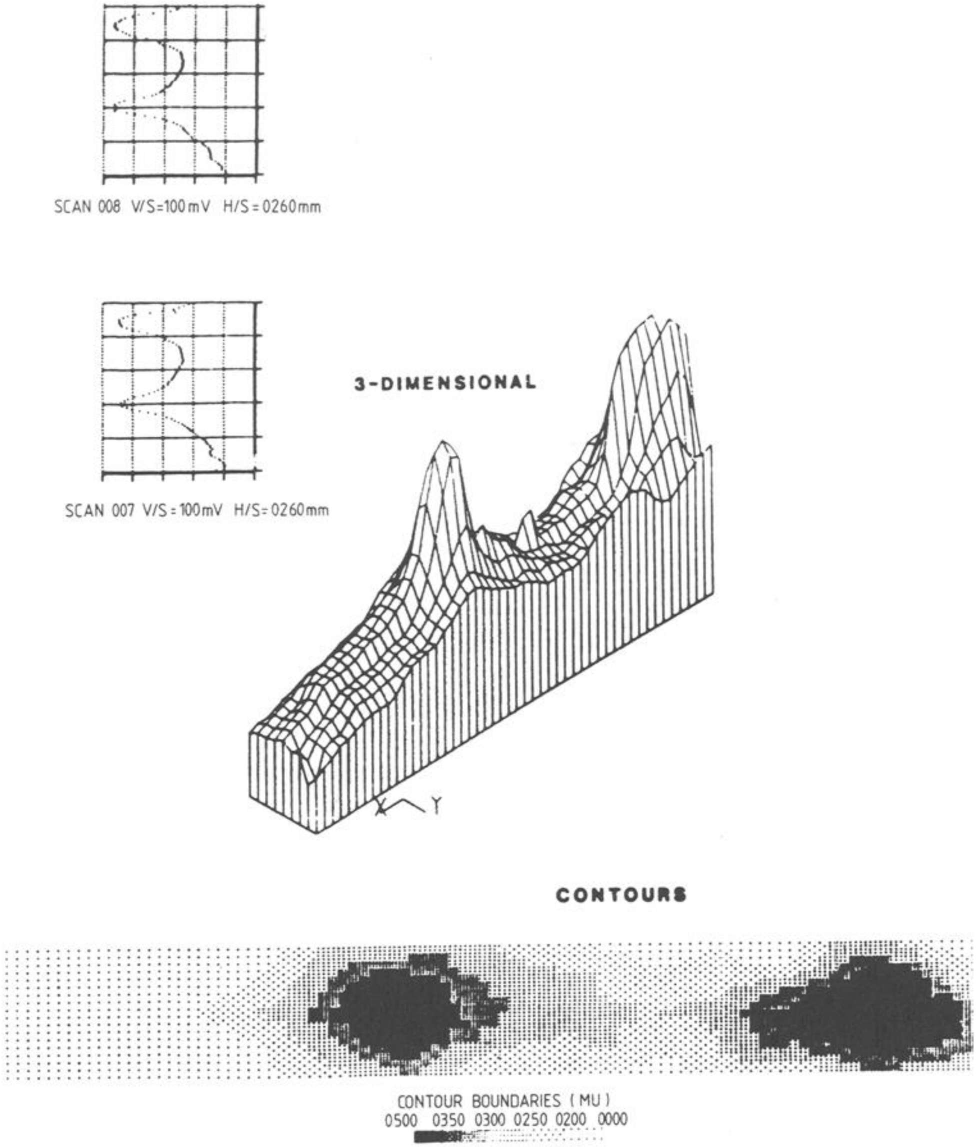

FIG. 4—*Data Bucket presentation of the results.*

enables the operator to use the Wheel as a distance measuring device to ease the task of marking-out the structure for subsequent measurement.

The functions and various programs of the Data Bucket are controlled by a Pocket Terminal, connected to it by a serial linelink using a coiled flexible cable.

A particular advantage of the Potential Wheel's design is that it can be used in any attitude, unlike a conventional Cu/$CuSO_4$ half-cell which is difficult to use upside down. It also has fewer possible problems of contact than a multiple cell array. These features are exploited by providing a telescopic extension to the Wheel to enable its use overhead, for example, on the underside of parking lot decks or high up walls without requiring immediate access

Reproducibility

The results of reproducibility checks are shown in Fig 5 for a test block with salt placed against the bars in two drill holes from behind the block There is a variation of up to 45 mV between repetitions, at individual points in areas of steep gradient, but the variation reduces to 10 mV in the most anodic and cathodic areas. A statistical analysis of the data in the figure shows an overall standard deviation of 7 5 mV about the mean for each set of three points. The junction effect mentioned earlier would account for up to 8 mV variability Drift in the half-cell is negligible and therefore the most significant source of error is probably minor deviations in the path taken across the surface in areas of rapidly changing potential where gradients of up to 70 mV/cm have been measured

Long-term drift of the system has been found to be negligible when the equipment is properly maintained

Thermal effects are shown in Figs 6, 7, and 8 by comparing the Potential Wheel (Ag/AgCl half-cell) with a conventional $Cu/CuSO_4$ half-cell Work was done in a constant temperature room at 25°C with no account taken of the change in potential of the rebar due to temperature effects The standard hydrogen potentials and temperature coefficients for Ag/AgCl and $Cu/CuSO_4$ are given in Table 2

The actual laboratory Wheel results at 40 to 100 mV are more negative than the $Cu/CuSO_4$ half-cell at 11°C, dropping to 0 to 70 mV difference at 35°C It would appear either that experimental variations are more significant that the temperature coefficients even in a laboratory experiment, or that changes in potential of the steel are more significant than those of the instrumentation.

Experience in Use

To date, the Potential Wheel has been used in the United Kingdom, Australia, and Hong Kong over the last two years

The Wheel has been found to be capable of scanning up to 400 m/h over a day or more of investigation in practical site conditions with good access The Data Bucket can accept 1000 readings per s With 120 readings/m, the wheel can travel at about 8 m/s In practice, 1 m every 1 to 5 s is a practical limit to the running speed in the present configuration for a hand-held device The bucket holds up to 128 scans or up to 15 866 readings At 5 mm measurement interval, this is equal to 80 m of data, at a more usual measurement interval of 50 mm for a large scale survey, 800 m of data can be accumulated before down-loading or plotting is necessary

Figures 9 and 10 show a 10 by 10 76 m area of soffit of a chloride contaminated bridge (3% chloride by weight of cement). The high level of visible surface defects was consistent with high (negative) potentials In other areas with low concrete resistivity and high potentials, no corrosion-related defects were visible indicating that corrosion risk is high and steps must be taken before delamination starts Data collection over the approximately 100 m^2 area took only 3 h, including establishing rebar connections and marking out This shows the true value of the device, in scanning large areas of concrete to check for rebar corrosion which is underway but has not yet caused visible damage, thus providing an early warning of damage and enabling cheaper repairs to be effected

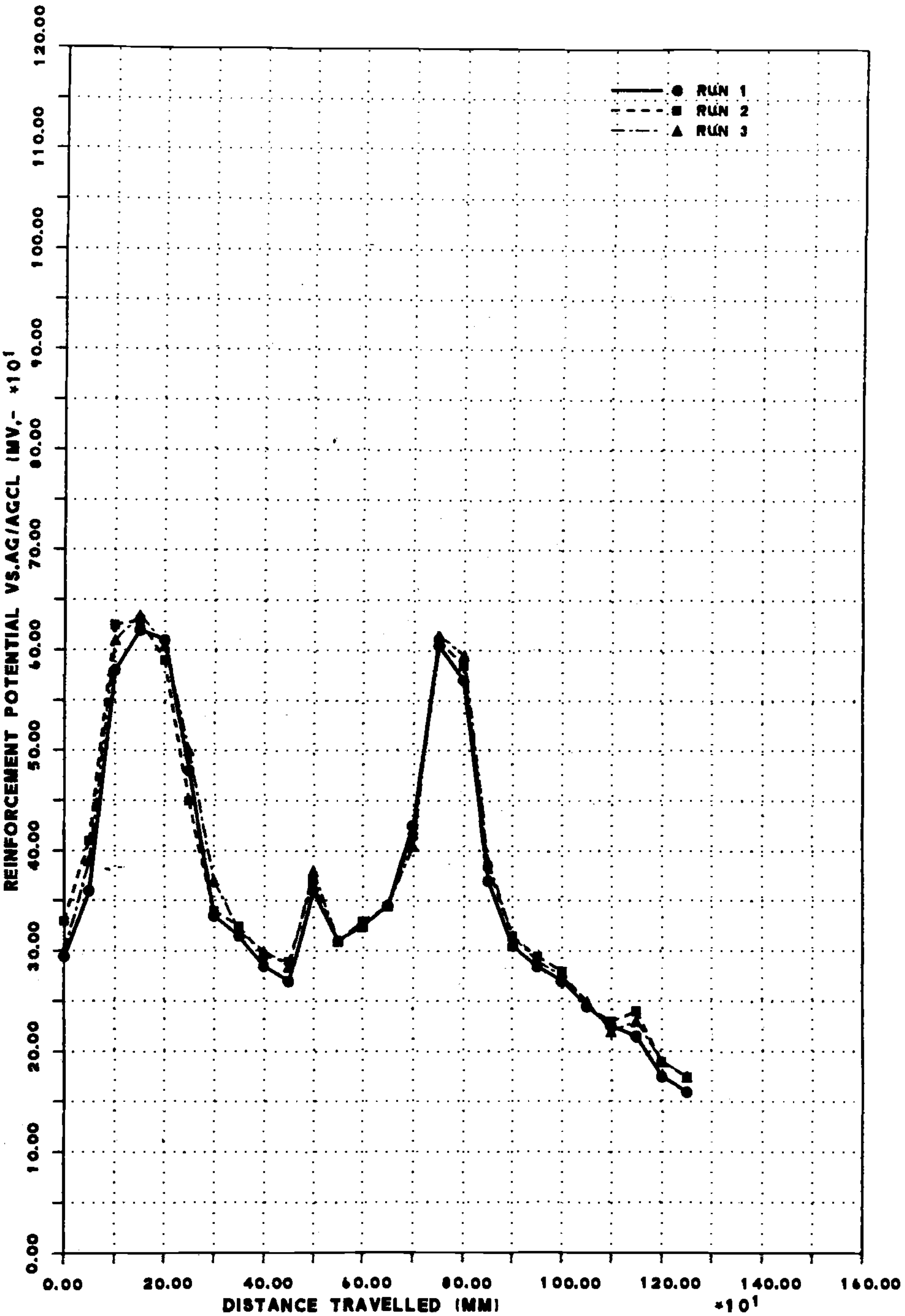

FIG. 5—*Potential Wheel repeatability assessment.*

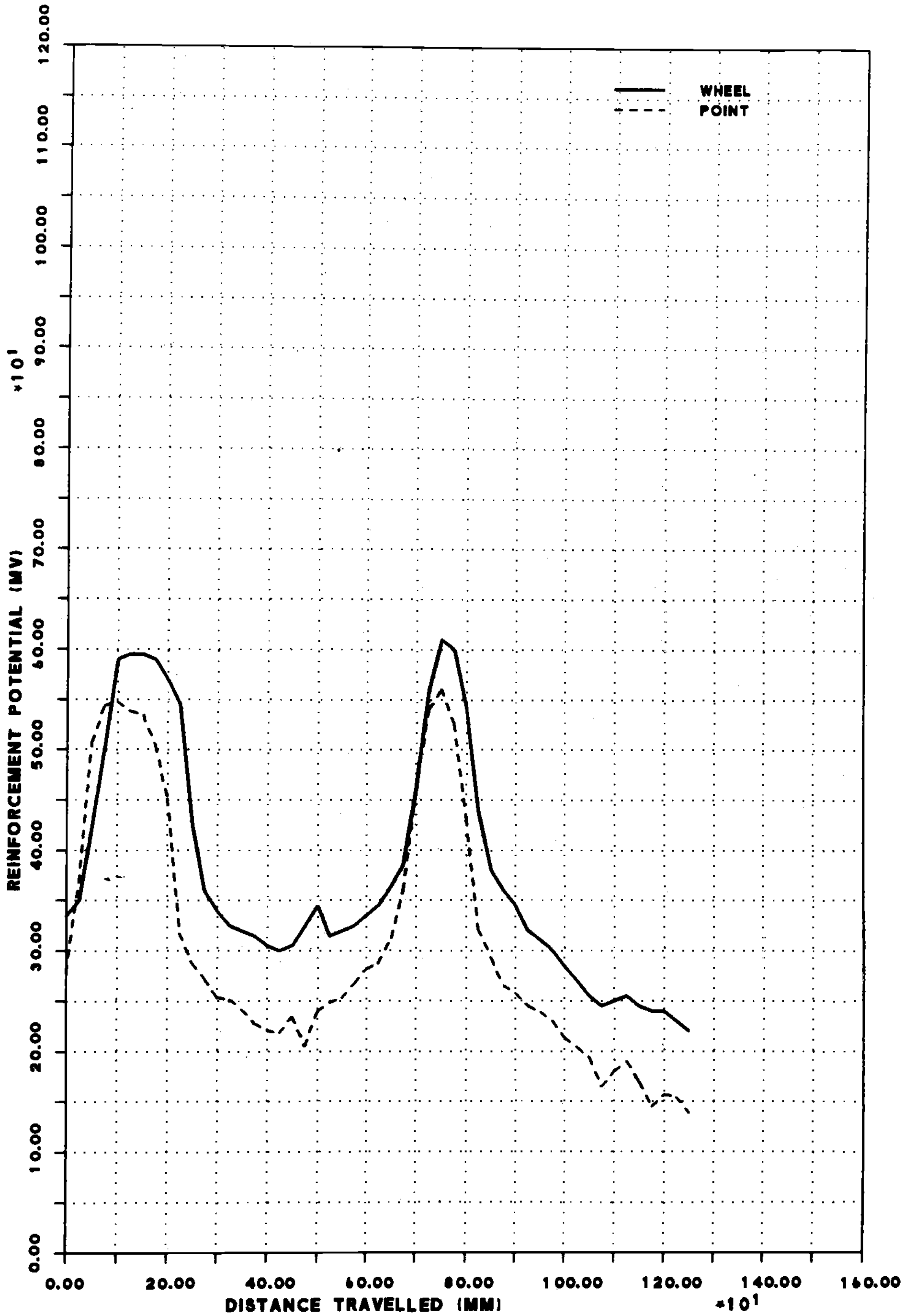

FIG. 6—*Potential Wheel comparative assessment 11°C Line 5.*

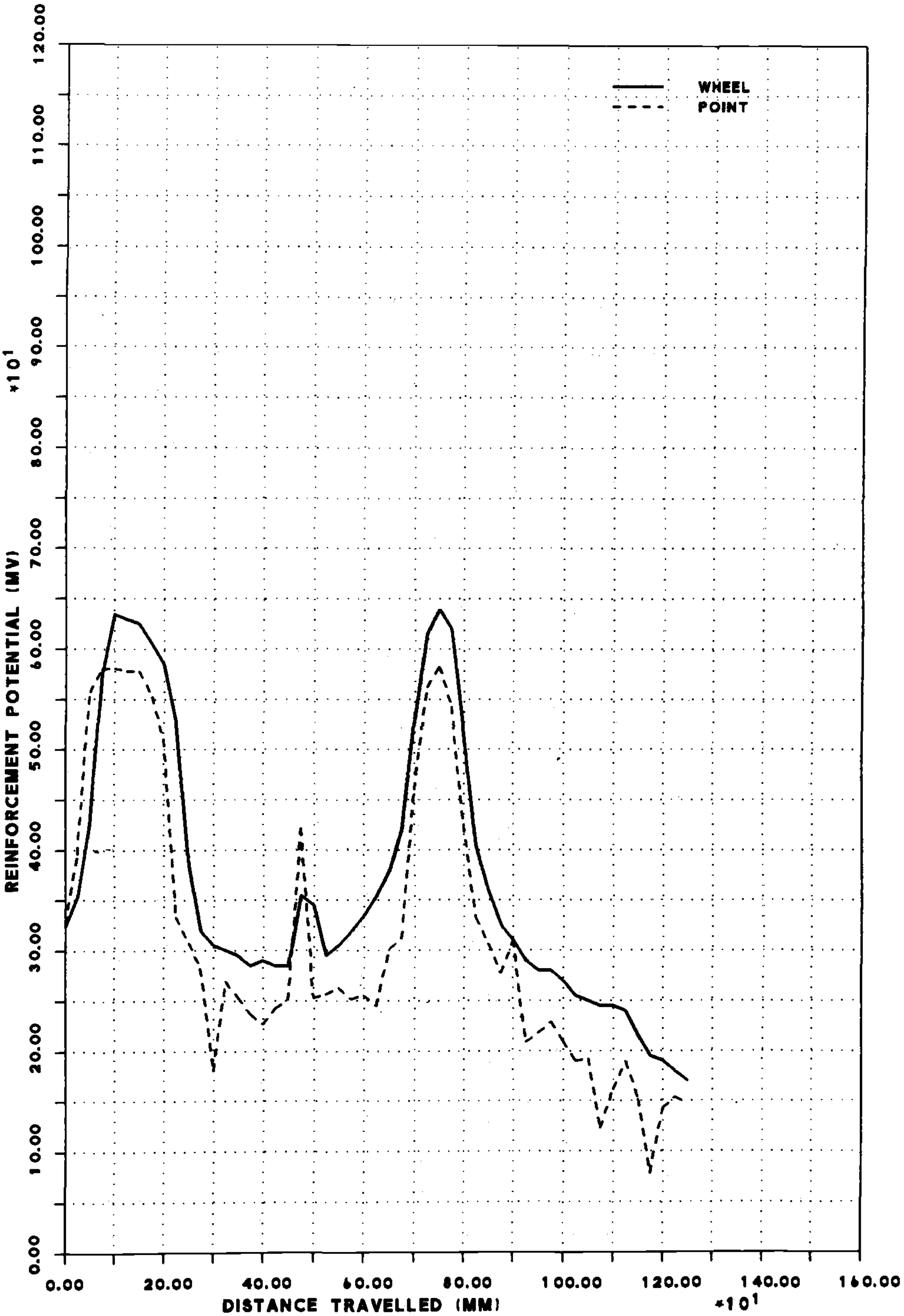

FIG. 7—*Potential Wheel comparative assessment 20°C Line 5.*

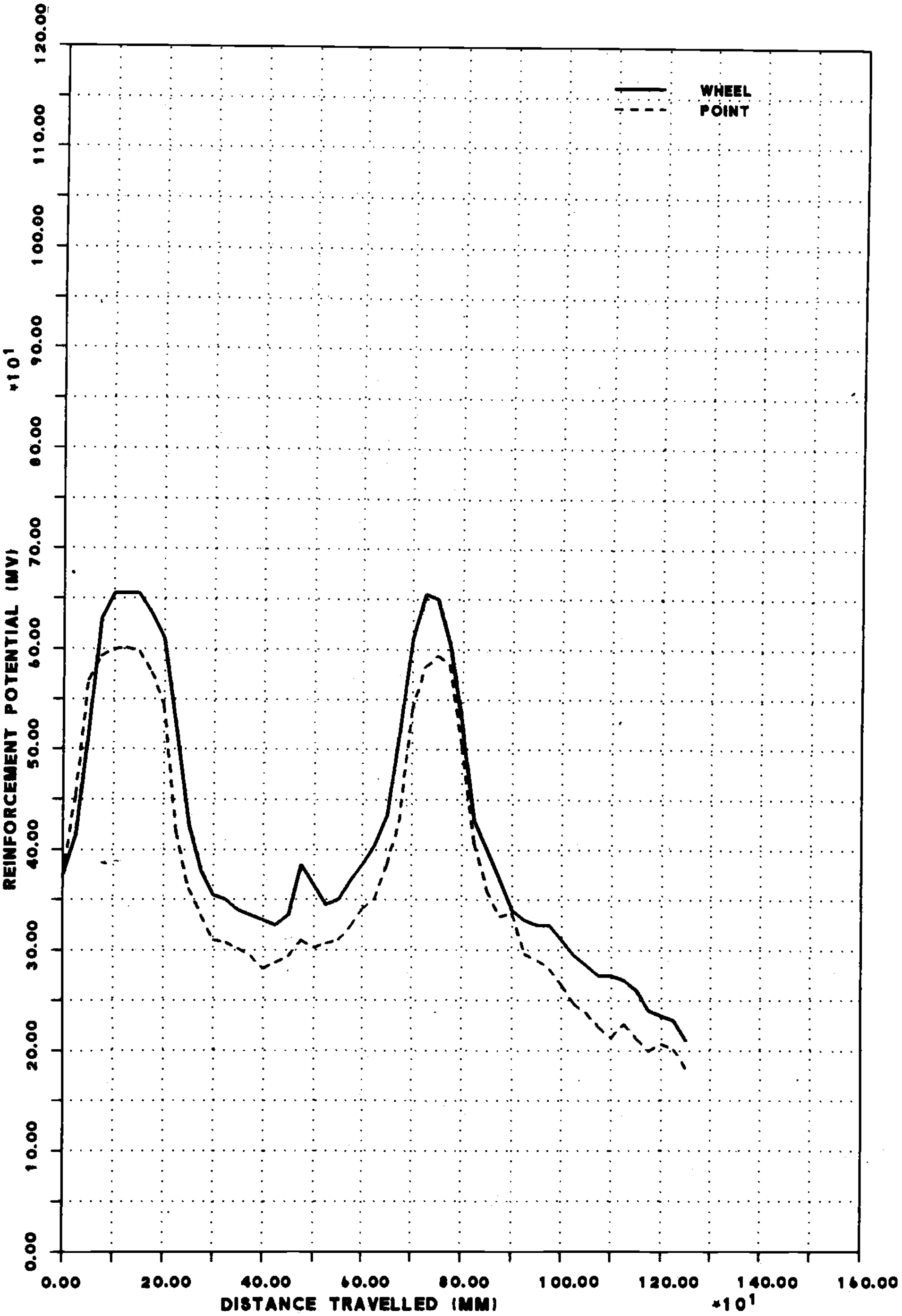

FIG. 8—*Potential Wheel comparative assessment 33°C Line 5.*

TABLE 2—*Reference electrode temperature coefficients* [6] $E = E_{25^\circ} + \frac{dE}{dt} \cdot t$.

Name	Cell	E_{25°, V	$\frac{dE}{dt}$	E, V		
				11°C	20°C	30°
Silver chloride	Ag/AgCl/KCl/(0.1 N)	0.2881	-6.5×10^{-4}	0.291	0.291	0.28
Copper sulfate	Cu/CuSO$_4$/CuSO$_4$(saturated)	0.316	9×10^{-3}	0.303	0.311	0.320

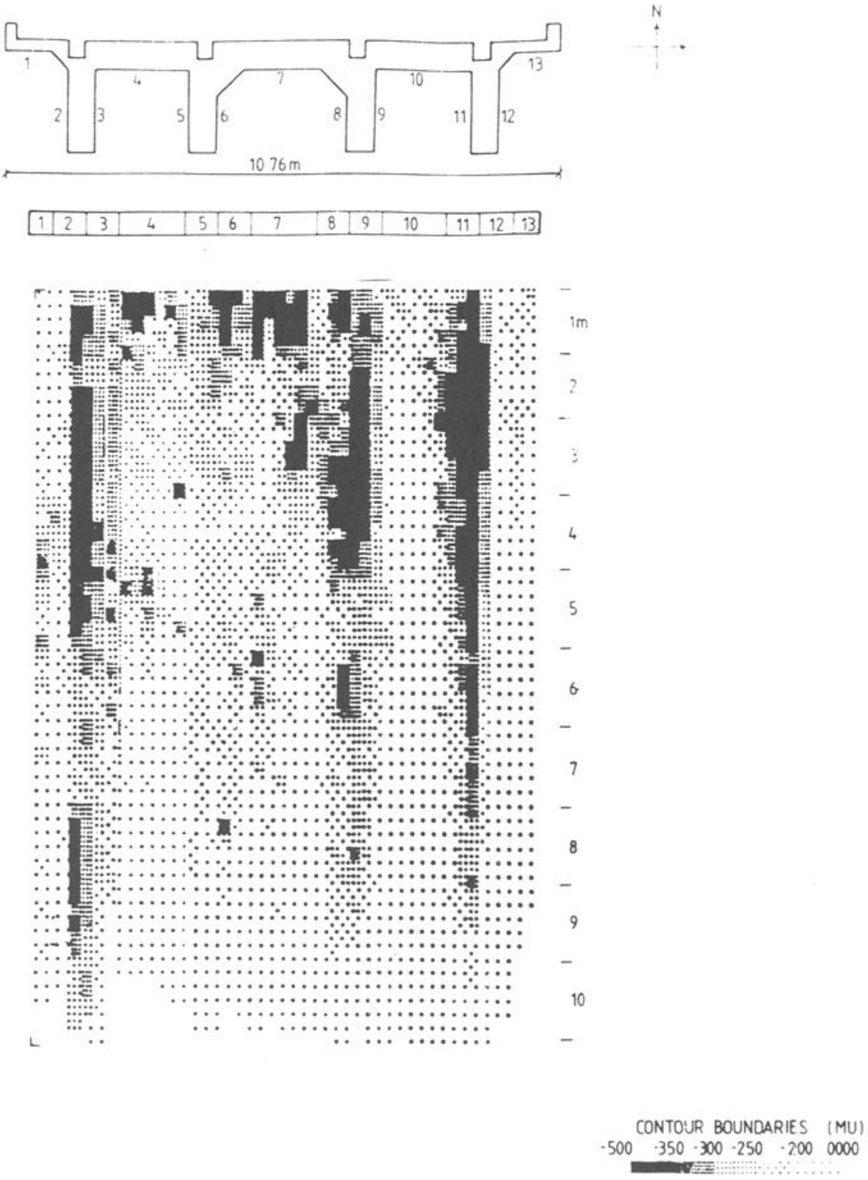

FIG. 9—*Potential map of the bridge soffit.*

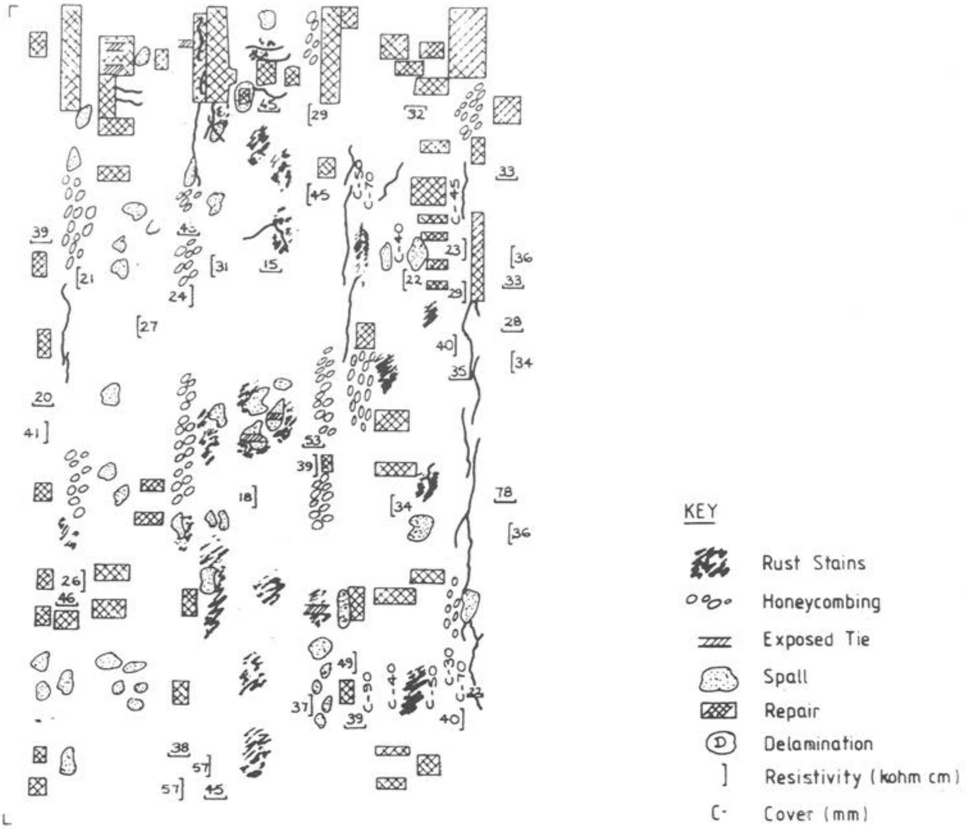

FIG. 10—*Visual survey of a bridge soffit.*

Conclusions

1. A Potential Wheel has been developed for rapid scan surveying of corrosion damaged reinforced concrete.
2. The device includes a rapid response half-cell, a wheel connection, and a Data Bucket microprocessor data storage system.
3. The system is ideal for rapid scanning of soffits, walls, and, in fact, virtually any surface.
4. Laboratory testing has shown the Wheel to be comparable to or better than a standard copper/copper sulfate half-cell, in terms of reproducibility, stability, and temperature effects.
5. Extensive site use has shown the wheel to be a practical and economical method of surveying.

Acknowledgments

The authors wish to thank Taylor Woodrow for permission to publish this paper and the staff of the laboratory who assisted in carrying out the work described in this paper.

References

[1] ASTM Test Method for Half-Cell Potentials of Uncoated Reinforcing Steel in Concrete (C 876-87)
[2] Van Daveer, J R , *Proceedings,* American Concrete Institute, Vol 12, 1975, p 697
[3] Williams, N J M and Lawrence, P F , "Fundamental Mechanisms of Corrosion of Steel Reinforcements in Concrete Immersed in Seawater," Concrete in the Oceans Technical Report No 6, CIRIA/UEG, Dept of Energy, UK
[4] Baker, A F , *Proceedings,* Seminar on Corrosion in Concrete, London Press Center, 1986
[5] Pathmanaban, S , *Proceedings,* Seminar on Corrosion in Concrete, London Press Center, 1987
[6] Uhlig, H H , *The Corrosion Handbook,* Wiley, New York, 1948

B. Borgard,[1] *C. Warren,*[2] *S. Somayaji,*[3] *and R. Heidersbach*[4]

Mechanisms of Corrosion of Steel in Concrete

REFERENCE: Borgard, B , Warren, C , Somayaji, S , and Heidersbach, R , **"Mechanisms of Corrosion of Steel in Concrete,"** *Corrosion Rates of Steel in Concrete, ASTM STP 1065,* N S Berke, V Chaker, and D Whiting, Eds , American Society for Testing and Materials, Philadelphia, 1990, pp 174–188

ABSTRACT: The corrosion of metals in concrete is a multibillion dollar problem which affects the construction, transportation, and many other industries While much has been written about the problem, and numerous reports have appeared which discuss how this corrosion can be controlled, little has appeared on the mechanism whereby this corrosion occurs

It is well known that highway structures corrode, for the most part, due to the influence of deicing salts or marine environments Relatively little has appeared about the equally severe corrosion problems which occur in buildings and other nonhighway structures Most of these structures are not exposed to the salts present in highway structures, yet they still corrode

This paper discusses how all forms of concrete and similar cementitious environments protect embedded metals It discusses the three protection mechanisms—passive film formation, changes in the conductivity of the electrolyte, and mineral scales—that have been used to explain how corrosion in concrete occurs It also presents evidence to explain how, and why, corrosion occurs in these structures, even in the absence of deicing salts, marine environments, or other salt sources Examples are discussed including buildings, marine piers, foundations, and highway structures

KEY WORDS: corrosion, concrete, mortar, masonry, deicing salts, marine environments, chloride, reinforcing steel, cracks, potential-pH (Pourbaix) diagrams, passivity, protective scales, steels

The corrosion of reinforced concrete and of other concrete structures is a multibillion dollar problem in the United States and many other countries [*1–3*] The collapse of the Berlin Congress Hall (Fig 1) [*4*] and of a parking garage in Minnesota (Fig 2) [*5*,*6*] are but two examples of spectacular failures which have been widely-publicized in recent years Other corrosion problems in buildings (Figs 3 and 4), and highway structures (Fig 5) produce maintenance and replacement costs While they are less spectacular, these maintenance and replacement problems are far more common and represent most of the reason for concern about corrosion in concrete

Reinforced concrete has been in use for over 100 years, and, in general, the environment provided by concrete proves protective of the embedded steel Many of the problems associated with corrosion in concrete can be attributed to the presence of salts from the environment This association with salt has led to two problems, (1) a misunderstanding of

---

[1] Engineer, Cortest Laboratories, Houston, TX

[2] Engineer, Compaq, Houston, TX

[3] Professor of Civil Engineering, California Polytechnic State University, San Luis Obispo, CA 93407

[4] Professor and head, Metallurgical and Materials Engineering Department, California Polytechnic State University, San Luis Obispo, CA 93407

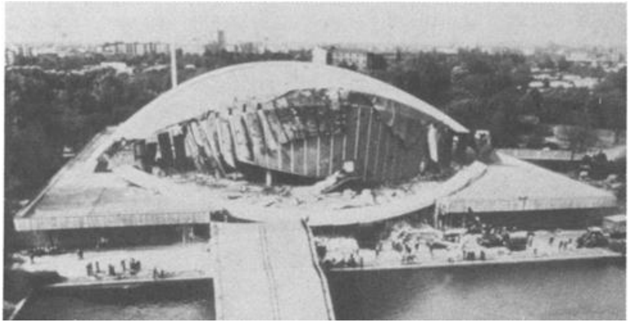

FIG. 1—*The collapse of the Berlin Congress Hall* [*4*].

the role of salts in the corrosion process for reinforced concrete structures and (2) a false sense of security for concrete structures in the absence of salt. The structures shown in Figs. 1 and 4 corroded in the absence of salts or chloride-containing additives. This type of corrosion is not well, documented, at least in part because it occurs on buildings which may be involved in litigation and not available for public scrutiny.

A careful review of the corrosion-in-concrete literature reveals at least three possible mechanisms whereby concrete may protect steel from corrosion:

1. Wet concrete is a base, and bases cause iron and steel to form protective oxides (passive films) which protect the metal from further reaction with their environments.
2. Concrete is a high-resistance electrolyte which limits galvanic corrosion.

FIG. 2—*Collapse of a salt-damaged parking garage* [*6*].

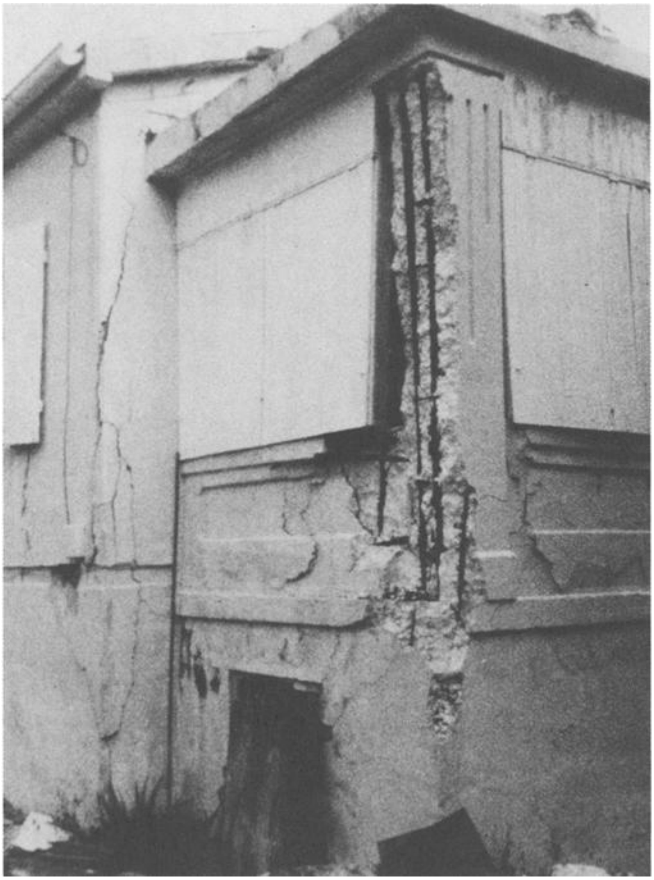

FIG. 3—*Corrosion of government housing in Key West, Florida.*

3. Mineral scales form on metals in concrete environments—the scales protect the steel from reacting with the environment.

This paper discusses each of these possibilities and how they relate to salts, cracking, freeze-thaw cycles, and other environmental concerns.

Passivity

One of the first National Bureau of Standards reports used the concept of passivity to explain how concrete protected steel from corrosion. The term "passivity," as used before 1920, predates modern understanding of protective films, crystalline structures in solids, and many other modern concepts. This early National Bureau of Standards report [7] should not be cited as supporting the concept of passive films on carbon steel in concrete environments.

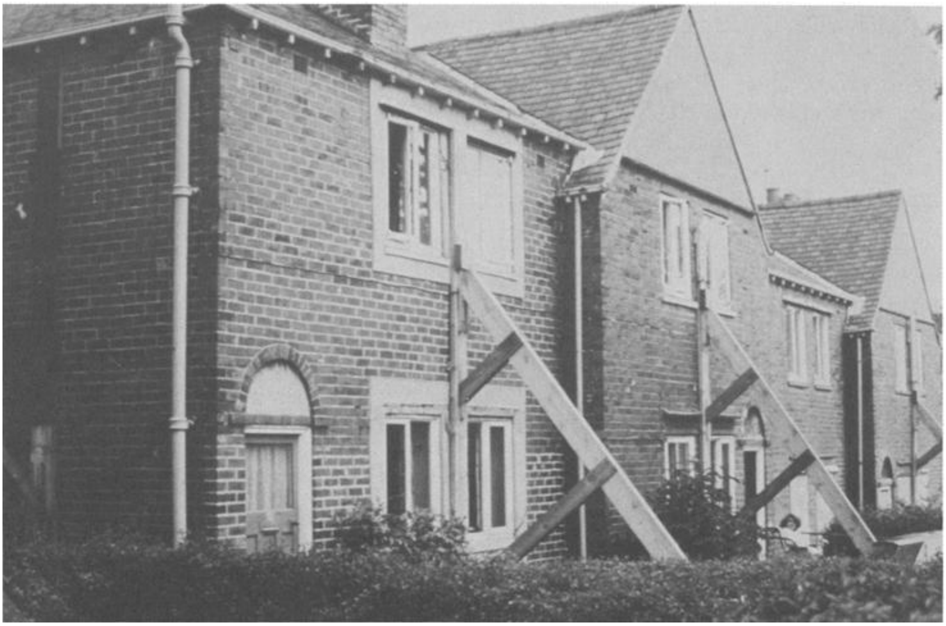

FIG. 4—*Collapse of masonry walls due to corroded wall ties.*

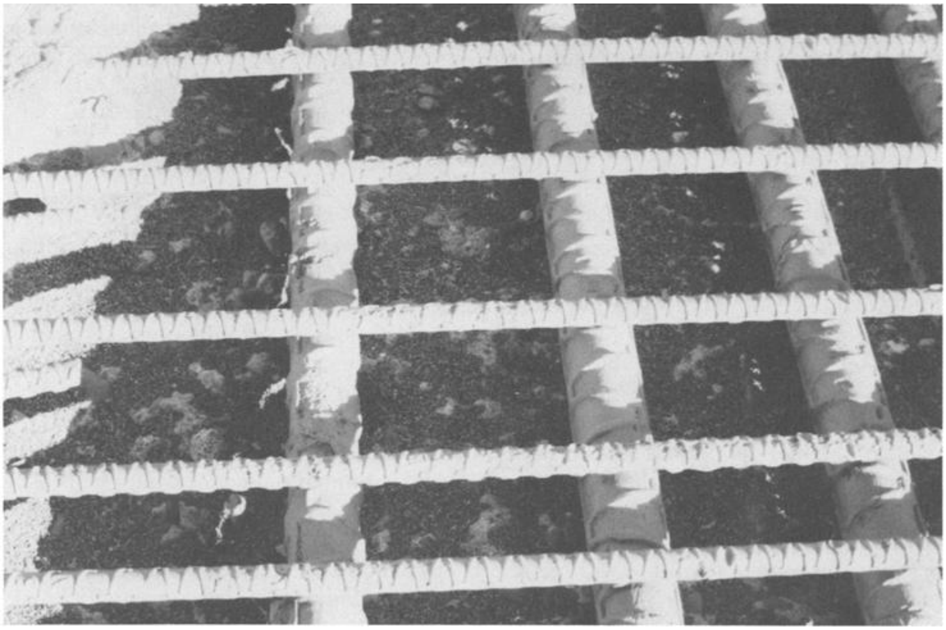

FIG. 5—*Corrosion of reinforcing steel due to pavement overlay cracks* [29].

The concept of passivity was reintroduced in 1964 by Cornet and co-workers [*8*] who cited the then popular concept of potential-pH (Pourbaix) diagrams to explain how concrete, with a pH of approximately 12.8, protects steel from corrosion. The passivity concept, introduced with no *experimental* evidence to support the protective passivity *mechanism*, has gained in popularity and is widely cited in recent literature [*1,9–11*].

Potential-pH Diagrams

Figure 6 shows a potential-pH (Pourbaix) diagram for iron in water with Fe_2O_3 as a protective (passive) film [*12*]. These diagrams, based on equilibrium thermodynamics, define three regions in potential-pH space:

1. Immunity—the metal is thermodynamically stable and is immune to corrosion.
2. Corrosion—ions of the metal are thermodynamically stable, and, under most conditions, corrosion will occur at a rate which cannot be predicted thermodynamically.
3. Passivity—compounds of the metal are thermodynamically stable. These compounds, or passive films, may protect the substrate from further reactions with the environment and may be protective.

Unfortunately, thermodynamics cannot be used to predict whether or not a film will be protective of its substrate.

The dotted lines of Fig. 6 represent the regions of thermodynamic stability for oxygen (above Line a), water (between Lines a and b), and hydrogen (below Line b). Passive films cover most of the high-pH region between Lines a and b. This was the basis for Cornet's comments that passivity could be used to explain why corrosion does not normally occur in concrete.

Unfortunately, the extrapolation of thermodynamics in water to practice in concrete continues to this day. Many authors assume the idea of protective films is well-accepted in the corrosion community without realizing the serious limitations of applying thermodynamic "passivity"—as defined by potential-pH diagrams—to actual kinetic situations. Most corrosion textbooks discuss potential-pH diagrams and their limitation [*13–16*].

Corrosion of Carbon Steel

Carbon steel, such as is used in reinforcing bars, prestressing wire, and post-tensioning cables does form passive films [*17–19*], but they are not protective in mortar or concrete [*20*]. Corrosion control is achieved when needed for exposure to bases by alloying (changing the composition of the passive film), by use of oxidizing corrosion inhibitors (chromates, phosphates, nitrates, etc.), and by the use of oxygen scavengers, mechanical deaerators, or cathodic protection. All of these approaches are discussed in the corrosion literature [*14*], and most of them have been applied to the corrosion of steel embedded in concrete [*1*].

One of the more important concepts introduced to the corrosion in concrete literature by Cornet and co-workers was the idea that passive films formed on metals would be broken down, or "depassivated," by the presence of chloride ions. Many other authors have adopted this idea [*1,21–25*], and it has become so widespread that it is sometimes cited in the corrosion-in-concrete literature with no reference to the source of the idea [*22,24*].

Stratfull, one of the earlier researchers in this field, adopted the idea of passivity breakdown because, in his work, there was no correlation between the amount of chlorine detected in bridge decks and the amount of corrosion experienced [*21*]. This suggested to Stratfull

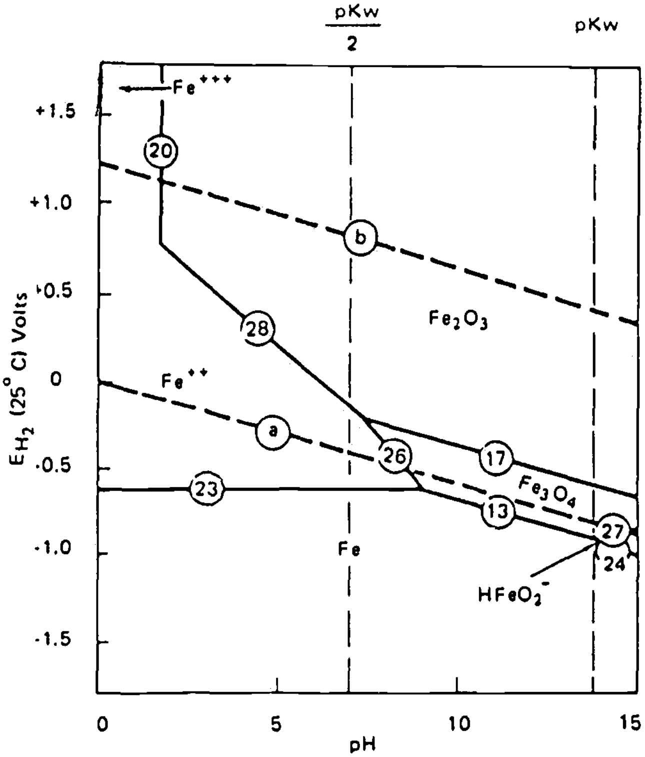

FIG. 6—*Potential-pH(Pourbaix) diagram for iron* [12].

that a minimum level of chlorine was necessary to initiate passivity breakdown and excess chlorine would not affect corrosion.

There are many reasons for the variations that have been reported in the chlorine levels associated with the onset of corrosion of steel in concrete. Differences in cement chemistry, concrete mix conditions, and exposure variables can all affect the protection that concrete affords to embedded steel [1,11,24–28]. Unfortunately, localized variations in chlorine content are seldom reported. The electron microprobe (a scanning electron microscope equipped with an X-ray spectrometer) has been used to show how high chlorine levels are found at the corrosion shown in Fig. 5, whereas little chlorine is found on the uncorroded steel only millimeters away [29]. These localized chlorine concentrations cannot be detected using the techniques commonly reported in the corrosion-in-concrete literature [1,22–23].

Some researchers have shown that increased chlorine levels can cause reductions in corrosion rates under certain circumstances [30]. Chlorine salts have been reported to act as corrosion inhibitors, although the exact mechanism may not have been explained correctly [31]. Relatively high levels of chlorine are necessary to initiate corrosion of steel in concrete [22–23]. These high levels, and the fact that chlorine can reduce corrosion in some cases [30–31], are indications that corrosion in concrete is not related to the breakdown of passive films on carbon steel. Titanium and stainless steel are more corrosion resistant than carbon steel. Localized depassivation can lead to stress corrosion cracking of these corrosion-resistant metals. This is avoided by keeping chlorine to part per billion levels [32–34]. It is unlikely that these corrosion-resistant metals would resist *lower* chlorine levels than corrosion-susceptible carbon steels This suggests that passivity is *not* the mechanism which causes protection of steel from corrosion in concrete environments

Passivity Summary

This discussion of passivity can be summarized by the following

1 Passive films are *not* protective for carbon steels in most high-pH environments Oxidizers, corrosion inhibitors, or other means must be used to prevent corrosion in bases

2 Wide variations in chlorine levels have been associated with the onset of corrosion of carbon steel in concrete These levels are higher than the levels necessary to depassivate stainless steel, titanium, and other corrosion-resistant alloys

The foregoing information suggests that other reasons must be found to explain why concrete normally protects steel from corrosion

Concrete as an Electrolyte

Stratfull published a paper in 1968 with experimental evidence showing that salt ingress reduced the electrical resistivity of concrete [*35*] This experimental work, published in the same volume of the same journal as Cornet's passivity hypothesis [*8*], has received relatively less attention, even though, unlike Cornet's paper, it presented experimental evidence from an actual highway bridge in California

Table 1 shows the effects of electrical resistivity on corrosion rates in soil [*36*] The corrosion rates shown in Table 1 are based on long-term studies at the National Bureau of Standards [*36,37*] The effects of resistivity are discussed in underground corrosion texts [*38–40*] and have several similarities to corrosion in concrete In general, corrosion rates are affected by moisture levels, salt contents, and dissolved oxygen levels The same parameters affect corrosion rates in concrete [*41*] A level of 10 000 ohm-cm has been suggested as "critical resistivity to support corrosion" in concrete [*22,42*] This is the same resistivity level shown in Table 1 for the dividing line between moderate corrosion rates and mild, or less corrosive, soil conditions

A number of other studies have appeared showing correlations between electrical resistivity or a-c impedance and corrosion rates or both [*43–49*] Unfortunately, these studies are either based on small laboratory samples or they report average corrosion rates on actual structures The severity of localized corrosion, such as shown in Fig 5, cannot be estimated using electrochemical techniques, at least as normally used [*1,16,49*]

TABLE 1—*Corrosion activity in soils* [36]

Resistivity, ohm-cm	Anticipated Corrosion Activity
Low, 0 to 2 000	severe
Medium, 2 000 to 10 000	moderate
High, 10 000 to 30 000	mild
Very high, 30 000 plus	unlikely

Mineral Scales

The formation of mineral scales, precipitates of chemical compounds, on metal surfaces is a common means of corrosion control. Protective scales form on circulating water pipes [*50–55*], oil field production tubing [*56,57*], and boiler walls [*58*] where passive films do not form [*59*]. These scales also form on metals in cementitious environments.

Steel can often be removed from concrete after many years with no indication that it has ever been exposed to a wet environment. Figure 5 [*29*] and Fig. 7 [*60*] show steel with no indications of exposure to moisture adjacent to other portions of the same steel which have been extensively corroded. When steel like this is removed from concrete, it is very instructive to examine the adjacent cementitious material. It is shiny and has no water deposits or other indications of moisture after the concrete curing cycle.

This is very similar to the behavior of water pipes used in hard water service. While soft waters (high in sodium and potassium) are generally corrosive, hard waters (higher in calcium and magnesium) are less corrosive [*50*] and produce localized or pitting corrosion [*51*].

The lack of corrosion at many locations on Fig. 5 is quite comparable to the corrosion in oil-field production tubing. This tubing is frequently protected from corrosion by the presence of carbonate scales. These carbonate scales become unprotective at locations where turbulence wears them away and allows very deep localized corrosion [*57,61*].

Carbonation of concrete is commonly considered to be one possible cause of corrosion [*1,62*]. The reduced pH of concrete is assumed to cause a loss of passivity. Figure 6 shows that passive films are maintained on steel surfaces down to pHs of 6 and less depending on the electrochemical potential. Of course, Fig. 6 cannot be used to predict whether or not a passive film is protective or not.

FIG. 7—*Corrosion at void in concrete* [*60*].

It is more likely that protective scales, high in calcium, form on metal surfaces in concrete environments A number of papers on corrosion in concrete have suggested this [*24,28,63–67*]

Several authors have suggested that concrete pore water is the environment to which reinforcing steel is exposed [*23,68–70*] While this "pore water" may model the unreacted water in cement pastes, it ignores the low solubility, and likelihood of scale formation, from waters high in calcium Since portland cements are high in calcium, and form high-calcium reaction products [*71*], the formation of high-calcium scales is likely A recent laboratory study into the nature of these scales found them protective and "for active corrosion to start, formation of voids at the steel-mortar interface is a necessary condition" [*20*]

Calcium-containing scales have been used to control corrosion for many years [*14,50–55,58*], and they are likely to explain why corrosion is normally retarded, or completely prevented, by concrete [*20*] It is interesting to note that calcium carbonate scales are used for protection of oil-field production tubing even in the presence of chloride levels far higher than seawater [*56*] This suggests corrosion in concrete, like corrosion in oil and gas production, can be explained by the mechanical failure of carbonate scales

Cracks and Corrosion

One of the first reports on corrosion-in-concrete research used embedded electrodes which corroded and cracked the surrounding concrete [*7*] The samples and cracks were similar to Fig 8, taken from a 1940s study of electrolysis in railroads [*71*] Since this early research, most publications have implied that corrosion causes cracking in concrete [*1*] While there can be no doubt corrosion caused by impressed currents can cause cracking in concrete [*7,55*], the evidence in the absence of external electrical currents is much less convincing.

One obvious correlation between cracking and corrosion is the increased incidence of structural cracking in highway bridges that accompanied the increased use of deicing salts on highway bridges Figure 9 shows a sidewalk in the United States which has cracked and crumbled due to the presence of deicing salts No corrosion was involved A recent study of highway bridges in Japan discusses freeze-thaw damage in concrete highway bridges with no mention of corrosion on these reinforced concrete bridges [*72*] Salt water can enter bridge structures through freeze-thaw cracks and cause corrosion

The freeze-thaw cracking pattern shown in Fig 9 is different from the cracking and deterioration of the pipe shown in Fig 10. The concrete pipe shown in Fig 10, on a southern California beach, is not subject to freeze-thaw damage Cores of the concrete pipe shown in Fig 10 revealed many cracks caused by wave action and unrelated to the location of embedded wire reinforcement

Figure 11 shows the cracking pattern on a concrete core removed from a fence wall on a beach in central California Half-cell potential measurements were made using the ASTM Half Cell Potentials of Reinforcing Steel in Concrete (C 876-80) method This commonly used procedure [*1,23,73*] indicated that the concrete should be cracked, presumably due to corrosion Examination of the metal surface revealed only superficial corrosion—less than is common on many construction sites prior to placing concrete around the reinforcing steel

The crack widths shown in Fig 11 are an accurate representation of the crack patterns on this core—which is typical of cores obtained in our research If corrosion had produced these cracks, the cracks should be wider near the steel The opposite pattern, cracks which are wider away from the steel, is common on cores obtained from a marine seawall, the wall shown in Fig 11, and an Interstate highway bridge All of the cracks from these structures seem to come from structural sources and none from corrosion

Figures 12 and 13 show corrosion resulting from deicing salts in parking garages The

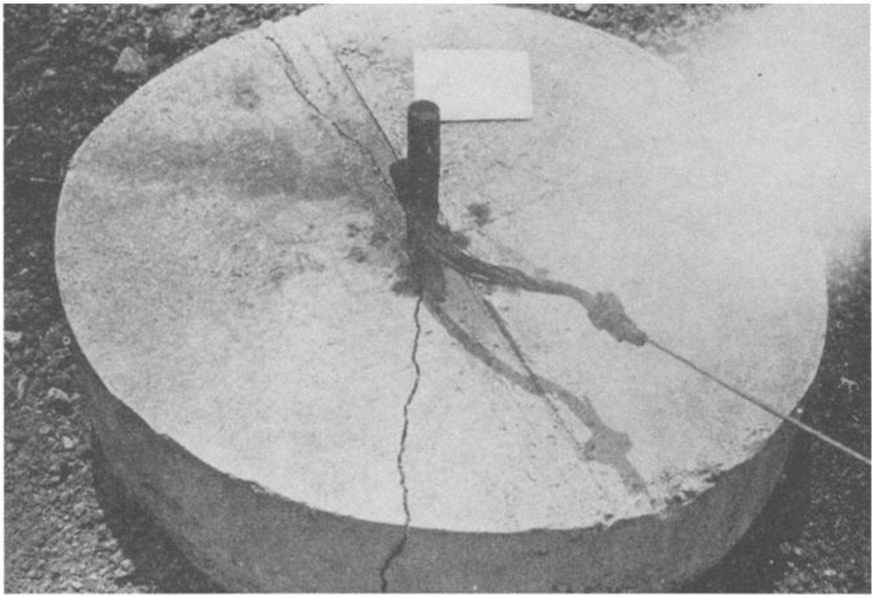

FIG. 8—*Cracked concrete cylinder due to impressed-current corrosion of embedded steel* [*71*].

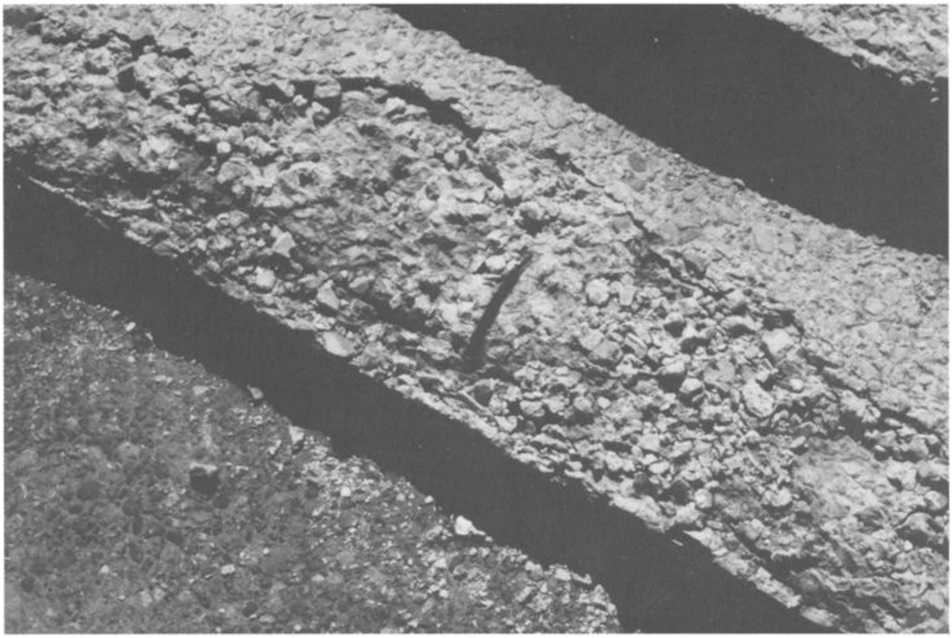

FIG. 9—*Salt-induced freeze-thaw damage on sidewalk in Missouri.*

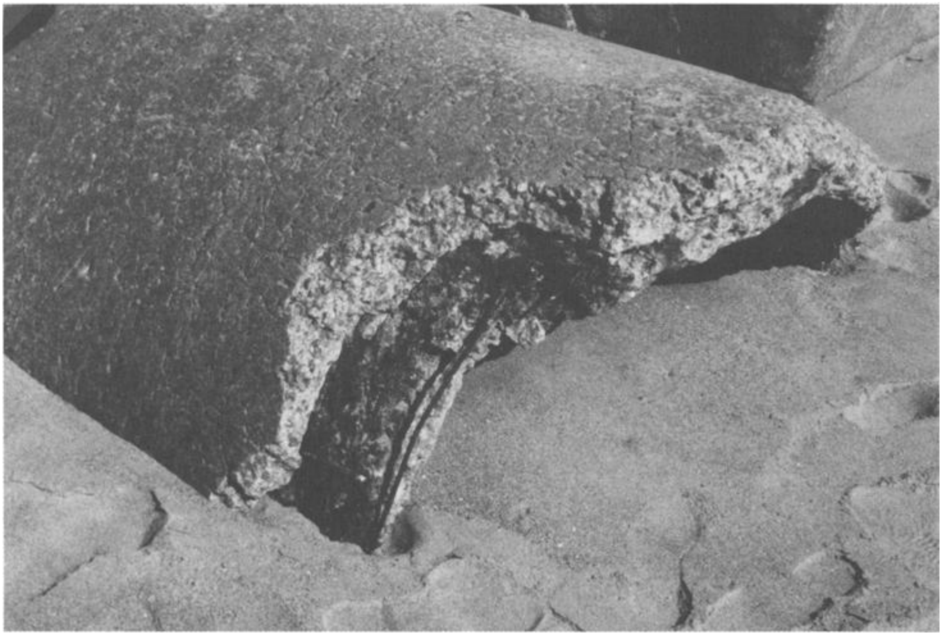

FIG. 10—*Corrosion on reinforced concrete drain pipe on beach in Ventura, California.*

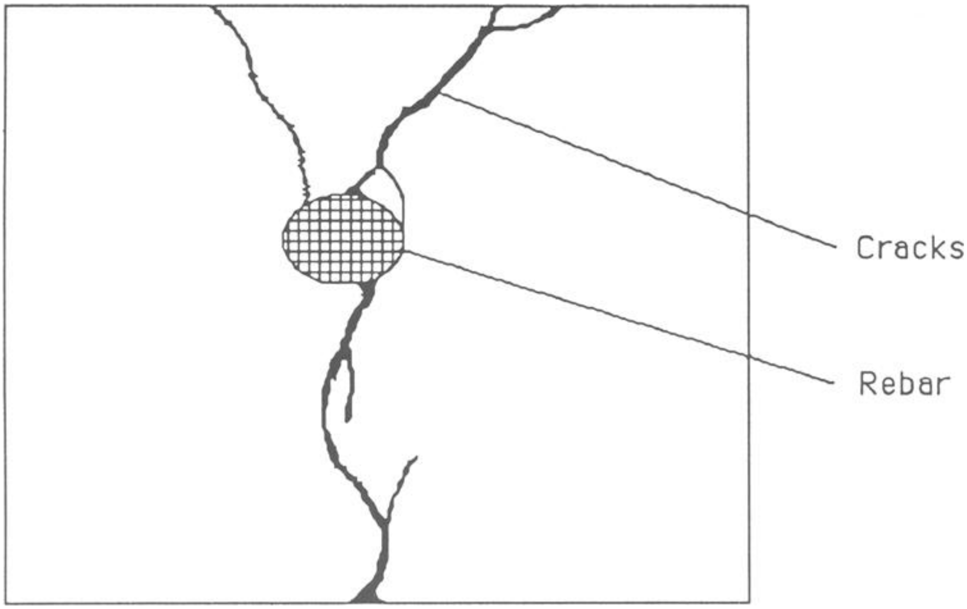

FIG. 11—*Cracking pattern on concrete core from reinforced concrete wall in Avila Beach, California.*

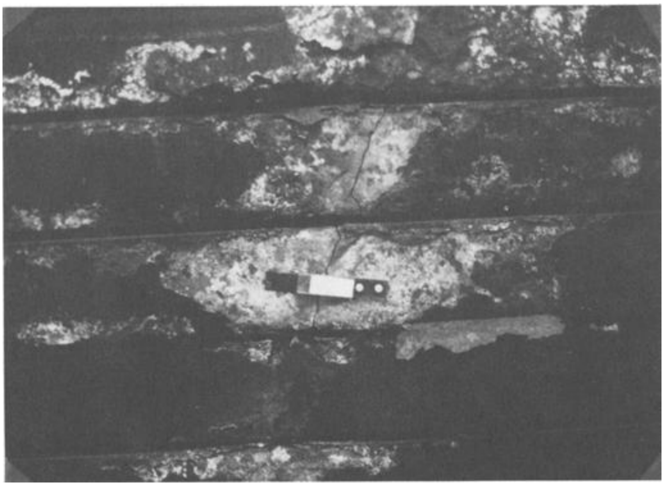

FIG. 12—*Cracks and corrosion on permanent-form concrete parking garage floor in New Haven, Connecticut* [5].

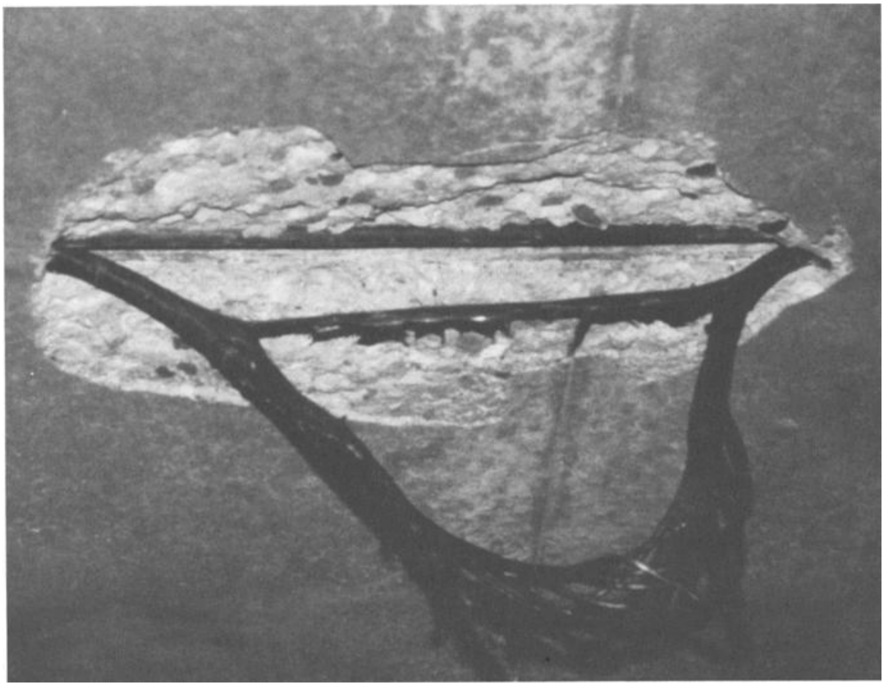

FIG. 13—*Broken corroded post-tensioning cable in roof of parking garage.* (Photo courtesy of J. Slater).

crack in Fig 12 led to the corrosion of the permanent metal forms beneath this parking garage floor The corrosion shown in Fig 12 is typical of the corrosion on this building, which may have to be demolished due to the parking garage corrosion It is not known whether pre-existing cracks were associated with the post-tensioning cable shown in Fig 13 [*5*]

A recent survey of highway bridge decks in the New York City area showed that the most likely cause of corrosion was inadequate cover over the reinforcing steel [*74*] Bridges with corrosion were almost identical to similar bridges with virtually no deck corrosion problems Half-cell potential measurements did not prove reliable and spalls and problem areas had to be located by other means The authors of this study concluded that corrosion was caused by cracking allowing salt water to penetrate to the level of reinforcing steel The deeper cracks supposedly healed [*75*] and kept the steel dry

As previously stated, most corrosion in concrete literature claims that corrosion causes cracks Unfortunately, crack patterns similar to those shown in Fig 11 are seldom reported When they are reported, it is usually from experimental exposures that do not undergo the flexural loading experienced by actual structures [*76*] These unloaded cracks could heal and may produce misleading results Since uncracked concrete is a "laboratory curiosity" (Ref *1*, p 49), the need exists for laboratory exposures involving loaded cracked samples The limited number of reports available confirm that cracking or voids are necessary to produce corrosion in the absence of external electric current sources [*26,77–80*]

Most authorities feel that cracks transverse to embedded steel can be considered less important than those parallel to embedded steel [*9*] This has been offered as a criticism of the loaded laboratory studies [*26,77–80*] just cited

Whether cracks can cause corrosion or are normally the result of corrosion will remain subject to debate [*9,81*]

Summary

A review of available information leads us to believe the resistance of embedded steel to corrosion is probably due to the presence of a protective mineral scale which keeps the embedded metal from becoming wet Low conductivity concrete or the presence of passive films may be also important

This report has shown that corrosion in concrete is often due to the presence of voids (Fig 7) or cracks (Figs 5 and 12) Whether cracking preceeds most corrosion or is a result of corrosion cannot be answered at this time

Acknowledgments

This work was supported by the National Science Foundation

References

[*1*] Slater, J , *Corrosion of Metals in Association with Concrete, ASTM STP 818,* American Society for Testing and Materials, Philadelphia, 1983

[*2*] Cady, P in *Chloride Corrosion of Steel in Concrete, ASTM STP 629,* American Society for Testing and Materials, Philadelphia, 1977, pp 3–11

[*3*] Litvan, G and Bickley, J in *Concrete Durability,* J Scanlon, Ed , American Concrete Institute SP 100, Detroit, 1987, pp 1503–1525

[*4*] Isecke, B , *Materials Performance,* Vol 21, No 12, Dec 1982, p 36

[*5*] Heidersbach, R , "Chapter 3—Corrosion," *Attorney's Guide to Corrosion,* I Kuperstein and N Salters, Eds , Matthew Bender, New York, 1986

[*6*] "Salt Flattens Old Garage," *Engineering News Record,* June 4, 1984, p 11

[*7*] Rosa, E , McCollum, B , and Peters, O , "Electrolysis in Concrete," National Bureau of Standards Technologic Paper No 18, 1918

[*8*] Cornet, I , Ishikawa, T , and Bresler, B , *Materials Protection,* Vol 7, No 3, March 1968, pp 44–47

[*9*] Darwin, D , Manning, D , Hognestad, E , Beeby, A , Rice, P , and Ghowrwal, A , *Concrete International,* Vol 7, No 5, 1985, p 20

[*10*] *Corrosion of Reinforcing Steel in Concrete,* Society of Chemical Industry, A Crane, Ed , London, 1983

[*11*] Sorenson, B and Maahn, E , *Nordic Concrete Research,* Vol 1, No 1, 1982, p 1

[*12*] Pourbaix, M , *Atlas of Electrochemical Equilibria in Aqueous Solutions,* National Association of Corrosion Engineers, Houston, 1974, pp 307–321

[*13*] Skorchelletti, V , *The Theory of Metal Corrosion* (translated from the Russian), Ketterpress Enterprises, Jerusalem, Israel, 1976, pp 192–201 (available from National Technical Information Service as TT 75-50013)

[*14*] Uhlig, H and Revie, W , *Corrosion and Corrosion Control,* Wiley, New York, 1985, pp 107–114, 414–415

[*15*] Atkinson, J and Van Droffelaar, *Corrosion and Its Control,* National Association of Corrosion Engineers, Houston, 1982, pp 14–15, 19–22

[*16*] Fontana, M , *Corrosion Engineering,* McGraw-Hill, New York, 1986, pp 452–454

[*17*] Berke, N in *Corrosion Effects of Stray Currents and the Techniques for Evaluating Corrosion of Rebars in Concrete, ASTM STP 906,* V Chaker, Ed , American Society for Testing and Materials, Philadelphia, 1986, pp 78–91

[*18*] Gernov, Y , Tomov, T , and Georgiev, *Journal of Applied Electrochemistry,* Vol 5, 1975, pp 351–358

[*19*] Rechberger, P , *Zement-Kalk-Gips,* Vol 36, No 10, 1983, pp 582–590

[*20*] Yonezawa, T , Ashworth, V , and Proctor, R , *Corrosion,* Vol 44, No 7, 1988, pp 489–499

[*21*] Stratfull, R , Van Matre, V , and Halterman, J , "Corrosion Autopsy of a Structurally Unsound Bridge Deck," California Highway Report CA-HY-MR-5116-8-72-41, Nov 1972

[*22*] Hope, B and Ip, A , *Materials Journal,* American Concrete Institute, July-Aug 1987, pp 306–314

[*23*] Wheat, H and Eliezer, Z , *Corrosion,* Vol 41, 1985, pp 640–645

[*24*] Mehta, P in *Chloride Corrosion of Steel in Concrete, ASTM STP 629,* American Society for Testing and Materials, Philadelphia, 1977, pp 12–19

[*25*] Lankard, D , *Proceedings,* Corrosion/76, Paper No 17, National Association of Corrosion Engineers, Houston, March 1976

[*26*] Tuuti, K , *Cracks and Corrosion,* Swedish Cement and Concrete Research Institute, Report 6 78

[*27*] Tuuti, K , *Nordic Concrete Research,* Vol 1, No 1, 1982, p 19

[*28*] Page, C and Treadaway, K , *Nature,* Vol 297, May 13, 1982, p 109

[*29*] Lloyd, J and Heidersbach, R , *Concrete International,* Vol 7, No 5, 1985, p 45

[*30*] Griffin, D and Henry, R , *Proceedings,* American Society for Testing and Materials, Vol 63, 1963, pp 1046–1079

[*31*] Arber, M and Vivian, H , *Australian Journal of Applied Science,* Vol 12, No 3, Sept 1961, pp 339–347

[*32*] Strauss, S , *Power,* Nov 1978, pp 14–17

[*33*] Barber, D and Lister, D , *Proceedings,* Water Chemistry and Corrosion Problems in Nuclear Power Plants, IAEA-SM-264/15, Vienna, 22–26 Nov 1982

[*34*] Barber, D and Van Borla, J , *Proceedings,* 1988 JAIF International Conference on Water Chemistry in Nuclear Reactors, 19–22 April 1988

[*35*] Stratfull, R , *Materials Protection,* Vol 7, No 3, 1968, p 29

[*36*] Romanoff, M , "Underground Corrosion," National Bureau of Standards Circular 579, 1957

[*37*] *Underground Corrosion, ASTM STP 741,* E Escalante, Ed , American Society for Testing and Materials, Philadelphia, 1980

[*38*] Parker, M , *Pipeline Corrosion and Cathodic Protection,* Gulf Publishing, Houston, 1962

[*39*] Peabody, A , *Control of Pipe Line Corrosion,* National Association of Corrosion Engineers, Houston, 1967

[*40*] Wranglen, G , *Corrosion and Protection of Metals,* Chapman and Hall, New York, 1985, pp 131–132

[*41*] Gjorv, O , Vennesland, O , and El-Busaidy, A , "Diffusion of Dissolved Oxygen Through Concrete," Corrosion/76, Paper No 17, National Association of Corrosion Engineers, Houston, March 1976

[42] Hope, B , Ip, A , and Manning, D , *Cement and Concrete Research,* Vol 15, 1985, pp 525–534

[43] Escalante, E and Ito, S , "Measuring the Rate of Corrosion of Steel in Concrete," *The Measurement and Correction of Electrolyte Resistance in Electrochemical Tests, ASTM STP 1056,* American Society for Testing and Materials, Philadelphia, 1989, pp 180–190

[44] John, G , Searson, P , and Dawson, J , *British Corrosion Journal,* Vol 10, 1981, pp 102–106

[45] Andrade, C and Gonzalez, J , *Werkstoffe und Korrosion,* Vol 29, 1978, pp 515–519

[46] Macdonald, D , McKubre, M , and Urquidi-Macdonald, M , *Corrosion,* Vol 44, 1988, pp 2–6

[47] Thompson, N , Lawson, K , and Beavers, J , *Corrosion,* Vol 44, 1988, pp 581–589

[48] Feliu, S , Gonzalez, J , Andrade, C and Feliu, V , *Corrosion,* Vol 44, 1988, p 761–767

[49] Slater, J , "Constraints in Measurement Techniques for Corrosion of Steel in Concrete," Corrosion/78, Paper No 121, National Association of Corrosion Engineers, Houston, March 1978

[50] *The Corrosion Handbook,* H Uhlig, Ed , Wiley, New York, 1948

[51] Boffardi, B in *Metals Handbook, 9th Edition, Volume 13—Corrosion,* L Korb and D Olson, Eds , American Society for Metals, International, Metals Park, OH, 1987, pp 487–497

[52] McCauley, R and Abdullah, M , *Journal of the American Water Works Association,* Vol 50, 1958, pp 1419–1428

[53] Stumm, W , *Journal of the American Water Works Association,* Vol 48, 1956, pp 300–310

[54] Powell, S , Bacon, H , and Lill, J , *Industrial Engineering Chemistry,* Vol 37, 1945, pp 842–846

[55] Comeaux, R , *Materials Performance,* Vol 17, No 11, pp 9–21

[56] *Corrosion Control in Petroleum Production,* National Association of Corrosion Engineers, Houston, 1979

[57] Craig, B , *Practical Oilfield Metallurgy,* PennWell Books, Tulsa, 1984

[58] *Handbook of Industrial Water Conditioning,* Betz Laboratories, Trevose, PA, 1980

[59] Townsend, H , *Proceedings,* 4th International Congress on Metallic Corrosion, Sept 1969, Amsterdam, pp 477–487

[60] Monfore, G and Verbeck, G , *Journal,* American Concrete Institute, Vol 57, 1960, pp 491–515

[61] Heidersbach, R , *Proceedings,* Offshore Technology Conference, Paper No 4974, Houston, May 1985

[62] Hausman, D , *Journal,* American Concrete Institute, Feb 1964, p 514

[63] Page, C , *Nature,* Vol 258, 11 Dec 1975, pp 514–515

[64] Page, C , *Nature,* Vol 297, No 5862, 1982, pp 109–115

[65] Page, C and Vennesland, O , *Materiaux et Construction,* Vol 16, No 91, 1983, pp 19–25

[66] Page, C , Al Khalaf, M , and Ritchie, A , *Cement and Concrete Research,* Vol 8, 1978, pp 481–490

[67] Page, C , *Composites,* April 1982, pp 140–144

[68] Arup, H , "Galvanic Action of Steel in Concrete," Danish Corrosin Centre, Glostrup, Denmark, Aug 1977

[69] Gjorv, O and Vennesland, O , *Journal,* American Concrete Institute, Sept 1976, p 512

[70] Barneyback, R and Diamond, S , *Cement and Concrete Research,* Vol 11, 1981, p 279

[71] Carlson, E , *Corrosion,* Vol 1, 1945, pp 31–37

[72] Fujiwara, T in *Concrete Durability,* J Scanlon, Ed , American Concrete Institute SP 100, Detroit, 1987, pp 805–818

[73] Yonezawa, T , Ashworth, V , and Proctor, R , *Corrosion,* Vol 44, 1988, pp 489–499

[74] Burkowski, B and Engloi, *Concrete International,* Vol 10, No 11, Nov 1988, pp 25–33

[75] Neville, A , *Properties of Concrete,* Wiley, New York, 1975

[76] Beeby, A , *The Structural Engineer,* Vol 56A, No 3, March 1978, pp 77–81

[77] Rider, R and Heidersbach, R in *Corrosion of Reinforced Steel in Concrete, ASTM STP 713,* D Tonini and J Gaidis, Eds , American Society for Testing and Materials, Philadelphia, 1980, pp 75–92

[78] Nilsen, N and Espelid, B , "Corrosion Behavior of Reinforced Concrete Under Dynamic Loading," *Proceedings,* Corrosion/85, Paper No 261, National Association of Corrosion Engineers, Houston, March 1985

[79] Vennesland, O and Gjorv, O , *Materials Performance,* Vol 20, No 8, Aug 1981, pp 49–51

[80] Flick, L and Lloyd, J in *Corrosion of Reinforced Steel in Concrete, ASTM STP 713,* D Tonini and J Gaidis, Eds , American Society for Testing and Materials, Philadelphia, 1980, pp 93–101

[81] Mehta, P K in *Concrete in Marine Environment,* V Malhotra, Ed , American Concrete Institute SP 100, Detroit, 1988, pp 1–30

Author Index

Subject Index

ISBN 0-8031-1458-3